

Structure-Activity Relationship Studies of Albicidin's C-Terminal Dipeptide and N-terminal Cinnamoyl Residue

vorgelegt von

M. Sc.

Iraj Behroz

an der Fakultät II – Mathematik und Naturwissenschaften
der Technischen Universität Berlin
zur Erlangung des akademischen Grades

Doktor der Naturwissenschaften

- Dr. rer. nat. -

genehmigte Dissertation

Promotionsausschuss:

Vorsitzender: Prof. Dr. Reinhard Schomäcker

Erstgutachter: Prof. Dr. Roderich D. Süssmuth

Zweitgutachter: Prof. Dr. Thorsten Berg

Tag der wissenschaftlichen Aussprache: 10. Juni 2021

Berlin 2021

Zusammenfassung

Der vom pflanzenpathogenen Bakterium *Xanthomonas albilineans* synthetisierte Naturstoff Albicidin ist ein neuartiger und hochpotenter Gyrasehemmer mit hervorragenden antibakteriellen Eigenschaften sowohl gegen Gram-positive als auch gegen Gram-negative Bakterien. Nach der erstmaligen Beschreibung Mitte der 1980er Jahre vergingen drei Jahrzehnte bis zur vollständigen Strukturaufklärung des Peptidantibiotikums, auf welche unmittelbar die erste und skalierbare Totalsynthese folgte. Um den vielversprechenden Wirkstoff für die Verwendung als Arzneimittel in der Humanmedizin zu qualifizieren, bedarf es jedoch der Optimierung einiger pharmakokinetischer Eigenschaften – allen voran der Plasmastabilität und der Löslichkeit. Mit diesem Ziel wurden in den letzten Jahren zwei Studien zur Struktur-Aktivitäts-Beziehung (SAR) durchgeführt, welche zahlreiche Derivate mit Variationen der zentralen α -Aminosäure und der N-terminalen Cumarsäure hervorbrachten.

Diese Arbeit beinhaltet die Synthesen und Bioaktivitätsuntersuchungen von 38 neuen Albicidin-Derivaten, die in zwei voneinander unabhängigen Studien präsentiert werden. In der ersten Studie wird das bislang wenig erforschte C-terminale, aromatische Dipeptid systematisch untersucht, wobei die Bedeutung des Substitutionsgrades und des Substitutionsmusters, als auch die Art des Substituenten im Mittelpunkt stehen. Des Weiteren werden Derivate betrachtet, die ein heteroaromatisches bzw. ein alicyclisches Grundgerüst besitzen. Diese Derivate geben tiefe Einblicke in die SAR dieses Pharmakophors und liefern wichtige Hinweise für die Strukturoptimierung des Albicidins hin zu einem potenziellen präklinischen Wirkstoffkandidaten.

In der zweiten Studie werden vor allem Verbindungen behandelt, bei denen das Methylacrylamid-Strukturmotiv durch eine Dreifachbindung ersetzt wurde, um einer photochemischen (*E*)-(*Z*)-Isomerisierung der *p*-Cumarsäure, die zu einem erheblichen Aktivitätsverlust führt, vorzubeugen. Die Ergebnisse zeigen, dass weitreichende strukturelle Veränderungen am N-Terminus toleriert werden und oftmals zu hochaktiven und robusteren Verbindungen führen. Einige der neu synthetisierten Diarylalkin-Analoga besitzen eine praktisch unverminderte antibakterielle Wirksamkeit. Daher stellt dieses Gerüst eine vielversprechende Alternative zur *p*-Cumarsäure dar und könnte als Grundlage für das Design von Derivaten mit wesentlich verbesserten pharmakologischen Eigenschaften dienen.

Abstract

In the light of the rapid emergence and spread of multidrug-resistant (MDR) pathogens and the dwindling options for the treatment of infected patients with conventional antibiotics, it is of utmost importance to explore innovative classes of drugs that possess unique structures and unparalleled mechanisms of action. Produced by the plant-pathogenic bacterium *Xanthomonas albilineans*, the natural product albicidin is an unprecedented and highly potent inhibitor of bacterial DNA gyrase with pronounced activity against Gram-positive and Gram-negative bacteria. Initially described in the mid-1980s, the elucidation of the structure and subsequently the first total synthesis of the antibiotic were accomplished almost three decades later. Despite being a promising lead structure, albicidin's pharmacokinetic properties – most notably the poor solubility and plasma stability – need to be improved to make it a viable drug candidate. For that reason, two structure-activity relationship (SAR) studies have been conducted in recent years, giving rise to many structural derivatives with variations of the central amino acid and the N-terminal *p*-coumaric acid, respectively.

This work describes the syntheses and biological evaluation of 38 new albicidin derivatives, which are presented in the context of two independent studies. The first study comprises a systematic investigation of the previously underexplored C-terminal aromatic dipeptide, focusing on the degree and pattern of substitution as well as on the nature of the substituents. Besides, derivatives containing heteroaromatic and alicyclic motifs are investigated. These derivatives provide a profound insight into the SAR of this pharmacophore and will support future efforts to optimize the structure of albicidin towards a potential clinical candidate.

Since the N-terminal *p*-coumaric acid moiety is prone to undergo photochemical (*E*)-(*Z*)-isomerization, which results in a significant loss of activity, the second study mainly deals with the replacement of the methacrylamide residue with an alkyne motif. The results suggest that extensive structural manipulations are tolerated at the N-terminus and often lead to highly active and more robust compounds. Some of the newly synthesized diaryl alkyne analogs display virtually undiminished antibacterial efficacies. Therefore, this scaffold represents a promising alternative to the *p*-coumaric acid and could potentially serve as a blueprint for designing albicidin derivatives with preserved activity that display enhanced pharmacological properties.

Publikationen

Teile dieser Arbeit wurden bereits veröffentlicht:

1. [I. Behroz](#), P. Durkin, S. Grätz, M. Seidel, L. Rostock, M. Spinczyk, J. B. Weston, and R. D. Süßmuth, *Extensive Structure-Activity Relationship Study of Albicidin's C-Terminal Dipeptidic p-Aminobenzoic Acid Moiety*, *Chem. Eur. J.* **2019**, 25, 16538–16543.
2. [I. Behroz](#), L. Kleebauer, K. Hommernick, M. Seidel, A. Mainz, S. Grätz, J. B. Weston, and R. D. Süßmuth, *Acetylenic Replacement of Albicidin's Methacrylamide Residue Circumvents Detrimental (E)-(Z)-Photoisomerization and Preserves Antibacterial Activity*, *Chem. Eur. J.* 10.1002/chem.202100523, **2021**.

Danksagung

An erster Stelle gilt mein Dank meinem Doktorvater Professor Dr. Roderich Süssmuth. Durch die Aufnahme in seine Arbeitsgruppe habe ich die Möglichkeit bekommen, an einem nach wie vor spannenden und hochrelevanten Thema zu forschen. Als Doktorand im Albicidin-Projekt wurde ich fachlich wie auch menschlich bestens auf das Berufsleben vorbereitet. Professor Süssmuth hat sich immer viel Zeit dafür genommen, wissenschaftliche Fragestellungen mit seinen Mitarbeitern zu erörtern und sich richtungsgebend in das Projekt einzubringen. Auch deshalb blicke ich auf eine erfolgreiche Doktorarbeit zurück. Für die Möglichkeit, an mehreren nationalen und internationalen Konferenzen teilnehmen zu dürfen, bin ich sehr dankbar. Herrn Professor Dr. Berg und Herrn Professor Dr. Schomäcker danke ich herzlich für die jeweilige Übernahme des Zweitgutachtens bzw. des Vorsitzes des Promotionsausschusses.

Ein großer Dank gilt meinen Kollegen aus dem „Team-Albi“. Dr. John Weston danke ich für die sehr gute Beratung und seine Unterstützung beim Verfassen von Publikationen. Dr. Stefan Grätz, Dipl.-Chem. Dennis Kerwat, Dr. Patrick Durkin und Dr. Leonard von Eckardstein danke ich für die lehrreiche Zusammenarbeit und die ständige Hilfsbereitschaft bei synthetischen Fragestellungen und darüber hinaus. Insbesondere während meiner Einarbeitung habe ich diese Hilfe sehr zu schätzen gewusst. M. Sc. Kay Hommernick, M. Sc. Leonardo Kleebauer und Marcello Spinczyk danke ich für die sehr gute Zusammenarbeit zum Ende meiner Laborzeit hin. Dr. Andi Mainz danke ich vielfach für seine kompetente und zielführende Unterstützung auch bei schwierigen Fragestellungen rund um die NMR-Spektroskopie. Ein großer Dank gilt auch Dipl.-Ing. Maria Seidel und Annette Poch für die Durchführung der zahlreichen biologischen Testierungen, die für unsere Arbeit unentbehrlich sind. Maria danke ich zudem für die Übernahme der organisatorischen Aufgaben, die uns das Leben im „Team-Albi“ deutlich erleichtert haben. Dr. Lida Rostock danke ich für die Durchführung der Experimente im Zusammenhang mit AlbA und AlbD.

Der gesamten Arbeitsgruppe Süssmuth möchte ich für die gute Zusammenarbeit und die starke Kollegialität in den letzten Jahren danken. Die vielen lustigen Momente, gemeinsamen Abende und die schönen MAS-Wochenenden werden mir noch lange in Erinnerung bleiben.

Danksagung

Ein besonderer Dank gilt Kati Winter, die im Hintergrund den organisatorischen und bürokratischen Aufwand auf sich genommen hat und der restlichen Arbeitsgruppe somit viele Hindernisse aus dem Weg geräumt hat.

Der Analytik-Abteilung des Instituts danke ich für die schnelle und zuverlässige Vermessung der zahlreichen Proben und die Instandhaltung der Messgeräte. Hier sind insbesondere Marc Griffel, Dr. Maria Schlangen, Samantha Voges und Dr. Sebastian Kemper hervorzuheben.

Auf privater Seite gebührt mein besonderer Dank schließlich meinen Eltern und meinem Bruder, die mich während der gesamten Zeit meines langen Studiums auf vielfältige Art und Weise unterstützt haben. Meiner Freundin Theresa danke ich von Herzen für die Kraft, die sie mir beim Schreiben dieser Arbeit gegeben hat.

Table of Contents

Abbreviations	17
List of Figures.....	21
List of Tables.....	23
List of Schemes	25
1 Introduction	27
1.1 The Antibiotic Resistance Crisis.....	27
1.1.1 General Introduction.....	27
1.1.2 The Evolution of Antibiotic Resistance.....	31
1.2 Antibacterial Drug Targets	34
1.2.1 Molecular Targets of Common Antibiotics	34
1.2.2 Bacterial DNA Gyrase	36
1.3 Small Molecule Gyrase Inhibitors	39
1.3.1 Aminocoumarins and Simocyclinones	40
1.3.2 Quinolones	42
1.3.3 Other Small-Molecule Gyrase Inhibitors.....	44
1.4 Albicidin.....	47
1.4.1 General Introduction.....	47
1.4.2 Structure Elucidation and Biosynthesis.....	48
1.4.3 Primary Uptake and Mode of Action	53
1.4.4 Mechanisms of Resistance	55
1.4.5 Total synthesis.....	60

Table of Contents

1.4.6	Previous SAR Studies	63
1.4.7	Cystobactamids/Coralmycins and Natural Albicidin Derivatives	68
1.4.8	Summary of Previous SAR Findings.....	70
2	Aim of this Work.....	73
3	Results and Discussion	75
3.1	Preliminary Remarks	75
3.2	Derivatives with Variations of the C-Terminal Dipeptidic <i>p</i> ABA Moiety	75
3.2.1	Syntheses of Modified E-F Dipeptides	78
3.2.2	Synthesis of Tetrapeptides with Modified E-F Building Blocks.....	87
3.2.3	Final Assembly of E-F Derivatives of Albicidin.....	97
3.2.4	Biological Evaluation of E-F Derivatives of Albicidin	101
3.3	Derivatives with Variations of the N-Terminal A-B Building Block	107
3.3.1	Syntheses of A-B Derivatives of Albicidin.....	111
3.3.2	Biological Evaluation of A-B Derivatives of Albicidin	114
4	Summary and Outlook.....	117
4.1	Derivatives with Variations of the C-Terminal Dipeptide	117
4.2	Derivatives with Variations of the N-Terminal A-B Building Block	120
5	Experimental Part.....	123
5.1	General Information.....	123
5.1.1	Reagents and Solvents	123
5.1.2	Chromatography	123
5.1.3	Analytical Methods.....	124
5.1.4	Nomenclature.....	124

5.2	Synthetic Protocols.....	124
5.2.1	General Procedures (GPs)	124
5.2.2	Derivatives with Variations of the C-Terminal Dipeptidic <i>p</i> ABA Moiety	127
5.2.3	Derivatives with Variations of the N-terminal A-B Building Blocks	186
5.3	Biological Assays.....	204
5.3.1	Microdilution Assay.....	204
5.3.2	DNA Gyrase Inhibition Assay	205
6	References	207
7	Appendix.....	219

Abbreviations

A

A domain	adenylation domain
ABC	ATP binding cassette
ACP	acyl carrier protein
ADPNP	5'-adenylyl- β,γ -imidodiphosphate
AL	acyl-CoA ligase
AMR	antimicrobial resistance
aq	aqueous
AT	acyltransferase
ATPase	adenosine triphosphatase

B

Boc	<i>tert</i> -butyloxycarbonyl
BTC	bis(trichloromethyl) carbonate, triphosgene

C

C domain	condensation domain
CD	circular dichroism
CIP	ciprofloxacin
CNS	central nervous system
CoA	coenzyme A
CRE	carbapenem-resistant Enterobacteriaceae
CTD	C-terminal domain

D

DCC	dicyclohexylcarbodiimide
DDD	defined daily dose
DH	dehydrogenase
DIPEA	diisopropylethylamine
DMF	<i>N,N</i> -dimethylformamide
DMSO	dimethyl sulfoxide

E

EEDQ	2-ethoxy-1-ethoxycarbonyl-1,2-dihydroquinoline
EGCG	(-)-epigallocatechin-3-gallate
<i>ent</i>	enantiomer

equiv..... equivalent
ESBL.....extended-spectrum β -lactamase
ESI..... electrospray ionization
FDA..... U. S. Food and Drug Administration

G

G-segment..... gate segment

H

HGT..... horizontal gene transfer
HIV..... human immunodeficiency virus
HMBC.....heteronuclear multiple bond coherence
HPLC..... high-performance liquid chromatography
HR-MS.....high-resolution mass spectrometry
HSQC..... heteronuclear single quantum coherence
HTH.....helix-turn-helix

I

IC₅₀..... half-maximal inhibitory concentration
ICU..... intensive care unit

K

K_d..... equilibrium dissociation constant
KS.....ketosynthase
KT..... ketoreductase
MCA..... (E)-3-(4-hydroxyphenyl)-2-methylacrylic acid, 2-methylcoumaric acid
MCR.....mobilized colistin resistance
MDR..... multidrug-resistant
MerR..... mercury resistance
MGE..... mobile genetic element
MIC..... minimum inhibitory concentration
MRSA..... methicillin-resistant *S. aureus*
MT.....methyl transferase

N

NBTI..... novel bacterial topoisomerase inhibitor
NMR..... nuclear magnetic resonance
NOESY.....nuclear Overhauser effect spectroscopy
NRPS.....nonribosomal peptide synthetase

NTD.....	N-terminal domain
O	
OAt.....	azabenzotriazole
ORF	open reading frame
P	
<i>p</i> ABA	<i>para</i> -aminobenzoic acid
<i>p</i> AHBA.....	<i>para</i> -aminohydroxybenzoic acid
<i>p</i> AHMBA	<i>para</i> -amino-2-hydroxy-3-methoxybenzoic acids
PCP.....	pentachlorophenol
<i>p</i> HBA	<i>para</i> -hydroxybenzoic acid
pl.....	isoelectric point
PKS.....	polyketide synthase
PMSF.....	phenylmethylsulfonyl fluoride
<i>p</i> NBA.....	<i>para</i> -nitrobenzoic acid
<i>p</i> NBC.....	<i>para</i> -nitrobenzoyl chloride
POM.....	pivaloyloxymethyl
PPB.....	plasma protein binding
PPL.....	Priority Pathogens List
R	
r.t.	room temperature
S	
SAM	(<i>S</i>)-adenosyl methionine
SAR.....	structure-activity relationship
T	
T domain	thiolation domain
TE domain.....	thioesterase domain
TFA.....	trifluoroacetic acid
TFAA	trifluoroacetic anhydride
THF.....	tetrahydrofuran
TipA.....	thiostrepton-induced protein A
TLC.....	thin-layer chromatography
TopoIV	topoisomerase IV
<i>t</i> _R	retention time
T-segment.....	transport segment

Abbreviations

U

UTIurinary tract infection

V

VGTvertical gene transfer

VREvancomycin-resistant enterococci

WHOWorld Health Organization

List of Figures

Figure 1. The evolution and spread of antibiotic resistance.....	32
Figure 2. Structures of selected antibiotics in clinical use.	35
Figure 3. Molecular model for the “two-gate mechanism” of gyrase activity.	38
Figure 4. Structures of selected aminocoumarins.	41
Figure 5. Structures of selected quinolone antibiotics.	43
Figure 6. Structures of natural cyclothialidine and an improved synthetic analog.	45
Figure 7. Structures of catechin-based polyphenols found in green tea.....	45
Figure 8. Necrotic symptoms of leaf scald disease on sugarcane leaves.	47
Figure 9. Structure of the polyketide and peptide antibiotic albicidin (1).....	49
Figure 10. Proposed model of albicidin biosynthesis.....	52
Figure 11. Albicidin derivatives with variations of the central α -amino acid.	65
Figure 12. Albicidin derivatives with variations of the N-terminal coumaric acid moiety.	67
Figure 13. Structures of albicidin (1), cystobactamid 919-2 (31), and coralmycin A (32).....	69
Figure 14. SAR summary of natural and synthetic albicidins and related cystobactamids.	71
Figure 15. Structures of synthesized E-F analogs of AzaHis-albicidin 16 (Part 1).....	76
Figure 16. Structures of synthesized E-F analogs of AzaHis-albicidin 16 (Part 2).....	78
Figure 17. HR-LCMS analysis of the crude product mixture of 231 and 231a.	94
Figure 18. Proton NMR spectrum of ethylene glycol-containing albicidin derivative 52.....	99
Figure 19. Proton NMR spectra of N-methylated albicidin derivative 56.....	101
Figure 20. Gyrase inhibition assay for albicidin variants with modified E-F building blocks.	106
Figure 21. Photochemical (E)-(Z)-isomerization of albicidin’s cinnamoyl residue.....	108
Figure 22. Structures of albicidin derivatives with variations of the A-B building block motif.	110
Figure 23. Gyrase inhibition assay for albicidin analogs with modified A-B building blocks.	116
Figure 24. Summary of the bioactivity of selected albicidin derivatives.	118
Figure 25. Proposed E-F derivatives of albicidin for future SAR studies.....	119
Figure 26. Summary of the bioactivity of selected albicidin derivatives.	120
Figure 27. Proposed incorporation of the acetylene group as amide bond isosteres.....	121

List of Tables

Table 1. Priority Pathogens List (PPL) published by the WHO in 2017.	30
Table 2. Syntheses of final albicidin derivatives with modified pABAs (Part 1).....	98
Table 3. MIC values for albicidin derivatives with modified E-F building blocks (S1 panel)..	103
Table 4. MIC values for albicidin derivatives with modified E-F building blocks (S2 panel)..	104
Table 5. MIC values for albicidin derivatives with modified A-B building blocks.	115

List of Schemes

Scheme 1. Retrosynthetic strategy for the total synthesis of albicidin (1).....	61
Scheme 2. Synthesis of E-F dipeptides with sequential deletion of substituents.	79
Scheme 3. Synthesis of orthogonally protected dihydroxybenzoic acids.....	80
Scheme 4. Synthesis of tetrasubstituted O-alkylation precursors.....	81
Scheme 5. Scope and limitations of O-alkylation reactions of phenols 105 and 106.....	82
Scheme 6. Syntheses of ethoxy-substituted E-F dipeptides.	83
Scheme 7. Synthesis of the ethylene glycol-containing E-F dipeptide.	84
Scheme 8. Syntheses of heteroaromatic E-F dipeptides.	85
Scheme 9. Synthesis of an N-methylated E-F dipeptide.	86
Scheme 10. Syntheses of isophthalic acid and cyclohexyl-containing dipeptides.	86
Scheme 11. Syntheses of D-E-F tripeptides with sequential deletion of E-F substituents.	88
Scheme 12. Syntheses of C-D-E-F tetrapeptides with sequential deletion of E-F substituents.	89
Scheme 13. Synthesis of C-D-E-F tetrapeptides containing ethoxy-substituted pABAs.....	91
Scheme 14. Synthesis of a C-D-E-F tetrapeptide with an ethylene glycol-containing pABA... ..	92
Scheme 15. Syntheses of C-D-E-F tetrapeptides containing pyridines.....	93
Scheme 16. Synthesis of a C-D-E-F tetrapeptide containing an amide bond isostere.	95
Scheme 17. Synthesis of isophthalic acid and cyclohexyl-containing C-D-E-F tetrapeptides..	96
Scheme 18. Syntheses of final albicidin derivatives with modified pABAs (Part 2).....	100
Scheme 19. Syntheses of albicidin derivatives with modified A-B building blocks (Part 1). .	112
Scheme 20. Syntheses of albicidin derivatives with modified A-B building blocks (Part 2). .	113

1 Introduction

1.1 The Antibiotic Resistance Crisis

1.1.1 General Introduction

At the beginning of the 20th century, infectious diseases, such as cholera, diphtheria, pneumonia, tuberculosis, and syphilis, still accounted for high morbidity and mortality rates worldwide. At that time, the average life expectancy in the US was below 60 years.^[1] The advent of antibiotics in the early 1920s marked the turning point in modern medicine and dramatically improved the public health response to bacterial infections. Potent antibiotics have become indispensable for both prophylactic and therapeutic measures by shielding patients from potentially lethal infections and allowing complex medical procedures, such as surgery, chemotherapy, and dialysis, to take place at relatively low risk of infection.^[2] While antibiotic resistance is an ancient natural phenomenon, its spread in human pathogens is a recent development on an evolutionary time scale.^[3] The exceptional effectiveness of antibiotics has made them a universal remedy in the eyes of the public and has resulted in their widespread and lavish use in human health care, animal husbandry, and plant agriculture over the past 70 years.^[4] A recent study with data from 76 countries showed that the worldwide consumption of antibiotics rose by 65% between the years 2000 and 2015, reaching 34.8 billion defined daily doses (DDDs). More importantly, the antibiotic consumption rate in that period climbed by 39% from 11.3 to 15.7 DDDs per 1,000 inhabitants. Mainly driven by low- and middle-income countries, the study predicts a further 200% increase in consumption by the year 2030.^[5]

General practitioners who prescribe antibiotics based on suspicion of a bacterial infection, rather than based on lengthy test results, are mainly responsible for their overuse in human healthcare. This practice is often caused by patients and their relatives demanding a prompt

response to illnesses and doctors succumbing to the pressure.^[6] For example, many antibiotics are prescribed against upper respiratory tract infections that are usually caused by viruses against which antibiotics are ineffective.^[7] Because life-threatening infections require immediate action, patients in hospital settings are often administered multiple antibiotics simultaneously. The impracticality of identifying infectious diseases and their causative agents in due time often forces clinicians to randomly administer antibiotics. Some patients prematurely discontinue a prescribed treatment, thereby unknowingly fostering resistance development.^[8] In many countries, antibiotics can still be purchased over the counter, which gives rise to improper self-medication and overuse.^[9] The gross application of antibiotics in livestock and crops considerably contributes to the emergence and spread of resistant bacteria. Valuable clinical drugs that are regarded as last resorts against potentially lethal infections in humans, such as colistin, are used on a massive scale worldwide. The immoderate use of antibiotics has increased the selective pressure on bacteria, stimulated their natural adaption to the antibiotic threat, and ultimately led to the incurrence of multidrug-resistant (MDR) strains.^[10] Resistant bacteria can spread among livestock and people through food, direct contact with the animals, or contaminated air. The foodborne pathogen *Salmonella* Heidelberg, for example, is a prime example of zoonosis and can cause disease in both cattle and humans.^[11]

Today, the rapid emergence and spread of antibiotic resistance are among the greatest threats to human and animal health worldwide. Previously potent antibiotics are becoming increasingly ineffective, depriving patients of life-saving medications. Even the strongest weapons in our therapeutic arsenal, such as last resort polymyxins and carbapenems, are facing limitations due to the incessant emergence of pan-resistant pathogenic bacteria.^[12,13] The most common bacterial pathogens associated with antibiotic resistance are referred to by the acronym *ESKAPE*, which encompasses the Gram-positive species *Enterococcus faecium* (*E. faecium*) and *Staphylococcus aureus* (*S. aureus*) as well as the Gram-negative species *Klebsiella pneumoniae* (*K. pneumoniae*), *Acinetobacter baumannii* (*A. baumannii*), *Pseudomonas aeruginosa* (*P. aeruginosa*), and *Enterobacter* spp.^[14] Together with *Escherichia coli* (*E. coli*)^[15] and *Clostridioides difficile* (*C. difficile*)^[16], they are the principal cause of hospital-acquired (nosocomial) infections. The most prevalent types are urinary tract infections, bloodstream infections, surgical site infections, and pneumonia.^[17] They are

difficult to treat because they are frequently caused by MDR pathogens, including methicillin-resistant *S. aureus* (MRSA), vancomycin-resistant enterococci (VRE), extended-spectrum β -lactamase (ESBL) producing *E. coli*, and carbapenem-resistant Enterobacteriaceae (CRE)^[18] Due to their highly restrictive outer membrane permeability, Gram-negative microorganisms are of special concern^[19] According to the WHO, approximately 15% of all hospitalized patients are affected by nosocomial infections. Many hospitals and hospital-type health care environments are predestined for the evolution of highly MDR bacterial strains. Possible risk factors include inadequate hygiene, the prolonged and intensive use of antibiotics, the extended stay of patients in intensive care units (ICUs), the susceptibility of immunocompromised patients to infections, and the lack of awareness of prevailing infections and knowledge on how to prevent them among patients and health care personnel.^[20]

The most prescribed antibiotics, e.g., cephalosporins and fluoroquinolones, derive from known compound classes that are remnants of the 'golden era' of antibiotic research (the 1940s to 1960s). The development of enhanced structural analogs does not suffice anymore to keep pace with the spread of resistance. There is an urgent demand for truly novel chemical scaffolds with unprecedented mechanisms of action.^[21] Novel antibiotic agents are classified innovative if they fulfill at least one of the following criteria: the absence of cross-resistance to existing antibiotics, a new chemical class, a new molecular target, or a new mechanism of action.^[22] The clinical pipeline for first-in-class antibiotics is running dry because of increasingly stringent regulatory barriers and major pharmaceutical companies abandoning antibiotic research for the more profitable field of chronic diseases.^[1] The scope of the problem has reached alarming levels. According to the World Health Organization (WHO), the number of annual deaths attributable to antimicrobial resistance (AMR) could reach ten million by the year 2050. Additionally, an associated increase in global health expenses by \$1.2 trillion is anticipated.^[23]

The antibiotic resistance crisis has become an important topic of public debate in the last couple of years and has been recognized as a major global health challenge by regulatory, economic, and political bodies, such as the WHO, the International Monetary Fund, and the World Bank.^[24] In 2015, the WHO and its member states have acknowledged the devastating prospect of a post-antibiotic era and outlined the objectives to combat antimicrobial resistance in a Global Action Plan. A designated 'One Health' approach calls for the combined

international effort of stakeholders in human and animal health care as well as agriculture to cope with the problem.^[25] Many governments across the world have adopted national programs, e.g. the German Antimicrobial Resistance Strategy 2020 (DART 2020) to meet the requirements.^[26] Even if all precautionary measures envisaged by the WHO are successful, the development of novel anti-infectives, either antibiotics or alternative therapeutics, will remain crucial. Recently, a Priority Pathogens List (PPL) was drawn up by the WHO in collaboration with the Division of Infectious Diseases at the University of Tübingen to promote and guide research and development of new antibiotics. The list includes members of 12 families of bacteria with critical, high, and medium antibiotic resistance (Table 1). The purpose of the PPL is to help prioritize incentives and funding, to help harmonize public health requirements with research and development priorities, and to facilitate global coordination.^[27]

Table 1. Priority Pathogens List (PPL) published by the WHO in 2017.

A global priority list of 12 bacteria to guide research and development of new antibiotics.^[28]

Priority	Pathogens	Antibiotic Resistance
Critical ^a	<i>Acinetobacter baumannii</i>	carbapenems
	<i>Pseudomonas aeruginosa</i>	carbapenems
	Enterobacteriaceae ^b	carbapenems and 3 rd generation cephalosporins
High	<i>Enterococcus faecium</i>	vancomycin
	<i>Staphylococcus aureus</i>	methicillin, vancomycin-intermediate and -resistant
	<i>Helicobacter pylori</i>	clarithromycin
	<i>Campylobacter</i>	fluoroquinolones
	<i>Salmonella spp.</i>	fluoroquinolones
	<i>Neisseria gonorrhoeae</i>	3 rd generation cephalosporins, fluoroquinolones
Medium	<i>Streptococcus pneumoniae</i>	penicillin-non-susceptible
	<i>Haemophilus influenzae</i>	ampicillin
	<i>Shigella spp.</i>	fluoroquinolones

^aMycobacteria were not reviewed as it already is a globally established priority.

^bEnterobacteriaceae include *Klebsiella pneumoniae*, *Escherichia coli*, *Enterobacter spp.*, *Serratia spp.*, *Proteus spp.*, *Providencia spp.*, and *Morganella spp.*

1.1.2 The Evolution of Antibiotic Resistance

Antibiotic resistance is an ancient response of microorganisms to environmental threats.^[3] Many bacteria and fungi produce and release antimicrobial secondary metabolites as part of their natural defense mechanism. This gives them an edge over other microbes in their proximity when competing for nutrients in a distinct habitat. Bacteria have likely been exposed to antibiotics for hundreds of millions of years and have developed a variety of resistance mechanisms to uphold reproduction and survive in their presence. They are believed to have acquired resistance genes against many of those antibiotics directly from their original producers, which they have coexisted with in the same ecological space. Most antibiotics in clinical use today are either natural products that originate from isolates discovered by the screening of soil samples or their structural derivatives.^[28,29] These include the various generations of penicillins and cephalosporins from fungi^[30] and a wealth of antibiotics from different strains of the bacterial genus *Streptomyces*.^[31] Prominent examples include streptomycin, actinomycin, erythromycin, vancomycin, and tetracycline.^[32] Chemical modifications are introduced either semi-synthetically, e.g. for many β -lactam antibiotics, or by total synthesis as for the second-generation erythromycins, i.e. clarithromycin and azithromycin. Only a few entirely synthetic antibiotic classes, such as the fluoroquinolones and oxazolidinones, are of significant clinical importance.^[33]

Bacterial resistance can be divided into two classes, namely intrinsic or natural resistance and acquired resistance. Intrinsic resistance arises from the presence of genes in the bacterial genome which produces resistance phenotypes, i.e., structural and functional characteristics that allow bacteria to withstand the effect of an antibiotic. This type of resistance predates antibiotic chemotherapy and is present in all bacterial species. It is commonly associated with the non-permeability of the outer membrane of Gram-negative bacteria, the activity of multidrug efflux systems, the lack of affinity of the antibiotic for the bacterial target, and the production of enzymes that inactivate the antibiotic.^[34,35] An example is the innate resistance of *Mycoplasma* against β -lactams, such as penicillins and cephalosporins. This genus of bacteria lacks a cell wall and thus is not susceptible to these inhibitors of bacterial cell wall synthesis.^[36] Another example is the impermeability of the outer membranes of most Gram-negative bacteria to the large glycopeptide antibiotic vancomycin.^[37,38] The intrinsic resistance of *P. aeruginosa* against the broad-spectrum antibiotic tetracycline is often linked to the

presence of active efflux systems.^[39] Some antibiotics targeting components of intrinsic resistance, such as polymyxins, have been known for over 50 years. They are a class of cyclic cationic lipopeptides acting as outer membrane permeabilizing agents.^[40] These molecules are powerful antibiotics on their own, but also serve as a gateway for hydrophobic antibiotics when used in combination. The clinical application of polymyxins was discontinued due to associated toxicity. However, due to the emergence of life-threatening infections caused by MDR strains of *A. baumannii*, *P. aeruginosa*, and *K. pneumoniae*, colistin (polymyxin E) was reintroduced in the 1980s as a last-resort antibiotic.^[41]

Acquired resistance refers to the ability of bacteria to withstand the action of antibiotics they were previously susceptible to. This can result from spontaneous genetic mutations and vertical gene transfer (VGT)^[42], from the acquisition of resistance genes from other bacteria through horizontal gene transfer (HGT)^[43] or from a combination of both mechanisms. When antibiotics exercise selective pressure on populations of bacteria, they annihilate susceptible strains while allowing resistant ones to survive and propagate (Figure 1).^[44] The genetic blueprint for such resistance is passed on to their offspring through VGT. Due to the rapid generation time of bacteria, e.g. 20 min for *E. coli*^[45], resistant populations quickly evolve and act as a source of resistance genes for other strains.

Mutations resulting in resistance mitigate the antibiotic activity through the following mechanisms: alteration of the antibiotic target^[46], enzymatic modification of the antibiotic

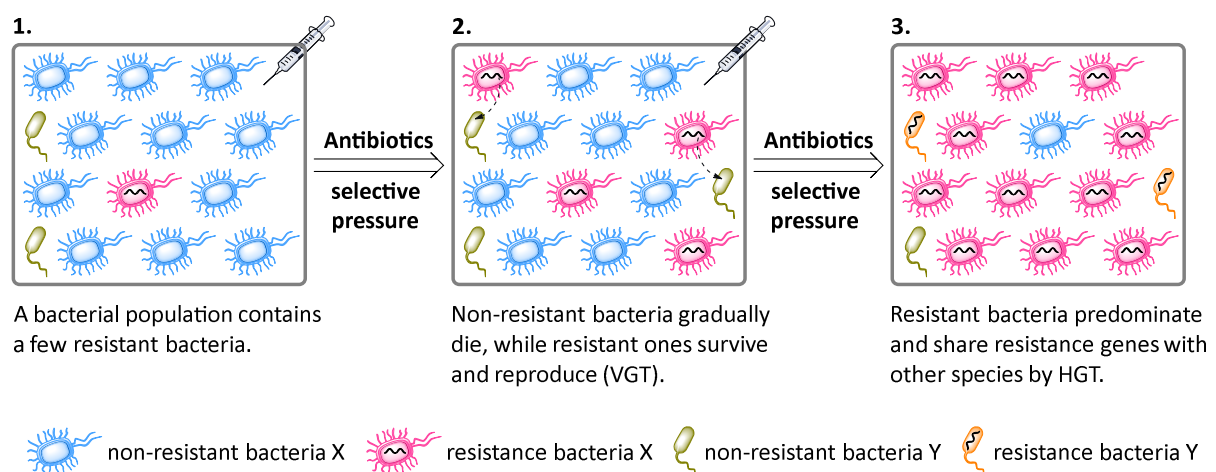


Figure 1. The evolution and spread of antibiotic resistance. A simplified illustration of antibiotic resistance development driven by evolutionary pressure under antibiotic exposure and promoted by vertical gene transfer (VGT) and horizontal gene transfer (HGT).

warhead^[47], decrease in antibiotic uptake, and activation of efflux mechanisms.^[48,49] Therefore, acquired bacterial resistance is very diverse and broad in complexity. The acquisition of genetic information from foreign bacteria through HGT has been an essential process for bacterial evolution and one of the main reasons for the emergence and spread of antibiotic resistance. Three main types of HGT allow bacteria to acquire foreign DNA: direct uptake and incorporation of exogenous DNA (transformation), bacteriophage-mediated DNA transfer from one bacterial cell to another (transduction), and the transfer of DNA by direct cell-to-cell contact (conjugation). The most important strategy for the development of resistance in clinically important pathogens involves conjugation.^[50] This strategy employs mobile genetic elements (MGEs) to allow the exchange of genetic information among bacteria. The most relevant MGEs for the development and spread of MDR bacteria are plasmids and transposons.^[51] Since conjugation requires cell-to-cell contact, it frequently occurs in densely populated bacterial communities. The human gut of hospitalized patients, for example, is a major pool for antibiotic resistance genes that have been selected due to overexposure to antibiotics.^[52]

The global emergence and dissemination of plasmid-mediated resistance in Gram-negative pathogens belonging to the family of Enterobacteriaceae, such as *E. coli* and *K. pneumoniae*, is of great concern.^[53] Resistance to β -lactam antibiotics conferred by ESBLs, AmpCs, cephalosporinases, and carbapenemases are encoded in genes mostly located on conjugative plasmids.^[54] Recently, the first mobilized colistin resistance (MCR-1) gene was found in *E. coli* and nine additional Enterobacteriaceae species.^[55] These plasmids often additionally transfer resistance to aminoglycosides, fluoroquinolones, trimethoprim/sulfamethoxazole (co-trimoxazole), and other antibiotics. The combination of chromosomally encoded and plasmid-mediated resistance results in bacteria that are virtually immune against our entire antibiotic arsenal. Lately, these extensively drug-resistant pathogens have received considerable media coverage and are often termed 'superbugs' in the vernacular.^[56]

1.2 Antibacterial Drug Targets

1.2.1 Molecular Targets of Common Antibiotics

Antibiotics are natural, synthetic, or semi-synthetic chemical substances that either kill (bactericidal) or inhibit the growth (bacteriostatic) of bacteria by disrupting metabolic processes essential to their survival. Bactericidal antibiotics can eradicate an infection independently, whereas bacteriostats rely on the host defense mechanism to exterminate an infection. Whether bacteria are bactericidal or bacteriostatic can also depend on the concentration.^[57,58] Five main bacterial targets have been identified for most of the antibiotics currently on the market: cell wall synthesis, protein synthesis, DNA gyrase, DNA-directed RNA polymerase, and metabolic enzymes.^[59] β -Lactam antibiotics, such as penicillins, cephalosporins, monobactams, and carbapenems, as well as the glycopeptide vancomycin and the epoxide fosfomycin are examples of cell wall synthesis inhibitors and thus act bactericidal.^[60,61] The recently discovered teixobactin^[62] inhibits peptidoglycan biosynthesis by binding to the highly conserved motifs of lipid II and lipid III, which are precursor molecules of peptidoglycan and teichoic acid, respectively.^[63] Teixobactin is one of few examples of target-specific antibiotics for which resistance has not been found yet. It is currently in preclinical development (NovoBiotic Pharmaceuticals, LLC).^[64] Other bactericides include fluoroquinolones and aminocoumarins, which prevent bacterial DNA replication by inhibiting gyrase activity.^[65,66] Prokaryotic DNA-directed RNA polymerase is an essential enzyme for DNA transcription and the cellular target of the semi-synthetic bactericide rifampicin.^[67]

Examples of bacteriostatic drugs targeting metabolic enzymes include sulfonamides and trimethoprim, which interfere with the folic acid pathway. While the former act as competitive inhibitors of the enzyme dihydropteroate synthase, the latter binds to dihydrofolate reductase. Co-trimoxazole is used to exploit the potential synergistic effects of trimethoprim and sulfamethoxazole.^[68-70] However, the combination of different antibacterial drugs can also be disadvantageous. For example, bacteriostatic agents, such as tetracyclines and chloramphenicols, are believed to decrease the bactericidal activity of penicillin in pneumococcal infections.^[71,72] Another drug target mechanism involves the disruption of bacterial protein synthesis, which is associated with the inhibition of the ribosomal RNA

(rRNA) subunit 30S by aminoglycosides and tetracyclines, the inhibition of the 50S subunit by macrolides, chloramphenicol, lincosamide, and streptogramins.^[73,74] The oxazolidinone antibiotics, e.g. linezolid, are unique in that they block the initiation of protein synthesis rather than an advanced step.^[75,76] It is important to note that the classification of an antibiotic as purely bactericidal or bacteriostatic is only valid under strict laboratory conditions *in vitro* and does not necessarily hold *in vivo* under clinical conditions. Hence, most antibacterials are better characterized as potentially being both bactericidal and bacteriostatic.^[57]

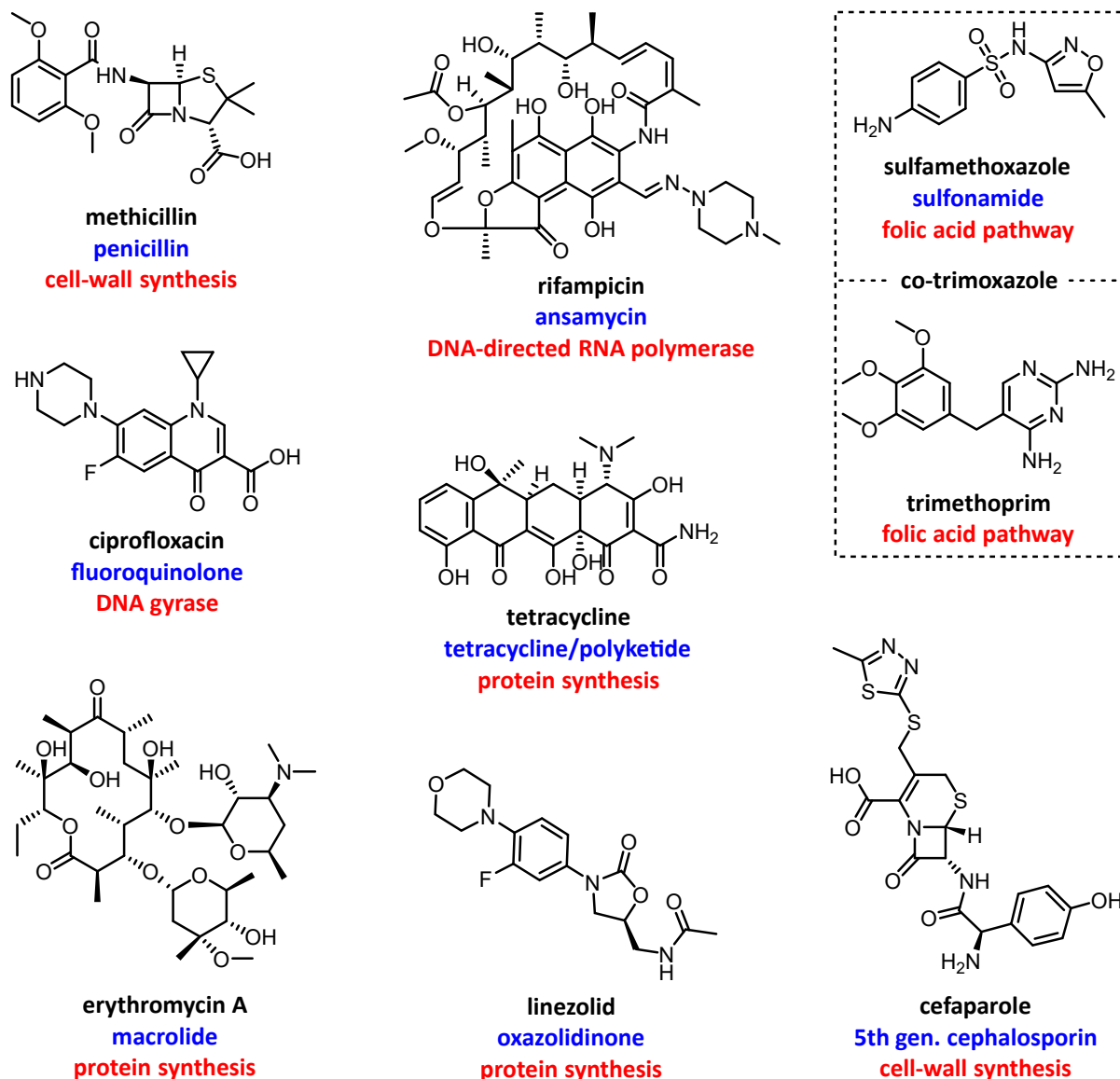


Figure 2. Structures of selected antibiotics in clinical use.

A small selection of currently marketed antibiotics is depicted. The corresponding antibiotic classes (blue) and their bacterial drug targets (red) are highlighted.

1.2.2 Bacterial DNA Gyrase

The Role of Topoisomerases in Bacteria

The (circular) chromosome of a bacterium in its relaxed state is too large to fit into the nucleoid region of a prokaryotic cell. In *E. coli*, the DNA is compacted by approximately a 1000-fold, which is accomplished in part by a process known as supercoiling, where the double-stranded DNA molecules are twisted and coiled into condensed shapes.^[77] DNA replication and transcription are processes that require unwinding of double-stranded DNA by helicase before DNA and RNA polymerases can act on the single strands.^[78] This disruption is very fast, e.g. 100,000 base pairs per minute for *E. coli*, and results in overwound DNA molecules and the accumulation of supercoils. If not released, the increasing mechanical stress will ultimately halt unwinding and stop the replication process.^[79]

As a response to these problems, nature has developed topoisomerases. These enzymes catalyze changes in the topology of DNA by creating transient breaks in the backbone using a conserved tyrosine as the catalytic residue. Besides interconverting relaxed and supercoiled forms, they can promote catenation and decatenation as well as introduce and remove knots of circular DNA. Topoisomerases are responsible for the adjustment of the delicate equilibrium of DNA supercoiling, both to facilitate protein interactions with the DNA and to prevent excessive supercoiling. Since they are present in all cell types, display vulnerable mechanistic features, and are essential to survival, they have become important drug targets for antibacterial and anticancer medication.^[80–82]

Topoisomerases are divided into two subclasses, type I and type II, based on whether they are involved in the transient disruption of one (type I) or both (type II) DNA strands. Type II topoisomerases include DNA gyrase and topoisomerase IV (TopoIV).^[83,84] While all topoisomerases can relax supercoiled DNA, only DNA gyrase can introduce negative supercoils in closed-circuit double-stranded DNA. Gyrase is vital to all bacteria but absent from higher eukaryotes, making it an attractive drug target in antibiotic research.^[85] Discovered by GELLERT *et al.* in 1976 in the wake of studies on two classes of DNA synthesis inhibitors, the coumarins and quinolones, the gyrase enzyme has been the topic of extensive research ever since.^[86]

Structure and Functionality of DNA Gyrase

The best-studied gyrase enzyme is that of *E. coli*, which consists of two protein subunits, GyrA and GyrB, with molecular weights of 97 and 90 kDa, respectively. These two subunits associate to form the heterotetrameric A₂B₂ complex in the active enzyme.^[83] Similarly, topoisomerase IV is composed of two ParC and ParE subunits. GyrA/ParC contains the active-site tyrosine and is responsible for cleaving and recombining both strands of DNA, while GyrB/ParE displays adenosine triphosphatase (ATPase) activity that provides the energy required for supercoiling. The mechanism of gyrase activity is not fully understood yet, but a proposed model, known as the “two-gate mechanism” (Figure 3), is strongly supported by biochemical and structural data.^[87,88] Despite the lack of high-resolution structures of the holoenzyme, the ensemble of X-ray structures for the individual domains from various bacterial species and the fusion of a GyrA domain with a GyrB domain provides a good mechanistic understanding.^[89–97]

Gyrase performs a complex series of topological changes resulting in the passage of a transport segment (T-segment) of DNA through a transient break in the gate segment (G-segment) of the same DNA molecule. This process is ATP-dependent, and the two phosphate termini of the broken G-segment are covalently connected to a pair of catalytical tyrosines in the GyrA domain to form a transient 5'-phosphotyrosyl protein. Two negative supercoils are introduced into the DNA molecule at the expense of two equivalents of ATP per reaction cycle. Chiral wrapping of the DNA around a specialized domain of the enzyme before strand passage ensures the directionality of topoisomerisation, which gives gyrase its unique ability to introduce negative supercoils. In the absence of ATP, the enzyme still catalyzes the relaxation of supercoiled DNA, essentially by the reversed mechanisms.^[98,99] Gyrase has become an attractive cellular drug target because every stage of the catalytic cycle can potentially be disrupted by small molecule inhibitors, for example by impeding DNA binding, DNA cleavage, strand passage, and ATP hydrolysis. The success of many currently employed antibiotics stems from their ability to exploit this vulnerability.^[85,100]

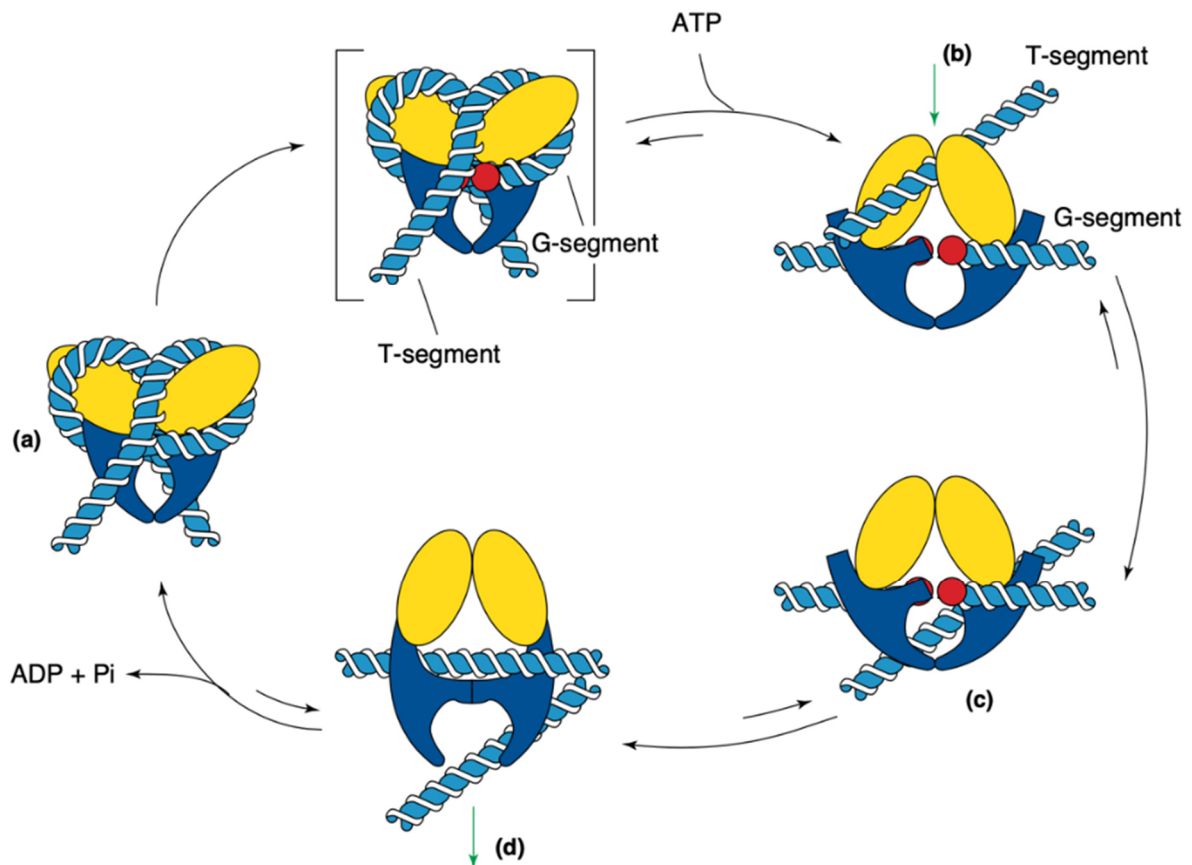


Figure 3. Molecular model for the “two-gate mechanism” of gyrase activity.

(a) Initiated by the interaction of the G segment of DNA (light blue and white) with the N-terminus of gyrase, the GyrA subunits (dark blue) and GyrB subunits (yellow) wrap DNA around a positive supercoil. The locations of the active sites (red circles) in the GyrA domains are indicated in the complex shown in parentheses. (b) The N-gate is closed upon binding of ATP, which traps the T-segment of DNA, followed by a temporary double-strand break in the G-segment. (c) The T-segment is transported through the open gate into the void of the GyrA dimer. (d) The G-segment is reconnected, and the T-segment released through a transient opening of the GyrA dimer, resulting in the introduction of two negative supercoils. The green arrows in steps (b) and (d) indicate the direction of the T-segment passage. The hydrolysis of the second equivalent of ATP opens the GyrB domain and resets the enzyme for the next supercoiling cycle. Adapted from COUTURIER *et al.*^[97] and DIGHE *et al.*^[98]

1.3 Small Molecule Gyrase Inhibitors

The antibacterial activity of gyrase-inhibiting small molecules rests upon two main mechanisms of action. In the first mechanism, the enzymatic activity of gyrase is inhibited, for example by blocking the ATPase activity of the GyrB subunit. The most notable member of such an ATP-competitive GyrB inhibitor is the aminocoumarin novobiocin.^[101,102] The second mechanism involves the stabilization of the covalent gyrase-enzyme complex (poisoning), which prevents the relegation of the disconnected G-segment. The fluoroquinolone ciprofloxacin is the most important member of these cleavage-complex stabilization agents.^[98,103] Intensive mechanistic studies have confirmed that complex stabilization is the most efficient mode of action of gyrase inhibition. This is because comparably low concentrations of a target-bound inhibitor can provoke a series of events, including chromosome fragmentation, induction of the SOS response, and production of reactive oxygen.^[85,104]

In addition to coumarins and quinolones, many other gyrase inhibitors, of both natural and synthetic origin, have been discovered in the past four decades. Some of these compounds and their analogs are highly effective antibiotics currently undergoing preclinical trials. Only a few novel bacterial topoisomerase inhibitors (NBTIs) have advanced to clinical trials, with the investigational drug gepotidacin (GSK2140944) currently undergoing phase III human trials for the treatment of uncomplicated urogenital gonorrhoea caused by *Neisseria gonorrhoeae*.^[105,106] Recently, the orally bioavailable spiropyrimidinetrione antibiotic zoliflodacin has successfully finished phase II trials.^[107] None of these compounds have made it into clinical practice yet. Due to the essential role of type II topoisomerases in bacteria and the complexity of the gyrase catalytic cycle, innovative gyrase inhibitors will likely continue to play an important role in the search for new antibacterial therapeutics in the future. The following chapter provides a concise overview of aminocoumarins and quinolone antibiotics as the currently two most important gyrase-targeting antimicrobials. To demonstrate the structural variety of gyrase-inhibiting small molecules, the cyclothialidines and catechin-based polyphenols are briefly introduced as well.

1.3.1 Aminocoumarins and Simocyclinones

Aminocoumarins were the first class of gyrase-inhibiting antibiotics in clinical use, with novobiocin exhibiting a half-maximum inhibitory concentration (IC₅₀) of 250 nM against *E. coli* gyrase.^[86,108] Structurally, all members of this class contain at least one 3-amino-4,7-dihydroxycoumarin ring. The classical aminocoumarins, including novobiocin, clorobiocin, coumermycin A₁, and rubradirin as well as the simocyclinones (Figure 1), were isolated from different *Streptomyces* and *Actinoallomurus* species.^[109–112] To date, many derivatives have derived from genetic manipulation, metabolic engineering, mutasynthesis, and chemical synthesis.^[113–117] Despite the limited structural resemblance of the classical aminocoumarins to ATP, they block the reaction between ATPase and bacterial type II topoisomerases by overlapping with the ATP binding site at the GyrB/ParE subunit.^[100,118] The mode of action of the structurally more complex simocyclinones, which contain an angucyclinone polyketide motif in addition to the aminocoumarin moiety^[119], appears to be entirely different from that of classical aminocoumarins. Studies by FLATMAN *et al.* have revealed that the ATPase domain of GyrB is not the target of simocyclinone D8.^[108] It was shown that the compound does not stabilize the enzyme-DNA cleavage complex either. Instead, it was found to antagonize the ability of fluoroquinolones to induce cleavage complex formation. The authors proposed that simocyclinones inhibit gyrase activity by binding to a DNA binding site located at the GyrA subunit, which constitutes an entirely new mode of action. It may also be possible that simocyclinones stabilize a conformation of the enzyme incapable of binding to DNA. Recently, Sissi *et al.* proposed the existence of a simocyclinone binding site in the GyrB subunit as well.^[120] Further mechanistic studies will be needed to elucidate the prevailing mode of action. Compared to the simocyclinones, little attention was paid to rubradirin.^[121] The multifunctional ansamycin antibiotic acts as a selective inhibitor of enzymatic peptide chain initiation^[122], whereas its aglycone is a potent inhibitor of RNA polymerase.^[123] This aglycon moiety, containing an ansamacrolide, also acts as a potent inhibitor of the immunodeficiency virus (HIV) reverse transcriptase.^[124]

In the early 1950s, pharmaceutical companies put in a big effort to discover new classes of antibiotics by microbial natural product screening. Novobiocin was discovered independently within two years (1955–1956) by the companies Upjohn, Pfizer, Merck, and Lepetit, and finally

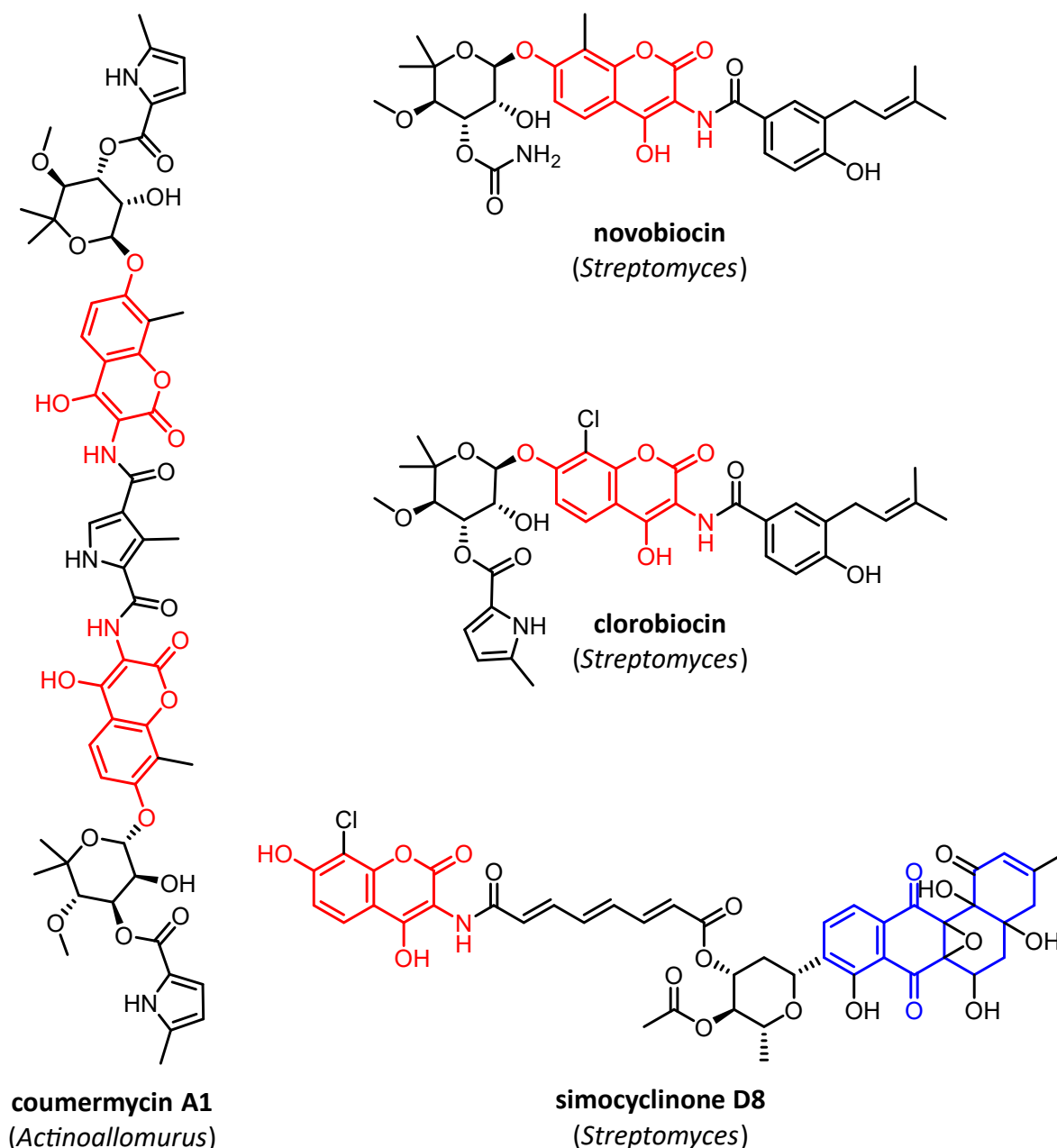


Figure 4. Structures of selected aminocoumarins.

The 3-amino-4,7-dihydroxycoumarin scaffold present in all aminocoumarin antibiotics is highlighted in red. The angucyclinone motif present in simocyclinones is highlighted in blue.

introduced to the market by Upjohn under the trade name Albamycin in the early 1960s.^[125–128] Novobiocin was primarily used to treat infections caused by penicillin-resistant *S. aureus* and less frequently to treat pneumococcal pneumonia.^[129,130] It quickly became superfluous when penicillinase-stable penicillins, such as methicillin and oxacillin, and the first-generation cephalosporins were introduced. In the 1980s, the coumarin class regained attention for its activity against MRSA, which had already become a clinical concern by that time, and different fluoroquinolone-resistant bacterial strains.^[126,131] Owing to its poor efficacy against Gram-

negative bacteria, low bioavailability, low solubility, high plasma protein binding, and eukaryotic toxicity, novobiocin ultimately became obsolete and the U. S. Food and Drug Administration (FDA) withdrew its approval for the oral form of the drug in 2011.^[132]

1.3.2 Quinolones

Quinolones are one of the most successful classes of antibiotics currently on the market and are considered the benchmark for gyrase inhibition. They bind to the DNA-gyrase or DNA-TopoIV cleavage complex, mediated by water-metal ion bridges, which connect the ketone function of quinolone to the serine and acidic residue of the enzymes.^[133,134] Also, cell-death can be evoked by the bacterial DNA stress response.^[135] Quinolones are entirely synthetic molecules deriving from nalidixic acid (Figure 5), the discovery of which is closely related to a by-product of the synthesis of the antimalarial agent chloroquine in 1962.^[136] Nalidixic acid was the first gyrase inhibitor introduced for clinical use in 1967. The first generation of quinolone and quinolone-related antibiotics, including nalidixic acid, oxolinic acid, and cinoxacin, showed no activity against Gram-positive pathogens. They were usually employed in the treatment of urinary tract infections (UTIs) except for those caused by *P. aeruginosa*.^[137] The first fluoroquinolone flumequine was patented in 1973 and showed limited antibacterial activity and sparse distribution into the body tissue. However, it provided the first indication that structural modifications of the chemical scaffold could bring about activity against Gram-positive bacteria.^[138] Following the discovery of improved fluoroquinolones, such as norfloxacin (1977, Kyorin Seiyaku) and ofloxacin (1980, Daiichi Seiyaku), ciprofloxacin (1980, Klaus Grohe, Bayer AG) was approved by the FDA for clinical use in 1987.^[139,140]

Second generation quinolones easily penetrate most bacterial cells and have improved pharmacokinetic properties compared to the first-generation quinolones, including favorable bioavailability, increased blood serum concentration, and higher volume of distribution.^[141,142] Ciprofloxacin quickly became one of the most prescribed antibiotics worldwide and is named alongside levofloxacin (1985, Daiichi Seiyaku) on the WHO's list of essential medicines.^[143–145] The latter is the pharmacologically active (*S*)-enantiomer of racemic ofloxacin.^[146] Although generally considered safe for eukaryotes, fluoroquinolones are sometimes associated with severe side effects involving gastrointestinal reactions, central nervous system (CNS) reactions, genotoxicity, photosensitive eruptions, Achilles tendon rupture, and additional

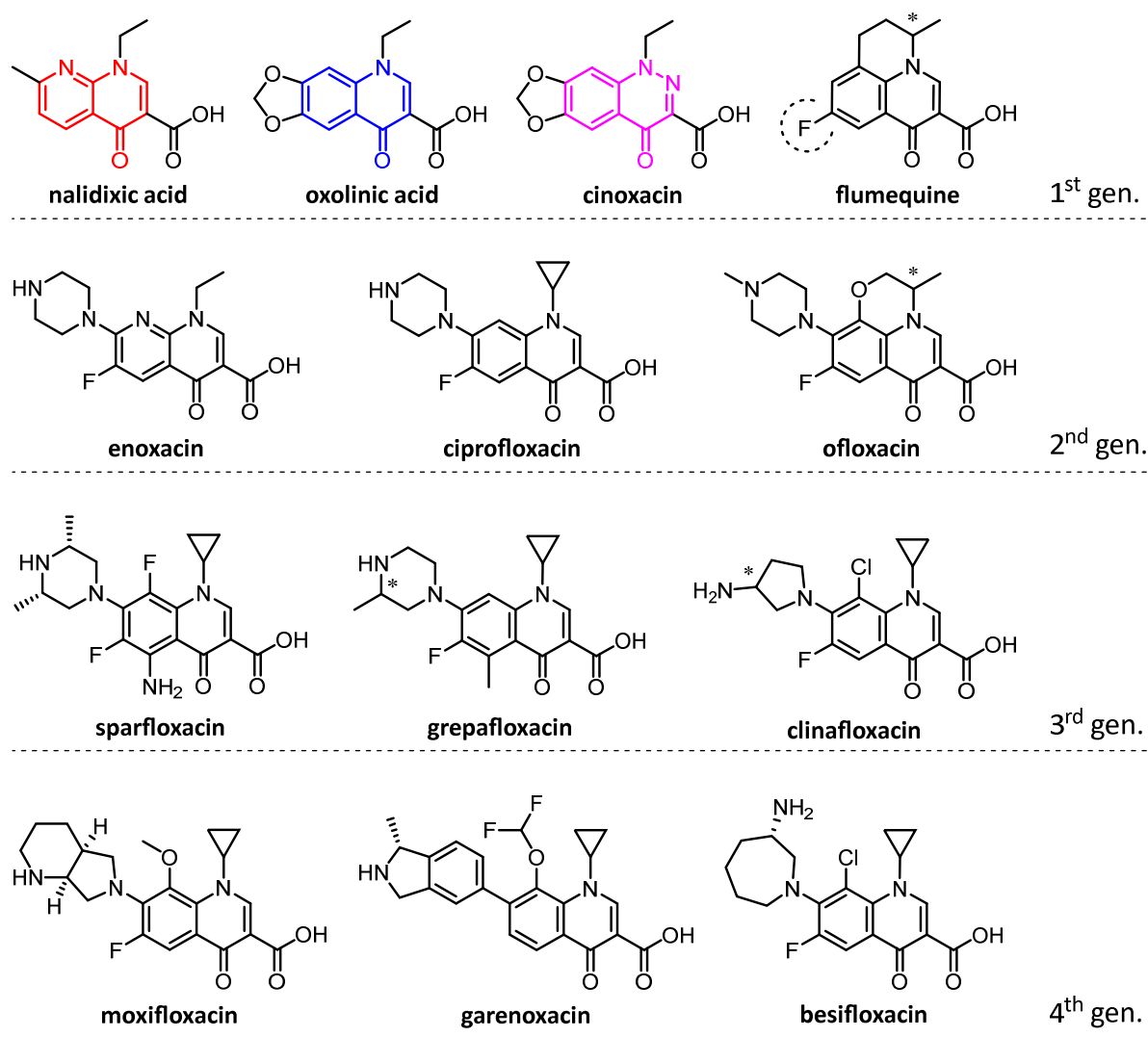


Figure 5. Structures of selected quinolone antibiotics.

Examples are shown for first-, second-, third-, and fourth-generation quinolone antibiotics. Classification might vary depending on the choice of reference.^[147] Apart from the quinolone ring (blue), core structures contain a naphthyridinone (red) and a cinnolinone (purple). The fluorine substituent eponymous to the fluoroquinolones is highlighted with a dotted circle in the structure of flumequine.

secondary adverse effects. The fluorine residue is crucial for the improved activity of fluoroquinolones over previous generations but is associated with genotoxicity.

Due to their over- and misuse, bacteria are increasingly becoming resistant to fluoroquinolone antibiotics. The mode of resistance involves genetic mutations and plasmid gene uptake that modify the drug targets, deactivate the drug, or reduce intracellular drug concentration by either decreased uptake or increased efflux. More than 90% of genetic mutations change the target enzymes' active site serine residues, resulting in reduced quinolone binding.^[65,148,149] Rising levels of *E. coli* resistance to fluoroquinolones have led to their replacement by third-

generation cephalosporins as the preferred drug in the treatment of UTIs.^[150] However, they are still the prevailing therapeutics against typhoid fever caused by *Salmonella* because of emerging resistance to previous first-line agents, such as ampicillin, chloramphenicol, and co-trimoxazole.^[151,152] Apart from resistant bacteria, the clinical application of fluoroquinolones is also threatened by its potential toxicity for children (arthralgia)^[153], elderly people (aortic rupture)^[154], and pregnant and breastfeeding women (teratogenic and mutagenic).^[155] The FDA has released several ‘black box’ warnings for fluoroquinolones on the risk of tendinitis, mental health issues, and hypoglycemia, among other things.^[156]

1.3.3 Other Small-Molecule Gyrase Inhibitors

Cyclothialidines

In 1992, the Swiss pharmaceutical company Hoffman-La Roche reported the cyclic peptide antibiotic cyclothialidine (Figure 6) as a new antibacterial lead structure from *Streptomyces filipinensis* after screening over 20,000 culture broths for gyrase inhibition in *E. coli*. Cyclothialidine's gyrase inhibitory activity turned out to be double that of novobiocin and considerably higher than that of ciprofloxacin (29-fold).^[104,157,158] Like the classical aminocoumarins, cyclothialidine is a competitive inhibitor of the ATPase activity in the GyrB subunit. Notably, the lack of cross-resistance to aminocoumarins is indicative of different microenvironments for the ATP binding sites. Cyclothialidine's selectivity for bacterial gyrase versus mammalian type II topoisomerase is remarkable (63,000-fold) when compared to novobiocin (6,700-fold) and particularly to ciprofloxacin (70-fold).^[159] However, owing to insufficient penetration of the lipophilic cytoplasmic cell membrane, natural cyclothialidines hardly display any activity against intact bacterial cells. The lead optimization efforts were initially hampered by up to 96% plasma protein binding, high clearance due to glucuronidation of a key phenol moiety, and poor aqueous solubility. After years of SAR studies, Roche scientists came up with structurally simplified analogs with minimum inhibitory concentrations (MICs) below that of novobiocin against various Gram-positive pathogens. As depicted in Figure 6, one compound showed very good efficacy against *S. aureus* in animal infection models.^[160,161]

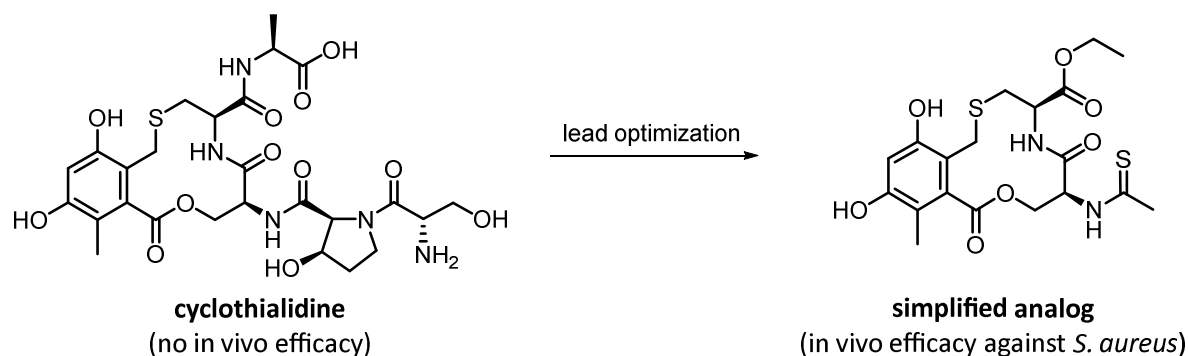


Figure 6. Structures of natural cyclothialidine and an improved synthetic analog.

Catechin-based polyphenols

Catechin-based polyphenols are ubiquitous flavonoids in green tea (*Camellia sinensis*) and other tea plants. They have been part of the human nutritional and medicinal regime for millennia and display versatile biological activities.^[162] Among other things, they are associated with antioxidant^[163], anticarcinogenic^[164], anti-inflammatory^[165], and antimicrobial properties.^[166] A regular cup of green tea contains more than 200 mg of catechin-based flavonoids, including (–)-epigallocatechin-3-gallate (EGCG, 40–60%), (–)-epicatechin-3-gallate (10–20%), (–)-epigallocatechin (10–20%), and (–)-epicatechin (4–6%) (Figure 1).^[167] Direct and indirect antimicrobial effects of catechins include damage to the bacterial cell membrane^[168], inhibition of fatty acid synthesis^[169], inhibition of enzyme activity^[170], and inhibition of inflammation triggered by oxidative stress.^[171]

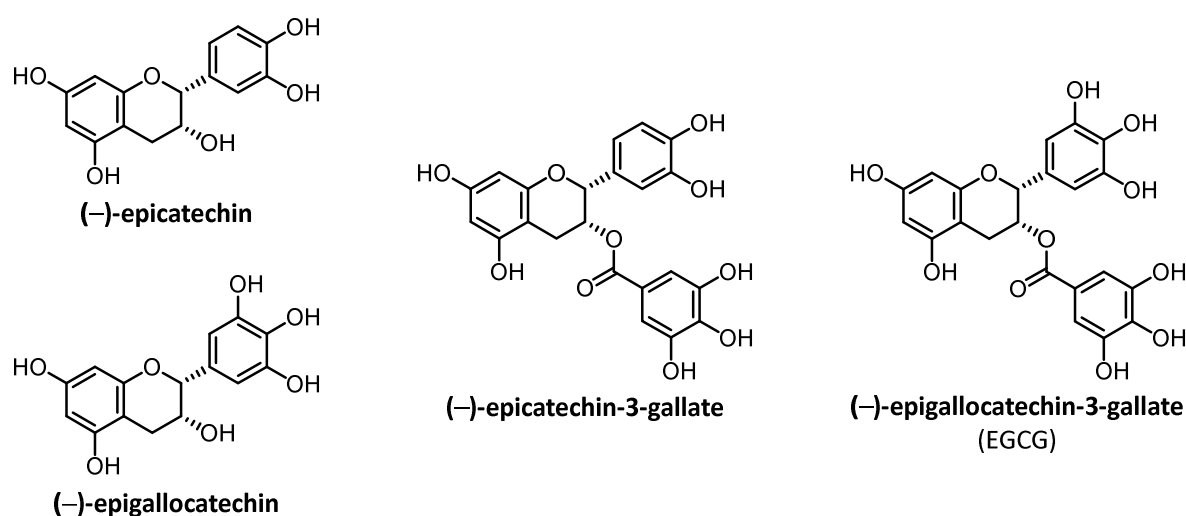


Figure 7. Structures of catechin-based polyphenols found in green tea.

High concentrations of EGCG may be cytotoxic and trigger genotoxic events in mammalian cells. It has been demonstrated that green tea catechins can act synergistically with commonly employed antibiotics. These liaisons include tetracycline against *S. aureus* and *S. epidermidis*^[172], penicillin, oxacillin, ampicillin/sulbactam, and imipenem against MRSA^[173], and chloramphenicol, ciprofloxacin, and cefotaxime against *E. coli*.^[174] In 2007, studies by GRADIŠAR *et al.* have confirmed the biological activity of some green tea catechins on DNA gyrase. The most active substance was found to be EGCG with a MIC of 10 μM for *E. coli* and an estimated IC_{50} of 50 μM in the gyrase supercoiling inhibition assay. Like the aminocoumarins, the mode of action was shown to involve blocking the ATP binding site of the GyrB subunit.^[167]

1.4 Albicidin

1.4.1 General Introduction

The bacterial genus *Xanthomonas* has caused crop failures in sugarcane, rice, soybean, cotton, wheat, and citrus species for many decades.^[176] The xylem-invading, Gram-negative species *Xanthomonas albilineans* (*X. albilineans*) is the causal organism of leaf scald disease in sugarcane, which is an economically important natural resource primarily used to produce sugar, rum, and bioethanol.^[175,177,178] In the early 1980s, Australian scientists ROBERT G. BIRCH and SURESH S. PATIL showed that chlorosis-inducing isolates of *X. albilineans* produce a mixture of antibacterial compounds in culture. The principal component of this mixture was isolated by high-performance liquid chromatography (HPLC) and given the trivial name albicidin. The phytotoxin was shown to block chloroplast differentiation, resulting in narrow white stripes and necrosis of infected leaves, ultimately killing the plant (Figure 8).^[179–181] production was suspected to play a dual role for *X. albilineans*, namely protection against secondary bacterial invaders and immobilization of the plant's defense response during the systemic invasion by the bacterium.^[182–184]



Figure 8. Necrotic symptoms of leaf scald disease on sugarcane leaves.

Infected sugarcane leaves show chlorotic white stripes after contamination by *X. albilineans*. Adapted from Daugrois *et al.*^[175]

Although the structure of albicidin was unknown at that time, the biological and chemical properties, which were distinct from any other known antibiotic classes, already drew attention to its potential medical application. Albicidin is rapidly bactericidal with low MIC values to a wide range of Gram-negative and Gram-positive bacteria, including clinically important species, such as *E. coli* ($0.063 \mu\text{g}\cdot\text{mL}^{-1}$), *A. baumannii* ($2.0 \mu\text{g}\cdot\text{mL}^{-1}$), *P. aeruginosa* ($1.0 \mu\text{g}\cdot\text{mL}^{-1}$), *E. faecium* ($2.0 \mu\text{g}\cdot\text{mL}^{-1}$) and *S. aureus* ($2.0 \mu\text{g}\cdot\text{mL}^{-1}$).^[184,185] It does not affect cultured mammalian cells at a concentration of $10 \mu\text{M}$ but interferes with DNA replication, transcription, and gene regulation by inhibiting the supercoiling activity of DNA gyrase from *E. coli* with an IC_{50} of $\sim 40 \text{ nM}$.^[186] While this value is broadly similar to that of other important gyrase inhibitors, such as ciprofloxacin ($\sim 700 \text{ nM}$) and novobiocin ($\sim 250 \text{ nM}$)^[108], albicidin's unusual structure and unique mode of action qualify it as a promising lead compound in the search for a new class of antibiotic drug.

The following subchapters will provide insights into albicidin's unusual structure, model of biosynthesis, proposed mode of action, and known resistance mechanisms. This will be followed by a summary of its first total synthesis, pharmacological challenges, and previous SAR studies. Finally, two structurally related classes of antibiotics, the cystobactamids and coralmycins, will be briefly introduced and compared to albicidin.

1.4.2 Structure Elucidation and Biosynthesis

Structure elucidation

The preliminary characterization of albicidin in 1985 by proton and ^{13}C nuclear magnetic resonance (NMR) spectroscopy and mass spectrometry (MS) had already suggested a phenolic acid-containing oligoaromatic composition with a molecular weight of approximately 842 Da. Yet, the full chemical structure remained hidden for another 30 years. Structural analysis was impeded by the extremely low production rate of 0.2 mg of purified compound per liter of culture in its slow-growing host organism *X. albilineans*. A 30-fold increase in the production rate was achieved in 1998 by using a chemically defined medium (SMG3) instead of a sucrose peptone medium.^[187] Nitrogen regulation of albicidin biosynthesis played a key role and antibiotic production was found to be the highest when only the required amino acids methionine and glutamic acid were added to the medium. Despite this progress, the amounts of albicidin obtained still did not suffice to allow full chemical characterization by NMR

spectroscopy. The assignment of albicidin's biosynthetic gene cluster by ROYER *et al.* in 2004 paved the way for the heterologous production in the fast-growing host bacterium *Xanthomonas axonopodis* pv. *vesicatoria*.^[177,188] Not only did this approach result in sixfold higher yield but the new system was readily modifiable by genetic engineering because the biosynthetic genes were cloned in plasmids. Finally, enhanced heterologous production and a revised purification protocol by preparative HPLC yielded quantities of albicidin large enough to allow structure elucidation by COCIANCICH *et al.* in 2014.^[189] Employing high-resolution MS (HR-MS) and 1- and 2D-NMR spectroscopy, the structure was shown to be composed of a non-proteogenic α -amino acid β -cyano-L-alanine at its center (L-Cya, building block C), which is surrounded by two *para*-aminobenzoic acids (*p*ABA-1 and *p*ABA-2, building blocks B and D). The C-terminal dipeptide consists of two *para*-amino-2-hydroxy-3-methoxybenzoic acids (*p*AHMBA-1 and *p*AHMBA-2, building blocks E and F). The N-terminus is acylated with (*E*)-3-(4-hydroxyphenyl)-2-methylacrylic acid, which equals a *para*-coumaric acid bearing a methyl group at the C=C double bond (MCA, building block A) (Figure 9). Albicidin's molecular formula $C_{44}H_{38}O_{12}N_6$ was revealed by HPLC-HR-Orbitrap electrospray ionization-MS (ESI-MS) analysis and corresponds to a molecular weight of 842.80 Da.

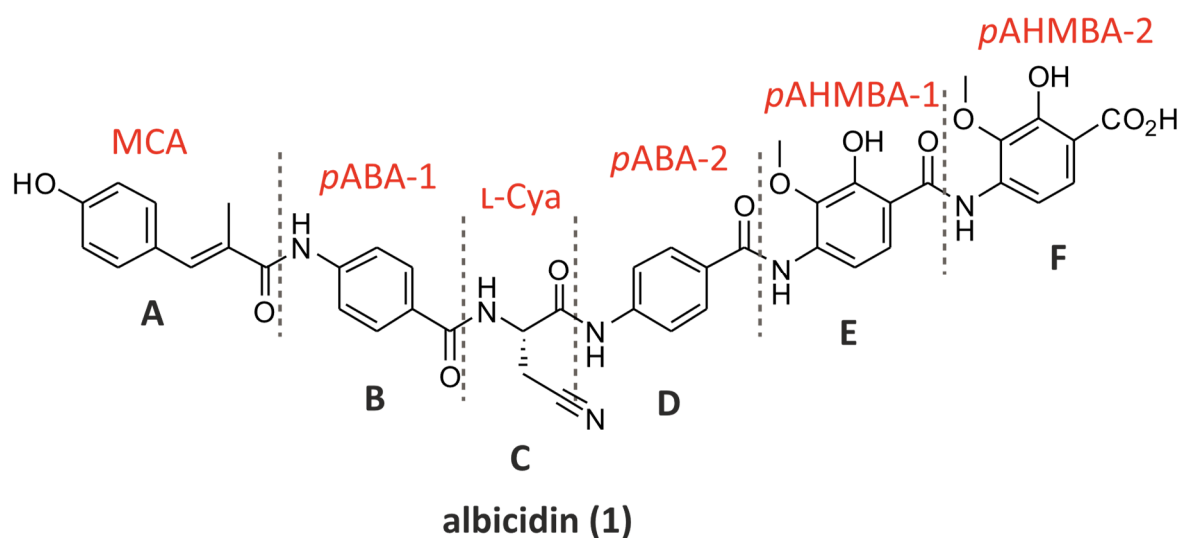


Figure 9. Structure of the polyketide and peptide antibiotic albicidin (1).

For unambiguous referencing, the N-terminal cinnamoyl moiety and the individual amino acids of the pentapeptide are assigned letters from A to F. Abbreviations for the systematic names of the individual fragments are highlighted in red.

A comparison of the HR-ESI-(+)-Orbitrap-MS/MS fragment spectra of ^{15}N -labeled and unlabeled albicidin unveiled its peptide backbone, the presence of six nitrogen atoms, and the

chemical formulae for the individual fragments. The sixth nitrogen atom was assigned to the nitrile group of the L-Cya building block by ^1H - ^{15}N heteronuclear multiple bond coherence (HMBC). The configuration of albicidin's only stereocenter was determined by chiral gas chromatography-MS (GC-MS) analysis. The correct order of the individual building blocks A-F was unambiguously confirmed by ^1H - ^{13}C HMBC and ^1H - ^1H Nuclear Overhauser Effect Spectroscopy (NOESY). The elucidation of albicidin's structure facilitated further studies regarding its biosynthesis and chemical synthesis.

Proposed model of biosynthesis

In addition to the information obtained on the gene cluster, the structure of albicidin was of great importance to put together the puzzle of its biosynthesis. According to the proposed model, the phytotoxin **1** is produced by a complex polyketide synthase/nonribosomal peptide synthetase (PKS-NRPS) biosynthetic machinery encoded by three gene clusters: XALB1, XALB2, and XALB3. The XALB1 cluster is 48,131 base pairs large and consists of 20 genes, which encode a variety of important functional products. These include the hybrid PKS-NRPS assembly line, NRPS and PKS associated proteins, enzymes responsible for precursor synthesis, an esterase, an albicidin transporter, gene regulation, resistance genes, and tailoring enzymes. The XALB2 and XALB3 gene clusters each encode one open reading frame (ORF), a phosphopantetheinyl transferase, and the heat shock protein HtpG.^[177,190–192]

The proposed formation of albicidin begins with the synthesis of the N-terminal MCA building block by the coordinated action of the three PKS modules (PKS-1-3) of *Alb01* (Figure 10, A) First, the MCA precursor molecule *para*-hydroxybenzoic acid (*p*HBA) is converted into the corresponding coenzyme A (CoA) ester *p*HBA-CoA by acyl-CoA ligase (AL) and loaded onto the first acyl carrier protein (ACP). Then, ketosynthase (KS) catalyzes the chain-elongation reaction of the ACP-bound substrate with an acyl extender unit (malonyl-CoA) provided by the *trans*-acting acyltransferase (AT) of *Alb13*. Subsequently, the introduction of the C–C double bond is achieved by the concerted action of dehydrogenase (DH) and ketoreductase (KR). Finally, a methyl transferase (MT) uses (*S*)-adenosyl methionine (SAM) to introduce a methyl group in the α -position of the preformed coumaric acid.

The assembly of the nonribosomal peptide (NRP) proceeds via the multienzyme thiotemplate mechanism.^[193,194] The collinearity rule predicts that five NRPS modules are needed for the

construction of the pentapeptide.^[195] A previously unknown A domain signature for the recognition of *pABA* building blocks represents an exceptional feature of albicidin biosynthesis. After being recognized and activated by the adenylation (A) domain of NRPS-1, *pABA*-1 (building block B) is loaded onto the downstream thiolation (T) domain. The 4'-phosphopantetheine prosthetic group of the holo-T1 domain serves as a swinging arm and delivers the tethered amino acid to the condensation (C) domain, where it undergoes peptide coupling to the upstream T0-bound MCA (building block A). The following incorporation of the central amino acid L-Cya (building block C) was expected to be carried out by the A domain of NRPS-2. However, neither L-Cya nor its precursor molecule L-Asn were activated by NRPS-2 in a radioactive ATP-PP_i exchange assay. Instead, L-Asn becomes activated by the single-standing and *trans*-acting module NRPS-2* of *Alb04* and stored as a thioester at the T2* domain. The formal dehydration of the L-Asn side chain through a phosphorylation and dephosphorylation sequence is mediated by a hitherto unknown type of dehydratase domain. The resulting T2*-bound L-Cya is then delivered to the T2 domain of the main assembly line by transthioation involving the shuttle protein *Alb11*.^[196]

The coupling of *pABA*-2 (building block D) by the NRPS-3 module proceeds analogously to the action of NRPS-1. Finally, *pAHMBA*-1 (building block E) and *pAHMBA*-2 (building block F) are incorporated by the performance of NRPS-4 and NRPS-5 of *Alb09*, respectively. The latter module additionally harbors the thioesterase (TE) domain responsible for the release of the final product **1**. Radioactivity-based substrate specificity assays revealed that 2- and 3-hydroxy-*pABA* (*pAHBA*) are the preferred substrates of NRPS-4 and NRPS-5 rather than *pAHMBA*. Therefore, it was proposed that hydroxylation of *pABA* by the benzoyl-CoA oxygenase-like enzyme *Alb12* occurs before recognition by the A domain of NRPS-4. The following methylation and hydroxylation of T4- or T5-bound *pAHBA* by the methyltransferase *Alb02* and the alleged hydroxylase *Alb08* leads to the formation of *pAHMBA*.^[197] The biosynthetic pathways of both the MCA precursor *pHBA*-CoA and the δ -amino acids *pABA* and *pAHMBAs* are believed to start from chorismate (Figure 10, B). Two possible ways have been contemplated for the delivery of *pABA*: either by the cluster-intrinsic genes *Alb17* and *Alb18* or by their respective homologs from primary metabolism (*pabAB* and *pabC*).^[198]

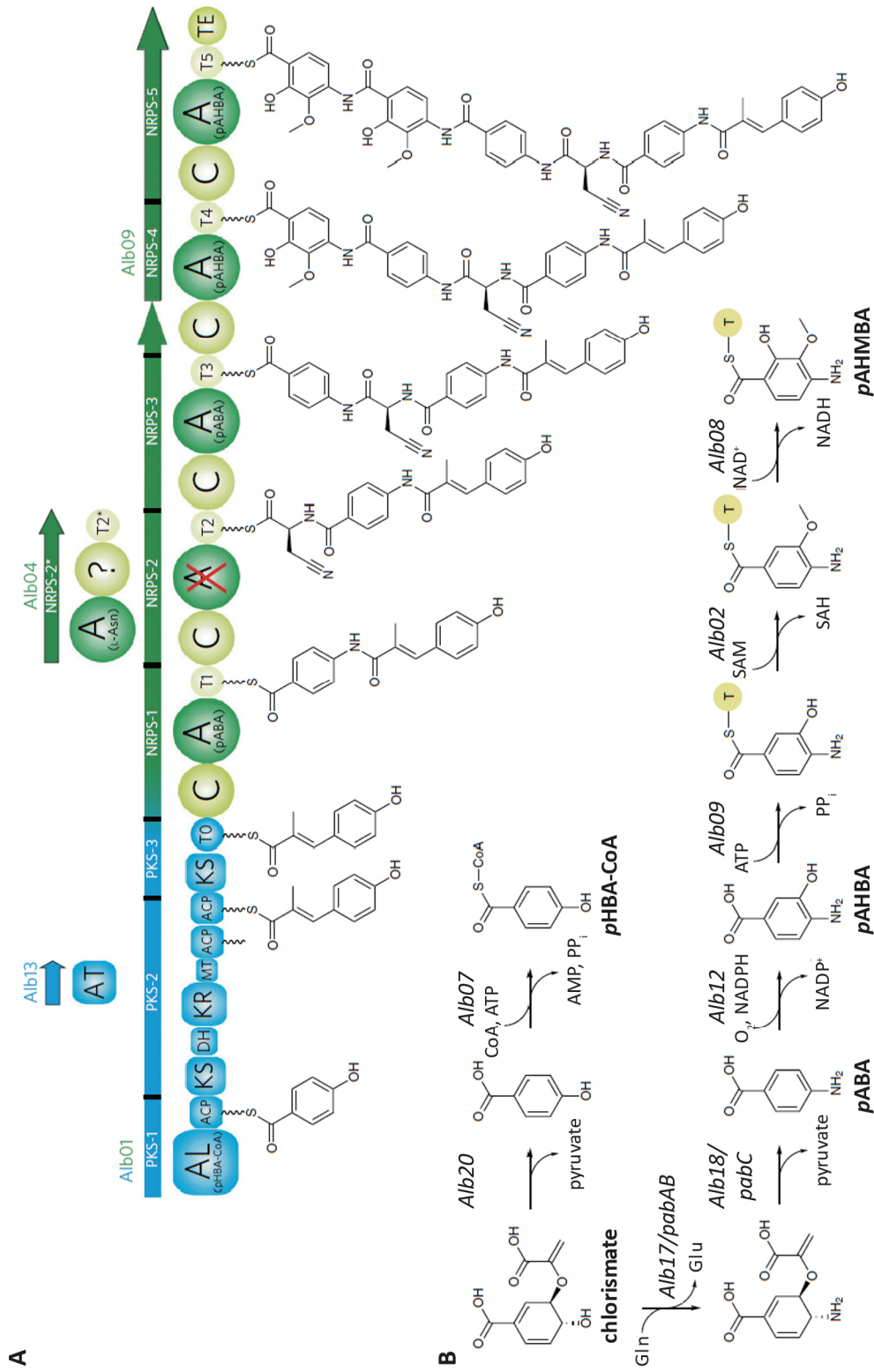


Figure 10. Proposed model of albicidin biosynthesis.

(A) The albicidin hybrid biosynthetic machinery comprises three PKS (blue) and five NRPS (green) modules jointly harboring the following domains: acyl-CoA ligase (AL), acyl carrier protein (ACP), ketosynthase (KS), acyltransferase (AT) dehydrogenase (DH), ketoreductase (KR), methyltransferase (MT), thiolation (T), condensation (C), adenylation (A) and thioesterase (TE). (B) Putative biosynthetic pathways for pHBA-CoA and pAHMBA starting from chlorismate. Adapted from Cociancich *et al.* with permission from the authors.^[186]

1.4.3 Primary Uptake and Mode of Action

Primary uptake by Tsx

The outer membranes of Gram-negative bacteria serve as a major permeability barrier against hydrophilic substances and potentially toxic chemicals, such as antibiotics.^[199–201] Various mechanisms of transport that enable nutrients and waste products to cross the outer membrane have been reported in the literature.^[202,203] For example, iron-chelator complexes (siderophores) and vitamin B₁₂ exploit highly specific receptor proteins as well as the energy-coupling function of TonB to be delivered to the periplasm.^[204–206] Non-specific porins, such as OmpC, OmpF, and PhoE, which are permanently open, water-filled, and do not bind their substrates. They are responsible for the TonB-independent, passive transport of various molecules into the cell. The flux of larger molecules (>600 Da) is restricted by the small pore diameter of these porins.^[207–210] At low external substrate concentrations, certain compounds depend on the active transport by substrate-specific channels operating independently of TonB, e.g. maltoporins (LamB)^[211,212] and sucrose porins (ScrY).^[213,214] As for the non-specific porins, transport occurs along a concentration gradient and does not require energy. However, in this case, it is accelerated by saturable substrate-specific binding. These channels are of great physiological significance for bacteria in low nutrient environments when uptake by general porins is insufficient.^[215,216]

Another example for a substrate-specific channel is the protein Tsx found in *E. coli*. Initially recognized as a receptor for the bacteriocin colicin K and the bacteriophage T6,^[217] the Tsx channel was later found to play an important role in the active uptake of all nucleosides and deoxynucleosides at concentrations below 1 μM except for cytidine and deoxycytidine.^[218,219] Also, it does not transport free bases and phosphorylated analogs of deoxynucleosides.^[220,221] Forming a 12-stranded β -barrel, the 272-residue Tsx protein is the smallest known channel-forming outer-membrane protein.^[221–223] The narrow and long, keyhole-shaped central pore contains aromatic residues on its inner wall – known as the 'greasy slide'.^[214,224] Its substrate specificity derives from a saturable, stereospecific ligand-binding site inside the channel. In addition to its role as a nutrient scavenger, the Tsx gateway makes *E. coli* susceptible to intrusion by harmful substances. Since albicidin is toxic to *E. coli* at a very low concentration, the Tsx protein is believed to contain a specific binding site for the aromatic peptide. Studies by Birch *et al.* have shown that albicidin-resistant strains of *E. coli* are resistant to

bacteriophage T6 as well, suggesting that active transport of albicidin via the Tsx-channel is the primary route of uptake at low concentrations of the antibiotic in the extracellular space.^[225]

The proposed mode of action

As mentioned previously, albicidin is a potent antibiotic that inhibits the supercoiling activity of bacterial and plant organellar DNA gyrase much more efficiently than other successful gyrase-inhibiting small molecules. The investigation of its full mode of action is the subject of ongoing research but preliminary findings point towards an entirely new mechanism of gyrase inhibition. Although DNA synthesis inhibition was identified as the primary mode of action by Birch *et al.*^[180], gyrase was initially dismissed as the molecular target of albicidin because no cross-resistance between the antibiotic and known inhibitors of GyrA (nalidixic acid) and GyrB (novobiocin, coumermycin A₁) was observed. However, direct binding of albicidin to DNA was ruled out as well, as mixing the antibiotic with *E. coli* did not change the thermal denaturation behavior of DNA or the absorption spectrum of the phytotoxin.^[180] In 2007 and 2008, HASHIMI *et al.* have conducted a series of experiments with albicidin and purified enzymes from wild-type *E. coli* and the plant *Arabidopsis thaliana* (*A. thaliana*) to investigate the compound's mode of action in more detail.^[184,226] Albicidin showed cross-resistance to *E. coli* strains harboring mutations associated with quinolone (GyrA S83L) and CcdB (GyrA R462C) resistance, suggesting a similar mode of action. Like quinolones, albicidin was found to target the GyrA subunit and stabilize the covalent DNA-gyrase complex, albeit with distinctive mechanistic features on a molecular level. While quinolones rapidly stabilize the gyrase-DNA cleavage complex in an ATP-independent fashion, albicidin requires the presence of ATP to efficiently do the same.

It was confirmed that albicidin's ability to stabilize the cleavage complex dramatically increases for relaxed (100-fold) or supercoiled (1000-fold) DNA in the presence of ATP. Increased activity was observed to a lesser extent also in the presence of the non-hydrolyzable ATP derivative 5'-adenylyl- β,γ -imidodiphosphate (ADPNP). Besides inhibiting the ATP-dependent DNA supercoiling activity of gyrase (IC₅₀ \approx 40 nM), albicidin was shown to inhibit ATP-dependent relaxation and decatenation of TopoIV (IC₅₀ \approx 300 nM) as well. However, it did not affect the ATPase activity of the GyrB subunit. This ATP-dependent mechanism of gyrase poisoning is reminiscent of how the plasmid-encoded proteinaceous toxins CcdB

(11.7 kDa)^[103,227] and microcin B17 (3.1 kDa)^[228,229] are suspected to act on gyrase. Remarkably, despite the size difference between albicidin (842 kDa) and the two toxins, gyrase activity is inhibited much faster by the former. Thus, albicidin can perhaps be viewed as an efficient small-molecule emulator of the toxins, which further spurs its potential as a clinical drug candidate.

1.4.4 Mechanisms of Resistance

To date, six resistance factors have been discovered for albicidin, which will be discussed in more detail in this chapter. These include mutations in *tsx* blocking the uptake of albicidin, self-protection of *X. albilineans* by the efflux pump AlbF and the DNA imitator AlbG, enzymatic hydrolysis of the peptide by the endopeptidase AlbD, and non-enzymatic trapping of the molecule by the binding proteins AlbA and AlbB. The path to develop a clinical candidate requires an optimized drug design guided by extensive structure-activity relationship studies, which will also require a deeper mechanistic understanding of these resistance processes.

Reduced albicidin uptake by mutations in tsx

Since efficient albicidin uptake depends on the presence of Tsx proteins, mutations in the *tsx* gene can induce resistance to albicidin. *E. coli* strains carrying insertion mutations that obstruct Tsx production have been shown to display a 100-fold increase in albicidin resistance.^[225] In 1993, FSIHI *et al.* isolated 38 albicidin-resistant *tsx* mutants that produced the full amount of Tsx but with defects in their channel properties. Characterization of each mutant by DNA sequence analysis exposed seven alleles, containing six different point mutations and one 39-base pair duplication. These mutations also resulted in the reduced deoxynucleoside-specific activity of Tsx. To rule out a complete collapse of the Tsx channel because of the mutations, the preserved ability of the mutant protein to operate as a non-specific porin was confirmed in strains lacking OmpC and OmpF using ¹⁴C-labeled serine as substrate.^[219]

Self-protection of X. albilineans with AlbF and AlbG

The discovery of albicidin as a potent bactericide had already prompted questions regarding the self-preservation of its original producer *X. albilineans*, which has developed a multi-faceted toolset to protect itself against the antibiotic. The first line of defense involves the highly regulated biosynthesis of albicidin itself. Besides, two gene sequences were found in

the biosynthetic gene cluster that cause resistance to albicidin by encoding the proteins AlbF and AlbG.^[177] First described by BOSTOCK *et al.* in 2006, the ATP binding cassette (ABC) transporter protein AlbF is a single-component antibiotic efflux pump that confers a high level of resistance specifically to albicidin. Remarkably, low-level heterologous expression of the cloned *albF* gene in *E. coli* has resulted in a 3000-fold higher resistance to albicidin without affecting the rapid uptake of the antibiotic through the Tsx channel.^[230] The other protein associated with self-protection is the DNA-mimicking pentapeptide repeat protein AlbG, which resembles quinolone resistance proteins Qnr^[231] and MfpA^[232,233] and competes with DNA for binding to gyrase, thus interfering with the mode of action of albicidin. AlbG was shown to convey a 30-fold increased resistance to albicidin when expressed in *E. coli*. It also inhibits the supercoiling activity of *E. coli* gyrase, albeit at high concentrations.^[184]

Enzymatic cleavage of albicidin by AlbD

During the search for a biocontrol agent for leaf scald disease in sugarcane, ZHANG and BIRCH discovered a gene (*albD*) in the bacterium *Pantoea dispersa* (*P. dispersa*) that is capable of efficient and irreversible detoxification of albicidin.^[234,235] AlbD was found to code for a 235-amino acid protein (AlbD) with a central Gly-Xaa-Ser-Xaa-Gly motif that is conserved in serine hydrolases. The purified AlbD protein displayed strong esterase activity on *para*-nitrophenyl butyrate as a substrate. Hydrolysis of the butyrate and inactivation of albicidin progressed in the absence of cofactors and both processes were strongly inhibited by the serine protease inhibitor phenylmethylsulfonyl fluoride (PMSF). In the light of these findings and with little knowledge of the chemical structure of albicidin, the authors incorrectly classified AlbD as an esterase.^[182] Strains of *X. albilineans* inoculated with *albD* did not evoke disease symptoms in sugarcane.^[181] Later, it was shown that the expression of *albD* in transgenic sugarcane plants suppressed chlorotic disease symptoms as well.^[236]

The structure elucidation and total synthesis of albicidin enabled unraveling the exact mechanism of resistance conferred by AlbD. In 2015, VIEWEG *et al.* demonstrated that recombinantly expressed and purified AlbD eliminates the antibacterial activity of synthetic albicidin in agar diffusion assays with *E. coli*.^[237] Analysis of the enzymatic cleavage products by HPLC-HR-ESI-(+)-Orbitrap-MS revealed two biologically inactive fragments resulting from hydrolysis of the amide bond between building blocks D (*p*ABA-2) and E (*p*AHMBA-1). It was therefore proposed that AlbD belongs to the class of endopeptidases, rather than esterases,

with a hitherto unprecedented capacity to hydrolyze peptide bonds between aromatic δ -amino acids. Following the high homology of AlbD to the family of serine endopeptidases, the active site catalytical triad of AlbD was shown to be composed of a serine (Ser₁₀₅), histidine (His₂₀₀), and an aspartic acid (Asp₁₆₉).

Subsequent incubation of truncated albicidin derivatives with AlbD exposed tripeptides *p*ABA-*p*AHMBA-1-*p*AHMBA-2 (D-E-F) and L-Cya-*p*ABA-*p*AHMBA-1 (C-D-E) as the enzyme's minimal cleavage motif. While the presence of a negative charge at the C-terminus hardly affected the cleavage efficiency of AlbD, molecular recognition was hampered by the presence of a positive charge at the N-terminus of the C-D-E tripeptide. The increased stability towards AlbD displayed by *ent*-albicidin (D-Cya as building block C) highlights the importance of the configuration at the stereocenter for efficient substrate cleavage. Short-length analogs of albicidin lacking either MCA (building block A) or both MCA and *p*ABA-1 (building block B) were found to be better substrates for the enzyme than albicidin itself, suggesting that the antibiotic might not be the natural substrate of AlbD.

Non-enzymatic trapping of albicidin by AlbA and AlbB

In addition to albicidin resistance conferred by enzymatic and irreversible cleavage by AlbD, non-enzymatic and reversible suppression of the antibiotic by the binding proteins AlbA and AlbB have been described. AlbA was first isolated by WALKER *et al.* in 1988 from *Klebsiella oxytoca* (*K. oxytoca*).^[238] Expression of the cloned *albA* resistance gene in *E. coli* effectively inactivated albicidin without blocking its uptake through the Tsx channel. The 25 kDa-protein was shown to trap its substrate with high affinity and selectivity.^[239] The reversible nature of the non-covalent binding interaction was demonstrated by heating the albicidin-AlbA complex at 100 °C for 30 min, which released the active antibiotic again, probably due to the denaturation of the protein. It was also shown that the binding affinity of AlbA, decreased by approximately 30% when the pH of the medium was lowered from 6 to 4. This was indicative of side-chain ionization of histidine (pKa = 6.0), which was further supported by stoichiometric analysis and site-directed mutagenesis of AlbA conducted by WENG *et al.*^[240] The authors identified His₁₂₅ as an essential residue for substrate binding and in later studies also detected a putative role of Lys₁₀₆, Trp₁₁₀, Tyr₁₁₃, Leu₁₁₄, Tyr₁₂₆, Pro₁₃₄, and Trp₁₆₂ in forming an albicidin binding pocket.^[241] Besides, the peptide sequence of AlbA was shown to have a 25% similarity

to the DNA binding motif of the transcriptional regulator proteins NifA and NtrC from *K. pneumoniae*.

Another albicidin-binding protein, AlbB, was isolated from *Alcaligenes denitrificans* (*A. denitrificans*) by BASNAYAKE *et al.* in 1995.^[242] As previously observed for *albA*, the *albB* gene conferred resistance to albicidin when expressed in *E. coli*, presumably without exerting catalytical inactivation of the antibiotic. A partial DNA sequence homology hinted towards an evolutionary relationship between the two distinct albicidin resistance genes from *K. oxytoca* and *A. denitrificans*. Based on an N-terminal amino acid homology, a conserved albicidin binding domain was hypothesized for both *albA* and *albB*.

Recently, a better understanding of the structure and binding mechanism of AlbA was provided by the work of ROSTOCK *et al.*, who have elucidated the crystal structure of the drug-binding domain of AlbA (AlbAS) in complex with albicidin.^[243] Far-ultraviolet (UV) circular dichroism (CD) spectroscopic analysis of AlbAS, both in the presence and absence of albicidin, underscored its α -helical secondary structure, which remained unaltered upon binding of albicidin.^[241] However, a significant rise in the melting temperature of AlbAS from 66 to 81 °C was observed as a result of ligand binding. Analysis of the ^1H - ^{15}N HSQC spectrum of ^{15}N -labeled AlbAS showed extensive line-broadening and signal overlap, which was credited to the internal dynamics of the protein. These effects were considerably reduced in the presence of albicidin, revealing a more rigid conformation of AlbAS in the substrate-bound state. Additionally, the binding strength between albicidin and AlbAS was determined. At first, the equilibrium dissociation constant (K_d) was estimated to be in the nM to μM range by performing ^1H - ^{15}N HSQC titration experiments. Due to the strong interaction, fluorescence quenching of AlbAS was monitored with increasing concentrations of albicidin to avoid ligand depletion effects. A K_d of 5.6 nM and a HILL coefficient (n) of 3.0 was determined, which underlined a high binding affinity of AlbAS towards albicidin and positive cooperativity, respectively.

A bioinformatic sequence similarity search suggested that AlbA and AlbB belong to the MerR family of transcriptional regulators^[238,242], whose members commonly activate a variety of MDR systems as a response to environmental stress.^[244] Prominent members of this family include BmrR from *Bacillus subtilis*^[245,246], SoxR from *E. coli*^[247], and the thiostrepton-induced

protein A (TipA) from *Streptomyces lividans*.^[248,249] AlbA displays high structural homology to the C-terminal thiopeptide-binding domain (TipAS) of TipA.^[250] Proteins belonging to the MerR family feature a highly conserved winged helix-turn-helix (HTH) DNA binding motif at the N-terminus. An alleged HTH motif that might be involved in DNA binding was found in AlbA and AlbB by bioinformatic analysis of the *K. oxytoca* and *A. denitrificans* genomes. Despite being distantly related in primary structure, AlbA and AlbB closely resemble each other in secondary structure according to structure predictions. A major difference between the two proteins is the isoelectric point (pI), which corresponds to a higher content of acidic residues for AlbA (15%, pI = 4.99) than AlbB (8%, pI = 10.15) and vice versa for basic residues.

The crystal structure of the albicidin-AlbAS complex revealed a pseudosymmetric tandem arrangement of an all- α -helical fold containing the N-terminal domain (NTD) and the C-terminal domain (CTD), which are connected by an elongated α -helical linker belonging to the CTD. Owing to decreased binding affinities towards albicidin compared to AlbAS, the truncated NTD and CTD constructs AlbAS_{NTD} and AlbAS_{CTD} no longer inactivated the antibiotic in agar diffusion assays with *E. coli*. AlbAS offers a predominately hydrophobic binding tunnel with the NTD and CTD encompassing the A-B-C and D-E-F fragments of albicidin, respectively. The aromatic side chain residues of F₁₆, W₂₇, W₁₃₃, and W₁₆₂ are involved in π -stacking to albicidin building blocks A, E, and F. At the same time, a salt bridge between the carboxylate of albicidin and R₁₈₁ of the CTD is believed to fix the molecule in a certain orientation. Albicidin adopts a V-shaped conformation in the binding tunnel, which is stabilized by several hydrogen bonds, especially between the side chain of N₇₅ and the amide bond nitrogen and oxygen atoms enclosing the central L-Cya building block. The capability of AlbAS to suppress the antibacterial effect of albicidin was significantly reduced when N₇₅, R₁₈₁, and Q₂₀₅ were replaced, suggesting an important role of these polar residues in ligand recognition.

The ability of AlbAS to capture albicidin derivatives was monitored by agar diffusion assays with *E. coli* and ¹H-¹⁵N HSQC spectroscopy, showing high ligand promiscuity concerning building blocks A and C. For example, the substitution of the N-terminal *para*-coumaric acid with a shorter *para*-hydroxybenzoic acid hardly impeded AlbA binding. Similarly, the replacement of the N-terminal phenolic hydroxy group with a fluorine atom was tolerated by AlbAS. The strong binding was also preserved when the central L-Cya building block was replaced by the sterically more demanding L-Thr. Since *ent*-albicidin was also arrested by

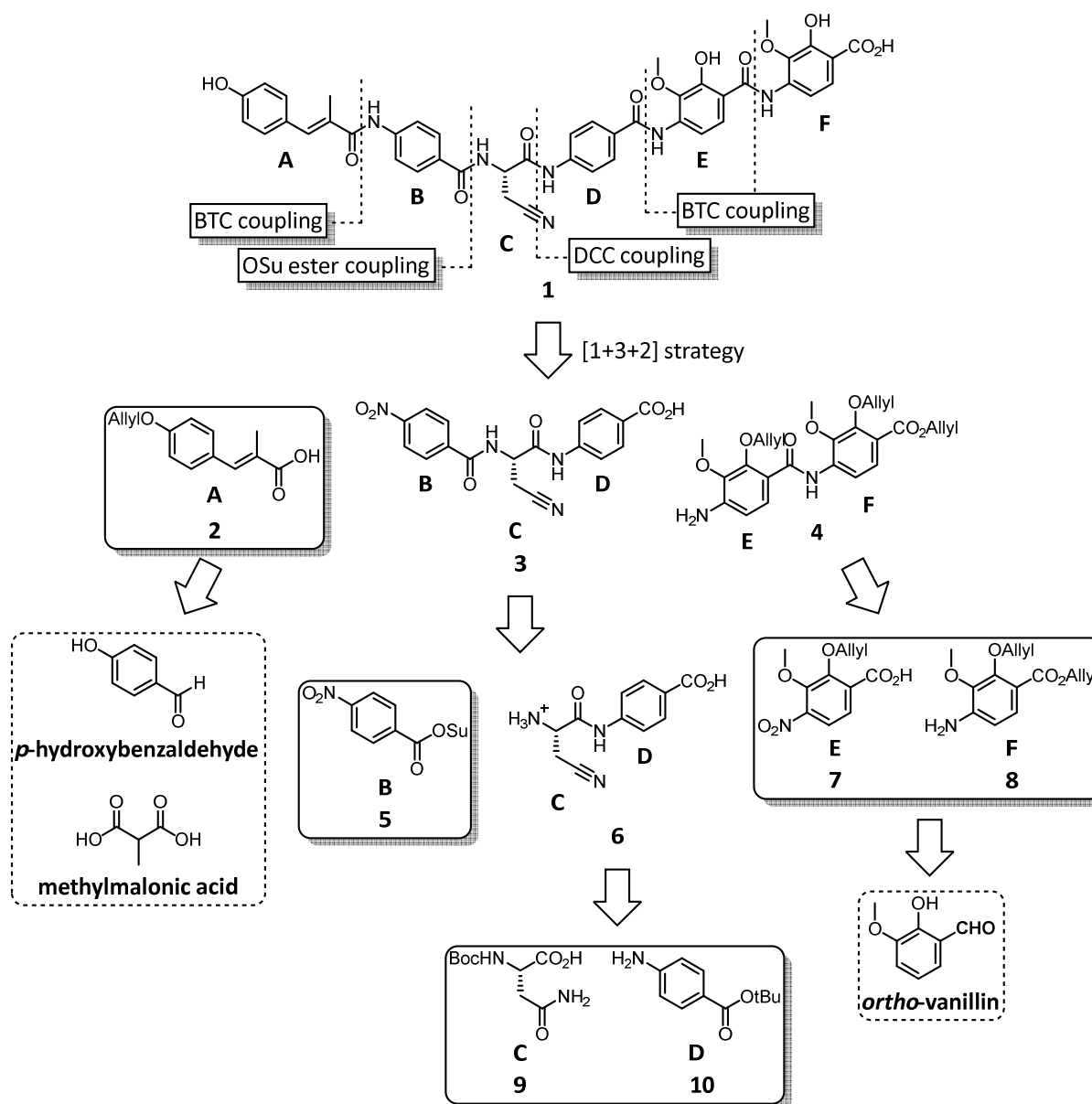
AlbAS, the stereochemistry of building block C was shown to be of minor importance for recognition, which underscores the fact that this moiety points into a void outside of the binding pocket. Finally, truncated albicidin derivatives consisting of either the A-B dipeptide, the D-E-F tripeptide, or the B-C-D-E tetrapeptide were employed to examine the binding contributions of the NTD and CTD. The findings support the alleged role of the CTD as an anchoring point for albicidin.

Initially believed to trap its substrate without catalyzing any chemical modification of the same, SIKANDAR and colleagues have recently claimed that AlbA promotes slow cyclisation of albicidin at the central Cya position to form a succinimide derivative that is 300-fold and 222-fold less active against *E. coli* and *S. aureus*, respectively.^[251]

1.4.5 Total synthesis

The increased amount of albicidin obtained by heterologous production had sufficed to conduct structural and biochemical analysis by HR-MS and NMR spectroscopy but had not satisfied the demand for proper bioactivity profiling and SAR studies. However, the above-mentioned findings on the structure of albicidin paved the way for the successful total synthesis, which was completed only months later by KRETZ *et al.*^[185,252] A [1+3+2]-coupling strategy was pursued to assemble albicidin (**1**). The three individual fragments obtained after the first retrosynthetic scission included the N-terminal hydroxycinnamate **2**, the central tripeptide **3**, and the C-terminal aromatic dipeptide **4**. The latter two fragments were further broken down into the individual building blocks **5** and **7–10** (Scheme 1).

Developing a feasible protecting group strategy posed one of the main challenges during the synthesis of albicidin. The nitrile group of the central amino acid was known to be readily hydrolyzed under basic conditions and the C–C double bond of the N-terminal coumaric acid was allegedly susceptible to reductive conditions, e.g., hydrogenolysis by H₂/Pd. Also, commonly used acid-labile groups, such as *tert*-butyl ethers and esters proved to be inefficient. Eventually, allyl protection of the hydroxy and carboxy moieties offered the most promising results. On the one hand, the introduction of the allyl groups to the precursor molecules **2**, **7**, and **8** proceeded under mild conditions and with high yields using K₂CO₃ and allyl bromide. On the other hand, the final deprotection step in the presence of Pd(PPh₃)₄ and



Scheme 1. Retrosynthetic strategy for the total synthesis of albicidin (1).

The [1+3+2]-approach for the assembly of albicidin's six building blocks A-F is depicted. An initial two-step fragmentation of the molecule gives compounds 2–4. The tripeptide 3 and the dipeptide 4 are further broken down into the mono building blocks 5, 9, 10 and 7–8, respectively.

phenylsilane allowed global cleavage of allyl esters and ethers to release the final product 1. Nitroarenes, as present in compounds 3, 5, and 7, served as masked anilines that could be reduced under very mild conditions using $\text{SnCl}_2 \cdot 2 \text{H}_2\text{O}$ without affecting the allyl protecting groups.

With a protecting group strategy in hand, synthetic pathways were outlined to prepare the individual fragments. Following literature protocols, the coumaric acid building block 2 was prepared in a KNOEVENAGEL-type reaction from 4-hydroxybenzaldehyde and methylmalonic

acid.^[253] The nitrile side chain of the central amino acid was formed by dehydration of Boc-Asn **9**. It has been known since the 1960s that side-chain unprotected Asn and Gln undergo dehydration during dicyclohexylcarbodiimide (DCC) or symmetric anhydride activation. These reactions usually proceed via cyclic isoimide intermediates that are highly prone to racemization.^[254–256] However, by using DCC in the absence of base and by fine-tuning the reaction conditions, an excellent enantiomeric excess ($ee = 98\%$) and a good yield of 64% could be obtained. Simultaneous removal of the acid-labile Boc and *t*Bu-ester protecting groups with HCl/dioxane (4 M) afforded the C-D dipeptide **6**, which was then coupled to the succinimide active ester **5** to build up the B-C-D tripeptide **3**. The C-terminal tetrasubstituted E-F dipeptide **4** was prepared from commercially available *ortho*-vanillin.^[257,258] Key reaction steps included aromatic nitration under standard conditions, the introduction of allyl groups, and the conversion of the benzaldehyde into the corresponding benzoic acid. Among the numerous oxidation methods available, the PINNICK oxidation was pursued because it met the criteria for mild reaction conditions and concomitant functional group tolerance to account for the vulnerability of the allyl group's C=C double bond.

Since **2** was found to considerably reduce the solubility of the peptide, the assembly of albicidin was started from the C-terminus. The intrinsically low nucleophilicity of anilines required activation of *p*-coumaric acid and *p*ABA derivatives by a strong coupling reagent to enable peptide bond formation. This was best accomplished by adopting a method established by JUNG *et al.* that employed bis(trichloromethyl) carbonate (BTC, triphosgene) for *in situ* acyl chloride formation.^[259,260] The triphosgene-mediated coupling of benzoic acid **7** and aniline **8** and subsequent reduction of the nitro group gave **4** in a combined yield of 72%. In the next step of the assembly, the same reaction sequence was used to couple the B-C-D tripeptide **3** to dipeptide **4** and once again reduce the nitro group to furnish the corresponding pentapeptide (not shown). Finally, after incorporating the N-terminal acyl moiety **2**, global allyl-deprotection afforded the desired product **1**. This first total synthesis of albicidin helped to confirm the previous structural assignment and enabled scalable and diversifiable synthesis to facilitate derivatization for subsequent SAR studies and lead optimization efforts.

In conformity with the values reported for the natural product, the IC₅₀ value for synthetic albicidin was approximately 40 nM. Notably, the antibacterial activity remained almost unchanged against ciprofloxacin-resistant (CIP-resistant) strains of *E. coli*. Besides, the

enantiomer of albicidin (*ent*-albicidin) was prepared and tested for both its gyrase-inhibiting capacity and antibacterial activity. Interestingly, both the IC₅₀ value and MIC values for a CIP-resistant *E. coli* strain remained unchanged, suggesting that the stereocenter of albicidin is of minor importance for its bioactivity. This was later investigated in more detail in SAR studies conducted to evaluate the role of building block C.

1.4.6 Previous SAR Studies

Despite its remarkable bioactivity, the physicochemical properties of albicidin need to be made more drug-like to achieve *in vivo* efficacy and meet the requirements for oral and parenteral administration. As for many other natural product-derived antibacterials, e.g. macrolides and glycopeptides, empirical rules to predict oral bioavailability of a compound, such as Lipinski's rule of five^[261], are of minor relevance.^[262] Albicidin's poor aqueous solubility, which is obvious by its hydrophobic structure and relatively high calculated partition coefficient between octanol and water (clogP = 5.2)^[263], is the most important property that needs to be enhanced by either structure optimization or an adequate formulation strategy, or both. The most common causes of low oral bioavailability are associated with poor solubility and low permeability. Finding the proper balance between aqueous solubility and moderate lipophilicity is crucial, e.g. to the absorption of the antibiotic from the small intestine into the bloodstream.^[264,265] Besides, it is known that bacterial efflux systems extrude amphiphilic and lipophilic molecules more effectively than hydrophilic compounds.^[266] In some cases, high lipophilicity is also related to increased plasma protein binding (PPB), e.g. to human serum albumin, lipoproteins, and glycoproteins, thereby reducing the amount of the pharmacologically active unbound fraction of the molecule.^[267] However, enhancing the polarity too much could impede albicidin's ability to penetrate the cytoplasmic membrane.^[268]

To identify albicidin's pharmacophoric regions, explore its chemical space, and subsequently improve its physicochemical properties and bioactivity profile, SAR studies are imperative. Together with studies on the mode of action and mechanisms of resistance, they provide vital information needed for the rational design of analogs with improved pharmacological characteristics. The scalable and diversifiable synthesis strategy employed in the total synthesis of albicidin has enabled the preparation of many structural analogs.^[185] In addition to variations of the N-terminal coumaric acid moiety (building block A)^[269], initial SAR studies

focused on the incorporation of various α -amino acids as building block C.^[270] A concise summary of the initial findings is given below, followed by a short introduction of the structurally related cystobactamids^[271] and coralmycins.^[272]

Variations of the central α -amino acid (building block C)

The first SAR study of albicidin was conducted by GRÄTZ *et al.* in 2016 and covered six derivatives with variations of the central β -cyanoalanine (Figure 11).^[270] To explore the role of charge, chirality, polarity, steric demand, and aromaticity on the bioactivity, and to find a viable replacement for the hydrolytically unstable cyano side chain, the amino acids Gly, Aib, Lys, Asp, Thr and 2-amino-3-(1*H*-1,2,3-triazol-4-yl)propanoic acid (AzaHis) were incorporated to prepare compounds **11–16**, respectively. For the most part, the [1+3+2] synthetic strategy was adapted from KRETZ *et al.*^[185], which was amended by an optimized peptide coupling protocol using HATU instead of DCC. The side chains of commercially available *N*-Boc amino acids Lys, Asp, and Thr were Allyl- or Alloc-protected, which enabled Pd-mediated global deprotection in the final step. An alternative [2+4] strategy, where the A-B dipeptide was coupled to the preassembled C-D-E-F tetrapeptide, was pursued to synthesize AzaHis-albicidin **16**.^[273] For this purpose, orthogonally protected AzaHis was prepared in two steps from commercially available propargylglycine following a literature protocol.^[274] Contrary to the cyano group present in the natural product, the robust triazole ring proved to be stable towards basic conditions, which allowed for convenient cleavage of the pivaloyloxymethyl (POM) protecting group of the triazole side chain with aq. KOH after completed assembly of the albicidin analog. All derivatives were tested alongside albicidin and the reference antibiotic apramycin for their antibacterial activity in a cell-based MIC assay against strains of *E. coli*, *Bacillus subtilis* (*B. subtilis*), *Micrococcus luteus* (*M. luteus*), and *Mycobacterium phlei* (*M. phlei*). Also, a target-directed *E. coli* gyrase supercoiling assay was performed to determine the capacity of these compounds to inhibit albicidin's primary molecular target. For better comparability, the gyrase assay was conducted at a substrate concentration of 40 nM, which corresponds to albicidin's IC₅₀.

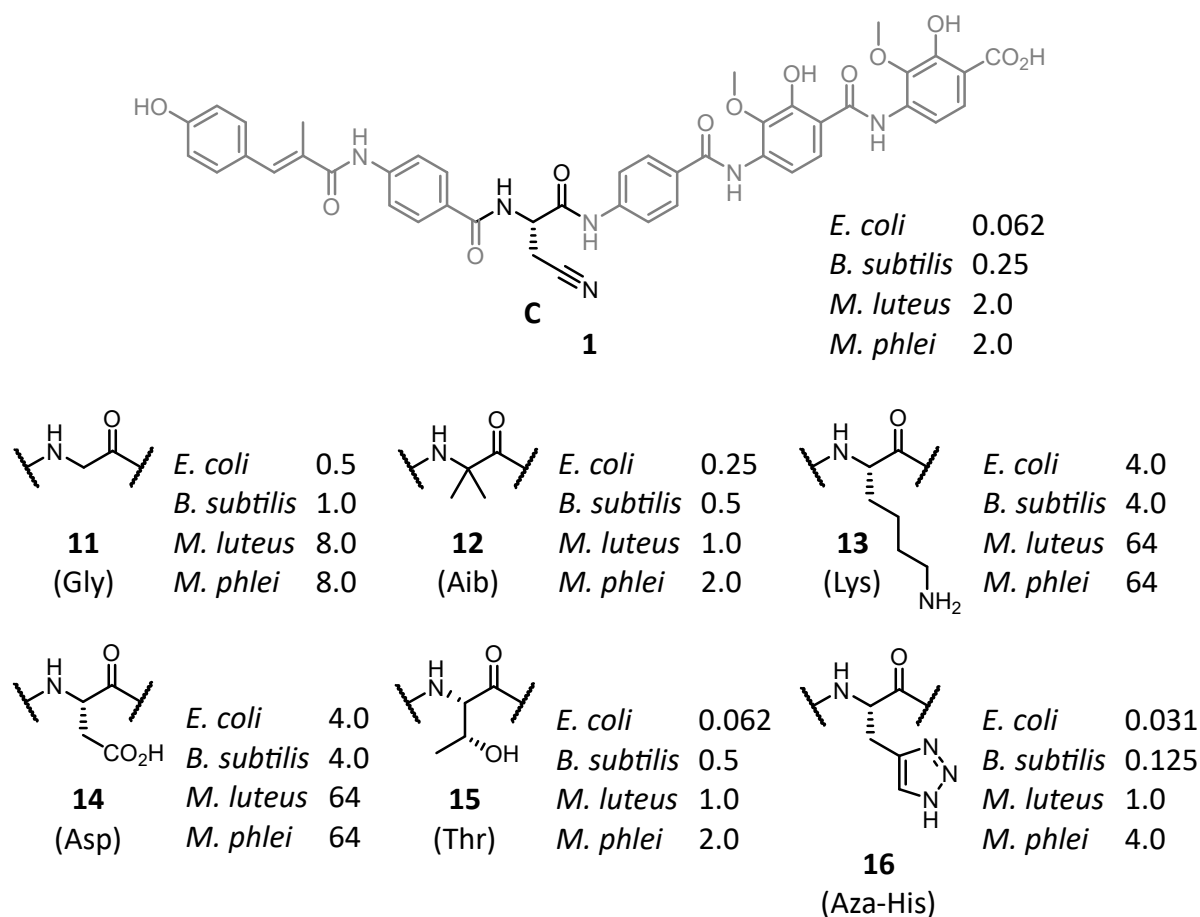


Figure 11. Albicidin derivatives with variations of the central α -amino acid.

A set of six albicidin derivatives with incorporation of various α -amino acids as building block C is shown. The MIC values for the strains *E. coli* DSM 1116, *B. subtilis* DSM 10, *M. luteus* DSM 1790, and *M. phlei* DSM 750 are given in $\mu\text{g}\cdot\text{mL}^{-1}$.

The tested compounds either matched or exceeded albicidin's potency, with analog **15** displaying a twofold lower IC_{50} towards gyrase than the natural product **1**. However, a different result was observed in the cell-based MIC assay. Notably, charged residues, as present in variants **13** and **14**, led to a significant loss of activity, possibly due to reduced cell-permeability. The partially retained activities of derivatives **11** and **12** suggested that chirality is not a prerequisite for bioactivity. Interestingly, the Thr-containing compound **15** was shown to be equally active as albicidin while being twice as soluble in water (unpublished results). The most promising results were obtained for the triazole-containing variant **16**, which exhibited superior activity to albicidin against the important Gram-negative *E. coli* strain and offered improved aqueous solubility and hydrolytic stability. Finally, its synthetic feasibility persuaded us to use AzaHis-albicidin **16** as the new template structure for SAR studies conducted as part of this thesis and beyond. In conclusion, the above-mentioned results

unfolded a high scope for variation at the central building block, which enables fine-tuning of albicidin's molecular properties, especially its solubility, without diminishing its bioactivity.

Variations of the N-terminal acyl moiety (building block A)

In 2015, PETRAS *et al.* identified an N-terminally carbamoylated albicidin analog with an extraordinary IC₅₀ of ~8 nM against gyrase, compared to 40 nM for **1**.^[275] Prompted by this finding, KERWAT *et al.* employed a combinatorial approach that was largely based on the original synthetic protocol to prepare a set of 14 derivatives with replacements of the N-terminal acyl moiety (Figure 12).^[269] The goal of this study was to assess the role of the position and nature of the substituents of the aromatic ring, the importance of the methacrylamide residue, and the relevance of the overall molecule length for antibacterial activity. Initially, the data obtained for variants **17** and **18** showed that substitution at the *ortho*- or *meta*-position virtually inactivated the corresponding derivatives. Interestingly, removing the substituent altogether did not affect the MIC values for analog **19** compared to **1**. A similar result was observed for analogs **20** and **21**, which bear a fluorine and trifluoromethyl group, respectively, in place of the *para*-hydroxy functionality. In medicinal chemistry, these substituents are commonly associated with improved metabolic stability and enhanced membrane permeability because of increased lipophilicity.^[276–278] The latter potentially facilitates the uptake of these derivatives via the T_{sx} channel, which might explain why only compound **21** inhibited gyrase and not the less lipophilic derivative **20**. A complete loss of activity was observed for carboxylic acid derivative **22**, demonstrating that a negative charge at the N-terminus is undesirable. The introduction of an aniline led to higher MIC values for analog **23** compared to **1** against all tested strains, except *M. luteus*, however, to a much lesser extent than for **22**.

Subsequently, the role of the methacrylamide residue was investigated. Removal of the methyl group provided compound **24**, which proved to be slightly less active than albicidin. Interestingly, omitting both the methyl and the *para*-hydroxy group did not worsen the potency of the corresponding derivative **25** compared to **24**. Since the C–C double bond was suspected to be prone to photochemical (*E*)-(*Z*)-isomerization^[279], resulting in a less active (*Z*)-isomer, it was formally reduced to furnish phenylpropionic acid derivatives **26** and **27**. While the hydroxy-fluorine exchange was favorable again, the loss of planarity was shown to dramatically increase the MIC values. To reduce the molecular weight, the short-length

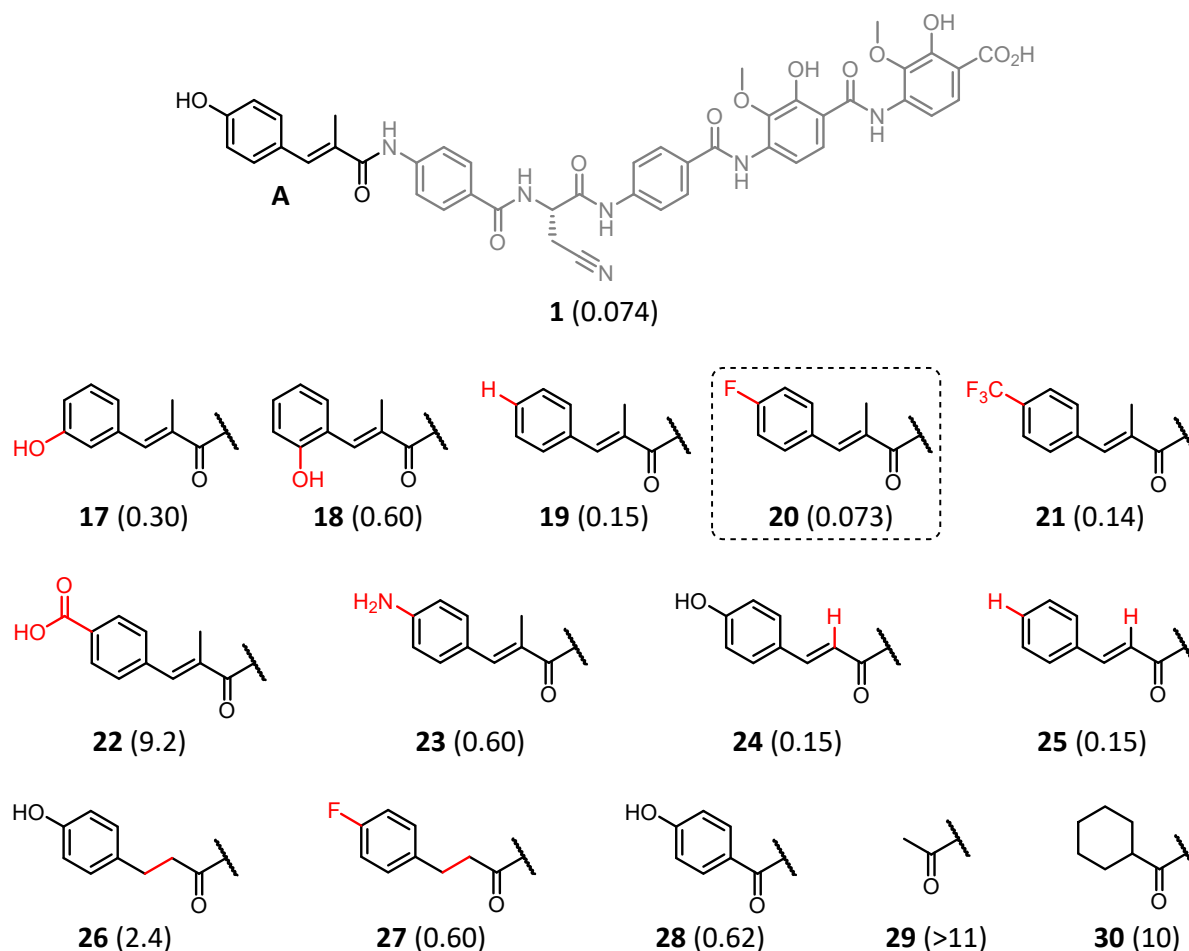


Figure 12. Albicidin derivatives with variations of the N-terminal coumaric acid moiety.

A set of 14 albicidin analogs with replacement of building block A is depicted. For full-length derivatives **17–27**, the structural modifications are shown in red. The most active derivative **20** is highlighted. The MIC values for the strain *E. coli* DSM 1116 in $\mu\text{g}\cdot\text{mL}^{-1}$ are given in brackets.

derivatives **28–30** were synthesized. Despite presenting similar activities to albicidin in the gyrase assay, the benzoic acid analog **28** and the cyclohexyl derivative **30** remained inactive in the cell-based assay. Finally, acetyl variant **29** was shown to be completely inactive, which is in accordance with the findings of VON ECKARDSTEIN *et al.*^[280] and Vieweg *et al.*^[237] that truncated analogs are virtually inactive.

The fact that some of the compounds failed to inhibit DNA gyrase while suppressing bacterial growth in the MIC assay might suggest an additional mode of action, such as the previously mentioned inhibition of TopoIV. However, the above-described experimental setup purported inactivity in the supercoiling assay for all derivatives with higher IC_{50} values than albicidin. In summary, albicidin's N-terminal acyl moiety was shown to have a high tolerance for structural variations. Unfortunately, the most active derivative, fluoro-albicidin **20**, still contains a

cinnamoyl residue. The inherent susceptibility of the cinnamate to photochemical (*E*)-(*Z*)-isomerization constitutes a major drawback and necessitates laborious precautionary measures during the synthesis, biological assessment, and storage of albicidin and respective analogs. This problem was addressed as part of this thesis and will be discussed in more detail in the results section.

1.4.7 Cystobactamids/Coralmycins and Natural Albicidin Derivatives

The cystobactamids represent another class of oligoaromatic gyrase inhibitors with high structural similarity to albicidin. First reported by BAUMANN *et al.* shortly after the elucidation of albicidin, they were isolated from the myxobacterial strain *Cystobacter* sp. Cbv34.^[271] Remarkably, the related coralmycins were isolated from *Corallococcus coralloides* M23, which is another myxobacterial strain, almost in parallel by KIM and co-workers in Korea.^[272] In addition to coralmycin A (**32**) and B (**33**), a third compound was isolated that was identified as the previously reported cystobactamid 919-2 (**31**) (Figure 13). Notably, the central β -methoxyasparagine (β -OMe-Asn) was originally reported to have a (2*S*,3*S*)-configuration. However, this assignment was shown to be incorrect by the Korean scientists and later revised to a (2*S*,3*R*)-configuration by Cheng *et al.*^[281] Recently, coralmycins **32** and **33** were also discovered as natural cystobactamid derivatives by HÜTTEL *et al.*^[282] The main structural differences to albicidin (**1**) include an *N*-terminal *para*-nitrobenzoic acid (*p*NBA) instead of the MCA, a β -OMe-Asn or β -methoxyaspartic acid (β -OMe-Asp) in place of the β -Cya as the central building block, and *iso*-propoxy groups in lieu of methoxy groups as decoration of the C-terminal *p*ABA units. Similar to albicidin and the fluoroquinolones, the cystobactamids are topoisomerase type II poisons. Based on a plasmid linearization assay and cross-resistance analysis, a partly overlapping, but not identical, primary binding site at the GyrA subunit was suggested for cystobactamids and quinolones. The cystobactamids are potent gyrase inhibitors, albeit with a sixfold higher IC₅₀ value for *E. coli* gyrase than albicidin. Also, their micromolar MIC values against various Gram-positive and Gram-negative bacteria are inferior to that of albicidin, which exhibits antibacterial activity at low nanomolar concentrations.

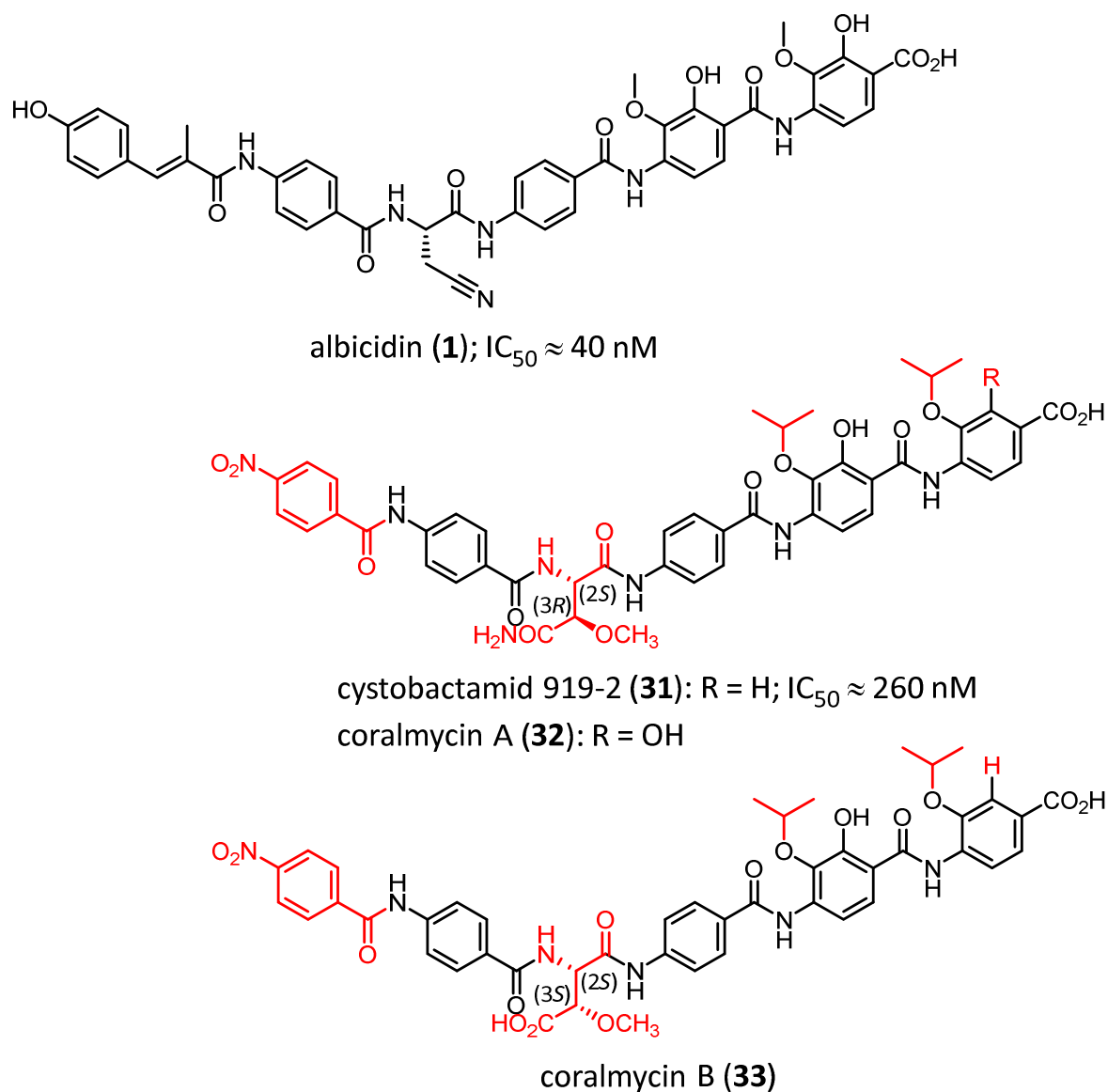


Figure 13. Structures of albicidin (1), cystobactamid 919-2 (31), and coralmycin A (32).

The structural moieties of cystobactamid/coralmycin that differ from albicidin are highlighted in red. IC_{50} values for gyrase are given for compounds **1** and **31**.

As previously shown for albicidin derivative **14** (Figure 11) the charged carboxylate side chain of the central amino acid has a detrimental effect on the activity of compound **33**. In 2017, VON ECKARDSTEIN *et al.* have reported the total syntheses and antibacterial assessment of eight natural albicidin derivatives from *Xanthomonas* strains, which were discovered through a non-targeted LC-MS/MS approach combined with spectral networking using Global Natural Product Social Molecular Networking (GNPS).^[280] This work provided many implications for the SAR of the albicidin and cystobactamid families and was paralleled by the total syntheses of natural cystobactamid derivatives reported independently by the KIRSCHNING^[282] and TRAUNER^[281] groups. The results of that study confirmed previous findings by KERWAT and

colleagues that an N-terminal aromatic building block is important for activity^[269], but also demonstrated the superiority of the MCA residue over *p*NBA as building block A. As expected, *O*-methylation and *O*-carbamoylation of MCA only had a minor effect on the MIC values. At the same time, carbamoylation resulted in very good gyrase inhibition, as reported by PETRAS *et al.*^[275] A direct comparison between albicidin derivatives bearing either β -Cya or β -OMe-Asn as the central amino acid revealed a higher activity of the former. Unlike the KIRSCHNING and TRAUNER groups' approach, VON ECKARDSTEIN's approach to the preparation of β -OMe-Asn allowed for the direct synthesis of L- β -OMe-Asn in both stereoconfigurations. Thereby, it was also shown that the (2*S*,3*R*)-isomer of β -OMe-Asn is slightly more potent than the (2*S*,3*S*)-isomer. In general, the bioactivity of the derivatives increased with the degree of substitution of the C-terminal *p*ABA dipeptide. Moreover, *iso*-propoxy groups proved to be beneficial by preserving activity even in the absence of the two hydroxy groups on building blocks E and F.

1.4.8 Summary of Previous SAR Findings

The biological evaluation of structurally diverse albicidin and cystobactamid derivatives have exposed ample possibilities for modifications regarding building blocks A, C, E, and F. As shown below (Figure 14, blue), the N-terminal acyl moiety requires at the very least an aromatic component and a minimum length to exhibit *in vitro* activity. Also, the coumaric acid motif present in albicidin is favored over the benzoic acid moiety present in cystobactamid. In general, a planar and rigid building block A seems to be the basis for *in vitro* potency, possibly due to increased uptake of the corresponding derivatives. The introduction of a charged residue in the *para*-position of the aromatic ring results in the loss of activity, which is most pronounced for a negative charge. Electron-withdrawing and lipophilic functional groups, such as F, CF₃, and CN, give slightly more active compounds than OH, OMe, and CONH₂. Regarding building block C, the incorporation of α -amino acids with charged residues dramatically decreases the antibacterial activity (Figure 14, red). Albicidin's L-Cya residue is matched by the polar L-Thr building block and slightly more favored than the β -OMe-Asn and β -OMe-Cya moieties present in some natural cystobactamid and albicidin derivatives. For the latter two, an increased potency was detected for the (2*S*,3*R*)-isomer over (2*S*,3*S*)-isomer. Combining the beneficial properties of polarity, planarity, and hydrolytic stability, AzaHis derivative **16** is the most active albicidin analog yet.

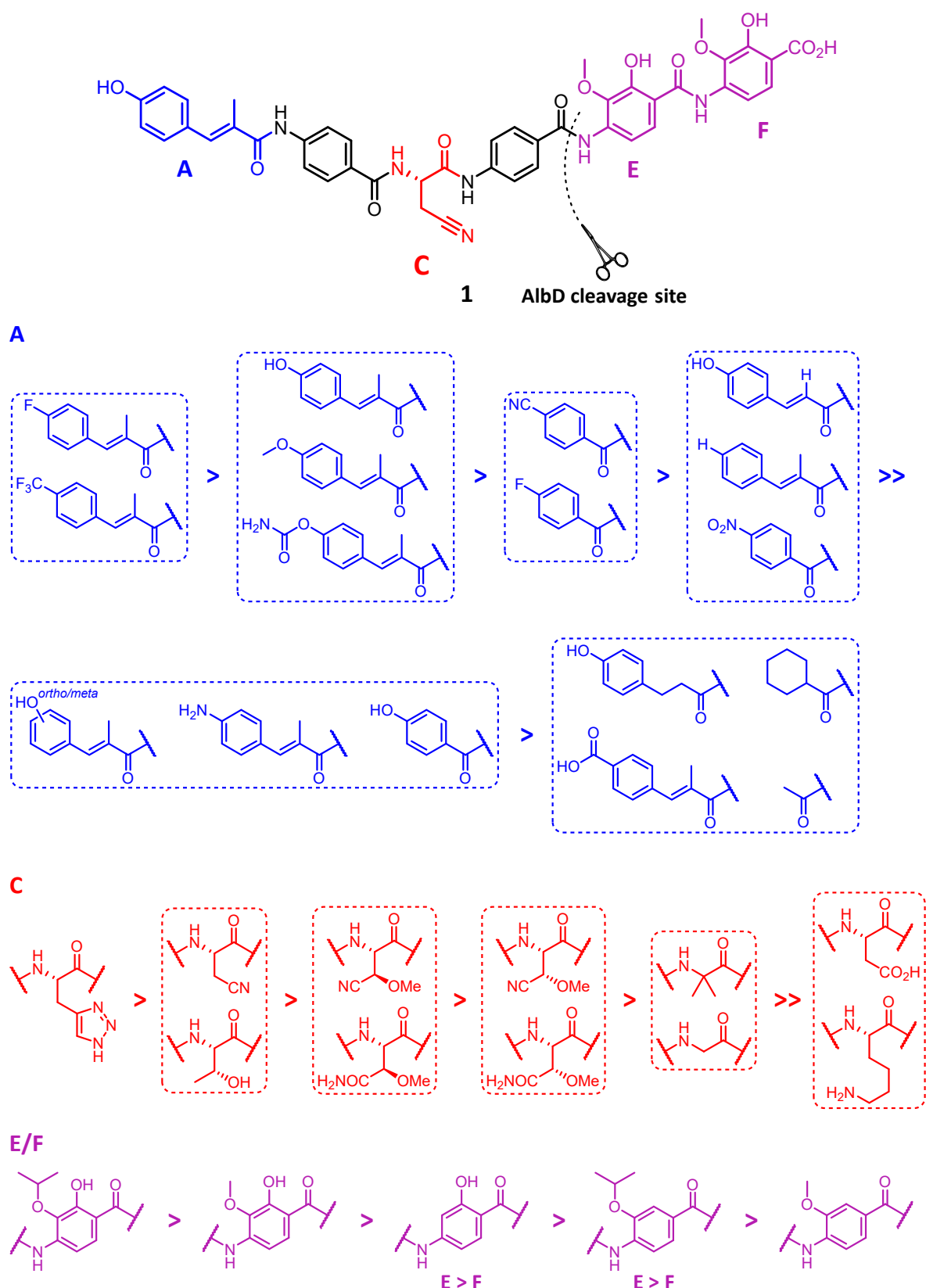


Figure 14. SAR summary of natural and synthetic albicidins and related cystobactamids.

The key findings of previous SAR studies with variations of building blocks A (blue), C (red), E/F (purple) are depicted. MIC values for *E. coli* and gyrase-inhibitory activities were taken as a basis to identify trends regarding the *in vitro* activity, which increases from left to right for the individual fragments.

Concerning the C-terminal aromatic dipeptide, *iso*-propoxy substituents are more favorable than methoxy groups and tetrasubstituted *p*ABAs give the most potent compounds (Figure 14, purple). However, as mentioned before, more hydrophobic substituents might confer lower aqueous solubility and higher plasma protein binding. Also, the hydroxy group seems to be more important than the alkoxy groups, especially when positioned at building block E.

2 Aim of this Work

The present work aims to provide insights into the complex SAR of albicidin through the synthesis and biological evaluation of a variety of its derivatives. The synthetic analogs investigated comprise variations of the C-terminal dipeptidic *p*ABA moiety (building blocks E-F) and the N-terminal cinnamate residue (building block A), respectively. A set of derivatives arising from the sequential deletion of the aromatic methoxy and hydroxy substituents represents the first systematic SAR study of the pharmacophoric E-F region of the molecule. Further derivatives result from heteroaromatic replacements of the phenolic core structure by pyridines as well as the introduction of more hydrophobic ethoxy substituents and a more hydrophilic ethylene glycolyl group instead of the methoxy groups. Also, the bioisosteric replacement of the susceptible amide bond between building blocks D and E is investigated as a potential means to protect the peptide's backbone against enzymatic hydrolysis by the endopeptidase AlbD. Since the inherent susceptibility of the cinnamate to photochemical (*E*)-(*Z*)-isomerization is deleterious to albicidin's bioactivity and requires tedious precautionary measures during its handling, a viable replacement for the methacrylamide moiety between building blocks A and B is desirable. A direct acetylenic linker is envisaged as a synthetically feasible surrogate for *trans*-configured amide bonds that mimics the planarity and rigidity of the natural A-B building block while increasing its photochemical stability. In that regard, variations of the N-terminal *para*-hydroxy group are carried out as well to explore the chemical space, identify beneficial modifications, and help fine-tune the antibiotic activity.

To determine the bioactivity of the new derivatives, cell-based MIC assays covering a broad range of Gram-positive and Gram-negative bacteria, including members of the *ESKAPE* group of pathogens, and target-based *E. coli* gyrase assays are performed. The conclusions drawn from these assays will support the SAR-guided rational design of future analogs in the search for an eligible preclinical drug candidate.

3 Results and Discussion

3.1 Preliminary Remarks

This chapter provides a detailed account of the synthesis of a variety of albicidin derivatives followed by the evaluation of their bioactivity profile and implications of the same for the peptide's SAR. Some of the experiments that were conducted by members of the SÜSSMUTH group other than the author but provide clarity and context and thus are important for the overall understanding of the results and will be described as well. Albicidin derivatives **42** and **43** were synthesized by DR. PATRICK DURKIN. Compounds **45** and **47** were prepared by DR. STEFAN GRÄTZ. Analogs **252** and **253** were synthesized by LEONARDO KLEEBAUER, MSc. and variant **254** was made by KAY HOMMERNICK, MSc. Gyrase inhibition and MIC assays were performed by Dipl. Biotechnol. MARIA SEIDEL. The experiments concerning the resistance factors AlbA and AlbD were carried out by DR. LIDA ROSTOCK at TU Berlin.

3.2 Derivatives with Variations of the C-Terminal Dipeptidic *p*ABA Moiety

To investigate the role of the substitution pattern of albicidin's E-F dipeptide in detail, a systematic approach was first taken. For this purpose, a set of derivatives arising from sequential deletion of the methoxy and hydroxy substituents and all possible permutations thereof were synthesized (Figure 15). The 15 analogs resulting from this procedure included four trisubstituted (**34–37**), six disubstituted (**38–43**), and four monosubstituted (**44–47**) variants as well as one unsubstituted compound (**48**). These compounds were designed to elaborate on the pharmacophoric E-F region of albicidin by pointing out the most favorable degree of substitution and the most beneficial combination of substituents for bioactivity. As mentioned previously, AzaHis-albicidin **16** served as the new template structure for all subsequent modifications, replacing the previous cyanoalanine building block in position C.

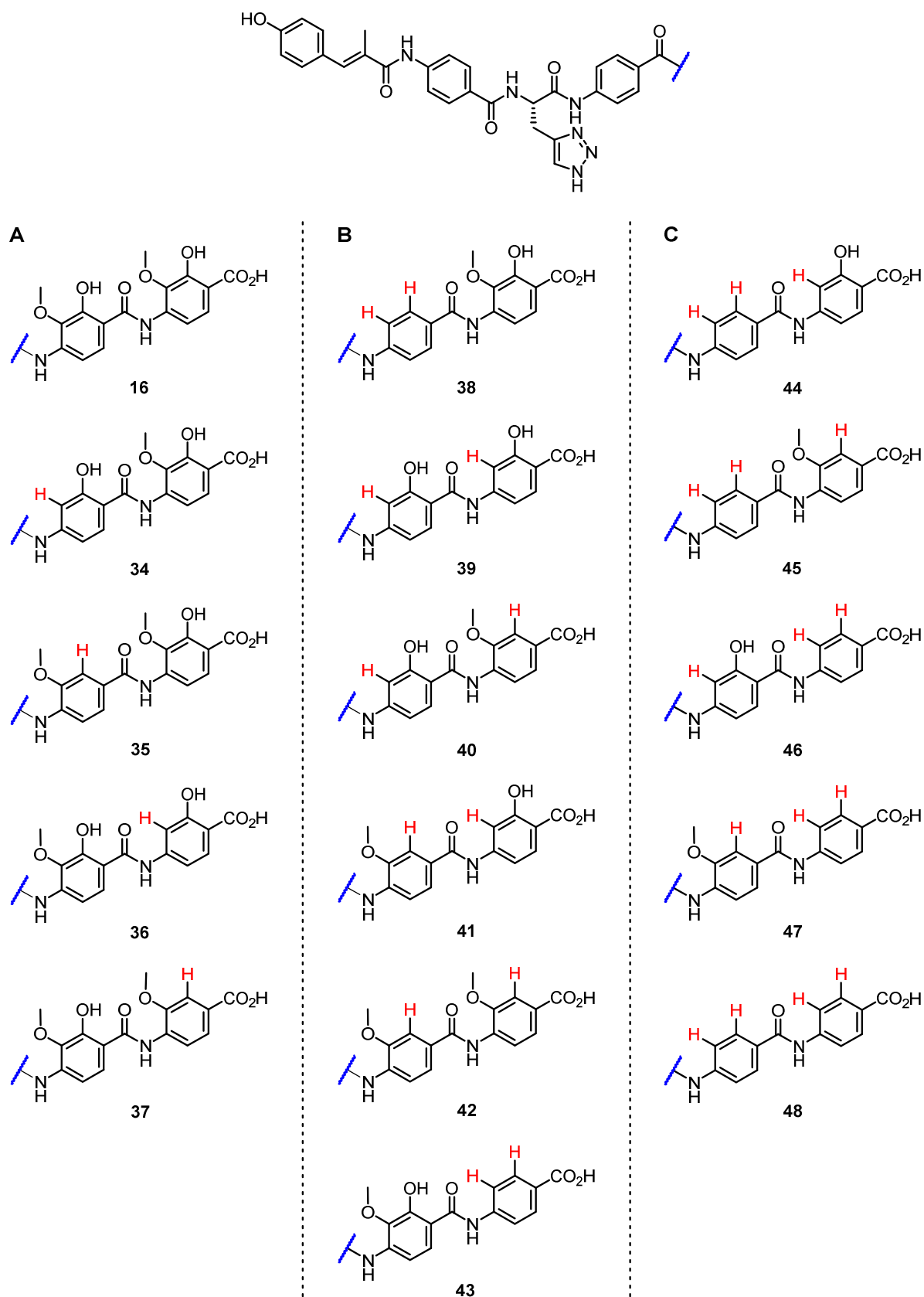


Figure 15. Structures of synthesized E-F analogs of AzaHis-albicidin 16 (Part 1).

Analogues arising from sequential deletion of the methoxy and hydroxy groups and permutations thereof are depicted. **A.** AzaHis-albicidin 16 and trisubstituted analogs 34–37. **B.** Disubstituted analogs 38–43. **C.** Mono- and unsubstituted analogs 44–48.

The second set of derivatives with variations of the C-terminal *p*ABA dipeptide contains ten synthetic analogs of compound **16** and covers a range of different modifications (Figure 16). The first three compounds (**49–51**) stem from replacing the methoxy groups of **16** by ethoxy groups, which allows to investigate the effect of more hydrophobic substituents at this position. Similarly, the ethylene glycol-containing analog **52** was synthesized to explore the effect of a more hydrophilic substituent and was also expected to increase the aqueous solubility of the molecule. Unlike the remaining compounds, this derivative was prepared with an A-B building block that contained a pyridine as building block B. As was demonstrated in the SÜSSMUTH lab by Dr. LEONARD VON ECKARDSTEIN, this heterocyclic replacement does not affect the bioactivity of the molecule significantly (unpublished results). To expand the chemical space for the SAR study, heterocyclic derivatives **53–55**, where the phenolic core structures of E and F are replaced by pyridines, were also synthesized.

Compound **56** contains an *N*-methylated amide bond between building blocks D and E and thus is meant to shield the peptide's backbone from enzymatic hydrolysis by AlbD. For the sake of completeness and clarity, this amide bond isostere will later be discussed together with additional isosteres that were not synthesized by the author but have recently been published by our group.^[273] Since very little is known about the role of the C-terminal carboxylic acid, the isophthalic acid derivative **57** was prepared as well. This dibenzoic acid was primarily chosen for its synthetic feasibility because the corresponding benzyl-protected building block E is commercially available. The increased polarity induced by the second carboxylic acid moiety potentially poses a challenge for the uptake of the molecule through the T_{scx} channel, but likely increases its aqueous solubility considerably. Finally, the *trans*-4-aminocyclohexylcarboxylic acid derivative **58** was synthesized, representing the only albicidin derivative with an alicyclic building block F. A direct comparison between **58** and its aromatic analog **43** will be helpful to understand the role planarity and rigidity at the C-terminus of the peptide play for its bioactivity.

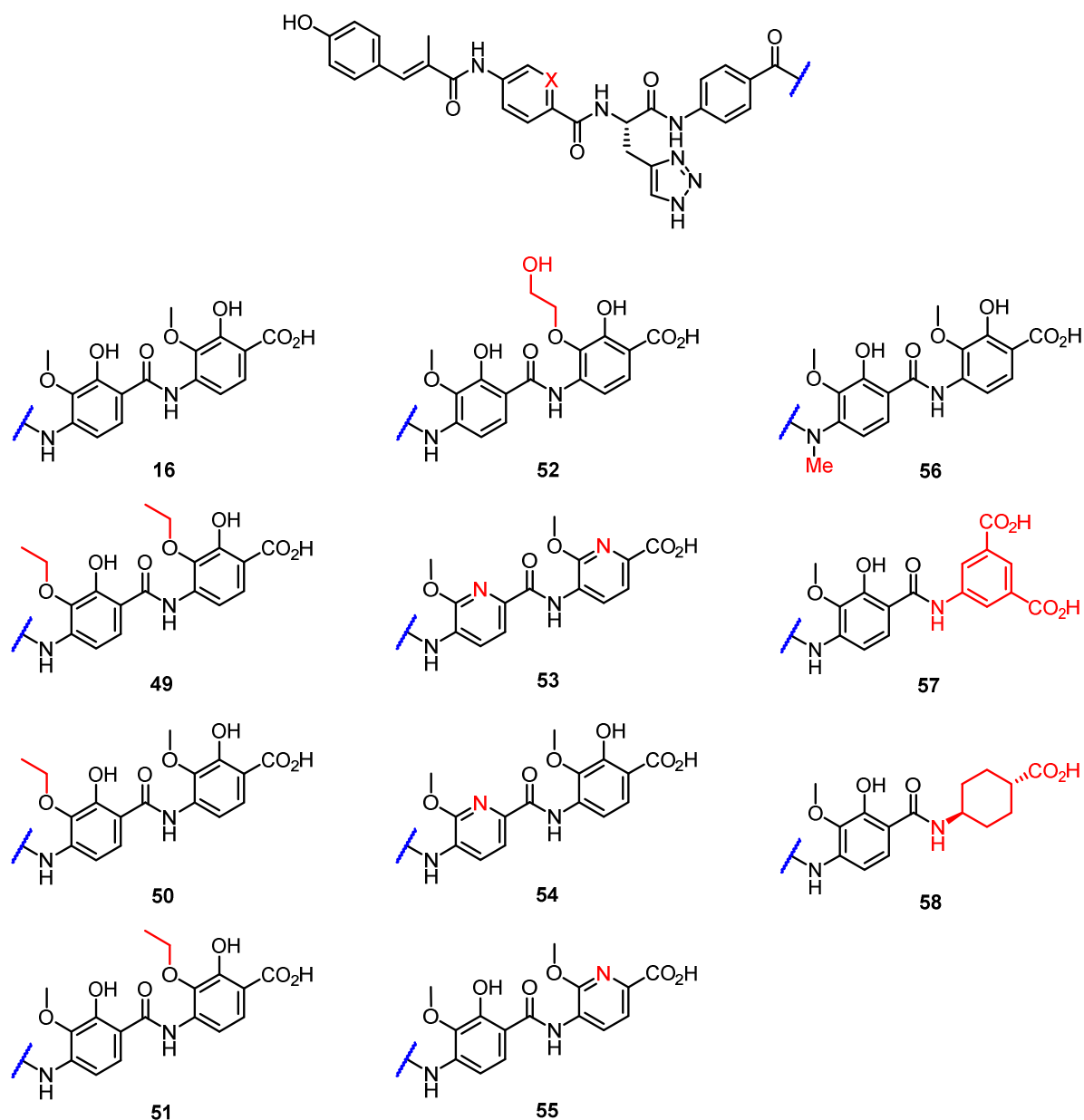


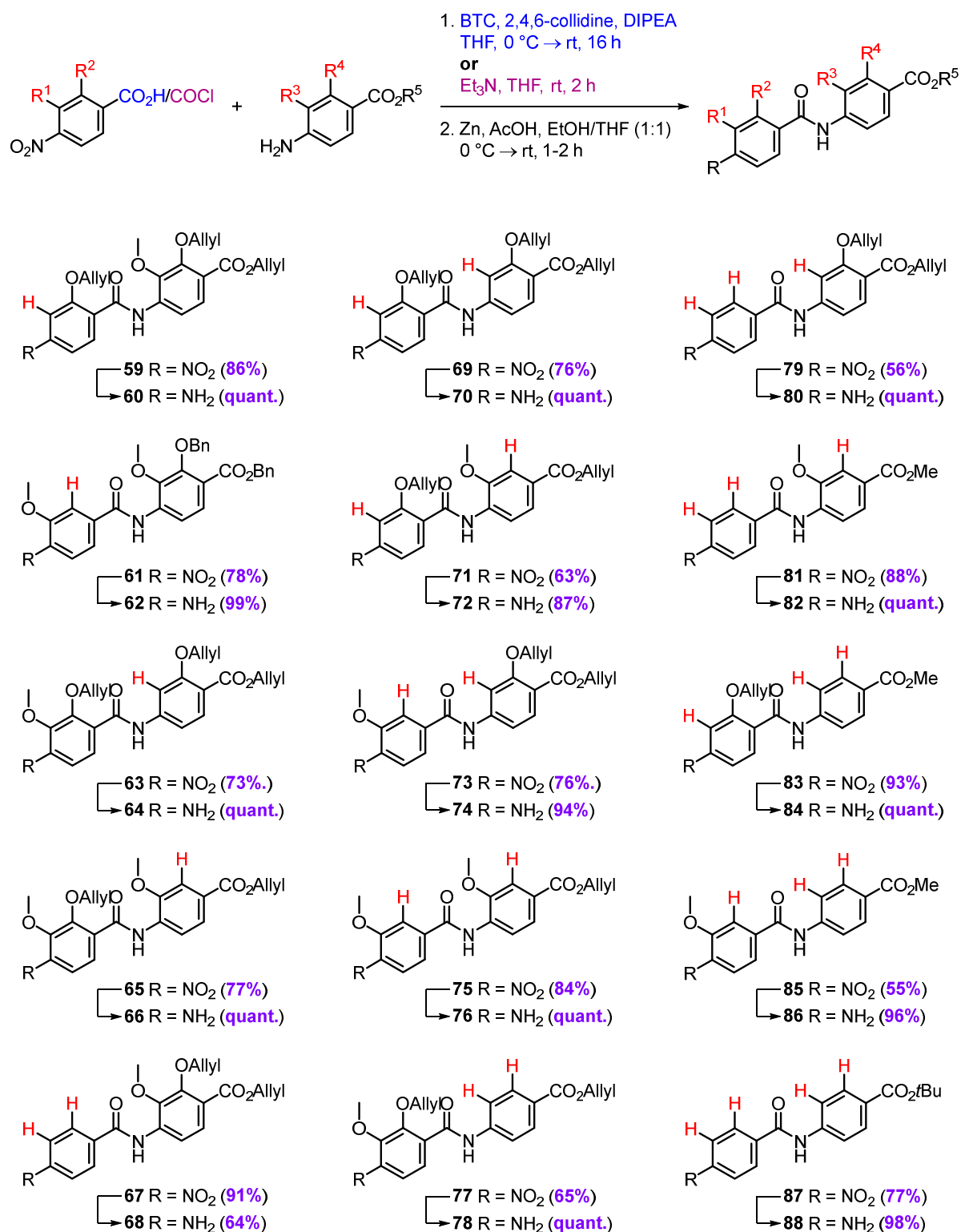
Figure 16. Structures of synthesized E-F analogs of AzaHis-albicidin 16 (Part 2).

The derivatives shown include variations of the methoxy groups (**49–52**), heteroaromatic replacements of the phenolic core structure (**53–55**), an amide bond isostere (**56**), an isophthalic acid variant (**57**) and a cyclohexyl analog (**58**). X = N for compound **52** and X = CH for all other compounds.

3.2.1 Syntheses of Modified E-F Dipeptides

The strategy for the syntheses of E-F dipeptides **59–88** is largely based on the original procedure reported by KRETZ *et al.*^[185] When starting from a commercially available or previously reported benzoic acid derivative (building block E)^[280], *in situ* activation of the electrophile as an acid chloride was achieved using triphosgene (Scheme 2, blue). When *para*-nitrobenzoyl chloride (*p*NBC) was employed, the addition of triethylamine in excess sufficed

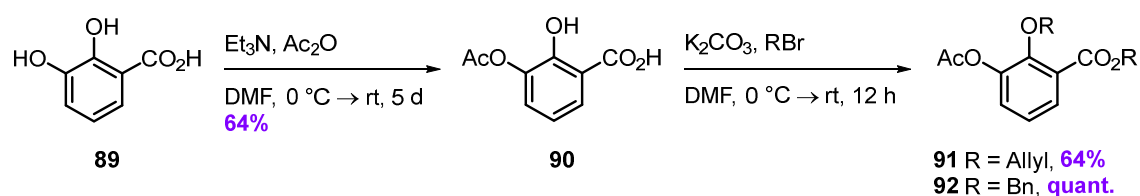
for the reaction to proceed (Scheme 2, purple). Subsequent reduction of the nitro group using Zn and AcOH afforded the desired dipeptides without further purification.



Scheme 2. Synthesis of E-F dipeptides with sequential deletion of substituents.

All *p*ABA derivatives used as starting materials were either commercially available or have been previously reported.

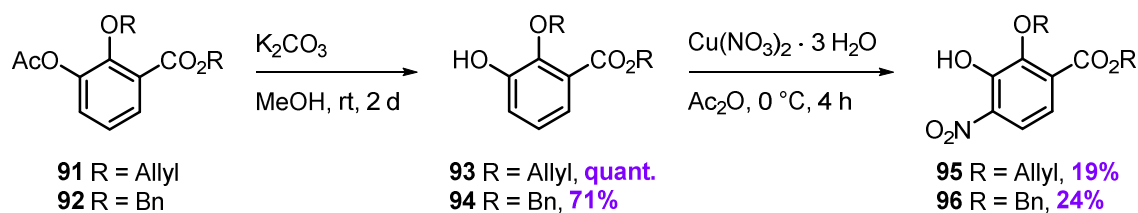
Since the original approach for the synthesis of the tetrasubstituted *p*ABA building blocks from *ortho*-vanillin did not allow for variations of the methoxy group, an alternative approach was followed to introduce different alkoxy substituents. Starting from commercially available 2,3-dihydroxybenzoic acid (**89**), the phenolic precursors **95** and **96** were synthesized in a multigram scale in four steps, partly in line with a protocol established in our group by Dr. MARIUS MORKUNAS. The regioselective acetylation of **89** proceeded slowly and was stopped after five days when no further conversion could be detected via TLC (Scheme 3). When the reaction was performed at $\sim 50\text{ }^{\circ}\text{C}$, a loss of selectivity was observed leading to a mixture of compounds. In the next step, **90** was treated with allyl bromide and benzyl bromide in the presence of a base, respectively, to yield the fully protected intermediates **91** and **92**.



Scheme 3. Synthesis of orthogonally protected dihydroxybenzoic acids.

A two-step reaction sequence was followed to introduce acetyl as well as allyl or benzyl protecting groups to 2,3-dihydroxybenzoic acid (**89**) to prepare compounds **91** and **92** via the intermediate ester **90**.

The subsequent selective cleavage of the acetyl group with K_2CO_3 in MeOH proceeded smoothly at r.t. to give phenols **93** and **94** in good to excellent yields (Scheme 4). However, a transesterification reaction between **91** and MeOH was observed at higher temperatures ($\sim 50\text{ }^{\circ}\text{C}$). In future attempts to reduce the reaction time, this problem can potentially be avoided by using a more inert solvent than MeOH. Finally, a mild nitration protocol involving $\text{Cu}(\text{NO}_3)_4 \cdot 3\text{H}_2\text{O}$ in acetic anhydride was employed to produce the desired tetrasubstituted phenols **95** and **96** with the nitro groups located at the *para*-position to the carboxylate. The low yields of 19% and 24%, respectively, can be accounted for by the additional formation of *ortho*-substituted regioisomers. Carrying out the nitration step prior to the removal of the acetyl group might help to improve the yield of the desired isomers and needs to be explored in the future.

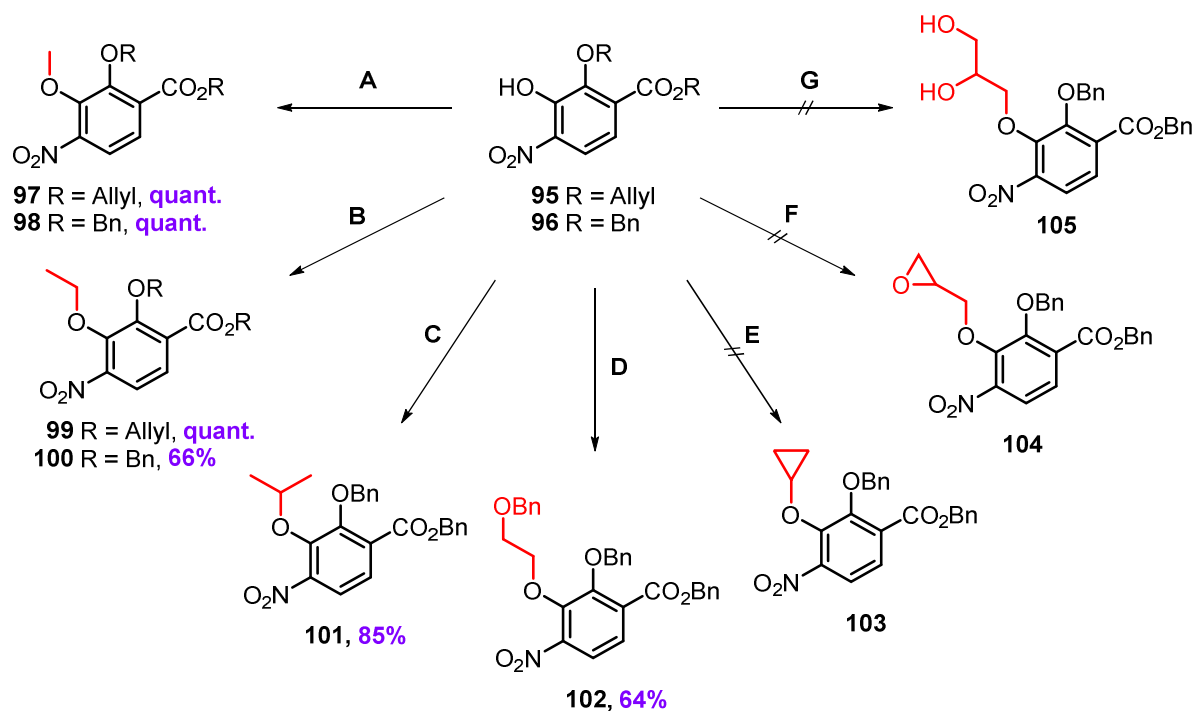


Scheme 4. Synthesis of tetrasubstituted *O*-alkylation precursors.

A selective deprotection and nitration sequence was employed to synthesize *O*-alkylation precursor molecules **95** and **96** from the trisubstituted diesters **91** and **92** via phenols **93** and **94**.

Compounds **95** and **96** were envisioned as universal precursors for *O*-alkylation reactions that could potentially be used to install numerous alkoxy groups in place of the methoxy group and thus facilitate the synthesis of albicidin derivatives with variations of the C-terminal dipeptide. Using commercially available alkyl halides, the introduction of methyl (**97** and **98**), ethyl (**99** and **100**), *iso*-propyl (**101**), and ethylene glycolyl (**102**) groups proceeded readily and with high yields. However, attempts to install cyclopropyl (**103**), 1,2-epoxypropyl (**104**), and propylene glycolyl (**105**) groups were to no avail, even at elevated temperatures (Scheme 5). The reactions were first performed on a test scale and monitored by MS. The successful reactions were repeated in a gram scale for compounds **99**, and **102**, which were later incorporated into albicidin derivatives.

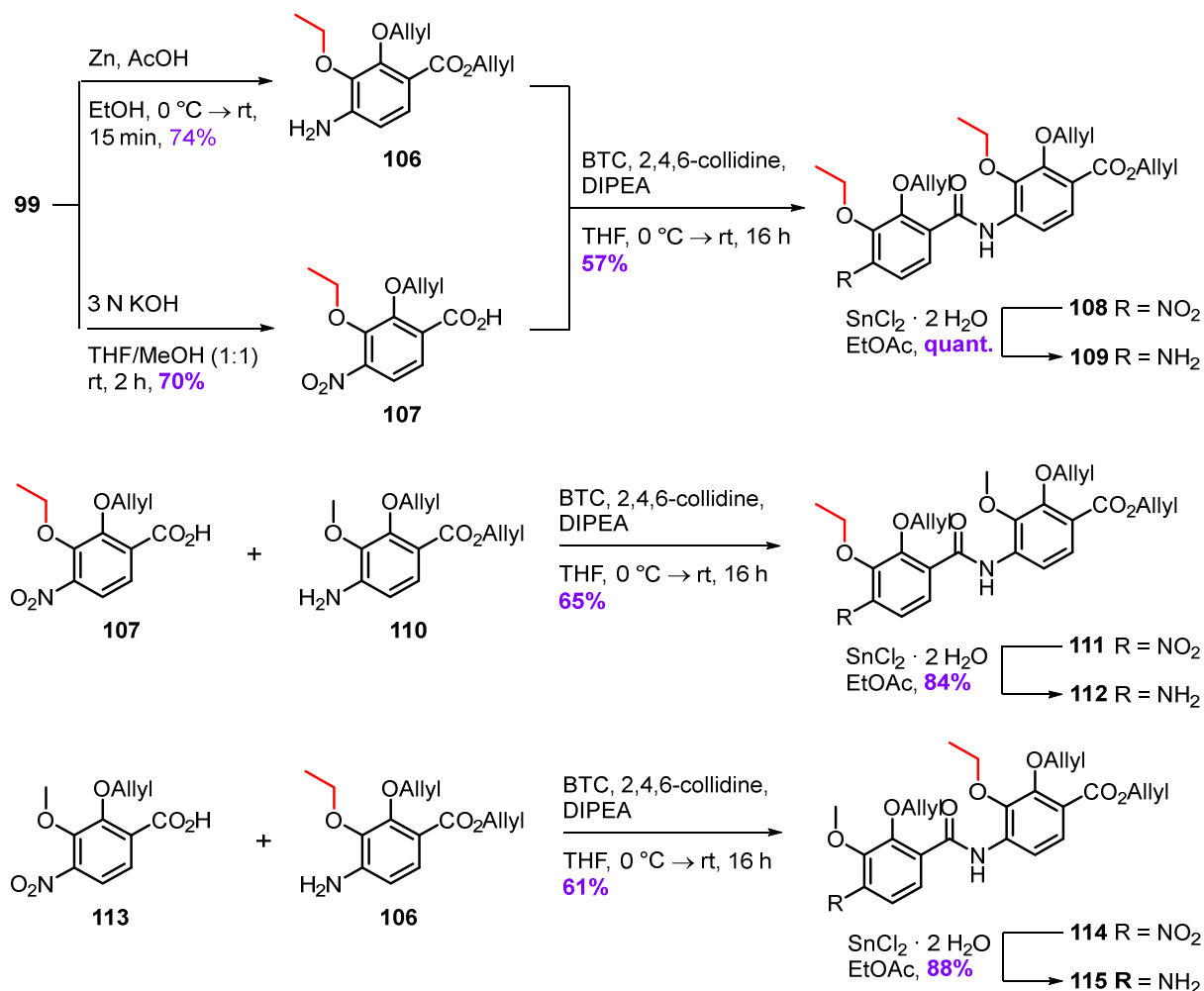
The feasibility of using benzyl protection is another clear advantage of this new pathway over the original one in that it allows cleavage of aliphatic benzyl ethers, as present in compound **102**, by Pd-catalysed hydrogenolysis. Aliphatic allyl ethers are inert towards Pd-mediated removal and thus render global deprotection nearly impossible. Since nitration follows only after the protection step in the original protocol, the aromatic substitution would occur at the benzyl group as well and lead to a wild mixture of compounds.



Scheme 5. Scope and limitations of *O*-alkylation reactions of phenols **105 and **106**.**

Reaction conditions: **A.** K₂CO₃, MeI, DMF, 40 °C, 16 h. **B.** K₂CO₃, EtBr, KI, DMF, 80 °C, 16 h. **C.** K₂CO₃, *iso*-PrBr, KI, DMF, 80 °C, 16 h. **D.** K₂CO₃, ((2-bromoethoxy)methyl)benzene, DMF, 110 °C, 16 h. **E.** Cs₂CO₃, cyclopropyl bromide, NaI, DMF, 170 °C, 3 d. **F.** Epibromohydrin, NaOH, H₂O/THF (10:3), r.t., 2 d; **G.** 3-Chloro-1,2-propanediol, NaOH, EtOH/H₂O (1:1), 120 °C, 4 d.

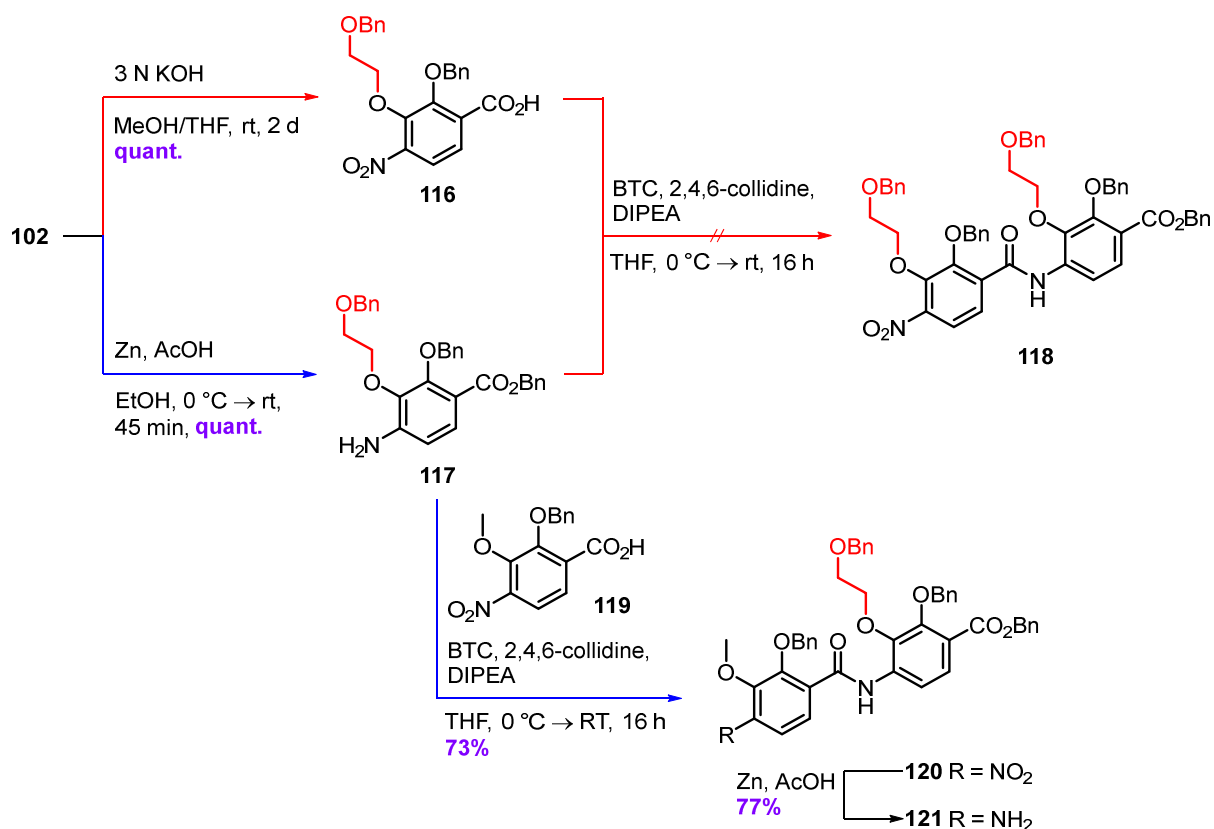
The fully protected and ethoxy-substituted building block **99** was treated with Zn and aq. KOH to obtain aniline **106** (building block F) and benzoic acid **107** (building block E), respectively. In triphosgene-mediated reactions, these were then coupled to each other or either of the methoxy-substituted building blocks **110** and **113** to obtain dipeptides **108**, **111**, and **114**. Since partial cleavage of the ethyl ether was observed during the reduction of the nitro group of **99** with Zn and AcOH, the original and milder method using SnCl₂ · H₂O was applied for the reduction of the three dipeptides to complete the E-F fragments **109**, **112**, and **115** (Scheme 6). This method results in similar yields but requires higher reaction temperatures, longer reaction times, and involves a tedious workup protocol. It should, therefore, be avoided whenever possible.



Scheme 6. Syntheses of ethoxy-substituted E-F dipeptides.

Starting from the fully protected precursor **99**, dipeptides **109**, **112**, and **115** were each prepared in three-steps via anilines **106** and **110**, benzoic acids **107** and **113**, and nitro dipeptides **108**, **111**, and **114**, respectively.

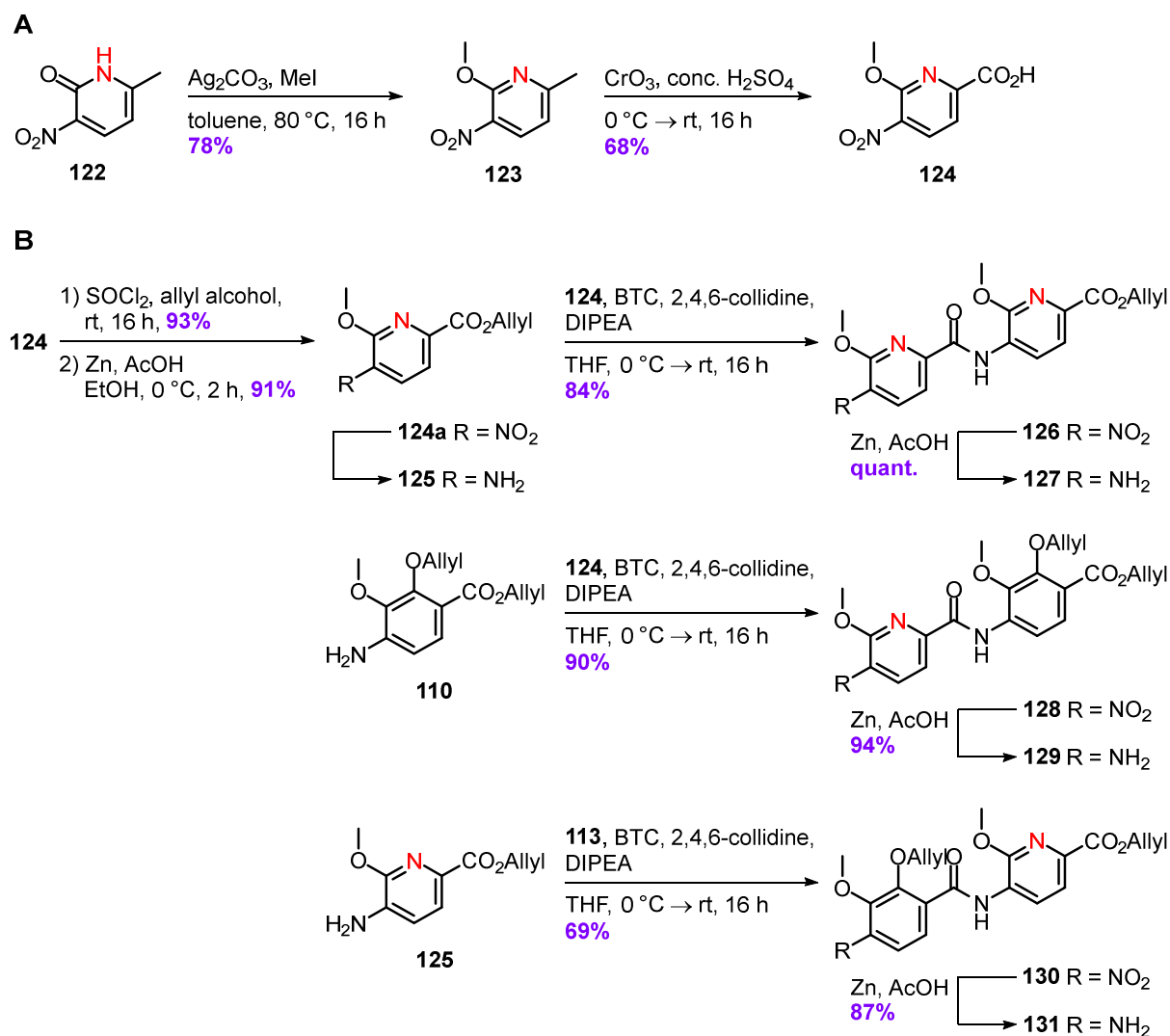
The ethylene glycol-containing dipeptide **121** was synthesized analogously to the ethoxy derivative **115** (Scheme 7, blue path). Since the protected ethylene glycol moiety was not prone to reductive cleavage, the nitro groups of **102** and **120** were reduced using Zn and AcOH again. As mentioned before, benzyl protecting groups were chosen instead of allyl groups because aliphatic benzyl ethers can easily be debenzylated by hydrogenolysis. An attempt to couple building blocks **116** and **117** did not yield the desired dipeptide **118** (Scheme 7, red path) Possibly, the reaction was prevented by the steric demand of the benzyl ether of **116** and particularly the benzyl-protected ethylene glycol moiety of **117**. Since triphosgene is a very powerful peptide coupling reagent, we refrained from screening additional reagents until we had evidence that the ethylene glycol group was beneficial for bioactivity in the first place.



Scheme 7. Synthesis of the ethylene glycol-containing E-F dipeptide.

Dipeptide **121** was synthesized in three steps from **102** (blue path). The attempted synthesis of the doubly substituted derivative **118** (red path) by the coupling of benzoic acid **116** to aniline **117** was unsuccessful.

To synthesize E-F dipeptides with the replacement of the phenolic core structure by pyridines, the commercially available nitropyridone **122** was first treated with MeI in the presence of Ag₂CO₃ to yield methoxypyridine **123**. Subsequently, a JONES-oxidation was performed at the methyl position of **123** to generate the picolinic acid derivative **124** (Scheme 8, A). Subsequently, **124** was allyl-protected using a standard procedure followed by the reduction of the nitro group to prepare aminopyridine **125**. The two building blocks **124** and **125** were then coupled to either of the original building blocks **110** and **113** by employing the previously mentioned triphosgene-mediated protocol to make dipeptides **126**, **128**, and **130** (Scheme 8, B). Finally, the reduction of the nitro groups proceeded smoothly and provided the desired E-F buildings **127**, **129**, and **131**.

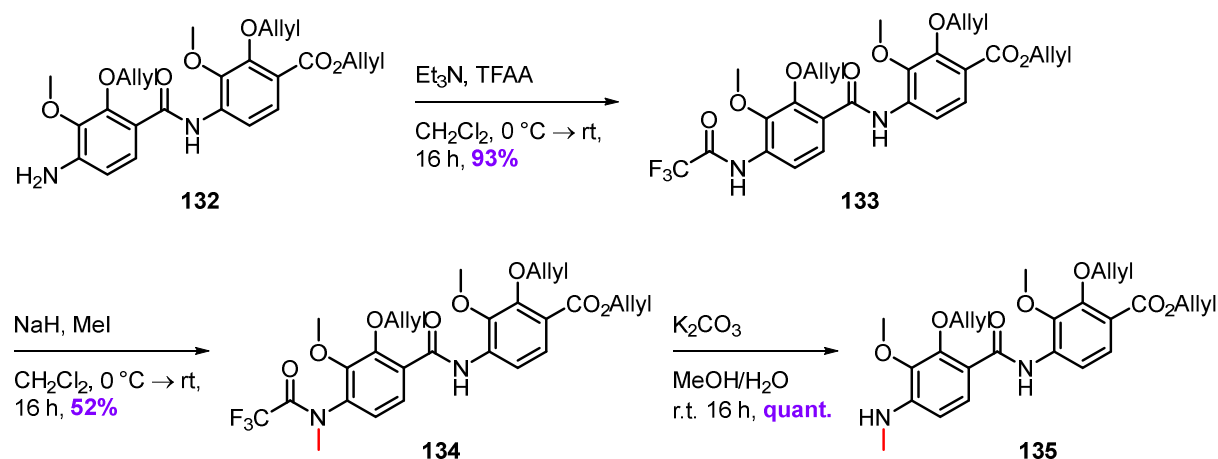


Scheme 8. Syntheses of heteroaromatic E-F dipeptides.

A. Two-step synthesis of picolinic acid derivative **124** from nitropyridone **122** via methoxypyridine **123**.

B. Synthesis of heteroaromatic dipeptides **127**, **129**, and **131**.

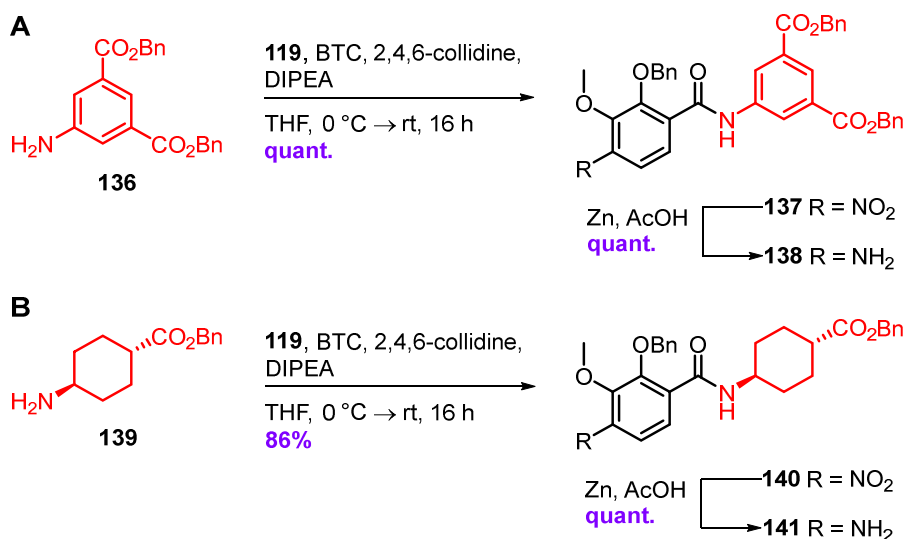
Introducing an amide bond surrogate between building blocks D and E through *N*-methylation of compound **132** required a detour as a direct treatment with MeI would have led to over-methylation of the aniline. This was avoided by installing a trifluoroacetyl protecting group using trifluoroacetic anhydride (TFAA) before methylation to obtain compound **133** in almost quantitative yield (Scheme 9).^[283] The electron-withdrawing effect of the TFA-group both prevents the second methylation and activates the amino group for the first one. As suggested by MS, the moderate yield of *N*-methyl amide **134** may be ascribed to the formation of a by-product carrying methyl groups at both amide moieties of the molecule. Finally, the protecting group was easily removed with K₂CO₃ in MeOH to afford the desired dipeptide **135**.



Scheme 9. Synthesis of an *N*-methylated E-F dipeptide.

Three-step linear sequence involving the protection of aniline **132**, methylation of the resulting trifluoroacetamide **133**, and deprotection of **134** to prepare *N*-methyl aniline **135**.

The syntheses of the final two E-F dipeptides, namely isophthalic acid derivative **138** and cyclohexyl derivative **141** (Scheme 10), were accomplished in high yields by employing the coupling strategy and nitro reduction method described above. Conveniently, dibenzyl 5-aminoisophthalic acid (**136**) and *trans*-4-aminocyclohexylcarboxylic acid (**139**) were readily available from commercial sources.



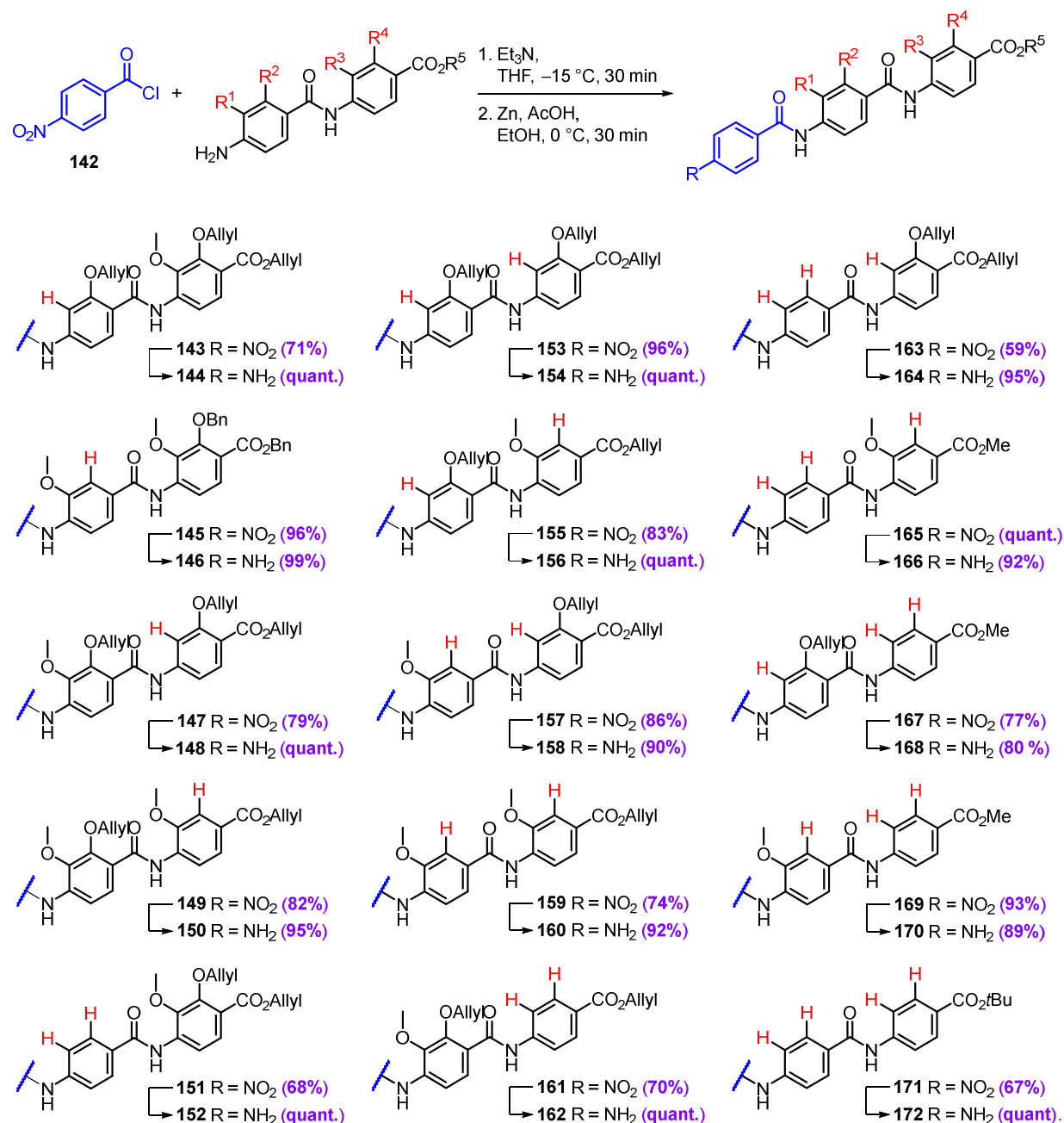
Scheme 10. Syntheses of isophthalic acid and cyclohexyl-containing dipeptides.

A. Synthesis of dibenzoic acid derivative **138** from 5-aminoisophthalic acid **136**. **B.** Synthesis of cyclohexyl derivative **141** from *trans*-4-aminocyclohexylcarboxylic acid **139**.

3.2.2 Synthesis of Tetrapeptides with Modified E-F Building Blocks

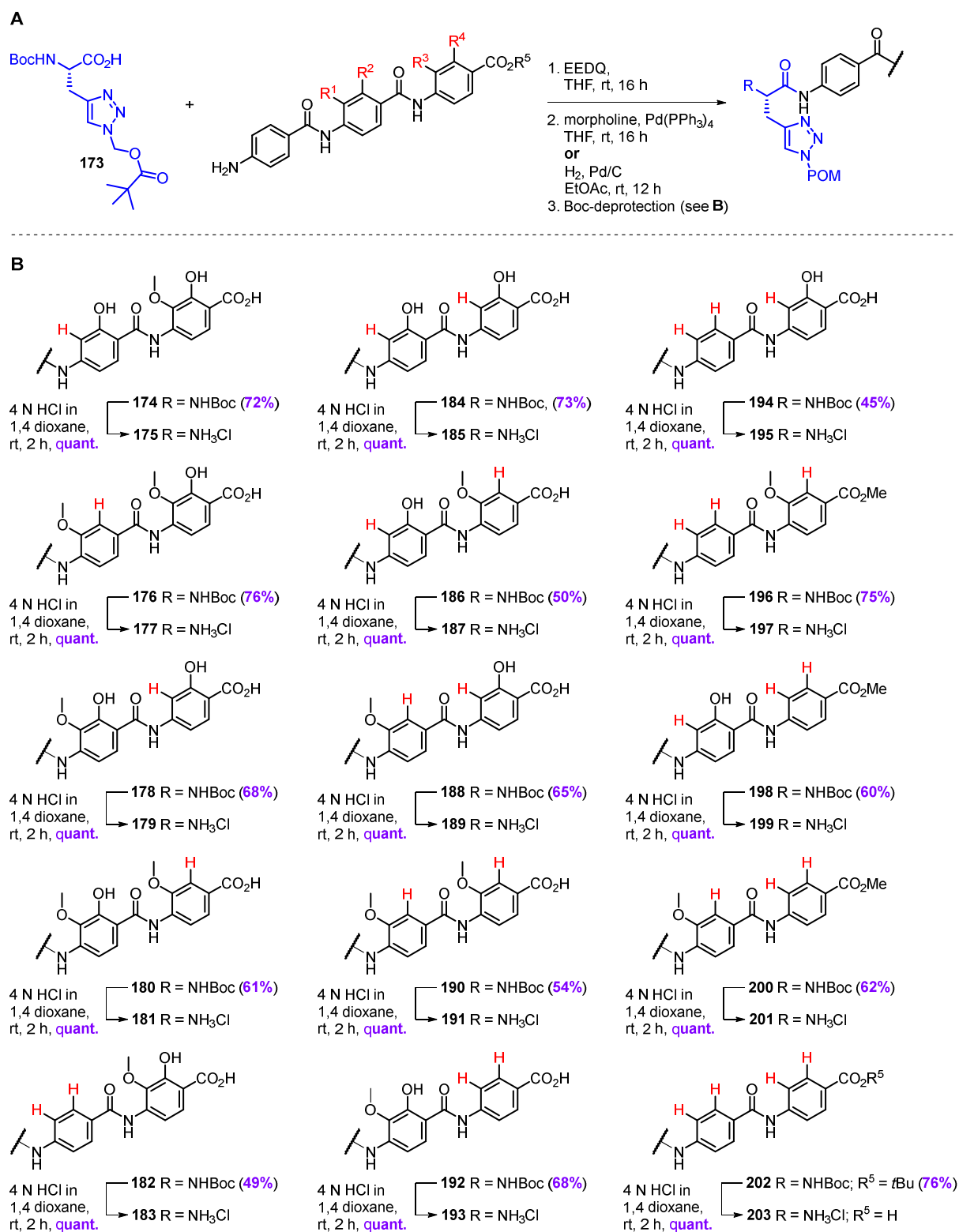
Starting from the E-F dipeptides described in Scheme 2, the assembly of albicidin derivatives was continued by preparing the corresponding C-D-E-F tetrapeptides in five steps. This was accomplished in two consecutive reaction sequences, each comprising a peptide elongation step and at least one deprotection step. The first reaction sequence involved the coupling of *p*NBC (**142**), an activated *p*ABA derivative, to the amino dipeptides followed by reduction of the products' nitro groups using Zn in EtOH in the presence of AcOH to afford tripeptides **143**–**172** (Scheme 11). Conveniently, the crude products of the coupling steps could be precipitated in diethyl ether to obtain analytically pure compounds that did not require further purification. However, the solubility of the tripeptides containing nitro groups in EtOH decreased with every deletion of substituents and was especially poor for the *p*ABA-*p*ABA-*p*ABA analog **97**. Nonetheless, the reaction proceeded in a “suspension-to-suspension” fashion. This problem was later avoided by using a mixture of EtOH and THF in various ratios as the solvent system.

The second reaction sequence involved the coupling of orthogonally protected AzaHis **173** to the tripeptides described in Scheme 11 via the formation of mixed anhydrides using 2-ethoxy-1-ethoxycarbonyl-1,2-dihydroquinoline (EEDQ) as a coupling reagent (Scheme 12). EEDQ is commonly known to suppress the epimerization of α -amino acids during peptide coupling reactions. Since an equimolar amount of quinoline is released during the activation of the carboxylic acid, no additional base is necessary. Quinoline serves as a weak base which keeps the nucleophile (amine) deprotonated without reacting with other components of the reaction mixture.^[284,285] The tetrapeptides were then allyl- and benzyl-deprotected, whenever applicable, by using Pd(PPh₃)₄/morpholine and Pd-catalyzed hydrogenolysis, respectively. Despite full reaction conversions, as monitored by TLC, allyl-deprotection often resulted in poor product yields. The loss can potentially be attributed to the laborious purification by column chromatography, which requires a quite polar solvent system (MeOH/CH₂Cl₂). Subsequently, the removal of the Boc groups in quantitative yield provided the analytically pure C-D-E-F tetrapeptides without further purification.



Scheme 11. Syntheses of D-E-F tripeptides with sequential deletion of E-F substituents.

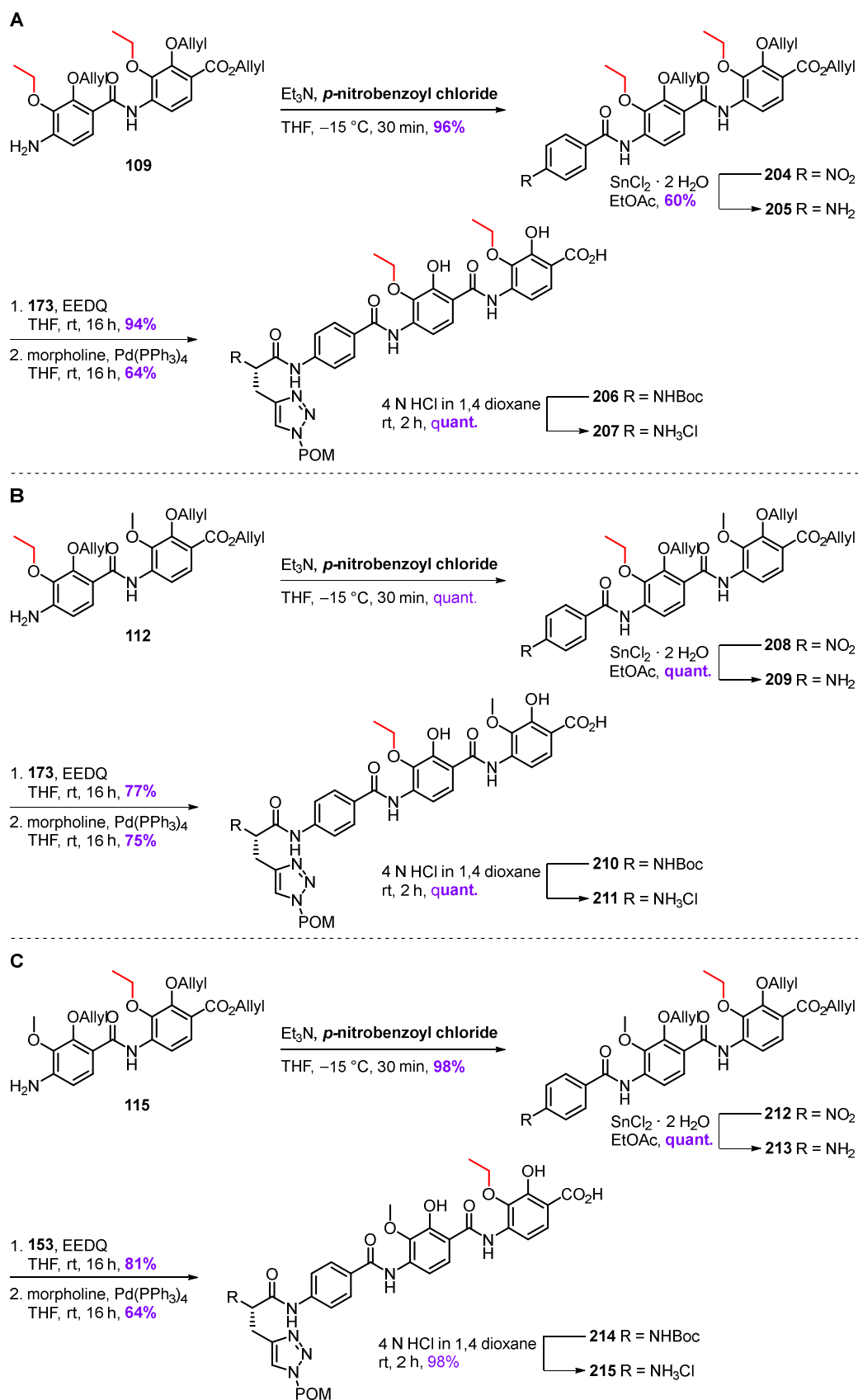
The amino dipeptides shown in Scheme 2 were each coupled to *p*NBC and the resulting compounds subsequently reduced to obtain the desired amino tripeptides. The yields of the individual coupling and reduction steps are given in brackets.



Scheme 12. Syntheses of C-D-E-F tetrapeptides with sequential deletion of E-F substituents.

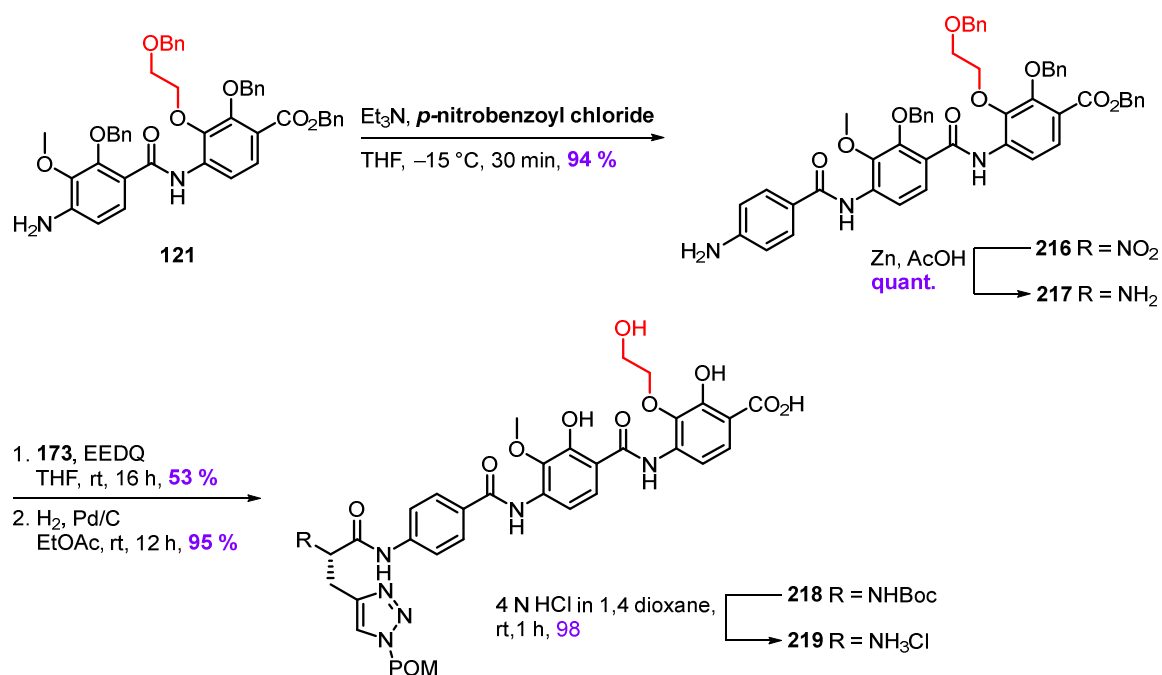
A. The amino tripeptides shown in Scheme 12 were each coupled to AzaHis **173** and subsequently allyl- or benzyl-deprotected if applicable. **B.** A final Boc-deprotection step provided the desired tetrapeptides. The yields of the individual deprotection steps are given in brackets.

The tetrapeptides containing ethoxy-substituted E-F moieties (**207**, **211**, and **215**; Scheme 13) were synthesized almost analogously to the compounds described above. The initial coupling of *p*NBC proceeded smoothly and afforded tripeptides **204**, **208**, and **212** in excellent yields. As mentioned before, $\text{SnCl}_2 \cdot \text{H}_2\text{O}$ was employed instead of Zn and AcOH for the reduction of the nitro groups to avoid reductive cleavage of the ethyl ether moieties. The moderate yield of 60% obtained for the doubly ethoxy-substituted aniline **205** resulted from the poor phase separation during the basic workup with saturated $\text{NaHCO}_3(\text{aq.})$ and could later be avoided for variants **209** and **213** by properly diluting the organic layer. The subsequent EEDQ-mediated coupling of AzaHis **173** to the reduced D-E-F tripeptides proceeded in high to excellent yields. Finally, the acidic hydrolysis of the N-terminal carbamates released the analytically pure target compounds **207**, **211**, and **215** without any loss. The ethylene glycol-containing tetrapeptide **219** was prepared via a similar route from its dipeptidic precursor **121** (Scheme 14). However, the allyl-deprotection step was replaced by a protocol for the removal of the benzyl protecting groups. The deprotection was achieved in a yield of 95% by applying standard conditions for Pd-mediated catalytic hydrogenolysis. Again, the final cleavage of the *tert*-butyl carbamate liberated the desired C-D-E-F tetrapeptide **219**.



Scheme 13. Synthesis of C-D-E-F tetrapeptides containing ethoxy-substituted *p*ABAs.

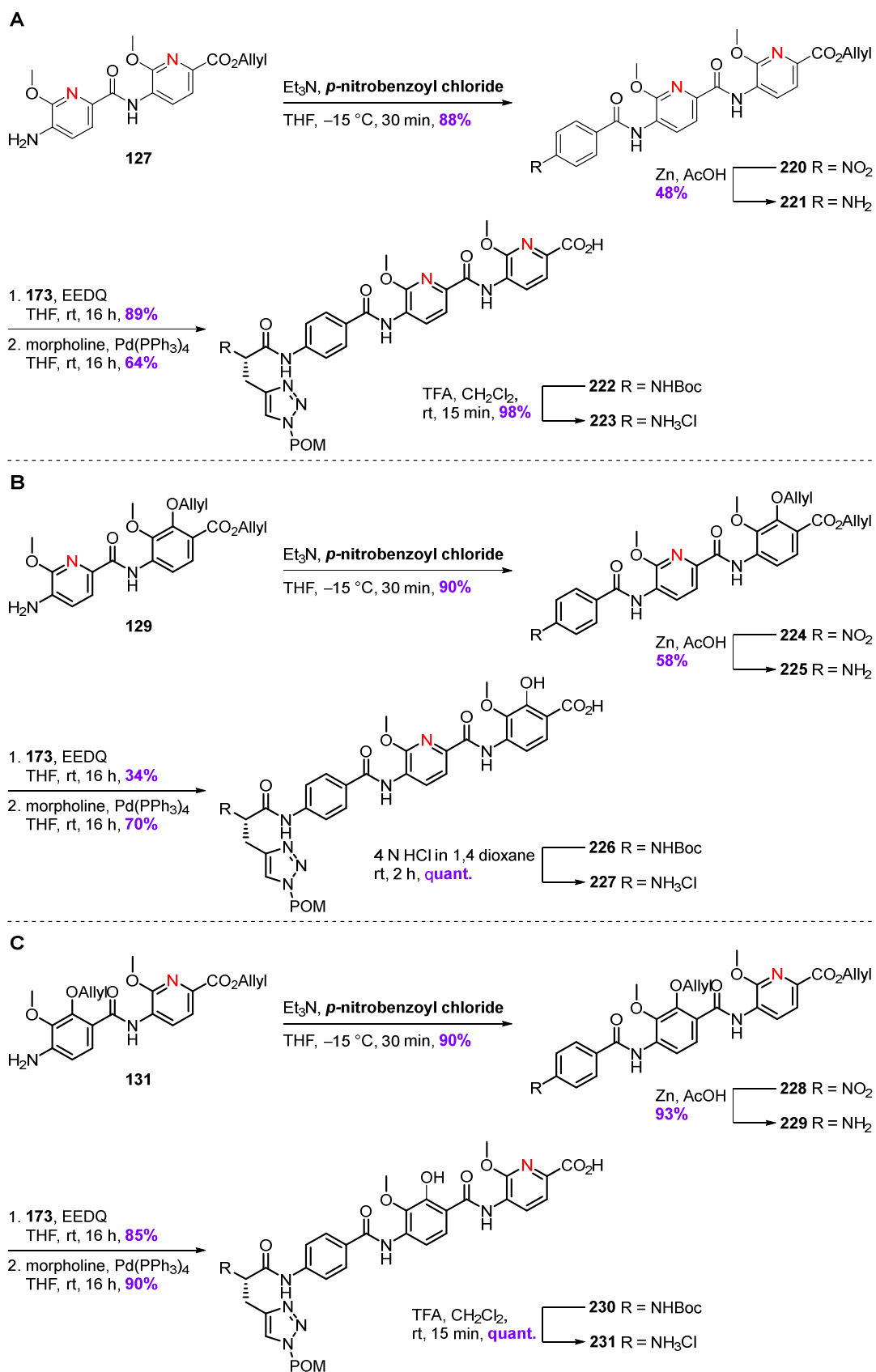
Five-step linear syntheses of allyl- and Boc-protected tetrapeptides **207** (A), **211** (B), and **215** (C) starting from dipeptides **109**, **112**, and **115**, respectively.



Scheme 14. Synthesis of a C-D-E-F tetrapeptide with an ethylene glycol-containing pABA.

A five-step linear synthetic route towards benzyl- and Boc-protected tetrapeptide **219** starting from the corresponding dipeptide **121** via tripeptide **217**.

When the same five-step synthetic sequence was employed to prepare the pyridine-containing tetrapeptides **223**, **227**, and **231** (Scheme 15), the reduction of the nitro groups of tripeptides **220** and **224** was hampered by the poor solubility of these compound in a mixture of EtOH/THF (3:1, v/v). A full reaction conversion was not achieved and the difficult isolation of the desired products by column chromatography likely caused the poor yields as mixed fractions were collected as well. In addition, the strikingly low yield of the EEDQ-mediated conversion of tripeptide **225** to the corresponding tetrapeptide was caused by the presence of residual AcOH from the previous nitro reduction step. As a quick reaction control via MS had revealed, AcOH acted as a competing electrophile in the reaction mixture to result in the formation of an N-terminally acylated tripeptide as the major product. To circumvent this problem, meticulous drying of the starting material under reduced pressure is mandatory.



Scheme 15. Syntheses of C-D-E-F tetrapeptides containing pyridines.

Five-step linear synthesis of allyl- and Boc-protected tetrapeptides **223** (A), **227** (B), **231** (C) starting from dipeptides **127**, **129**, and **131**, respectively.

Also, the Boc-deprotection step needed to be adjusted for the tetrapeptides bearing a methoxypyridine as building block F (**222** and **230**; Scheme 15). When the Boc-protected precursors **222** and **230** were treated with 4 N HCl in 1,4-dioxane at r.t. for one hour, a mixture of compounds was formed. However, only a single and desired product was detected under the same conditions in the case of variant **226**. The results suggested that only the C-terminal methoxypyridine was acid-labile, which was confirmed by HR-LCMS analysis of the crude product mixture for the reaction of compound **230** (Figure 17). The minor component of the mixture was identified as the desired Boc-deprotected tetrapeptide **231**. The methoxypyridine

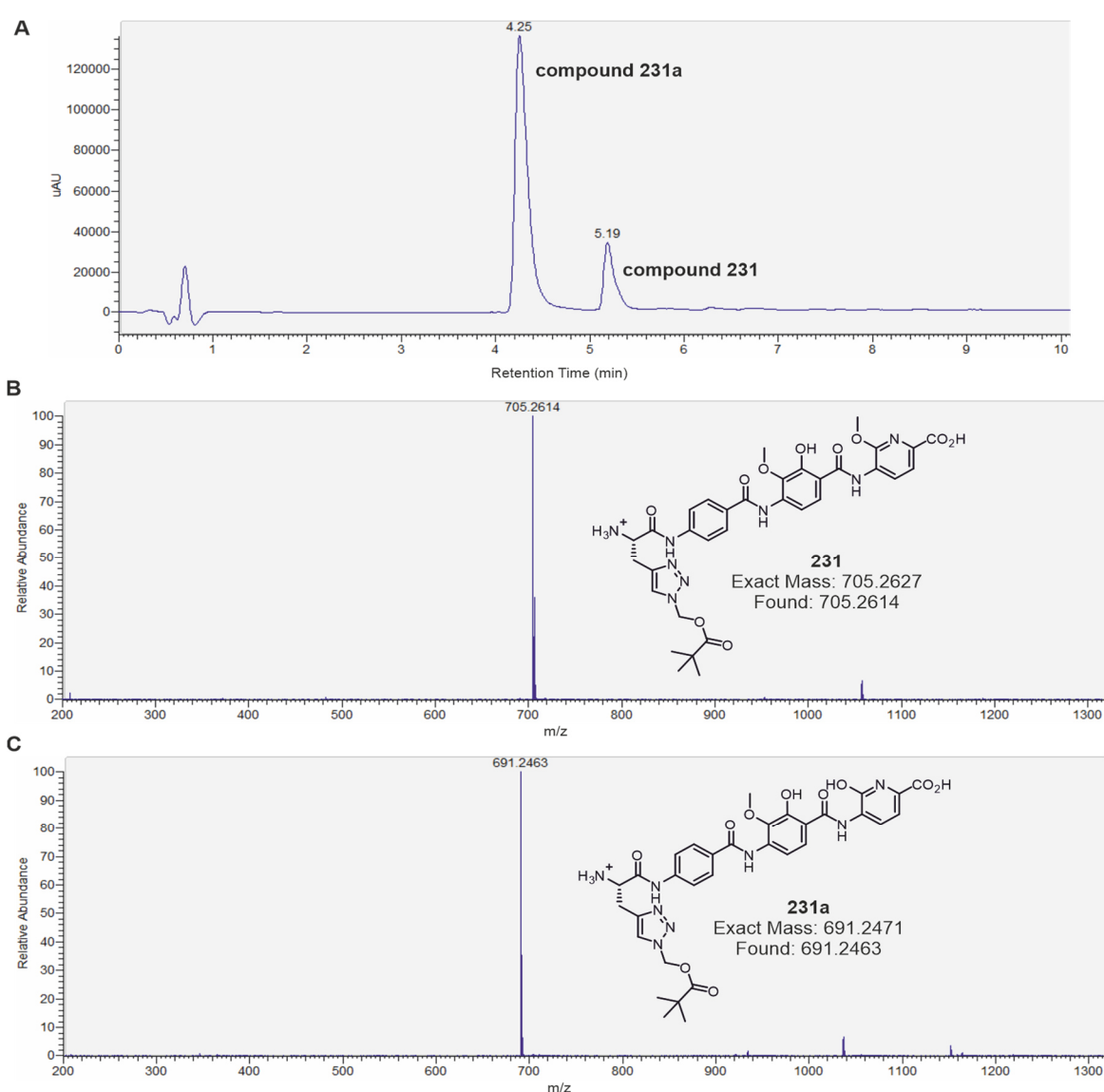
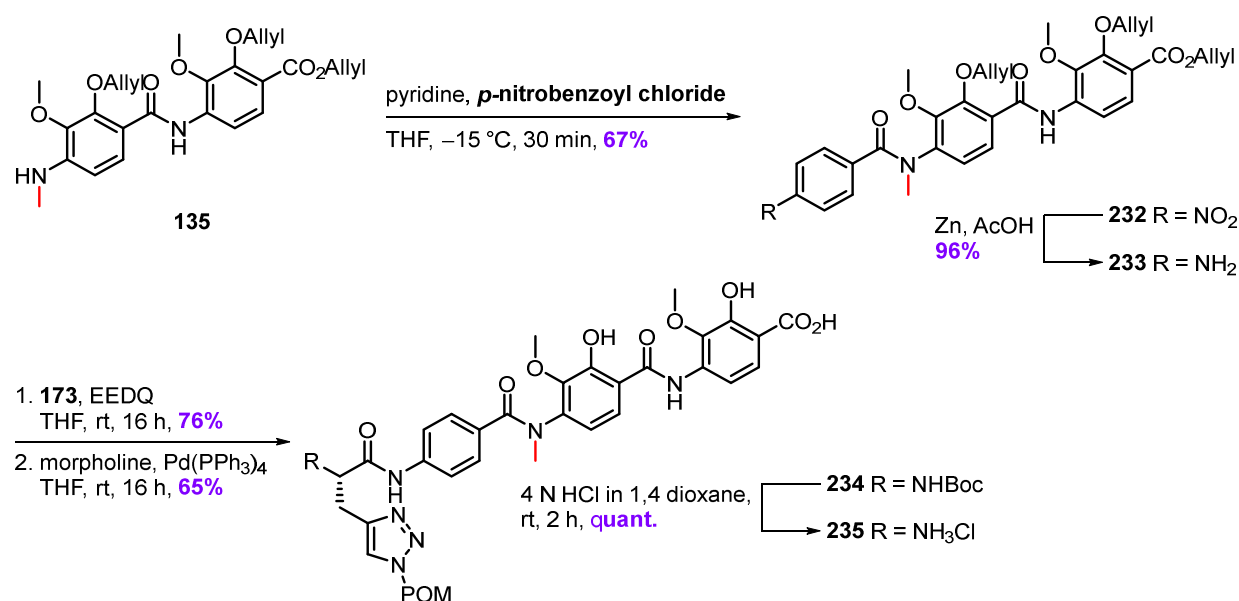


Figure 17. HR-LCMS analysis of the crude product mixture of 231 and 231a.

A. Excerpt of the UV chromatogram showing a mixture of two products. **B.** Extracted-ion chromatogram for the peak at $t_R = 5.19$ min reveals the minor analyte to be compound **231**. **C.** Extracted-ion chromatogram for the peak at $t_R = 4.25$ min shows the major analyte to be **231a**.

was then further converted to form the corresponding pyridone **231a**, which was shown to be the major component of the mixture. Repeating the reaction with trifluoroacetic acid (TFA) in dichloromethane and reducing the reaction time to only 15 min, finally afforded the desired product **231** in excellent yields again.

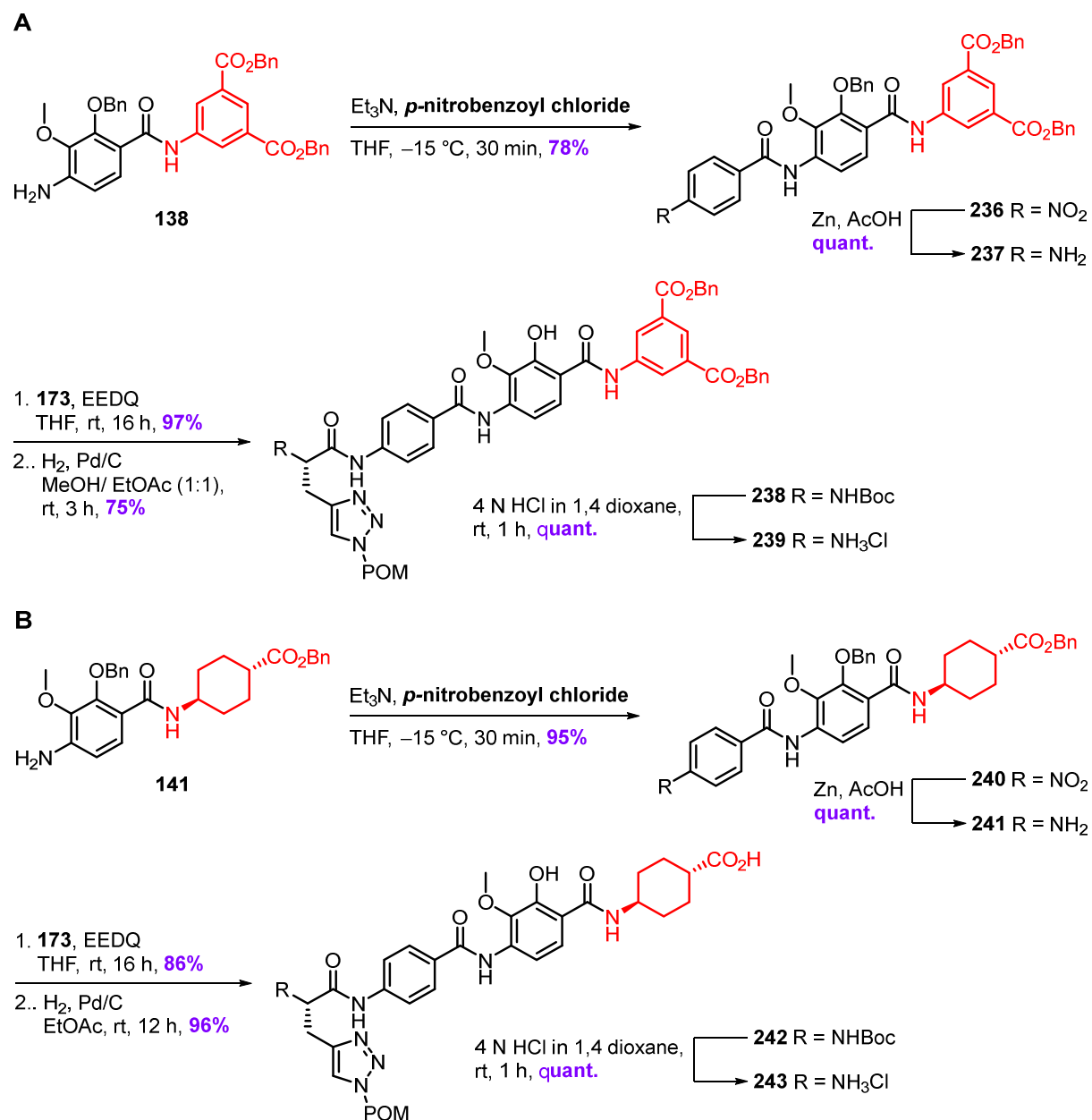
For the coupling of *p*NBC to the *N*-methylated E-F dipeptide **135**, pyridine turned out to be the more suitable base of choice than triethylamine (Scheme 16). When the latter was used, tripeptide **232** could only be detected in traces by MS. Presumably, the additional methyl group of **135** causes enough steric hindrance to stop the bulky triethylamine from deprotonating the methylated aniline when it is protonated to the corresponding hydrochloride by the HCl gas released during the reaction. Despite being less basic and a poorer HCl-scavenger than triethylamine, pyridine is a flat molecule that can potentially avoid repulsion by the methyl group and thus preserve the aniline's reactivity towards the electrophile by constantly deprotonating it.



Scheme 16. Synthesis of a C-D-E-F tetrapeptide containing an amide bond isostere.

Five-step linear synthesis of allyl- and Boc-deprotected tetrapeptide **235** starting from *N*-methylated dipeptide **135** via tripeptide **233**.

Finally, the pair of benzyl- and Boc-deprotected C-D-E-F tetrapeptides **239** and **243** containing isophthalic acid and cyclohexyl moieties as building block F, respectively, were synthesized analogously to the ethylene glycol-containing variant **219** in a straightforward fashion from the corresponding E-F dipeptides **138** and **141** (Scheme 17).



Scheme 17. Synthesis of isophthalic acid and cyclohexyl-containing C-D-E-F tetrapeptides.

A. Synthesis of dibenzoic acid derivative **239** starting from dipeptide **138** via tripeptide **237**. **B.** Synthesis of cyclohexyl derivative **243** starting from dipeptide **141** via tripeptide **241**.

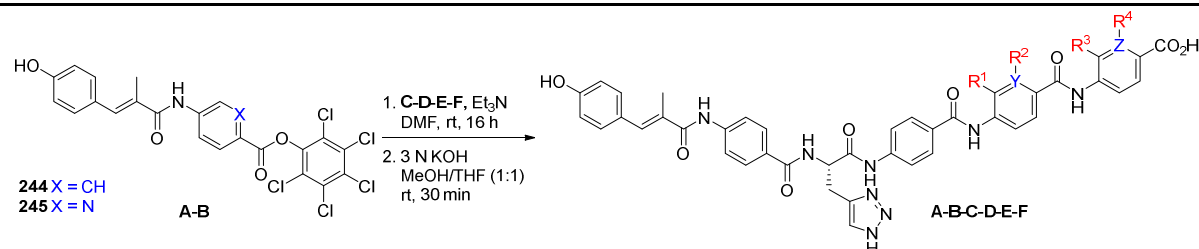
3.2.3 Final Assembly of E-F Derivatives of Albicidin

A [2+4] coupling strategy established in our group by Dr. Stefan Grätz was pursued to accomplish the final assembly of the full-length albicidin derivatives **34–55**.^[286] For this purpose, the preformed C-D-E-F tetrapeptide was coupled to an active ester of the corresponding A-B dipeptide. The activation of the dipeptides as pentachlorophenol (PCP) esters, rather than the previously used succinimide or azabenzotriazole (OAt) esters, led to higher reaction conversions and considerably facilitated the final purification step by reversed-phase preparative HPLC. The results for the syntheses of final albicidin analogs with sequential deletion of the substituents of the C-terminal dipeptide (**34–48**), sequential replacement of the methoxy groups with ethoxy groups (**49–51**), replacement of the methoxy group with an ethylene glycolyl moiety (**50**), and sequential replacement of the phenolic core structure with pyridines (**53–55**) are summarized in Table 2. After removing the solvent, the crude product of the initial coupling step was directly treated with 3 N KOH to remove the POM-protecting group of the AzaHis side chain and to saponify the remaining C-terminal methyl esters.

The targeted albicidin analogs were obtained from two consecutive steps in yields ranging from 2% for compound **41** to 25% for the doubly ethoxy-substituted derivative **49**. It is important to note that these yields do not adequately account for the conversion rate of the two-step reaction sequence. In general, full consumption of the tetrapeptides was achieved after 16 h and POM-deprotection was completed after 30 min. However, acidification of the basic solution after the final step led to the formation of a substantial amount of KCl that needed to be removed from the crude mixture. Since a simple aqueous workup was out of the question due to the relatively high polarity of the products, all volatiles, including water, were completely removed under reduced pressure and the solid residue taken up in DMSO. The resulting suspension was centrifuged, and the supernatant was directly injected into the preparative HPLC for the final purification. Despite washing the sediment multiple times with DMSO, a fair amount of product most likely remained in the pellet. In total, costly sample preparation in combination with losses attributable to the purification itself, as only the purest fractions were collected, amounted to the poor yields. As an example of a purified compound, the proton NMR spectrum for the ethylene glycol-containing derivative **52**, which features two characteristic triplet signals for the methylene units, is depicted in Figure 18.

Table 2. Syntheses of final albicidin derivatives with modified pABAs (Part 1).

A [2+4] assembly of final albicidin analogs with sequential deletion of the substituents of the C-terminal dipeptide (**34–48**), sequential replacement of the methoxy groups with ethoxy groups (**49–51**), replacement of the methoxy group with an ethylene glycolyl moiety (**50**), and sequential replacement of the phenolic core structure with pyridines (**53–55**) is depicted.



C-D-E-F	A-B-C-D-E-F	R ¹	R ²	R ³	R ⁴	X/Y/Z	Yield (2 steps)
175	34	H	OH	OMe	OH	C/C/C	8%
177	35	OMe	H	OMe	OH	C/C/C	5%
179	36	OMe	OH	H	OH	C/C/C	14%
181	37	OMe	OH	OMe	H	C/C/C	19%
183	38	H	H	OMe	OH	C/C/C	5%
185	39	H	OH	H	OH	C/C/C	6%
187	40	H	OH	OMe	H	C/C/C	23%
189	41	OMe	H	H	OH	C/C/C	2%
191	42	OMe	H	OMe	H	C/C/C	22%
193	43	OMe	OH	H	H	C/C/C	5%
195	44	H	H	H	OH	C/C/C	9%
197	45	H	H	OMe	H	C/C/C	18%
199	46	H	OH	H	H	C/C/C	12%
201	47	OMe	H	H	H	C/C/C	9%
203	48	H	H	H	H	C/C/C	12%
207	49	OEt	OH	OEt	OH	C/C/C	25%
211	50	OEt	OH	OMe	OH	C/C/C	21%
215	51	OMe	OH	OEt	OH	C/C/C	20%
219	52	OMe	OH	OEtOH	OH	N/C/C	14%
223	53	OMe	—	OMe	—	C/N/N	20%
227	54	OMe	—	OMe	OH	N/C/C	4%
231	55	OMe	OH	OMe	—	C/C/N	13%

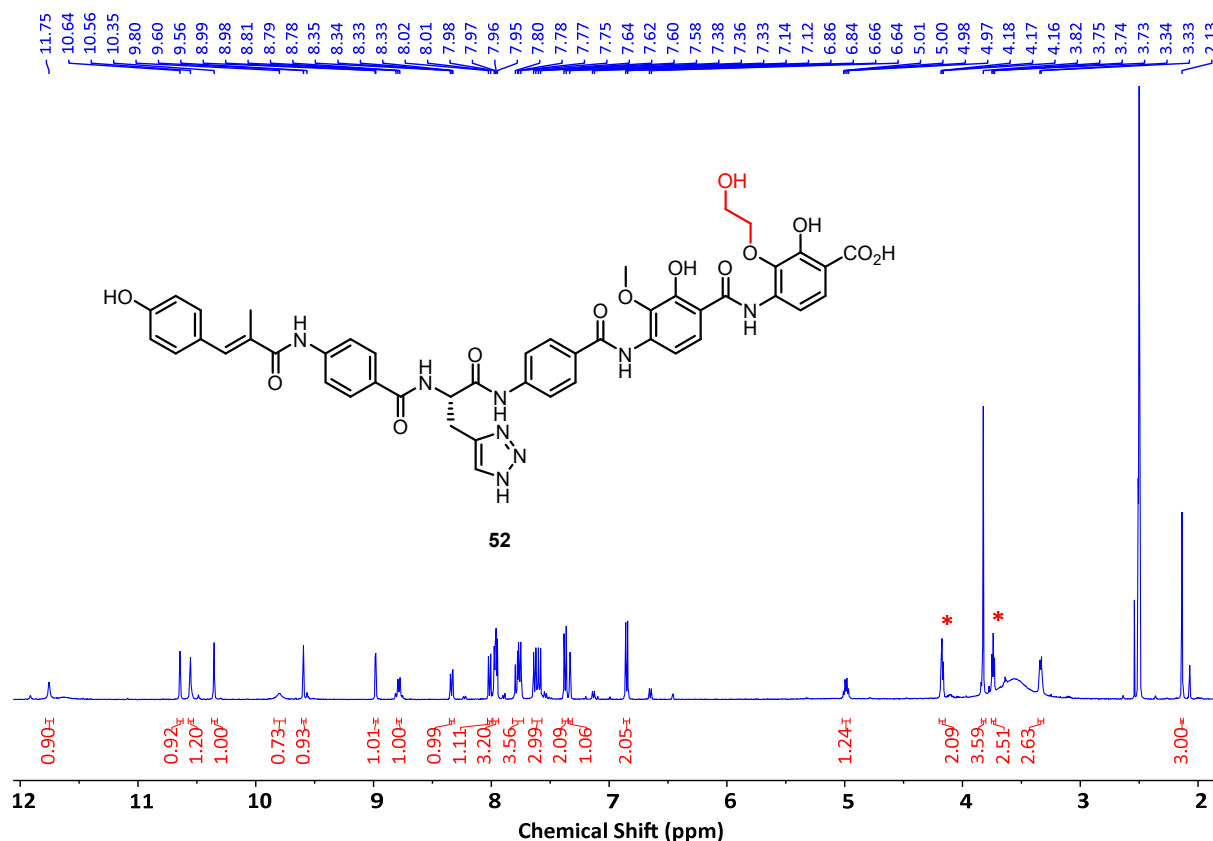
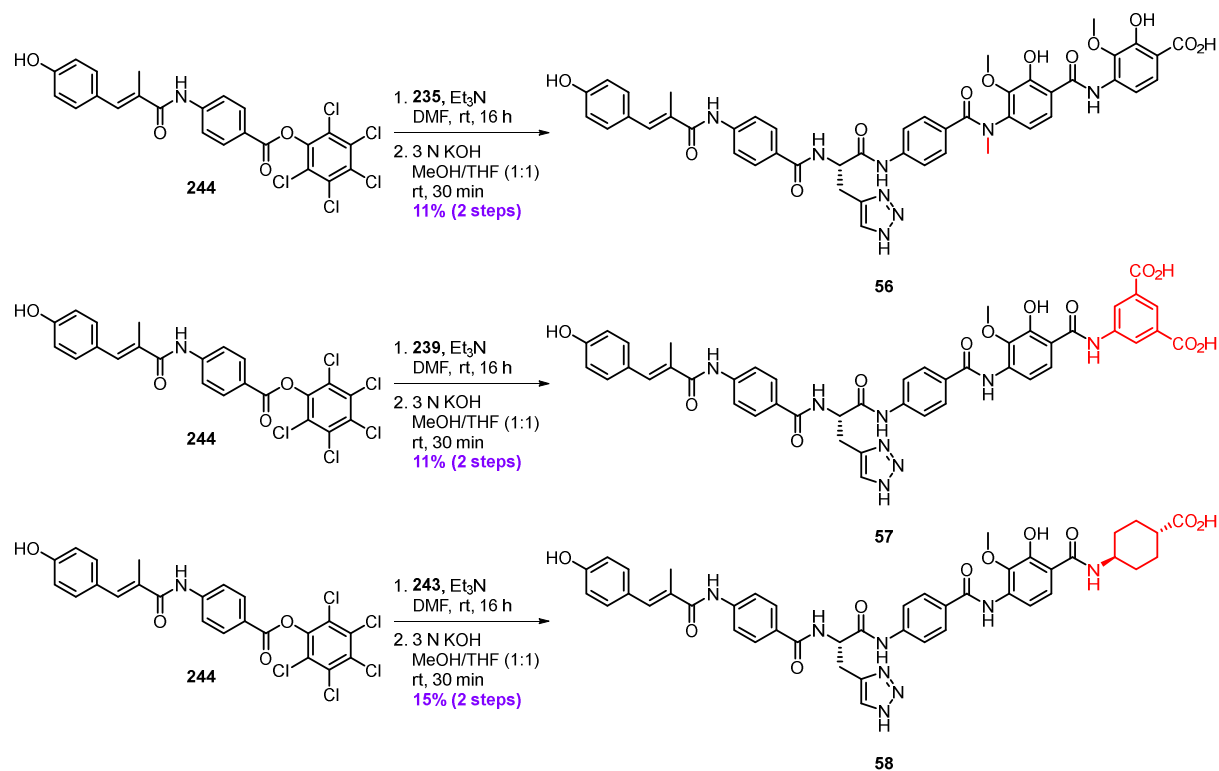


Figure 18. Proton NMR spectrum of ethylene glycol-containing albicidin derivative 52.

The two triplet signals of the methylene units of the glycol ether are highlighted with asterisks.

The final assembly of the remaining albicidin derivatives with modified E-F building blocks was again accomplished using the PCP-ester strategy (Scheme 18). Starting from the preassembled tetrapeptides **235**, **239**, and **243**, albicidin analogs **56–58** bearing an *N*-methylated amide bond isostere, an isophthalic acid moiety, and a cyclohexyl ring, respectively, were obtained in yields of 11–15% after purification by preparative HPLC. Provided that the retention time (t_R) observed by HR-LCMS is indicative of solubility, the dibenzoic acid variant **57** ($t_R = 7.15$ min) is likely to demonstrate a higher aqueous solubility than AzaHis-albicidin **16** ($t_R = 7.89$ min). The same would be true to a lesser extent for the cyclohexyl-containing compound **58** ($t_R = 7.63$ min).

**Scheme 18. Syntheses of final albicidin derivatives with modified *p*ABAs (Part 2).**

Two-step assembly of final albicidin analogs bearing an amide bond isostere (**56**), an isophthalic acid moiety (**57**), and a cyclohexyl ring (**58**).

In addition to the three singlet signals observed for natural albicidin, the proton NMR spectrum of the *N*-methylated variant **56** clearly shows a fourth singlet representing the newly introduced methyl group as a part of the amide bond surrogate (Figure 19).

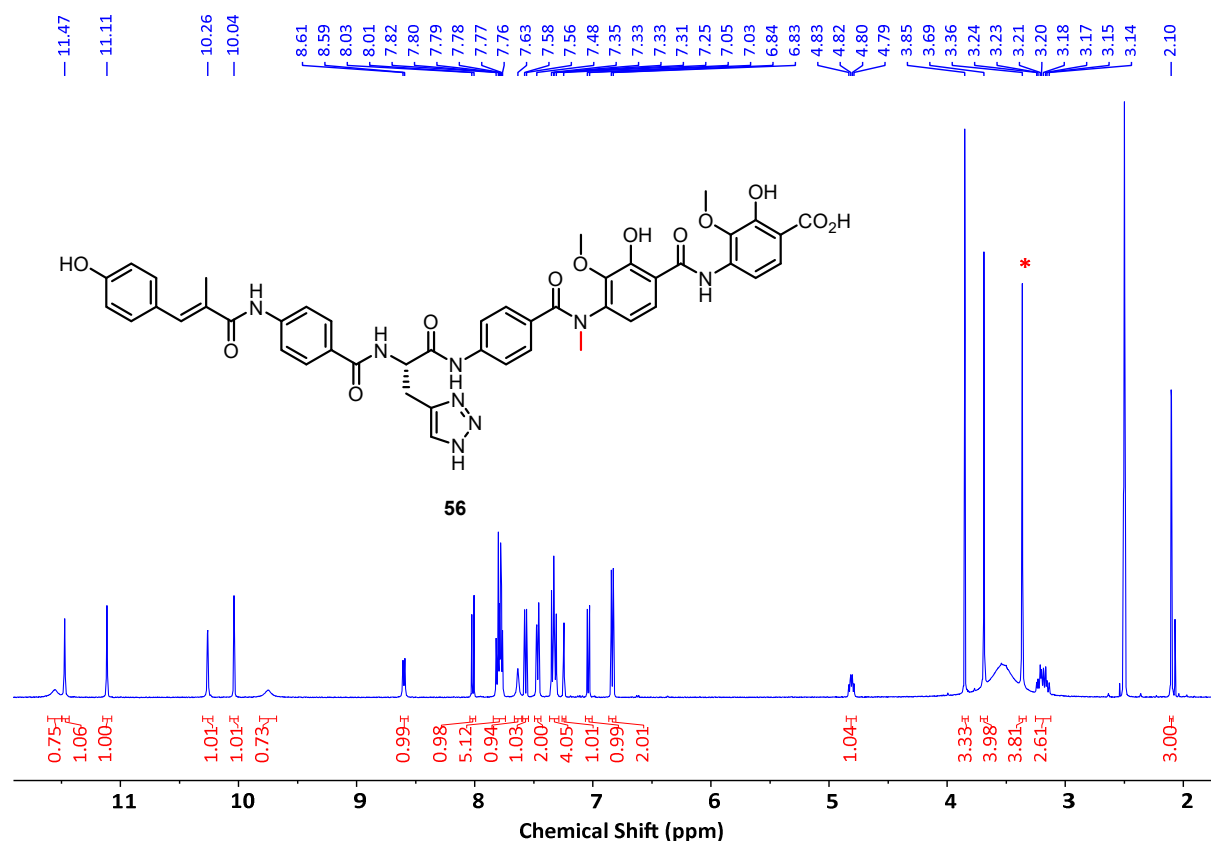


Figure 19. Proton NMR spectra of *N*-methylated albicidin derivative **56.**

The singlet signal of the newly introduced methyl group is highlighted with an asterisk.

3.2.4 Biological Evaluation of E-F Derivatives of Albicidin

The 25 newly synthesized albicidin derivatives with variations of the C-terminal E-F dipeptide were tested for their antimicrobial activities against a broad panel of S1 (Table 3) and S2 (Table 4) pathogens, including members of the particularly important *ESKAPE* group. For compounds **34–48**, it was found that removing any number of substituents led to a varying spectrum of potency but generally reduces overall activity. The MIC values for trisubstituted variants **34–37** suggest that the methoxy group in building block E is the most critical one regarding single deletions. For compound **34**, its absence leads to a significant drop of activity against both CIP sensitive and resistant strains of *S. aureus*, *B. subtilis*, and *M. luteus*, while the potency against the remaining panel, including all *E. coli* strains, remains similar for **34–37**. In general, the activity against Gram-positive pathogens gradually decreases with an increasing number of deletions of functional groups in E and F, leading to a complete loss of activity for the unsubstituted variant **48** and the monosubstituted derivatives **44–47**. Despite the lack of all substituents, the overall activity against Gram-negative pathogens only slightly decreases for

*p*ABA-*p*ABA analog **48**. Contrary to the remaining analogs from the deletion sequence, compound **16**, which bears a single methoxy group in building block E, displays an exceptionally low potency against all tested Gram-negative pathogens.

Although all ethoxy-substituted analogs showed high to very high activities throughout the series of tested pathogens – except for *Klebsiella* strains – the doubly ethoxy-substituted analog **49** stands out. It displays an increased spectrum of activity and the highest potency against Gram-positive *B. subtilis*, *M. phlei*, and most importantly CIP sensitive and resistant *S. aureus*. Remarkably, variant **49** is also highly potent on a CIP resistant strain of Gram-negative *A. baumannii*, with MIC values below those of compound **16** by a factor of 65. These results verify the trend that more hydrophobic substituents than the methoxy group are favorable for bioactivity. Previously, *iso*-propoxy groups have been shown to be beneficial for the antibacterial potency of natural albicidins and cystobactamids.^[271,280] However, recent experiments conducted in our group suggest that they are also detrimental to drug development purposes due to low solubility and high plasma protein binding (unpublished results). Therefore, the ethoxy group appears to constitute a threshold of tolerance regarding hydrophobicity that still displays bioactivity in the presence of plasma (data not shown). The ethylene glycol containing derivative **52** was only tested against the S1 panel of pathogens and showed a slightly diminished activity against Gram-negative strains compared to its parent compound **16**. Unlike the latter, it is completely inactive against *B. subtilis* but preserves moderate activity against *M. luteus*, and *M. phlei*. Based on the retention time during HR-LCMS analysis, compound **52** ($t_R = 7.96$ min) does not have a higher solubility than than azahis-albicidin **16** ($t_R = 7.89$ min).

Replacing the phenolic core structure of the E-F dipeptide with pyridines had diverse effects on the bioactivity of compounds **53–55**. While introducing a methoxypyridine as building block E only had a minor effect on the overall activity of **54**, a significant decrease of activity, particularly against the very important *P. aeruginosa* strains, was observed for variants **53** and **55**. Possibly, the deleterious effect caused by the pyridine in building block F of compound **55** is predominant and explains the poor activity observed for **53** as well. One could conclude that the hydroxy group in building block F is imperative, but a direct comparison of **55** with the trisubstituted and still active analog **37** negates that assumption and makes adverse electronic

Table 3. MIC values for albicidin derivatives with modified E-F building blocks (S1 panel).

MIC values are given in $\mu\text{g}\cdot\text{mL}^{-1}$ for ciprofloxacin (CIP), albicidin (**1**), AzaHis-albicidin **16**, and newly synthesized analogs **34–58** for an S1 panel of selected Gram-negative (*E. coli*, and *S. typhimurium*) and Gram-positive (*B. subtilis*, *M. luteus*, and *M. phlei*) bacteria. For a better overview, the activity is highlighted by a color code: 0.016–0.125 (dark green), 0.25–4.0 (light green), 8.0 (light red).

Entry	R ¹	R ²	R ³	R ⁴	<i>E. coli</i> DSM1116	<i>E. coli</i> BW25113	<i>S. typhimurium</i> TA100	<i>B. subtilis</i> DSM10	<i>M. luteus</i> DSM1790	<i>M. phlei</i> DSM750
CIP	OMe	OH	OMe	OH	0.063	0.063	0.063	0.25	1.0	2.0
1	OMe	OH	OMe	OH	0.063	0.063	0.063	0.25	1.0	2.0
16	OMe	OH	OMe	OH	0.016	n.d.	0.016	0.125	0.5	4.0
34	H	OH	OMe	OH	0.125	0.063	0.125	4.0	8.0	2.0
35	OMe	H	OMe	OH	0.125	0.125	0.063	1.0	2.0	2.0
36	OMe	OH	H	OH	0.125	0.031	0.016	0.5	0.5	1.0
37	OMe	OH	OMe	H	0.25	0.125	0.063	0.25	1.0	2.0
38	H	H	OMe	OH	0.063	0.031	0.063	4.0	8.0	4.0
39	H	OH	H	OH	0.125	0.063	0.016	1.0	0.5	2.0
40	H	OH	OMe	H	0.125	0.125	0.125	1.0	8.0	2.0
41	OMe	H	H	OH	0.25	0.125	0.125	2.0	4.0	4.0
42	OMe	H	OMe	H	1.00	0.25	0.25	1.0	4.0	8.0
43	OMe	OH	H	H	0.25	0.125	0.016	0.5	2.0	1.0
44	H	H	H	OH	0.25	0.063	0.125	8.0	8.0	8.0
45	H	H	OMe	H	0.25	0.063	0.125	8.0	8.0	8.0
46	H	OH	H	H	0.25	0.063	0.063	2.0	8.0	8.0
47	OMe	H	H	H	4.0	4.0	2.0	8.0	8.0	8.0
48	H	H	H	H	0.125	0.063	0.031	8.0	8.0	8.0
49	OEt	OH	OEt	OH	0.031	0.016	0.016	0.031	0.5	0.5
50	OEt	OH	OMe	OH	0.031	0.016	0.031	0.125	0.125	1.0
51	OMe	OH	OEt	OH	0.031	0.016	0.016	0.5	0.125	0.5
52	OMe	OH	OEtOH	OH	0.125	0.25	0.031	8.0	2.0	4.0
53	OMe	–	OMe	–	0.5	1.0	0.5	4.0	2.0	8.0
54	OMe	–	OMe	OH	0.063	0.063	0.016	0.5	0.25	1.0
55	OMe	OH	OMe	–	0.5	0.5	0.25	4.0	8.0	8.0
56	<i>N</i> -methylated albicidin				8.0	8.0	8.0	8.0	8.0	8.0
57	isophthalic acid albicidin				8.0	8.0	8.0	8.0	8.0	8.0
58	cyclohexyl albicidin				8.0	8.0	8.0	8.0	8.0	8.0

effects and *H*-bonding interactions between the nitrogen atom of the pyridine and the adjacent carboxyl group more likely.

The remaining compounds tested, including the *N*-methylated derivative **56**, isophthalic acid variant **57**, and the aliphatic cyclohexyl analog **58**, all turned out to be completely inactive in the MIC assays. An MS-cleavage experiment in the presence of AlbD was conducted for **56** to examine the stability of the amide bond surrogate. Simple *N*-methylation of the amide bond did not suffice to impede enzymatic cleavage. The results of additional peptide bond isosteres examined in our group have been published recently.^[273] There, a triazole moiety was identified as a viable structural motif to overcome cleavage by AlbD while preserving biological

Table 4. MIC values for albicidin derivatives with modified E-F building blocks (S2 panel). MIC values are given in $\mu\text{g}\cdot\text{mL}^{-1}$ for ciprofloxacin (CIP), albicidin (1), Azahis-albicidin 16, and newly synthesized analogs 34–51 and 53–56 for an S2 panel of selected Gram-negative (*E. coli*, *K. pneumoniae*, *A. baumannii*, and *P. aeruginosa*) and Gram-positive (*E. faecium*, *S. aureus*, and *S. Kentucky*) bacteria. For a better overview, the activity is highlighted by a color code: 0.016–0.125 $\mu\text{g}\cdot\text{mL}^{-1}$ (dark green), 0.25–4.0 $\mu\text{g}\cdot\text{mL}^{-1}$ (light green), 8.0–32.0 $\mu\text{g}\cdot\text{mL}^{-1}$ (light red), 64.0–128.0 $\mu\text{g}\cdot\text{mL}^{-1}$ (dark red).

Entry	R ¹	R ²	R ³	R ⁴	<i>E. coli</i> CIP res.	<i>E. coli</i> CIP sens.	<i>K. pneumoniae</i> CIP sens.	<i>A. baumannii</i> CIP res.	<i>P. aeruginosa</i> CIP res.	<i>P. aeruginosa</i> CIP sens.	<i>E. faecium</i> CIP res.	<i>E. faecium</i> CIP sens.	<i>S. aureus</i> CIP res.	<i>S. aureus</i> CIP sens.	<i>S. Kentucky</i> CIP res.	<i>S. Kentucky</i> CIP sens.
CIP					32.0	0.016	0.063	32.0	32.0	0.063	128.0	0.125	128.0	0.125	16.0	0.016
1	OMe	OH	OMe	OH	0.125	0.031	128.0	2.0	2.0	1.0	16.0	2.0	4.0	2.0	0.5	0.125
16	OMe	OH	OMe	OH	0.063	0.016	16.0	2.0	8.0	4.0	64.0	0.25	4.0	2.0	0.25	0.063
34	H	OH	OMe	OH	0.5	0.5	128.0	8.0	32.0	32.0	128.0	8.0	32.0	32.0	1.0	0.25
35	OMe	H	OMe	OH	0.5	0.25	128.0	8.0	32.0	16.0	8.0	4.0	16.0	4.0	1.0	0.125
36	OMe	OH	H	OH	0.5	0.25	128.0	8.0	32.0	4.0	16.0	2.0	2.0	1.0	0.25	0.125
37	OMe	OH	OMe	H	0.5	0.5	128.0	8.0	32.0	8.0	16.0	4.0	4.0	2.0	1.0	0.25
38	H	H	OMe	OH	0.5	0.25	128.0	8.0	32.0	32.0	32.0	16.0	32.0	8.0	0.25	0.125
39	H	OH	H	OH	0.5	0.25	128.0	8.0	32.0	8.0	16.0	16.0	2.0	1.0	0.25	0.125
40	H	OH	OMe	H	1.0	0.25	128.0	8.0	32.0	32.0	32.0	32.0	32.0	32.0	1.0	0.5
41	OMe	H	H	OH	1.0	0.25	32.0	16.0	32.0	32.0	128.0	8.0	8.0	4.0	0.5	0.25
42	OMe	H	OMe	H	2.0	0.5	128.0	16.0	32.0	32.0	128.0	32.0	8.0	4.0	0.5	0.5
43	OMe	OH	H	H	0.5	0.125	32.0	1.0	32.0	4.0	128.0	4.0	2.0	2.0	0.25	0.5
44	H	H	H	OH	0.5	0.125	16.0	4.0	32.0	32.0	128.0	4.0	2.0	2.0	0.25	0.125
45	H	H	OMe	H	0.5	0.25	128.0	4.0	32.0	32.0	128.0	128.0	32.0	32.0	0.25	0.25
46	H	OH	H	H	0.5	0.125	128.0	4.0	32.0	32.0	128.0	128.0	32.0	32.0	0.25	0.25
47	OMe	H	H	H	32.0	32.0	128.0	32.0	32.0	32.0	128.0	128.0	32.0	32.0	32.0	32.0
48	H	H	H	H	0.25	0.063	128.0	1.0	32.0	32.0	128.0	128.0	32.0	32.0	0.25	0.125
49	OH	OH	OH	OH	0.031	0.016	16.0	0.031	2.0	0.5	32.0	0.25	0.063	0.031	0.063	0.063
50	OH	OH	OMe	OH	0.25	0.031	128.0	0.5	64.0	64.0	128.0	0.063	0.063	0.063	0.125	0.063
51	OH	OH	OH	OH	0.5	0.031	128.0	0.5	4.0	1.0	128.0	0.063	0.125	0.125	0.063	0.125
53	OMe	-	OMe	-	8.0	4.0	128.0	128.0	128.0	128.0	64.0	2.0	16.0	8.0	16.0	8.0
54	OMe	-	OMe	OH	0.25	0.031	64.0	4.0	128.0	128.0	8.0	0.25	2.0	1.0	0.25	0.25
55	OMe	OH	OMe	-	8.0	2.0	128.0	128.0	128.0	128.0	128.0	128.0	16.0	16.0	8.0	4.0
56	N-methylated albicidin				128.0	128.0	128.0	128.0	128.0	128.0	128.0	128.0	128.0	128.0	128.0	128.0

activity. A direct comparison between compound **58** and its highly active aromatic counterpart **43** underpins the important role of a planar and rigid building block F. Further experiments will have to show whether aromaticity is a prerequisite at this position.

The results of the target-directed *E. coli* gyrase assay (Figure 20) are only partly consistent with the results obtained from the cell-based MIC assay (Table 3 and Table 4). Compared to the parent compound **1**, the inhibitory activities of albicidin derivatives with single deletions of the methoxy or hydroxy groups (**34–37**) are mostly preserved. The read-out of the assay by the naked eye suggests that compound **36**, which lacks a methoxy group in building block F, has the poorest activity among the four compounds of that series. The simultaneous deletion of two substituents appears to have no to little diminishing effect on the inhibitory potency of compounds **38–41**. However, variant **42** forms an exception: Lacking both hydroxy groups of the C-terminal dipeptide, almost only supercoiled DNA can be observed on the agarose gel, which is indicative for unimpeded gyrase activity. Removing all substituents, but the methoxy group in building block F, completely inactivates albicidin analog **47**. And with only the hydroxy moiety of building E in place, compound **46** suffers from a slightly decreased potency compared to **1**. The remarkably strong activity against Gram-negative bacteria observed in the MIC assay for the *pABA-pABA* analog **48** is also reflected in its gyrase-inhibiting capacity, which resembles that of the natural product.

The exceptionally high antibacterial activities observed for the ethoxy-substituted derivatives **49–51** in the cell-based assay are mirrored by their outstanding activity in the target-directed assay. This is not true for the ethylene glycol-containing derivative **52**, which is almost completely inactive in the gyrase assay. Another inconsistency is given for the heterocyclic albicidin variants **53–55**, with compound **54** displaying similar activity to **1**, while analogs **53** and **55** hardly inhibit gyrase at all. Surprisingly, the *N*-methylated albicidin analog **56**, which is completely inactive in the MIC assay, displays a moderate gyrase-inhibiting activity. Since there is clearly an interaction with albicidin's primary target, it needs to be determined with the help of additional experiments why no activity was observed against the sets of S1 and S2 pathogens. Presumably, the discrepancy can be traced back to albicidin resistance factors, which are known to impact the cellular uptake, enzymatic cleavage, and binding of albicidin

and its derivatives. As expected, the isophthalic acid and cyclohexyl variants **57** and **58** showed no activity in the gyrase assays at all.

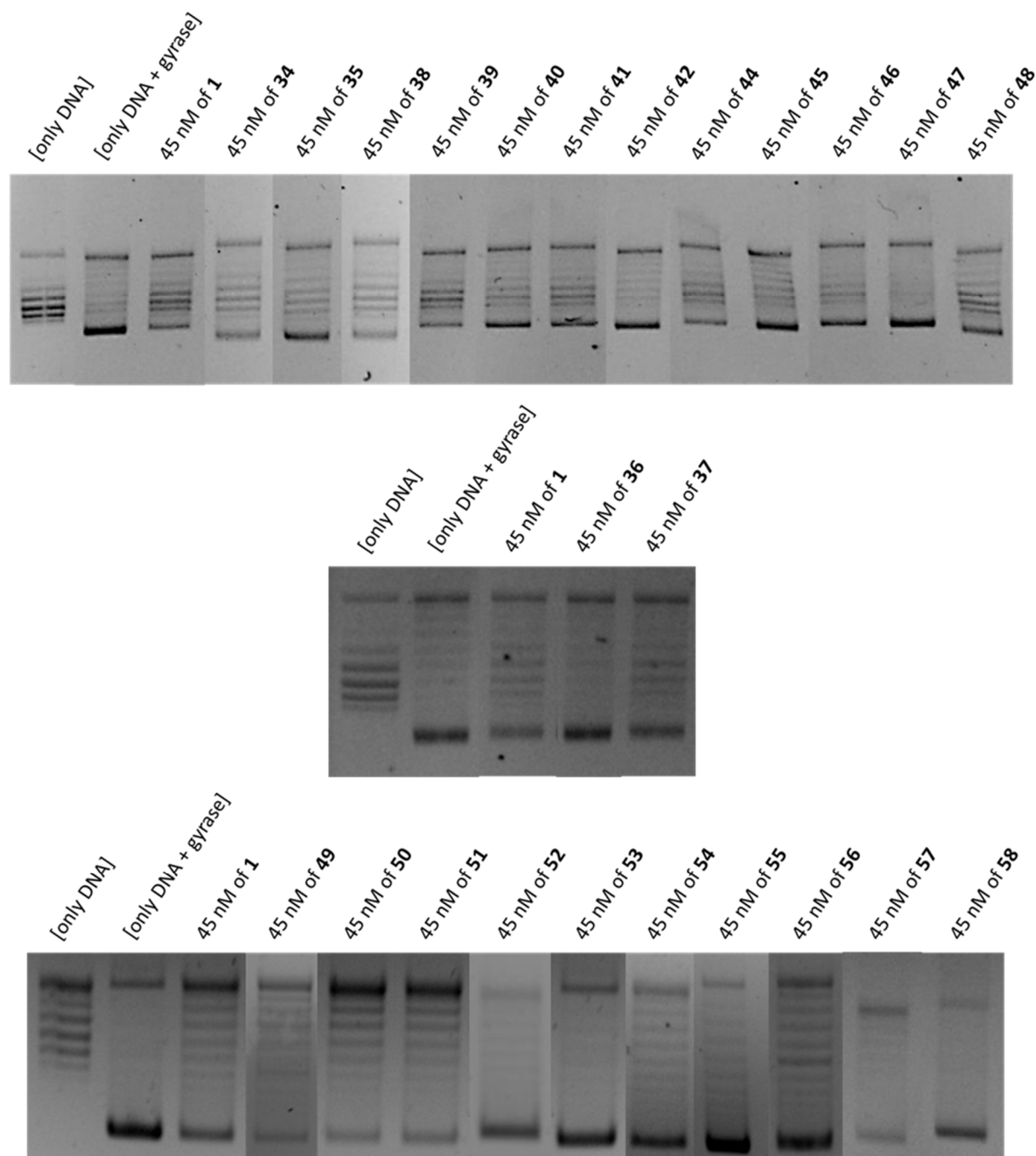


Figure 20. Gyrase inhibition assay for albicidin variants with modified E-F building blocks

Inhibition assay of the supercoiling activity of *E. coli* DNA gyrase for albicidin (**1**) and compounds **34**–**58**, except for **43**. The control experiment without enzyme and drug (left lane) shows relaxed DNA. Addition of DNA gyrase results in supercoiled DNA (second lane from left). All derivatives were tested at a concentration of 45 nM.

3.3 Derivatives with Variations of the N-Terminal A-B Building Block

Previous studies on albicidin's N-terminal acyl group have demonstrated that antibacterial activity can be retained upon exchange of the hydroxy group in *para*-position of the aromatic ring.^[269] However, every derivative with considerable activity reported thus far contained an (*E*)-configured cinnamoyl residue and was connected to the adjacent *p*ABA unit through an amide bond linker. In 1985, Birch and Patil had observed that albicidin gradually converted into another compound when stored in methanol at room temperature. This compound, which eluded before the natural product during HPLC analysis, exhibited diminished antibacterial activity.^[180] However, with the structure of albicidin being unknown at that time, the nature of the conversion also remained concealed. Similarly, in 2016 DR. STEFAN GRÄTZ observed a shoulder in the UV chromatogram of albicidin and some of its derivatives during purification by preparative HPLC. Knowing by then that the molecule contained many aryl amides as well as a cinnamoyl residue, he and DR. ANDI MAINZ considered both atropisomerism^[287] and (*E*)-(*Z*)-isomerism as potential causes for the conversion and validated the latter effect by performing a 2D NOESY experiment.^[286] In the past, cinnamates and their hydroxy derivatives, including *para*-coumaric acid, caffeic acid, ferulic acid, and sinapic acid, have been shown to rapidly undergo light-induced (*E*)-(*Z*)-isomerization and dimerization, e.g. in plant cell walls. The former two are known to isomerize from the (*E*)-form to the (*Z*)-form, and to a lesser degree in the opposite direction, to form an equilibrium mixture in which the (*E*)-isomer is the main component.^[279,288–290] The photoisomerization of cinnamamides is highly dependent on both *N*-alkylation and aromatic substitution.^[291,292]

To demonstrate the photochemical (*E*)-(*Z*)-isomerization for the cinnamoyl residue, a solution of freshly prepared albicidin (**1**) in DMSO-*d*₆ was exposed to UV light ($\lambda = 365$ nm) and monitored by ¹H NMR spectroscopy (Figure 21, A). The signals for the methyl group, the vinyl proton, and the *ortho*-protons of the aromatic ring are shifted upfield, indicating the presence of the (*Z*)-isomer. While only a small portion of the sample was converted after *t* = 2.5 h compared to the initial state (*t* = 0 h), almost complete conversion was detected after *t* = 16 h. At this point, the equilibrium state had already been reached and no further conversion was observed at *t* = 32 h. Interestingly, a separate experiment showed that by replacing the *para*-hydroxy group with an electron-withdrawing fluorine, the conversion can be slowed down

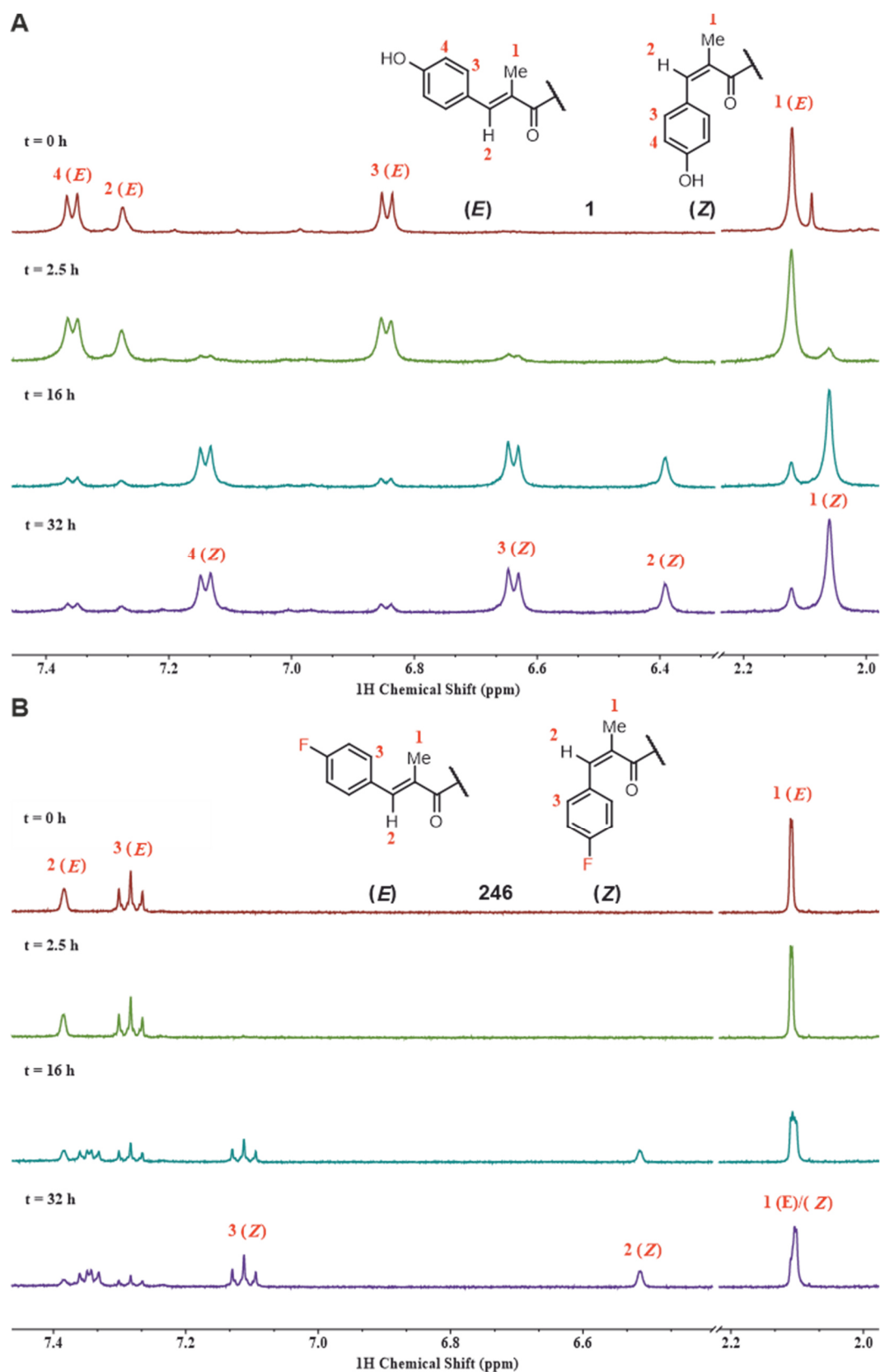


Figure 21. Photochemical (E)-(Z)-isomerization of albicidin's cinnamoyl residue.

Solutions of albicidin (**1**) (spectrum A) and fluoro-albicidin (**246**) (spectrum B) in DMSO-*d*₆ were each exposed to UV light ($\lambda = 365$ nm) and the conversion was monitored by ¹H NMR spectroscopy for 32 h to demonstrate the light-induced isomerization of albicidin's methacrylamide moiety.

(Figure 21, B). After 32 h, approximately 85% of the disfavored (*Z*)-isomer was present in the albicidin sample, compared to only 65% for the corresponding fluoro analog.

To circumvent this problem, a synthetically feasible structural modification was envisioned that could be considered a surrogate for *trans*-configured amide bonds and mimic the planarity and rigidity of albicidin's natural A-B building block while increasing its photochemical stability. We sought to replace the methacrylamide moiety between the cinnamate and the *p*ABA (building block B) with an alkyne, thus replacing the cinnamoyl-*p*ABA with diarylalkyne carboxylates. Hoping that a direct acetylenic linker between the two aromatic rings would be a viable replacement, a set of five acetylenic albicidin derivatives with varying substituents in the *para*-position of the N-terminal aromatic ring was synthesized (Figure 22, **247–251**). Based on previous findings^[269], the lipophilic methoxy and fluoro groups were included in addition to the “hydroneutral” cyano group and the hydrophilic hydroxy group.^[293] Methoxypyridine **249** was included to test the effect of a heterocyclic replacement of the aromatic ring adjacent to the *para*-substituent on the biological activity of these derivatives.

The use of the ethynyl group in pharmacologically active compounds dates back to as early as 1961 when the syntheses of analgesics of the prodine type containing ethynyl or substituted ethynyl groups in place of the 4-phenyl residue were reported.^[294] Ever since the acetylene group has been utilized as a potency enhancer, reactive warhead, nonpolar linear spacer, and nonclassical bioisostere. In the latter case it has served as a replacement for cyano, chloro, iodo, ethylene, carbonyl, ethyl, phenyl, cyclopropyl, and carboxamide groups.^[295] Among the few examples of FDA-approved drugs bearing internal or terminal alkynes are the HIV-1 reverse transcriptase inhibitor efavirenz (Sustiva[®], Bristol-Myers Squibb)^[296,297] and alkyne-containing steroidal drugs. Concerning toxicity, the species-dependent metabolism of efavirenz was shown to produce nephrotoxic glutathione conjugates in rats – but not in humans^[298,299] – while the steroidal drugs danazol^[300] and 17 α -ethynylestradiol^[301] are associated with a mechanism-based inactivation of CYP450 in the liver. Consequently, the preclinical assessment of alkyne-containing drug candidates demands the evaluation of metabolic pathways across CYP450 isoforms as well as the screening for reactive metabolites.

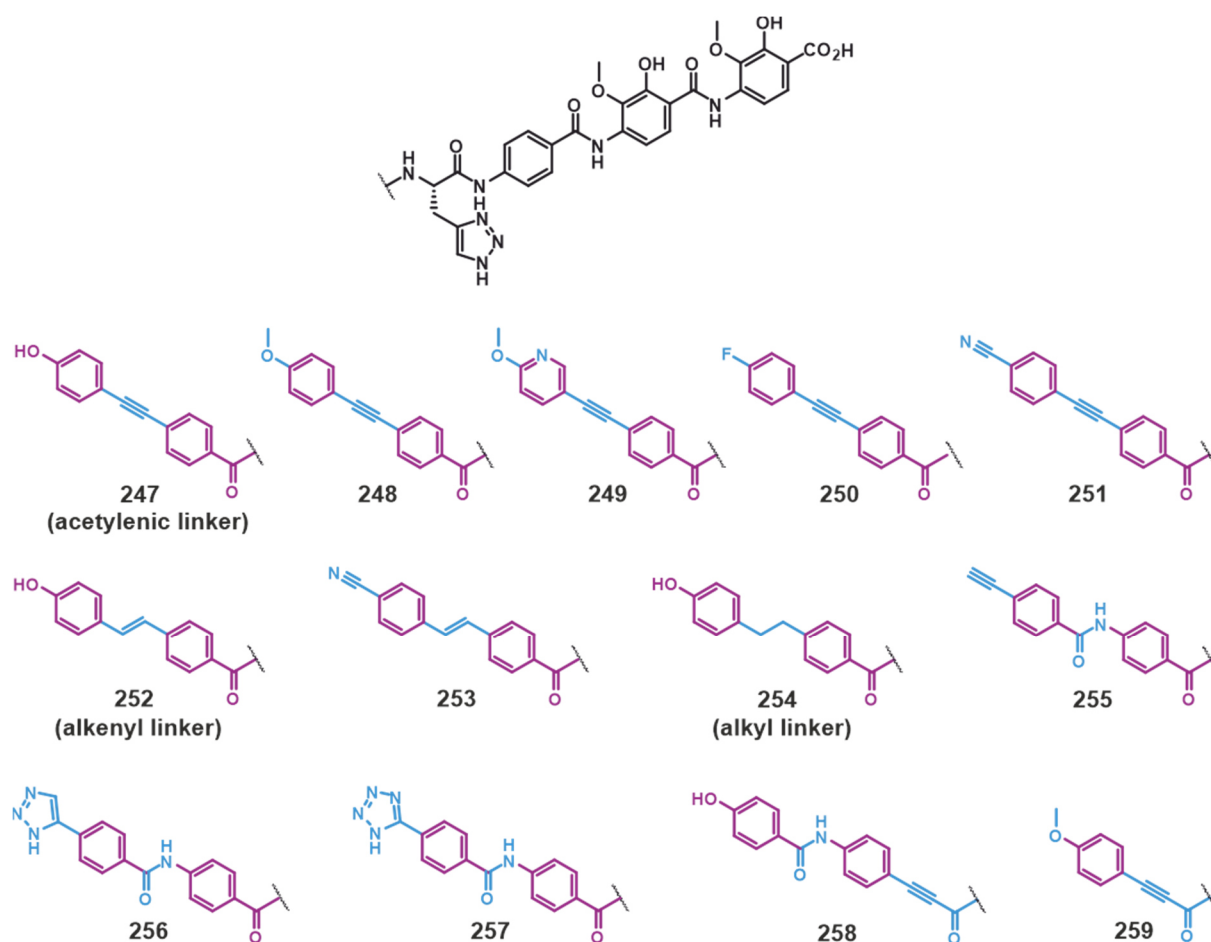


Figure 22. Structures of albicidin derivatives with variations of the A-B building block motif.

The set of compounds shown includes diaryl derivatives with acetylenic linkers (**247–251**), alkenyl linkers (**252** and **253**), and an alkyl linker (**254**). The remaining set comprises analogs bearing a terminal alkyne (**255**), a triazole ring (**256**), a tetrazole ring (**257**), a 4-hydroxybenzamide (**258**), and a truncated anisole (**259**). Unaltered structural features of albicidin are highlighted in purple. All deviations from the template structure are highlighted in blue.

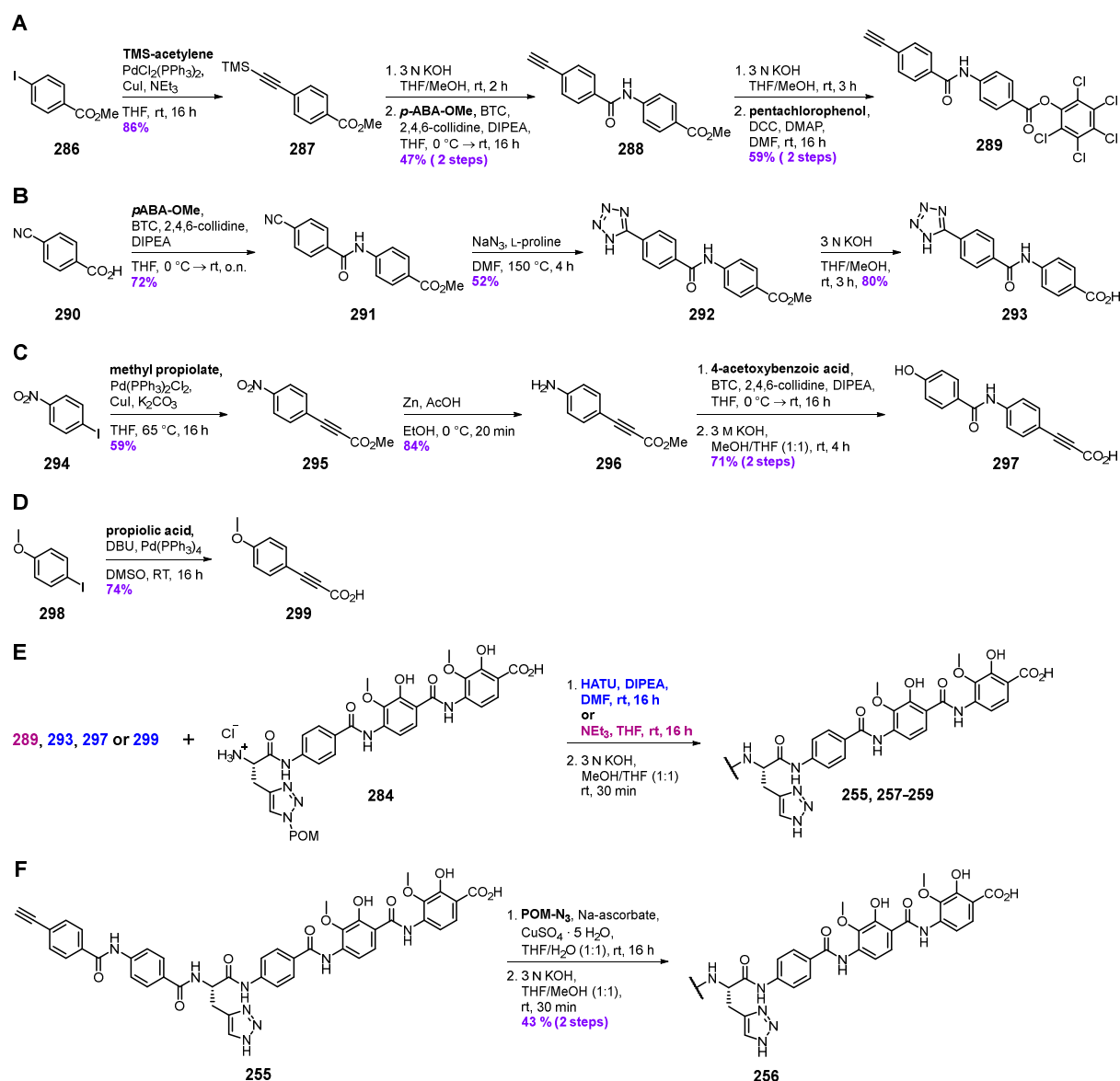
In addition to the diaryl alkyne motif as an alternative A-B building block, the corresponding *trans*-stilbene analogs **252** and **253** were prepared as well. Alkenes are prominent peptide bond isosteres because the C–C double bond closely mimics the C–N bond geometrically, while the electronic properties strongly differ from each other.^[302,303] To complete the picture, a fully saturated alkyl linker was incorporated into the molecule to give compound **254**. Being curious about the effect of an N-terminal alkyne on antibacterial efficacy, variant **255** was also added to the target list. With the terminal alkyne in place, a late-stage introduction of a triazole ring was projected to make analog **256**. Besides, derivative **257** bearing an acidic N-terminal head group was prepared by replacing the triazole ring with a tetrazole ring, which is commonly utilized in medicinal chemistry as a bioisosteric replacement for carboxylic

acids.^[304] Previously serving as an N-terminal head group (compound **255**) and as a direct linker between build blocks A and B (compounds **247–251**), the triple bond was relocated again to partake in the formation of an elongated hybrid alkyne-amide link between building blocks B and C. Thus, the 4-hydroxybenzamide **258** and the truncated anisole variant **259** complemented the list of newly synthesized A-B derivatives.

3.3.1 Syntheses of A-B Derivatives of Albicidin

The acetylenic A-B building blocks were prepared from commercially available aryl alkynes and aryl halides employing well-established Pd-mediated cross-coupling chemistry (Scheme 19, A-E).^[305,306] Having a fully saturated alkyl linker, compound **263** was prepared in a single step by catalytic hydrogenation of diaryl alkyne **262** (Scheme 19, A). The diaryl alkyne carboxylates **262**, **266**, **270** and **273** were then activated by HATU before being coupled to the preassembled tetrapeptide **284**. To prepare the cyano analog **251**, the carboxylate precursor **275** was activated by forming the corresponding PCP-ester **276** and coupled to the previously side-chain POM-deprotected tetrapeptide **285** (Scheme 19, H). This approach obviated the need for the final deprotection step using aqueous potassium hydroxide and thus preserved the nitrile. The commercially available styrene **278** was coupled to the aryl halides **277** and **281** through a HECK reaction to produce stilbenes **279** and **282**, respectively (Scheme 19, F and G).^[307] The final assembly of compounds **252** and **253** was achieved by employing the PCP-ester strategy described above.

The introduction of the N-terminal triple bond present in compound **255** was achieved by coupling the POM-protected tetrapeptide **284** to the activated acetylenic dipeptide **289**, the latter of which was prepared from methyl 4-iodobenzoate (**286**) in a five-step linear sequence initiated by a SONOGASHIRA reaction (Scheme 20, A).^[308] Subsequently, the alkyne in place was taken advantage of by performing a late-stage copper-catalyzed 1,3-dipolar cycloaddition of derivative **255** and POM-azide^[274], followed by removal of the protecting group to generate the triazole derivative **256** (Scheme 20, F).



Scheme 20. Syntheses of albicidin derivatives with modified A-B building blocks (Part 2).

A-D. Preparation of modified N-terminal building blocks **289**, **293**, **297**, and **299**. **E.** Assembly of final albicidin derivatives **255** and **257–259**. No coupling reagent was used for the reaction of PCP-ester **289** (red). All other A-B building blocks were coupled in the presence of HATU (blue). **F.** Synthesis of triazole **256** from its acetylenic precursor **255**.

The tetrazole-containing derivative **257** was prepared from benzonitrile **290** in five steps, involving an L-Pro catalyzed [3+2]-cycloaddition as the key step (Scheme 20, B and F).^[309] The 4-hydroxybenzamide **258** and the truncated anisole variant **259** were both synthesized from the readily available aryl iodides **294** and **298** employing the same synthetic strategies described above (Scheme 20, C and D).

3.3.2 Biological Evaluation of A-B Derivatives of Albicidin

To evaluate the antibacterial activity, MIC values were determined for the fluoroquinolone ciprofloxacin (CIP, reference standard), albicidin (**1**), AzaHis-albicidin (**16**) and the newly synthesized derivatives **247–259** for a panel of six different bacterial strains (Table 5). Also, a target-directed *E. coli* gyrase supercoiling assay was performed to determine the capacity of these compounds to inhibit albicidin's primary molecular target (Figure 23). We were pleased to find that the introduction of the acetylenic linker did not impair the antibacterial activity of the new compounds in the cell-based assay at all. Rather, all the tested derivatives remained highly active and produced MIC values in the range of albicidin (**1**). Regarding the *para*-substituents, the cyano analog **251** turned out to be the most active one, showing low MIC values like CIP and AzaHis-albicidin (**16**). As a direct comparison between the methoxy variant **248** and methoxypyridine **249** revealed, heterocyclic replacement of the aromatic ring did not have any effect on the activity of the compound. As expected, the loss of planarity and increased flexibility of compound **254**, as compared to the acetylenic analog **247**, led to a significant decrease of antibacterial activity of the molecule. For instance, an eightfold increase of MIC values was determined for both tested *E. coli* strains. However, except for slightly lower values for *B. subtilis* and *M. luteus* strains, the stilbene analog **252** exhibited similar potency to **254**. Interestingly, upon reduction of the acetylenic linker of the highly active cyano derivative **251**, the antibacterial activity of the resulting stilbene **253** was mostly retained. The MICs were slightly lower for *E. coli* and again slightly higher for *B. subtilis* and *M. luteus*. This appears to represent a general trend: by reducing the diaryl alkyne to the corresponding stilbene, the antibacterial activity slightly decreases for Gram-negative *E. coli* and increases for Gram-positive *B. subtilis* and *M. luteus*. Phenylacetylene **255** turned out to be highly active, and except for *B. subtilis* and *M. phlei*, the MIC values have the same order of magnitude as for AzaHis-albicidin **16** and CIP.

Table 5. MIC values for albicidin derivatives with modified A-B building blocks.

MIC values are given in $\mu\text{g}\cdot\text{mL}^{-1}$ for ciprofloxacin (**CIP**) albicidin (**1**), AzaHis-albicidin **16** and newly synthesized analogs **247–259** for a panel of selected Gram-negative (*E. coli* and *S. typhimurium*) and Gram-positive (*B. subtilis*, *M. luteus*, and *M. phlei*) bacteria. For a better overview, the activity is highlighted by a color code: 0.016–0.125 (dark green), 0.25–4.0 (light green), ≥ 8.0 (light red)

Entry	<i>E. coli</i> DSM1116	<i>E. coli</i> BW25113	<i>S. typhimurium</i> TA100	<i>B. subtilis</i> DSM 10	<i>M. luteus</i> DSM 1790	<i>M. phlei</i> DSM 750
CIP	0.016	≤ 0.016	≤ 0.016	0.125	1.0	0.25
1	0.063	0.063	0.016	0.25	2.0	2.0
16	0.016	n.d. ^b	≤ 0.016	0.125	0.5	1.0
247	0.063	0.125	0.031	2.0	2.0	1.0
248	0.063	0.125	≤ 0.016	0.25	0.5	1.0
249	0.063	0.063	≤ 0.016	0.25	0.5	1.0
250	0.031	0.031	0.016	0.25	0.25	0.5
251	≤ 0.016	0.031	≤ 0.016	0.25	0.25	1.0
252	0.5	0.25	0.125	0.5	1.0	4.0
253	0.031	0.063	≤ 0.016	0.063	0.031	1.0
254	0.5	0.25	0.125	2.0	2.0	4.0
255	0.031	0.016	≤ 0.016	0.125	2.0	8.0
256	0.063	0.125	0.063	1.0	0.125	2.0
257	2.0	4.0	2.0	≥ 8.0	8.0	8.0
258	0.5	0.5	0.5	≥ 8.0	≥ 8.0	≥ 8.0
259	≥ 8.0	≥ 8.0	≥ 8.0	≥ 8.0	≥ 8.0	≥ 8.0

^bnot determined

Despite improved activities against *M. luteus* and *M. phlei*, the higher MIC values determined for the remaining panel of pathogens for compound **256**, as compared to its precursor alkyne **255**, suggest that the presumably increased polarity, size, and capacity for hydrogen-bonding introduced to the molecule by the triazole ring have a deteriorating effect on the overall activity of **256**. Another aspect to be considered is the shift from a weakly to non-acidic C–H bond of the alkyne to a weakly basic triazole. Introduction of the negatively charged and acidic tetrazole head group resulted in a 30-fold decrease of activity against Gram-negative *E. coli* and *S. typhimurium* strains, as well as at least an eightfold decrease against Gram-positive *B. subtilis* and *M. luteus* for analog **257**. The truncated anisole variant **259** suffered from a complete loss of activity, which potentially stems from the unfavorable length of the molecule. Similarly, 4-hydroxybenzamide **258** displayed no activity against the Gram-positive strains and

a 30-fold lower activity against *E. coli* and *S. typhimurium*. The results of the target-directed *E. coli* gyrase assay (Figure 23) are consistent with the results obtained from the cell-based MIC assay. All acetylenic derivatives (**247–251**) inhibit the enzyme's activity at least as well as albicidin (**1**). Again, the cyano analog **251** turned out to be the most potent one, exhibiting similar activity to AzaHis-albicidin **2**. The partial loss of activity observed for the reduced analogs **252** and **254** is also reflected in their diminished capacity to inhibit gyrase. At the same time, cyano stilbene **253**, as well as phenylacetylene **255**, emerged highly potent against the molecular target. Consequently, the triazole derivative **256** showed a decreased activity as compared to its acetylenic precursor. Finally, the tetrazole variant **257**, 4-hydroxybenzamide **258**, and the truncated anisole **259** did not show any activity in this assay either.

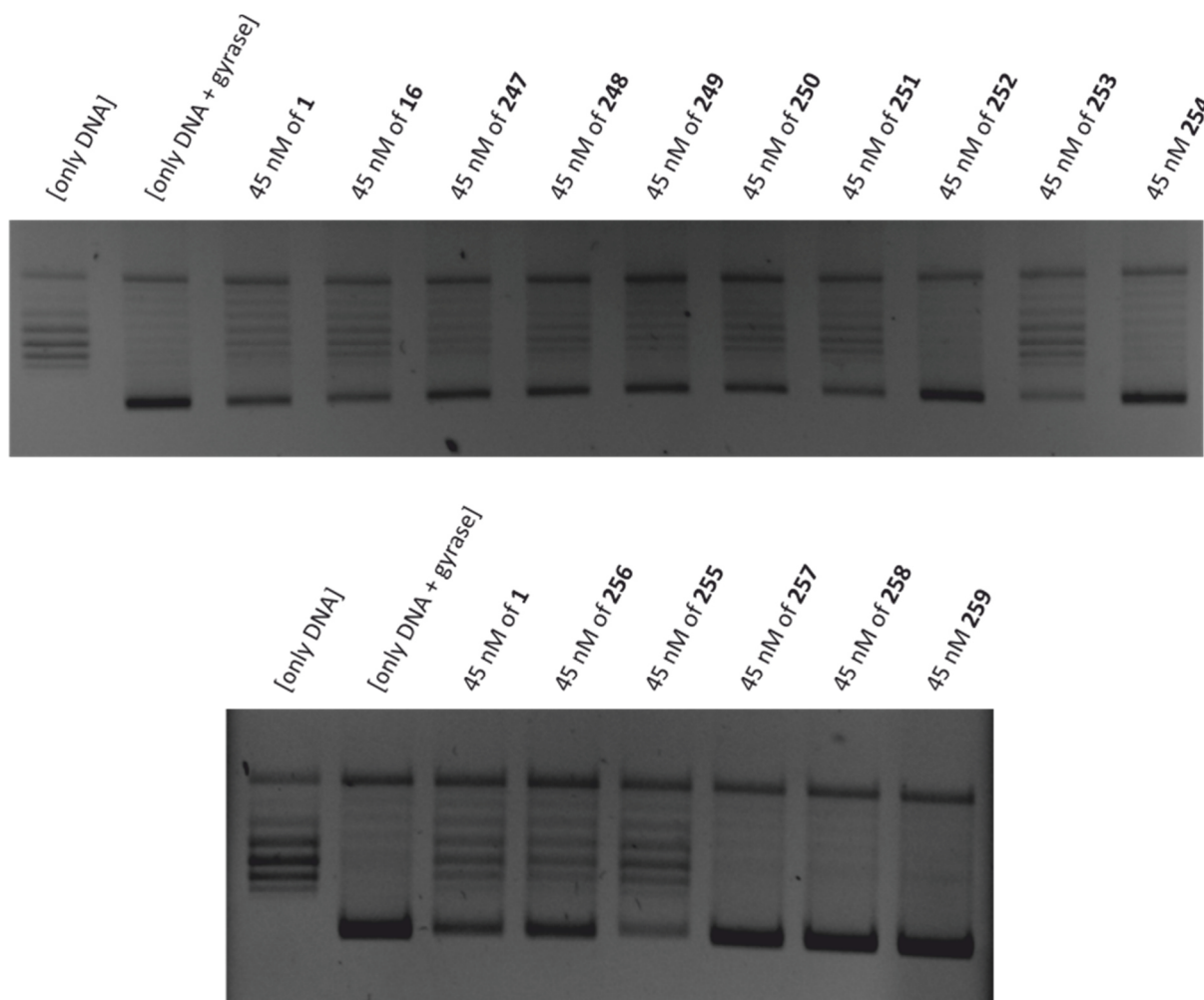


Figure 23. Gyrase inhibition assay for albicidin analogs with modified A-B building blocks.

Inhibition assay of the supercoiling activity of *E. coli* DNA gyrase for albicidin (**1**), AzaHis-albicidin (**2**), and compounds **247–259**. The control experiment without enzyme and drug (left lane) shows relaxed DNA. Addition of DNA gyrase results in supercoiled DNA (second lane from left). All derivatives were tested at a concentration of 45 nM.

4 Summary and Outlook

The Süssmuth group's long-term objective to transform albicidin from a promising lead compound with excellent antibacterial properties into a clinical drug candidate can only be accomplished through rational design, synthesis, and biological evaluation of a substantial number of structural analogs. These are imperative to identify key pharmacophoric regions and gain insight into the complex SAR of the molecule. An array of derivatives with manipulations in different fragments of the peptide have facilitated important studies on the mode of action and mechanisms of resistance as well. As previously mentioned, our lead optimization efforts have resulted in the incorporation of a triazole-containing surrogate as a replacement for the base-labile cyanoalanine. The resulting AzaHis-albicidin (**16**) has served as a template structure for all subsequent variants. The present work comprises 38 new derivatives with modifications of the C-terminal E-F dipeptide and the N-terminal A-B dipeptide, respectively. The most important SAR insights are summarized below and are used to identify trends and suggest possible target compounds for the future.

4.1 Derivatives with Variations of the C-Terminal Dipeptide

The sequential deletion of the methoxy and hydroxy substituents present in the C-terminal dipeptidic *p*ABA residue of albicidin has resulted in 15 new derivatives (compounds **34–49**) with a varying spectrum of antibacterial activity (Figure 24). The MIC values shown in Table 3 (S1 panel) suggest that removing one substituent at a time does not have a significant deleterious effect on the activity of compounds **34–37** against Gram-negative bacteria. At the same time, the reduced activity of derivative **34** against the Gram-positive *M. luteus* strain connotes that the methoxy group in building block E is the most critical one regarding single deletions.

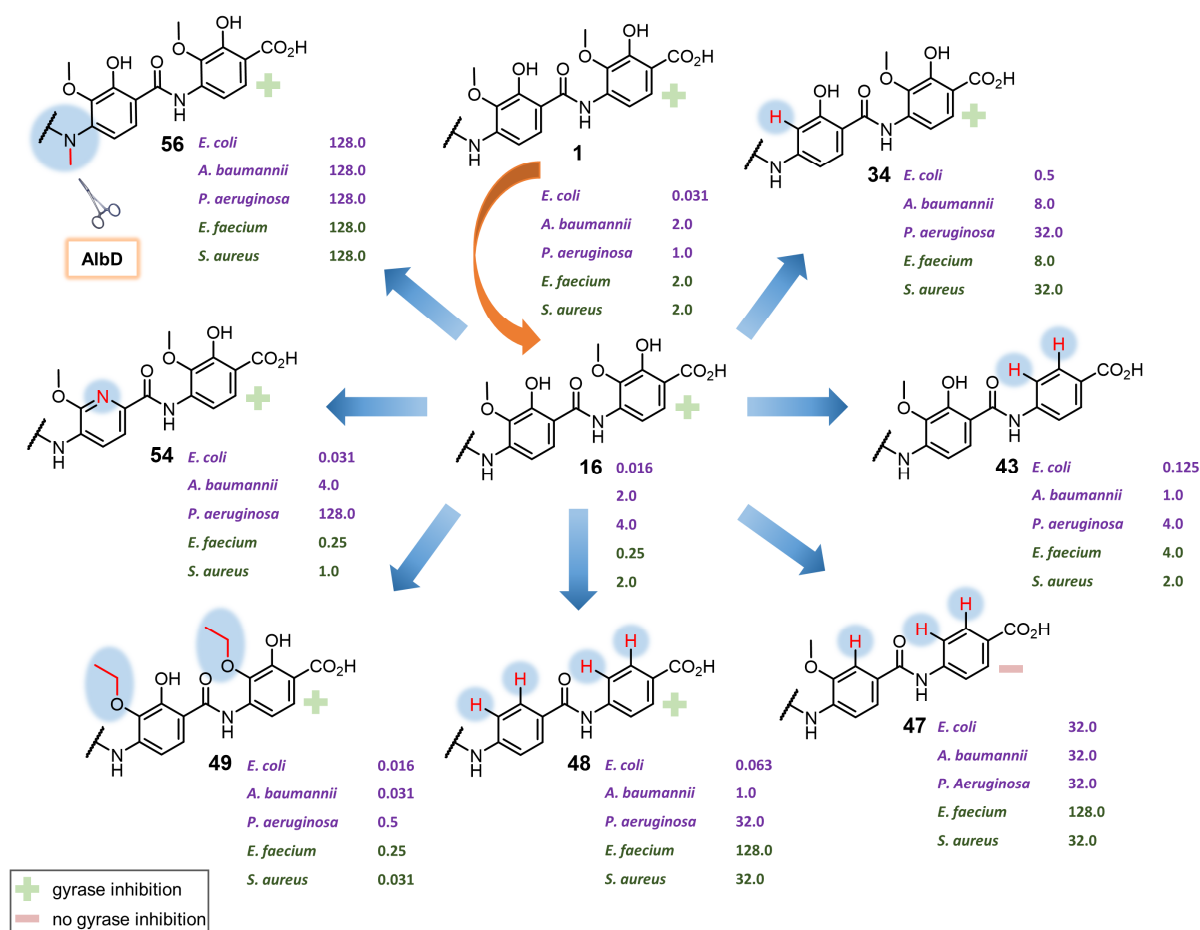


Figure 24. Summary of the bioactivity of selected albicidin derivatives.

MIC values are given in $\mu\text{g mL}^{-1}$ for selected albicidin derivatives. Values are shown for CIP sensitive strains of *E. coli*, *A. baumannii*, *P. aeruginosa*, *S. aureus*, and *E. faecium*. Gram-negative bacteria are highlighted in purple and gram-positive ones in green. The capacity of these variants to inhibit bacterial DNA gyrase is indicated with a green (+) for active and a light red (-) for inactive. For the complete list of investigated compounds, see Table 4 (S2 panel).

Except for compound **42**, which lacks both hydroxy groups and displays a slightly reduced activity profile against Gram-negative strains, double deletions appear to have little to no diminishing effect on the activity of the resulting derivatives **38–41** and **43** either. Remarkably, the activity against Gram-negative bacteria is mostly preserved even when three or all four substituents are omitted. Since compounds **44–48** are virtually inactive against all tested Gram-positive bacteria, the step from double deletions to triple and quadruple deletions of functional groups can be considered as an obstacle for anti-Gram-positive potency. However, the high degree of substitution of the aromatic dipeptide constitutes one of the biggest hurdles during the total syntheses of albicidin and respective analogs. Hence, fewer substituents potentially allow the synthetic chemists to resort to commercially available or easy-to-synthesize building blocks, which has the potential to dramatically facilitate and

expedite analog synthesis. Another important finding concerns the nature of the underlying aromatic ring. We have shown that bioactivity can be fully preserved when a methoxy pyridine is used as building block E. Therefore, a synthetic hybrid of the heteroaromatic albicidin variant **54** and compound **43**, which bears an unsubstituted *p*A BA residue as building block F, would be much easier to synthesize and likely exhibit excellent antibacterial properties (Figure 25, compound **300**). Furthermore, it would be interesting to see whether the loss of activity against Gram-positive pathogens observed for compound **48** can be restored by introducing a pyridine in building block E (compound **301**).

While deletions in E and F have been shown to cause a loss of activity against Gram-positive bacteria, replacing the methoxy groups of the parent compound **16** successively by the more hydrophobic ethoxy groups results in quite the opposite. The ethoxy-albicidins **49–51** are highly active against both Gram-positive and Gram-negative bacteria, outperforming all other compounds in the cell-based assay. Overall, the doubly ethoxy-substituted derivative **49** emerges as the most potent compound in the series, exhibiting good to very good activities against all tested S1 and S2 pathogens, except for *Klebsiella* strains (Table 4). Knowing from previous studies that *iso*-propoxy groups are also feasible in place of the methoxy groups^[271,272,280], one can conclude that more hydrophobic substituents are beneficial for bioactivity. However, as mentioned before, an overly hydrophobic albicidin derivative is detrimental to drug development purposes and the ethoxy groups potentially make for a good compromise in terms of druggability. Some additional possibilities to include the ethoxy group in future derivatives are depicted in Figure 25 (compounds **302** and **303**).

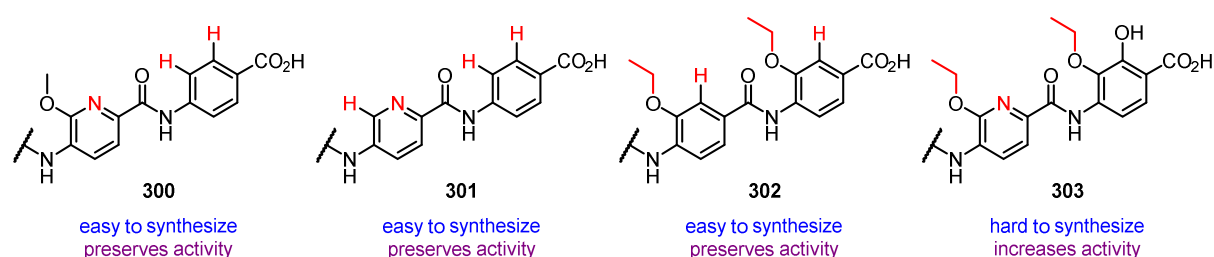


Figure 25. Proposed E-F derivatives of albicidin for future SAR studies.

The proposed albicidin derivatives **300–303** are depicted. The anticipated synthetic feasibility of the corresponding E-F dipeptides is indicated in blue and expected implications for the bioactivity of the final derivatives compared to the parent compound **16** is stated in purple.

4.2 Derivatives with Variations of the N-Terminal A-B Building Block

In our efforts to replace albicidin's unfavorable cinnamoyl residue we have synthesized and biologically tested 13 new derivatives with variations of the N-terminal A-B building block. We were pleased to find that our initial hypothesis that the acetylene group could serve as a surrogate for *trans*-configured amide bonds was validated in terms of bioactivity (Table 5). All variants bearing a diarylalkyne carboxylate (compounds **247–251**) preserved the excellent antibacterial properties of their parent compound **16**, with the cyano-substituted derivative **251** even slightly exceeding it (Figure 26). Interestingly, the corresponding stilbene analog **253** outperformed its acetylenic counterpart against Gram-positive bacteria. As expected, increasing the degree of freedom in the linker unit between the two aromatic rings even

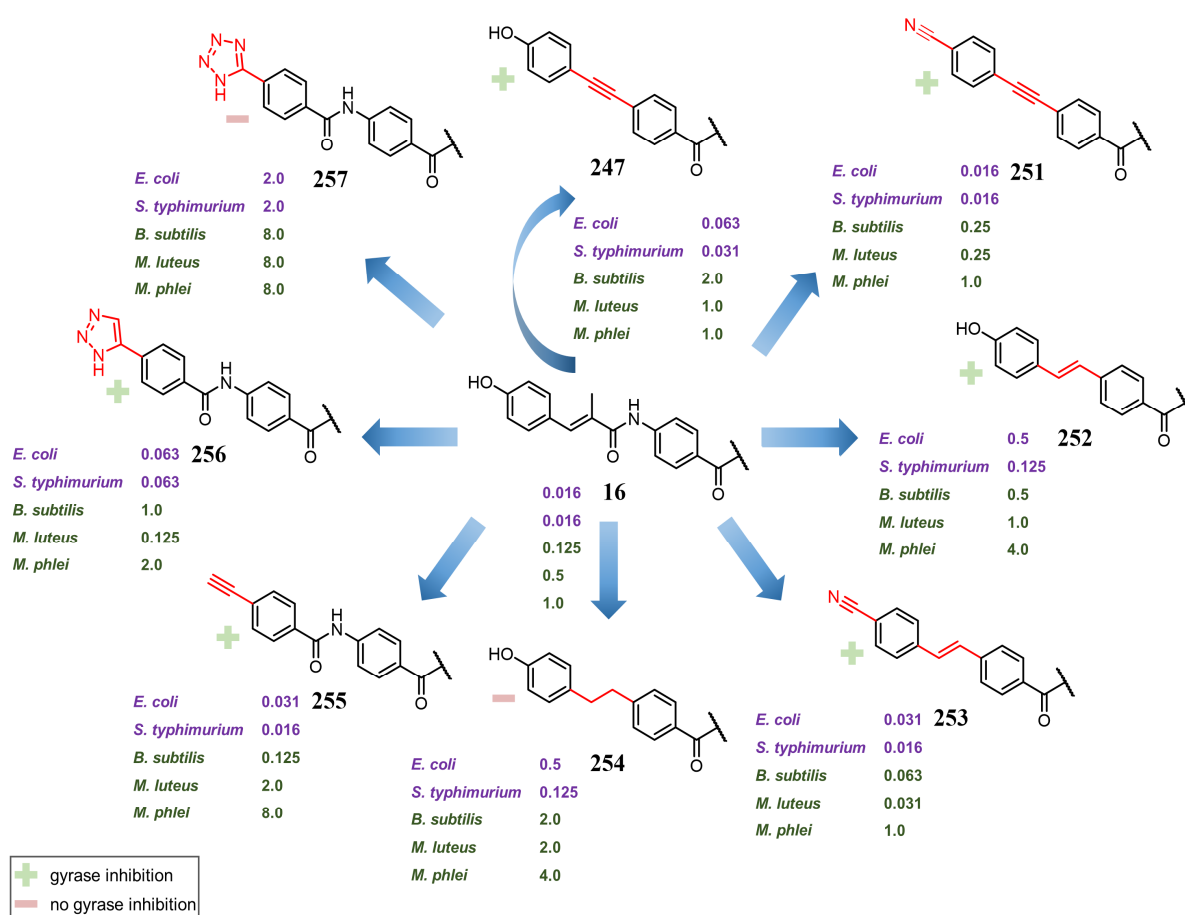


Figure 26. Summary of the bioactivity of selected albicidin derivatives.

MIC values are given in $\mu\text{g mL}^{-1}$ for selected albicidin derivatives. Values are shown for CIP sensitive strains of *E. coli*, *A. baumannii*, *P. aeruginosa*, *S. aureus*, and *E. faecium*. Gram-negative bacteria are highlighted in purple and gram-positive ones in green. The capacity of these variants to inhibit bacterial DNA gyrase is indicated with a green (+) for active and a light red (-) for inactive. For the complete list of investigated compounds, see Table 5.

further by introducing sp^3 -hybridized carbon atoms dramatically reduced the potency of the resulting diarylalkane derivative **254**. These results prompted us to consider utilizing the acetylene group in different parts of the molecule as well. In the future, it could potentially serve as a resilient amide bond isostere to protect albicidin from enzymatic hydrolysis by the endopeptidase AlbD. For this purpose, the internal alkyne would ideally be built into the C-terminal tripeptide D-E-F. As mentioned previously, the most vulnerable amide bond is the one between building blocks D and E followed by the one connecting building blocks C and D. While the diarylalkyne residue present in the proposed variant **304** is potentially accessible by Pd-mediated cross-coupling chemistry, incorporating the triple bond into compound **305** will prove much more difficult (Figure 27).

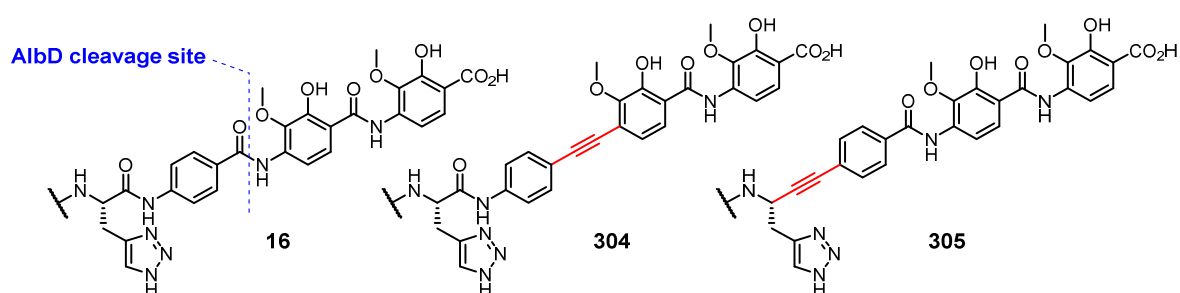


Figure 27. Proposed incorporation of the acetylene group as amide bond isosteres.

AzaHis-albicidin **16** is depicted alongside its proposed acetylenic derivatives **304** and **305**. The suggested structures have the potential to preserve bioactivity while defying enzymatic degradation by the resistance factor AlbD. The primary cleavage site of the enzyme is indicated in blue.

The alkyne moiety also proved worthwhile as a replacement for the hydroxy group in the *para*-position of the aromatic ring. Phenylacetylene **255** is not only highly active – particularly against Gram-negative pathogens – but its terminal alkyne is predestined to serve as a molecular handle, e.g., in further studies directed towards the elucidation of albicidin's mode of action and mechanisms of resistance.

5 Experimental Part

5.1 General Information

5.1.1 Reagents and Solvents

Commercially available reagents (*Carl Roth GmbH and Co. KG*, Karlsruhe, Germany; *Sigma-Aldrich*, Taufkirchen, Germany; *Iris Biotech GmbH*, Marktredwitz, Germany; *Orpegen*, Heidelberg, Germany; *ABCR*, Karlsruhe, Germany; *Alfa Aesar*, Karlsruhe, Germany; *Merk*, Darmstadt, Germany; *TCI*, Eschborn, Germany; *VWR International GmbH*, Darmstadt, Germany; *Acros*, Geel, Belgium) and solvents (*Fisher Scientific-Acros*, Schwerte, Germany) were used without further purification. Technical solvents were distilled in a 10 L rotary evaporator (*Büchi Labortechnik AG*, Flawil, Switzerland) prior to use. HPLC solvents (*Fisher Scientific-Acros*, Schwerte, Germany) and NMR solvents (*Deutero GmbH*, Kastellaun, Germany; *Sigma-Aldrich*, Taufkirchen, Germany) were used without further purification. Whenever necessary, reactions were carried out under an atmosphere of argon or nitrogen and in dry solvents.

5.1.2 Chromatography

Reactions and purifications were monitored by analytical thin layer chromatography (TLC) on aluminium-backed plates coated with *Macherey-Nagel* silica gel (60, F254) using solvent systems based on ethyl acetate, *n*-hexane, dichloromethane, and methanol. Analysis was performed by visualizing under UV light ($\lambda = 254$ nm), by staining with KMnO_4 -solution (KMnO_4 (3 g), K_2CO_3 (20 g), H_2O (300 mL), 5% $\text{NaOH}_{(\text{aq.})}$ (5 mL)) and with ninhydrin-solution (ninhydrin (0.3 g), AcOH (3 mL), *n*-BuOH (100 mL)). Flash chromatography was performed on silica gel (particle size 40–63 μm , *VWR Chemicals*, Darmstadt, Germany) and solvent mixtures based on ethyl acetate, *n*-hexane, dichloromethane, and methanol. Preparative HPLC was carried out

on a 1260 Infinity (*Agilent Technologies*, Waldbronn, Germany) system with a polymeric reversed phase column (PLRP-S 100A, 300 x 50 mm, particle size 10 μm , *Agilent Technologies*, Waldbronn, Germany). Eluent A was water with 0.1% trifluoroacetic acid and eluent B was acetonitrile with 0.1% trifluoroacetic acid. A flow rate of 70 mL min^{-1} was used.

5.1.3 Analytical Methods

^1H and ^{13}C NMR spectra were recorded at 298 K using Bruker Avance-II 400 MHz, Bruker Avance-III 500 MHz, or Bruker Avance-III 700 MHz instruments (*Bruker*, Karlsruhe, Germany). The chemical shifts are reported in parts per million (ppm) using the residual solvent peak as an internal reference ($\text{DMSO-}d_6$, CDCl_3). Multiplicity (br. s = broad singlet, s = singlet, d = doublet, dd = doublet of doublet, t = triplet, q = quartet, m = multiplet) and coupling constants (J =Hz) are quoted where applicable. NMR spectra were analyzed using the ACD/Spectrum Processor (*ACD/Labs*, Toronto, Ontario, Canada) or MestReNova (*Mestrelab Research S.L.*, Santiago de Compostela, Spain). HPLC-ESI-HRMS spectra were recorded on a QTrap LTQ XL (*Thermo Fisher Scientific*, Waltham, Massachusetts, USA) with an Agilent 1200 Series HPLC-System (*Agilent Technologies*, Waldbronn, Germany) using a reversed-phase C18 column (Hypersil 100, 150 x 4.6 mm, particle size 5 μm , *Thermo Fisher Scientific*, Waltham, Massachusetts, USA). Eluent A was water with 0.1% formic acid; eluent B was methanol with 0.1% formic acid. A flow rate of 3 mL min^{-1} was used. HRMS spectra were analyzed using XCalibur (*Thermo Fisher Scientific GmbH*, Bremen, Germany).

5.1.4 Nomenclature

Synthetic compounds were named according to the IUPAC nomenclature whenever reasonable. In all other cases comprehensible abbreviations were introduced.

5.2 Synthetic Protocols

5.2.1 General Procedures (GPs)

GP1 – Reduction of aromatic nitro compounds using zinc

To a solution or suspension of the aromatic nitro compound in either EtOH (abs.) or a mixture of EtOH (abs.) and THF was added AcOH. The resulting mixture was cooled down to 0 °C and

zinc powder was added carefully in portions. After fading of the exothermic reaction, the ice bath was removed, allowing the reaction mixture to warm up to r.t. Upon completion of the reaction (TLC monitoring), the solids were removed by filtration through a pad of Celite®, washed with little EtOAc and THF, and the filtrate was concentrated *in vacuo*. The acidic residue was taken up in EtOAc and carefully washed with saturated aq. NaHCO₃ (3×) and brine. After drying over anhydrous Na₂SO₄, the solvent was removed under reduced pressure to obtain either the analytically pure product or a crude product that required purification by column chromatography.

GP2 – Reduction of aromatic nitro compounds using SnCl₂

SnCl₂ · 2 H₂O was added to a solution of the aromatic nitro compound in EtOAc and the reaction mixture was stirred at 50 °C for 16 h. The reaction was quenched by the addition of saturated aq. NaHCO₃, followed by the separation of the two layers and extraction of the aq. layer with EtOAc (4×). The combined organic layers were washed with brine, dried over anhydrous Na₂SO₄, and concentrated *in vacuo* to obtain either the analytically pure product or a crude product that required purification by column chromatography.

GP3 – Hydrolysis of benzoic acid esters

To a solution of the benzoic acid ester in a mixture of THF and MeOH was slowly added 3 N KOH_(aq.). After complete conversion of the starting material (TLC monitoring), the reaction mixture was acidified to pH ~ 2 by the addition of 3 N HCl_(aq.). Workup method A: In case a precipitate was formed, it was isolated by filtration through a sintered funnel, washed with little water and dried under high vacuum to obtain the analytically pure product. Workup method B: In case no precipitate was formed, MeOH and THF were evaporated under reduced pressure and the aq. residue was extracted with EtOAc (3×). The combined organic layers were washed with brine, dried over anhydrous Na₂SO₄, and concentrated under reduced pressure to yield the analytically pure product.

GP4 – Peptide coupling via benzoyl chloride formation using BTC

Bis(trichloromethyl) carbonate (BTC, triphosgene) was added to a solution of the benzoic acid in dry THF and the solution was cooled down to 0 °C. 2,4,6-Collidine was added dropwise and the resulting suspension was stirred at that temperature for 45 min. Subsequently, a premixed solution of the aniline and DIPEA in dry THF was added dropwise to the suspension and the

reaction mixture was stirred for 16 h while warming up to r.t. After removing all volatiles under reduced pressure, the residue was taken up in EtOAc and washed with 1 N HCl_(aq.) (3×), saturated aq. NaHCO₃ (3×), and brine. The organic layer was dried over anhydrous Na₂SO₄ and concentrated *in vacuo* to obtain the crude product, which was purified by column chromatography on silica gel.

GP5 – Peptide coupling using pNBC and Et₃N

To a solution of the aniline in dry THF was added Et₃N and the mixture was cooled down to –15 °C. *p*-Nitrobenzoyl chloride (*pNBC*) was added in one portion and the reaction mixture was stirred at that temperature for 30 min. Ether was added to the solution and the resulting suspension was stirred for 1 h while warming up to r.t. The solids were isolated by filtration through a sintered funnel and washed with ether and little H₂O to obtain either the analytically pure product or a crude product that required purification by column chromatography.

GP6 – Peptide coupling via mixed anhydride formation using EEDQ

To a solution of the amino acid in dry THF was added EEDQ and the reaction mixture was stirred at r.t. for 15 min. A premixed solution of the tripeptide in dry THF was added slowly and the reaction mixture was stirred at r.t. for 16 h. The organic solvent was evaporated under reduced pressure and the residue was partitioned between EtOAc and 1 N HCl_(aq.). The organic layer was washed with 1 N HCl_(aq.) (2×), brine, dried over anhydr. Na₂SO₄, and concentrated *in vacuo* to afford the crude product, which was purified by column chromatography.

GP7 – Boc-deprotection using 4 N HCl in 1,4-dioxane

A solution of the Boc-protected tetrapeptide in 4 N HCl in 1,4-dioxane was stirred at r.t. for 1 h. Subsequently, all volatiles were removed under reduced pressure to obtain the crude product, which was taken up in H₂O and little CH₃CN and freeze-dried to afford the analytically pure desired product without further purification.

GP8 – Pd-mediated allyl-deprotection

The allyl-protected tetrapeptide was dissolved in dry THF and morpholine was added, followed by either Pd(PPh₃)₄ or Pd(Ph₃)₂Cl₂. The reaction mixture was stirred at r.t. for 16 h under the exclusion of light (aluminum wrap). After removing all volatiles under reduced pressure, the residue was taken up in EtOAc and washed with 1 N HCl_(aq.) (3×) and brine. The

organic phase was dried over anhydrous Na_2SO_4 and concentrated *in vacuo* to obtain the crude product, which was purified by column chromatography on silica gel.

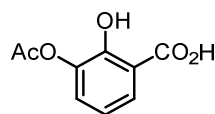
GP9 – Peptide coupling via active ester formation using PCP

The tetrapeptide (1.00 equiv) and the PCP active ester (1.20 equiv) were dissolved in a mixture of anhydrous DMF and Et_3N (5.0 equiv) was added. The reaction mixture was stirred at r.t. for 16 h under the exclusion of light. All volatiles were removed *in vacuo* and the residue was taken up in a mixture of THF and MeOH (1:1 v/v), and 3 N $\text{KOH}_{(\text{aq.})}$ was added dropwise at 0 °C. The ice bath was removed and after 15 min of stirring the suspension was acidified to pH \approx 2 by the addition of 3 N $\text{HCl}_{(\text{aq.})}$. The resulting suspension was concentrated under reduced pressure and the crude material was dissolved in DMSO and purified by HPLC (PLRP-S column, CH_3CN in H_2O).

5.2.2 Derivatives with Variations of the C-Terminal Dipeptidic *p*ABA Moiety

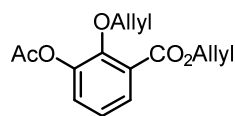
Syntheses of Modified E-F Dipeptides

3-Acetoxy-2-hydroxybenzoic acid (90**)**



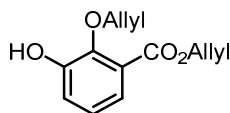
2,3-Dihydroxybenzoic acid (**89**) (15.0 g, 97.3 mmol, 1.00 equiv) was dissolved in DMF (450 mL) and cooled down to 0 °C. Et_3N (27.1 mL, 195 mmol, 2.00 equiv) was added dropwise followed by acetic anhydride (9.18 mL, 97.3 mmol, 1.00 equiv). The reaction mixture was stirred at r.t. for 5 d. After removing the solvent under reduced pressure, the residue was taken up in EtOAc and washed with brin (3x). The organic phase was dried over anhydrous Na_2SO_4 and concentrated *in vacuo* to afford the pure title compound **90** (12.2 g, 62.2 mmol, 64%) as a light-brown solid.

^1H NMR (400 MHz, $\text{DMSO}-d_6$) δ 7.67 (dd, $J=7.9, 1.6$ Hz, 1H), 7.27 (dd, $J=7.9, 1.6$ Hz, 1H), 6.85 (t, $J=7.9$ Hz, 1H), 2.27 (s, 3H). ^{13}C NMR (101 MHz, $\text{DMSO}-d_6$) δ 171.6, 168.4, 153.8, 138.8, 127.7, 127.4, 117.6, 20.4. HRMS (ESI): m/z calculated for $\text{C}_9\text{H}_8\text{O}_5$ $[\text{M}-\text{H}]^-$ 195.0288, found 195.0297 ($\Delta m = +4.6$ ppm).

3-Acetoxy-2-(allyloxy)allylbenzate (91)

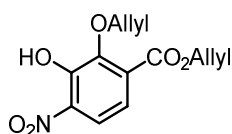
Benzoic acid **90** (6.00 g, 30.6 mmol, 1.00 equiv) was dissolved in DMF (250 mL) and treated with K_2CO_3 (12.7 g, 91.8 mmol, 3.00 equiv). The solution was cooled down to 0 °C and allyl bromide (5.29 mL, 61.2 mmol, 2.00 equiv) was added dropwise. After stirring at r.t. for 16 h, the mixture was extracted with EtOAc (4×) and washed with brine (5×). The combined organic layers were dried over anhydrous Na_2SO_4 and concentrated under reduced pressure. Purification of the crude product by column chromatography on silica gel (*n*-hexane/EtOAc, 8:1) afforded the title compound **91** (5.40 g, 19.5 mmol, 64%) as a colourless oil.

1H NMR (400 MHz, $DMSO-d_6$) δ 7.67 (dd, $J=1.7, 7.8$ Hz, 1H), 7.45 (dd, $J=1.7, 8.0$ Hz, 1H), 7.30 (t, $J=7.9$ Hz, 1H), 5.99–6.11 (m, 2H), 5.38–5.48 (m, 2H), 5.24–5.34 (m, 2H), 4.83 (dt, $J=1.4, 5.5$ Hz, 2H), 4.47 (dt, $J=1.4, 5.6$ Hz, 2H), 2.34 (s, 3H). ^{13}C NMR (101 MHz, $DMSO-d_6$) δ 168.6, 164.6, 149.8, 144.5, 133.7, 132.3, 128.1, 127.7, 126.3, 124.3, 118.3, 117.7, 75.1, 65.5, 20.5. HRMS (ESI): m/z calculated for $C_{15}H_{16}O_5$ $[M+H]^+$ 277.1071, found 277.1080 ($\Delta m = +3.2$ ppm).

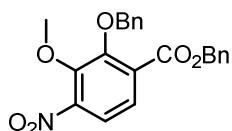
2-(Allyloxy)-3-hydroxyallylbenzoate (93)

To a solution of the allyl ester **91** (5.40 g, 14.5 mmol, 1.00 equiv) in MeOH (250 mL) was added K_2CO_3 (2.75 g, 20.0 mmol, 1.02 equiv) and the reaction mixture was stirred at r.t. for 2 d. After removing the solvent under reduced pressure, the residue was taken up in EtOAc, washed with 1 N $HCl_{(aq)}$ (2×), brine (3×), and dried over anhydrous Na_2SO_4 . The solvent was removed under reduced pressure and the crude product was purified by column chromatography on silica gel (*n*-hexane/EtOAc, 8:1) to afford the title compound **93** (3.59 g, 15.3 mmol, quant.) as a yellow oil.

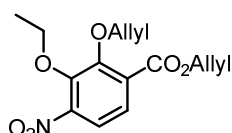
1H NMR (400 MHz, $DMSO-d_6$) δ 9.77 (s, 1H), 7.08–7.12 (m, 2H), 7.01–7.05 (m, 1H), 6.00–6.13 (m, 2H), 5.19–5.45 (m, 4H), 4.78 (dt, $J=1.5, 5.5$ Hz, 2H), 4.53 (dt, $J=1.4, 5.7$ Hz, 2H). ^{13}C NMR (101 MHz, $DMSO-d_6$) δ 165.7, 151.1, 145.3, 134.5, 132.6, 126.4, 124.0, 120.1, 120.0, 118.0, 117.3, 73.6, 65.1. HRMS (ESI): m/z calculated for $C_{14}H_{13}O_4$ $[M+H]^+$ 235.0965, found 235.0963 ($\Delta m = -0.9$ ppm).

Allyl 2-(allyloxy)-3-hydroxy-4-nitrobenzoate (95)

A solution of compound **93** (7.79 g, 33.3 mmol, 1.00 equiv) in acetic anhydride (300 mL) was cooled down to 0 °C and $\text{Cu}(\text{NO}_3)_2 \cdot 3 \text{H}_2\text{O}$ (4.82 g, 20.0 mmol, 0.600 equiv) was added in several portions. After stirring at 0 °C for 4 h, the reaction mixture was partitioned between ice water and EtOAc. The aq. phase was extracted with EtOAc (2×) and the combined organic phases were washed with 3 N HCl (aq.), dried over Na_2SO_4 , and concentrated under reduced pressure. Purification of the crude product by column chromatography on silica gel (*n*-hexane/EtOAc, 9:1) gave the title compound **95** (1.76 g, 6.33 mmol, 19%) as a yellow solid. ^1H NMR (500 MHz, $\text{DMSO}-d_6$) δ 7.76 (d, $J=8.8$ Hz, 1H), 7.28 (d, $J=8.8$ Hz, 1H), 6.02–6.12 (m, 2H), 5.25–5.47 (m, 4H), 4.84 (dt, $J=1.4, 5.6$ Hz, 2H), 4.58 (dt, $J=1.2, 6.0$ Hz, 2H). ^{13}C NMR (101 MHz, $\text{DMSO}-d_6$) δ 164.3, 147.7, 146.6, 139.7, 133.5, 132.1, 130.5, 119.6, 118.7, 118.6, 74.9, 65.8. HRMS (ESI): m/z calculated for $\text{C}_{13}\text{H}_{13}\text{NO}_6$ $[\text{M}+\text{H}]^+$ 279.0743, found 279.0972.

Benzyl 2-(benzyloxy)-3-methoxy-4-nitrobenzoate (98)

^1H NMR (500 MHz, $\text{DMSO}-d_6$) δ 7.74 (d, $J=8.5$ Hz, 1 H), 7.62 (d, $J=8.5$ Hz, 1 H), 7.42–7.46 (m, 2H), 7.32–7.39 (m, 8H), 5.33 (s, 2H), 5.04 (s, 2H), 3.92 (s, 3H). ^{13}C NMR (126 MHz, $\text{DMSO}-d_6$) δ 164.1, 151.9, 146.7, 146.6, 136.0, 135.4, 130.7, 128.5, 128.4, 128.4, 128.3, 128.3, 125.3, 119.4, 76.0, 67.1, 62.3. HRMS (ESI): m/z calculated for $\text{C}_{22}\text{H}_{19}\text{NO}_6$ $[\text{M}+\text{H}]^+$ 394.1285, found 394.1274 ($\Delta m = -2.8$ ppm).

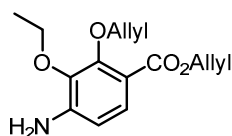
Allyl 2-(allyloxy)-3-ethoxy-4-nitrobenzoate (99)

Phenol **95** (1.39 g, 4.98 mmol, 1.00 equiv) was dissolved in DMF (50 mL) and successively treated with K_2CO_3 (757 mg, 5.48 mmol, 1.10 equiv), bromoethane (410 μL , 5.48 mmol, 1.10 equiv) and KI (30.0 mg, 180 μmol , cat.). After stirring at 80 °C for 16 h, the reaction was

stopped by the addition of ice water and the aq. solution was extracted with EtOAc (3×). The combined organic phases were washed with brine (5×), dried over anhydrous Na₂SO₄, and concentrated under reduced pressure. Purification of the crude product by column chromatography on silica gel (*n*-hexane/EtOAc, 10:1) afforded the title compound **99** (1.57 g, 5.11 mmol, quant.) as a yellow oil.

¹H NMR (400 MHz, DMSO-*d*₆) δ 7.72 (d, *J*=8.5 Hz, 1H), 7.58 (d, *J*=8.5 Hz, 1H), 5.98–6.09 (m, 2H), 5.34–5.45 (m, 2H), 5.24–5.32 (m, 2H), 4.81 (dt, *J*=1.2, 5.6 Hz, 2H), 4.57 (dt, *J*=1.2, 5.8 Hz, 2H), 4.17 (q, *J*=7.0 Hz, 2H), 1.30 (t, *J*=7.0 Hz, 3H). ¹³C NMR (101 MHz, DMSO-*d*₆) δ 164.0, 151.9, 146.9, 145.5, 133.2, 132.1, 125.0, 119.2, 118.7, 118.5, 75.0, 70.9, 65.9, 15.2.

Allyl 2-(allyloxy)-4-amino-3-ethoxybenzoate (**106**)

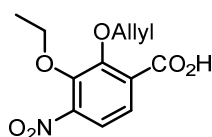


Reduction of the nitro group according to GP1:

- EtOH (20 mL), AcOH (4 mL)
- nitrobenzoate **99** (600 mg, 1.95 mmol, 1.00 equiv)
- Zn-dust (12.0 g)
- 0 °C to r.t., 15 min
- column chromatography: SiO₂, *n*-hexane/EtOAc, 10:1
- the title compound **106** (402 mg, 1.45 mmol, 74%) was obtained as a colourless oil

¹H NMR (400 MHz, DMSO-*d*₆) δ 7.33 (d, *J*=8.5 Hz, 1H), 6.46 (d, *J*=8.5 Hz, 1H), 5.92–6.14 (m, 2H), 5.70 (s, 2 H), 5.35 (ddq, *J*=17.2, 5.6, 1.7 Hz, 2H), 5.20 (ddq, *J*=13.7, 10.5, 1.4 Hz, 2H), 4.66 (dt, *J*=5.5, 1.4 Hz, 2H), 4.45 (dt, *J*=5.6, 1.3 Hz, 2H), 3.90 (q, *J*=7.0 Hz, 2H), 1.30 (t, *J*=7.0 Hz, 3H). ¹³C NMR (101 MHz, DMSO-*d*₆) δ 164.6, 153.2, 147.8, 137.7, 134.7, 133.2, 127.4, 117.4, 116.8, 110.9, 109.3, 74.0, 67.5, 64.1, 15.5. HRMS (ESI): *m/z* calculated for C₁₅H₁₉NO₄ (M+H)⁺ 278.1387, found 278.1387 (Δ*m* = ±0 ppm).

2-(Allyloxy)-3-ethoxy-4-nitrobenzoic acid (**107**)

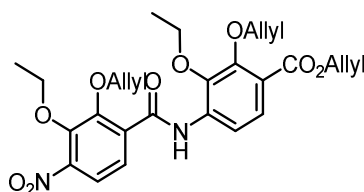


Hydrolysis of the allyl ester according to GP3:

- allyl ester **106** (800 mg, 2.60 mmol, 1.00 equiv.)
- THF (10 mL), MeOH (10 mL), 3 N KOH (aq.) (10 mL)
- 2 h, r.t., workup method A
- the title compound **107** (481 mg, 1.80 mmol, 70%) was obtained as a colourless solid

^1H NMR (400 MHz, DMSO- d_6) δ 13.51 (br. s, 1H), 7.67 (dd, $J=8.5, 0.8$ Hz, 1H), 7.53 (dd, $J=8.5, 0.8$ Hz, 1H), 5.98–6.12 (m, 1H), 5.38 (dt, $J=17.3, 0.8$ Hz, 1H), 5.21–5.29 (m, 1H), 4.58 (d, $J=5.8$ Hz, 2H), 4.12–4.22 (m, 2H), 1.26–1.34 ppm (m, 3H). ^{13}C NMR (101 MHz, DMSO- d_6) δ 164.6, 153.2, 147.8, 137.7, 134.7, 133.2, 127.4, 117.5, 116.8, 110.9, 109.3, 74.0, 67.5, 64.1, 15.5. HRMS (ESI): m/z calculated for $\text{C}_{12}\text{H}_{13}\text{NO}_6$ ($\text{M}-\text{H}$) $^-$ 266.0659, found 266.0665 ($\Delta m = +2.3$ ppm).

O₂N-E(Ethoxy-Allyl)-F(Ethoxy-Allyl)-OAllyl (108)



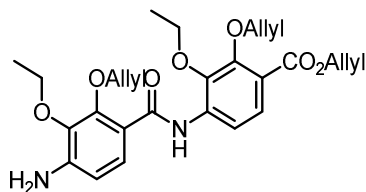
Peptide coupling using BTC according to GP4:

- benzoic acid **107** (435 mg, 1.63 mmol, 1.30 equiv) in THF (25 mL)
- 2,4,6-collidine (1.73 mL, 13.0 mmol, 8.00 equiv based on **107**)
- BTC (145 mg, 567 μmol , 0.30 equiv based on **107**)
- aniline **106** (349 mg, 1.26 mmol, 1.00 equiv) in THF (25 mL)
- DIPEA (2.26 mL, 12.6 mmol, 10.0 equiv)
- column chromatography: SiO_2 , n -hexane/EtOAc, 10:1
- the dipeptide **108** (377 mg, 716 μmol , 57%) was obtained as a yellow oil

^1H NMR (400 MHz, DMSO- d_6) δ 10.63 (s, 1H), 8.41 (d, $J=8.8$ Hz, 1H), 8.03 (d, $J=8.8$ Hz, 1H), 7.68 (d, $J=8.8$ Hz, 1H), 7.63 (d, $J=8.8$ Hz, 1H), 5.99–6.19 (m, 3H), 5.36–5.44 (m, 2H), 5.24–5.34 (m, 4H), 4.81 (dt, $J=1.4, 5.64$ Hz, 2H), 4.78 (d, $J=6.7$ Hz, 2H), 4.59 (dt, $J=1.3, 5.9$ Hz, 2H), 4.29 (q, $J=7.0$ Hz, 2H), 4.21 (q, $J=7.0$ Hz, 2H), 1.47 (t, $J=7.0$ Hz, 3H), 1.41 (t, $J=7.0$ Hz, 3H). ^{13}C NMR (101 MHz, DMSO- d_6) δ 15.2, 15.3, 65.1, 69.2, 70.9, 74.5, 75.6, 115.5, 117.7, 118.1, 119.5, 120.2, 121.1, 125.0, 126.0, 132.4, 132.6, 132.9, 133.9, 136.3, 142.0, 145.1, 146.7, 150.5, 151.3,

162.0, 164.5. HRMS (ESI): m/z calculated for $C_{27}H_{30}N_2O_9$ $[M+H]^+$ 527.1951, found 527.2024 ($\Delta m = 13.8$ ppm).

H₂N-E(Ethoxy-Allyl)-F(Ethoxy-Allyl)-OAllyl (109)

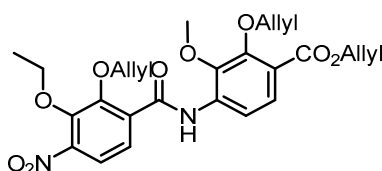


Reduction of the nitro group according to GP2:

- nitro dipeptide **108** (325 mg, 617 μ mol, 1.00 equiv)
- EtOAc (15 mL)
- $SnCl_2 \cdot 2 H_2O$ (696 mg, 3.09 mmol, 5.00 equiv)
- dipeptide **109** (334 mg, 673 μ mol, quant.) was obtained as a brown oil

1H NMR (400 MHz, $DMSO-d_6$) δ 10.63 (s, 1H), 8.41 (d, $J=8.8$ Hz, 1H), 8.03 (d, $J=8.8$ Hz, 1H), 7.68 (d, $J=8.8$ Hz, 1H), 7.63 (d, $J=8.8$ Hz, 1H), 5.99–6.19 (m, 3H), 5.36–5.44 (m, 2H), 5.24–5.34 (m, 4H), 4.81 (dt, $J=1.4, 5.64$ Hz, 2H), 4.78 (d, $J=6.7$ Hz, 2H), 4.59 (dt, $J=1.3, 5.9$ Hz, 2H), 4.29 (q, $J=7.0$ Hz, 2H), 4.21 (q, $J=7.0$ Hz, 2H), 1.47 (t, $J=7.0$ Hz, 3H), 1.41 (t, $J=7.0$ Hz, 3H).

O₂N-E(Ethoxy-Allyl)-F(Allyl)-OAllyl (111)

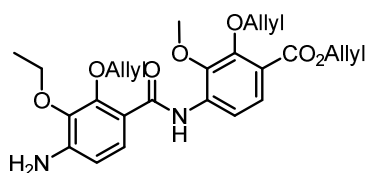


Peptide coupling using BTC according to GP4:

- benzoic acid **107** (396 mg, 1.48 mmol, 1.30 equiv) in THF (15 mL)
- 2,4,6-collidine (1.57 mL, 11.8 mmol, 8.00 equiv based on **107**)
- BTC (132 mg, 444 μ mol, 0.30 equiv based on **107**)
- aniline **110** (300 mg, 1.14 mmol, 1.00 equiv) in THF (5 mL)
- DIPEA (1.98 mL, 11.4 mmol, 10.0 equiv)
- column chromatography: SiO_2 , n -hexane/EtOAc, 10:1
- the dipeptide **111** (382 mg, 741 μ mol, 65%) was obtained as a yellow solid

^1H NMR (400 MHz, $\text{DMSO-}d_6$) δ 10.43 (s, 1H), 8.20 (d, $J=8.8$ Hz, 1H), 7.68–7.82 (m, 2H), 7.56 (d, $J=8.8$ Hz, 1H), 5.93–6.16 (m, 3H), 5.32–5.45 (m, 3H), 5.19–5.31 (m, 3H), 4.71–4.81 (m, 4H), 4.53 (d, $J=5.8$ Hz, 2H), 4.22 (q, $J=7.0$ Hz, 2H), 3.88 (s, 3H), 1.34 (t, $J=7.0$ Hz, 3H). ^{13}C NMR (101 MHz, $\text{DMSO-}d_6$) δ 164.5, 162.4, 151.2, 150.5, 146.6, 145.0, 143.3, 136.0, 133.9, 133.2, 132.6, 126.0, 124.9, 121.1, 119.7, 119.3, 118.2, 117.9, 115.7, 75.3, 74.6, 70.9, 65.2, 61.1, 15.3. HRMS (ESI): m/z calculated for $\text{C}_{26}\text{H}_{28}\text{N}_2\text{O}_9$ $[\text{M}+\text{Na}]^+$ 535.1687, found 535.1681 ($\Delta m = -1.1$ ppm).

$\text{H}_2\text{N-E(Ethoxy-Allyl)-F(Allyl)-OAllyl}$ (**112**)

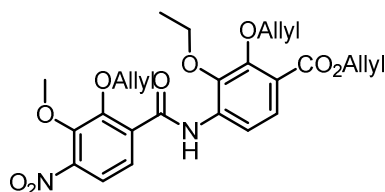


Reduction of the nitro group according to GP2:

- nitro dipeptide **111** (353 mg, 617 μmol , 1.00 equiv)
- EtOAc (15 mL)
- $\text{SnCl}_2 \cdot 2 \text{H}_2\text{O}$ (777 mg, 3.44 mmol, 5.00 equiv)
- dipeptide **112** (278 mg, 579 μmol , 84%) was obtained as a yellow oil

^1H NMR (400 MHz, $\text{DMSO-}d_6$) δ 10.64 (s, 1H), 8.35 (d, $J=8.8$ Hz, 1H), 7.58 (d, $J=8.8$ Hz, 1H), 7.53 (d, $J=8.8$ Hz, 1H), 6.57 (d, $J=8.8$ Hz, 1H), 5.97–6.15 (m, 3H), 5.81 (s, 2H), 5.33–5.44 (m, 3H), 5.21–5.30 (m, 3H), 4.73–4.81 (m, 4H), 4.52 (dt, $J=5.6, 1.3$ Hz, 2H), 3.95 (q, $J=7.0$ Hz, 2H), 3.86–3.90 (m, 3H), 1.36 (t, $J=7.0$ Hz, 3H). ^{13}C NMR (101 MHz, $\text{DMSO-}d_6$) δ 164.5, 163.1, 151.1, 150.7, 147.9, 142.0, 137.3, 136.3, 134.0, 133.1, 132.7, 127.0, 126.4, 119.4, 119.3, 118.1, 117.8, 114.4, 112.8, 110.2, 74.7, 74.5, 67.6, 65.0, 60.9, 15.5. HRMS (ESI): m/z calculated for $\text{C}_{26}\text{H}_{30}\text{N}_2\text{O}_7$ $[\text{M}+\text{H}]^+$ 483.2126, found 483.2123 ($\Delta m = -0.6$ ppm).

$\text{O}_2\text{N-E(Allyl)-F(Ethoxy-Allyl)-OAllyl}$ (**114**)



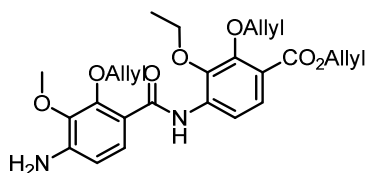
Peptide coupling using BTC according to GP4:

- benzoic acid **113** (475 mg, 1.88 mmol, 1.30 equiv) in THF (15 mL)

- 2,4,6-collidine (1.99 mL, 15.0 mmol, 8.00 equiv based on **107**)
- BTC (166 mg, 563 μmol , 0.30 equiv based on **107**)
- aniline **106** (400 mg, 1.44 mmol, 1.00 equiv) in THF (5 mL)
- DIPEA (2.51 mL, 14.4 mmol, 10.0 equiv)
- column chromatography: SiO_2 , *n*-hexane/EtOAc, 10:1
- the dipeptide **115** (454 mg, 878 μmol , 61%) was obtained as a yellow solid

^1H NMR (400 MHz, $\text{DMSO-}d_6$) δ 10.44 (s, 1H), 8.22 (d, $J=8.8$ Hz, 1H), 7.68–7.89 (m, 2H), 7.56 (d, $J=8.8$ Hz, 1H), 5.96–6.16 (m, 3H), 5.33–5.45 (m, 3H), 5.21–5.30 (m, 3H), 4.77 (dt, $J=5.5$, 1.5 Hz, 2H), 4.72 (d, $J=6.5$ Hz, 2H), 4.54 (d, $J=5.8$ Hz, 2H), 4.12 (q, $J=7.0$ Hz, 2H), 4.00 (s, 3H), 1.35 (t, $J=7.0$ Hz, 3H). ^{13}C NMR (101 MHz, $\text{DMSO-}d_6$) δ 164.5, 162.0, 151.3, 150.4, 146.3, 146.2, 142.0, 136.3, 133.9, 133.0, 132.6, 132.4, 126.1, 125.1, 121.1, 120.4, 119.5, 118.2, 117.7, 75.7, 74.5, 69.3, 65.2, 62.2, 15.4. HRMS (ESI): m/z calculated for $\text{C}_{26}\text{H}_{28}\text{N}_2\text{O}_9$ $[\text{M}+\text{H}]^+$ 513.1868, found 513.1865 ($\Delta m = -0.6$ ppm).

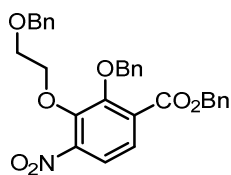
H₂N-E(Allyl)-F(Ethoxy-Allyl)-OAllyl (115)



Reduction of the nitro group according to GP2:

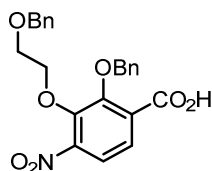
- nitro dipeptide **114** (454 mg, 886 μmol , 1.00 equiv)
- EtOAc (15 mL)
- $\text{SnCl}_2 \cdot 2 \text{H}_2\text{O}$ (999 mg, 4.43 mmol, 5.00 equiv)
- dipeptide **115** (376 mg, 780 μmol , 88%) was obtained as a yellow oil

^1H NMR (400 MHz, $\text{DMSO-}d_6$) δ 10.65 (s, 1H), 8.34 (d, $J=8.8$ Hz, 1H), 7.54 (dd, $J=9.8$, 8.8 Hz, 2H), 6.57 (d, $J=8.5$ Hz, 1H), 5.94–6.16 (m, 3H), 5.87 (s, 2H), 5.17–5.47 (m, 6H), 4.73 (dd, $J=17.6$, 5.8 Hz, 4H), 4.54 (d, $J=5.5$ Hz, 2H), 4.09 (q, $J=7.0$ Hz, 2H), 3.76 (s, 3H), 1.36 (t, $J=7.0$ Hz, 3H). ^{13}C NMR (101 MHz, $\text{DMSO-}d_6$) δ 164.5, 163.0, 151.3, 150.5, 147.4, 140.9, 137.8, 137.7, 134.1, 133.0, 132.7, 127.0, 126.4, 119.9, 119.3, 118.0, 117.6, 114.3, 113.0, 110.2, 75.1, 74.4, 69.1, 65.0, 59.6, 15.4. HRMS (ESI): m/z calculated for $\text{C}_{26}\text{H}_{30}\text{N}_2\text{O}_7$ $[\text{M}+\text{H}]^+$ 483.2126, found 483.2122 ($\Delta m = -0.8$ ppm).

Benzyl 2-(benzyloxy)-3-(2-(benzyloxy)ethoxy)-4-nitrobenzoate (102)

Phenol **96** (200 mg, 527 μmol , 1.00 equiv) was dissolved in DMF (15 mL) and successively treated with K_2CO_3 (80.0 mg, 580 μmol , 1.10 equiv), and ((2-bromoethoxy)methyl)benzene (170 mg, 791 μmol , 1.50 equiv). After stirring at 110 $^\circ\text{C}$ for 16 h, the reaction was stopped by the addition of ice water and the aq. solution was extracted with EtOAc (5 \times). The combined organic phases were washed with brine (3 \times), dried over anhydrous Na_2SO_4 , and concentrated under reduced pressure. Purification of the crude product by column chromatography on silica gel (*n*-hexane/EtOAc, 10:1) afforded the title compound **102** (172 mg, 335 μmol , 64%) as a yellow oil.

^1H NMR (400 MHz, $\text{DMSO-}d_6$) δ 3.66–3.69 (m, 2H), 4.29–4.31 (m, 2H), 4.44 (s, 2H), 5.06 (s, 2H), 5.32 (s, 2H), 7.22–7.43 (m, 15H), 7.60 (d, $J=8.6$ Hz, 1H), 7.73 (d, $J=8.6$ Hz, 1H). ^{13}C NMR (101 MHz, $\text{DMSO-}d_6$) δ 67.2, 68.9, 72.1, 73.9, 75.9, 119.5, 125.2, 127.4, 127.5, 128.2, 128.3, 128.4, 128.5, 130.8, 135.5, 136.1, 138.1, 145.9, 146.9, 151.7, 164.2. HRMS (ESI): m/z calculated for $\text{C}_{30}\text{H}_{27}\text{NO}_7$ [$\text{M}+\text{Na}$] $^+$ 536.1680, found 536.1673 ($\Delta m = +1.3$ ppm).

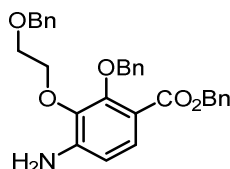
2-(Benzyloxy)-3-(2-(benzyloxy)ethoxy)-4-nitrobenzoic acid (116)

To a solution of benzyl ester **102** (410 mg, 798 μmol , 1.00 equiv) in a mixture of THF (7 mL) and MeOH (7 mL) was added 3 N $\text{KOH}_{(\text{aq.})}$. After stirring the reaction mixture at r.t. for 2 d, the organic solvents were removed under reduced pressure. The aq. residue was taken up in EtOAc and washed with 3 N $\text{HCl}_{(\text{aq.})}$ and brine (3 \times). The organic phase was dried over anhydrous Na_2SO_4 and concentrated *in vacuo* to afford the title compound **116** (354 mg, 836 μmol , quant.) as a yellow oil.

^1H NMR (400 MHz, $\text{DMSO-}d_6$) δ 3.67–3.70 (m, 2H), 4.30–4.32 (m, 2H), 4.45 (s, 2H), 5.08 (s, 2H), 7.25–7.35 (m, 8H), 7.44–7.46 (m, 2H) 7.55 (d, $J=8.5$ Hz, 1H), 7.71 (d, $J=8.5$ Hz, 1H). ^{13}C NMR (101 MHz, $\text{DMSO-}d_6$) δ 68.9, 72.2, 73.8, 75.7, 119.5, 124.8, 127.5, 128.2, 128.3, 128.6, 132.6,

138.1, 145.9, 146.4, 151.4, 166.1. HRMS (ESI): m/z calculated for $C_{23}H_{21}NO_7$ $[M-Na]^-$ 422.1234, found 422.1255 ($\Delta m = +5.0$ ppm).

Benzyl 4-amino-2-(benzyloxy)-3-(2-(benzyloxy)ethoxy)benzoate (**117**)

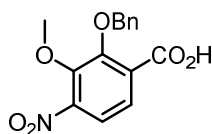


Reduction of the nitro group according to GP1:

- EtOH (20 mL), AcOH (4 mL)
- nitrobenzoate **102** (250 mg, 487 μ mol, 1.00 equiv)
- Zn-dust (2.30 g)
- 0 °C to r.t., 45 min
- the title compound **117** (235 mg, 487 μ mol, quant.) was obtained as a brown oil

1H -NMR (400 MHz, $CDCl_3$) δ 3.58–3.60 (m, 2H), 4.08–4.10 (m, 2H), 4.41 (s, 2H), 4.95 (s, 2H), 5.21 (s, 2H), 6.46 (d, $J=8.6$ Hz, 1H), 7.21–7.35 (m, 15H), 7.49 (d, $J=8.6$ Hz, 1H). ^{13}C NMR (101 MHz, $CDCl_3$). δ 66.4, 69.3, 72.6, 73.4, 76.1, 111.0, 115.1, 128.0, 128.2, 128.4, 128.6, 128.7, 136.6, 137.6, 137.8, 139.6, 145.2, 153.9, 165.5. HRMS (ESI): m/z calculated for $C_{30}H_{29}NO_5$ $[M+H]^+$ 483.2119, found 483.2121 ($\Delta m = +0.4$ ppm).

2-(Benzyloxy)-3-methoxy-4-nitrobenzoic acid (**119**)



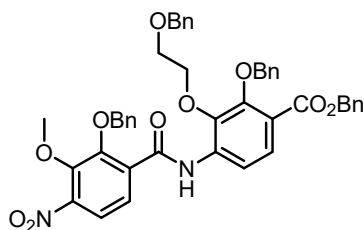
Hydrolysis of the allyl ester according to GP3:

- benzyl ester **98** (300 mg, 763 μ mol, 1.00 equiv.)
- THF (10 mL), MeOH (10 mL), 3 N KOH (aq.) (10 mL)
- 2 h, r.t., workup method A
- the title compound **119** (230 mg, 763 μ mol, quant.) was obtained as a colourless solid

1H NMR (400 MHz, $DMSO-d_6$) δ 13.61 (s, 1H), 7.72 (d, $J=8.6$ Hz, 1H), 7.57 (d, $J=8.5$ Hz, 1H), 7.53–7.46 (m, 2H), 7.46–7.32 (m, 3H), 5.07 (s, 2H), 3.93 (s, 3H). ^{13}C NMR (101 MHz, $DMSO-d_6$) δ 166.0, 151.5, 146.7, 146.2, 136.4, 132.5, 128.4, 128.3, 124.9, 119.3, 75.9, 62.3, 40.2, 39.9,

39.7, 39.5, 39.3, 39.1, 38.9. HRMS (ESI): m/z calculated for $C_{15}H_{13}NO_6$ $[M+H]^+$ 302.0670, found 302.0668 ($\Delta m = -0.7$ ppm).

Ethylene glycol-containing nitro dipeptide (**120**)

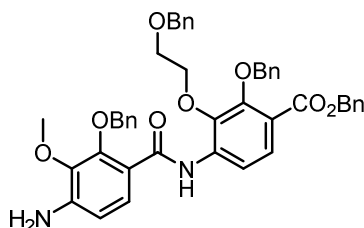


Peptide coupling using BTC according to GP4:

- benzoic acid **119** (295 mg, 972 μ mol, 2.00 equiv) in THF (10 mL)
- 2,4,6-collidine (1.03 mL, 7.78 mmol, 8.00 equiv based on **119**)
- BTC (86.5 mg, 292 μ mol, 0.30 equiv based on **107**)
- aniline **117** (235 mg, 486 μ mol, 1.00 equiv) in THF (3 mL)
- DIPEA (0.846 mL, 4.86 mmol, 10.0 equiv)
- column chromatography: SiO_2 , *n*-hexane/EtOAc, 6:1
- the dipeptide **120** (273 mg, 355 μ mol, 73%) was obtained as an orange oil

1H NMR (400 MHz, $DMSO-d_6$) δ 10.23 (s, 1H), 8.20 (d, $J=8.8$ Hz, 1H), 7.73 (d, $J=8.6$ Hz, 1H), 7.63 (dd, $J=14.8, 8.7$ Hz, 2H), 7.48–7.41 (m, 2H), 7.45–7.29 (m, 10H), 7.32–7.21 (m, 3H), 7.20–7.11 (m, 3H), 7.07–7.00 (m, 2H), 5.31 (s, 2H), 5.14 (s, 2H), 4.98 (s, 2H), 4.24 (s, 2H), 4.12–4.07 (m, 2H), 3.91 (s, 3H), 3.58–3.52 (m, 2H), 1.17 (t, $J=7.1$ Hz, 1H). ^{13}C NMR (101 MHz, $DMSO-d_6$) δ 164.6, 161.9, 151.2, 150.4, 146.2, 141.8, 137.7, 136.7, 136.5, 136.1, 135.3, 133.5, 129.1, 128.7, 128.5, 128.5, 128.3, 128.3, 128.2, 128.1, 127.3, 127.1, 126.4, 125.0, 120.9, 119.7, 115.3, 76.6, 75.3, 72.6, 71.9, 68.5, 66.3, 62.1, 54.9. HRMS (ESI): m/z calculated for $C_{45}H_{40}N_2O_{10}$ $[M+H]^+$ 769.2756, found 769.2757 ($\Delta m = -0.1$ ppm).

Ethylene glycol-containing nitro dipeptide (**121**)



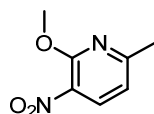
Reduction of the nitro group according to GP1:

- EtOH (15 mL), AcOH (5 mL)

- nitrobenzamidobenzoate **120** (260 mg, 338 μmol , 1.00 equiv)
- Zn-dust (5.0 g)
- 0 °C, 1 h
- column chromatography: SiO_2 , *n*-hexane/EtOAc, 4:1–3:1
- the title compound **121** (250 mg, 260 μmol , 77%) was obtained as a brown oil

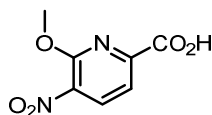
^1H NMR (400 MHz, $\text{DMSO-}d_6$) δ 10.51 (s, 1H), 8.29 (d, $J=8.8$ Hz, 1H), 7.54 (d, $J=8.8$ Hz, 1H), 7.49 (d, $J=8.7$ Hz, 1H), 7.46–7.29 (m, 13H), 7.29–7.22 (m, 3H), 7.18 (dd, $J=5.0, 1.9$ Hz, 3H), 7.08 (dd, $J=6.4, 2.9$ Hz, 2H), 6.57 (d, $J=8.7$ Hz, 1H), 5.86 (s, 2H), 5.29 (s, 2H), 5.12 (s, 2H), 4.95 (s, 2H), 4.28 (s, 2H), 4.01–3.94 (m, 2H), 3.72 (s, 3H), 3.49 (dd, $J=5.7, 3.5$ Hz, 2H). ^{13}C NMR (101 MHz, $\text{DMSO-}d_6$) δ 164.7, 163.1, 150.9, 150.7, 147.3, 141.0, 137.9, 137.9, 137.8, 136.8, 136.2, 135.9, 129.2, 128.5, 128.5, 128.4, 128.3, 128.2, 128.1, 128.1, 128.0, 127.4, 127.3, 126.9, 126.4, 119.2, 114.4, 113.7, 110.3, 76.0, 75.1, 72.3, 72.1, 68.7, 66.1, 59.7. HRMS (ESI): m/z calculated for $\text{C}_{45}\text{H}_{40}\text{N}_2\text{O}_{10}$ $[\text{M}+\text{H}]^+$ 738.2936, found 739.3000 ($\Delta m = +8.6$ ppm).

2-Methoxy-6-methyl-3-nitropyridine (**123**)



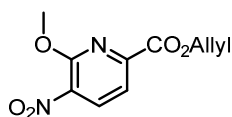
6-Methyl-3-nitropyridin-2(1*H*)-one (**122**) (7.00 g, 45.4 mmol, 1.00 equiv) was dissolved in toluene (120 mL), then Ag_2CO_3 (13.8 g, 50.0 mmol, 1.10 equiv) was added followed by MeI (5.65 mL, 90.8 mmol, 2.00 equiv). The reaction mixture was stirred at 80 °C for 16 h. After filtration through a pad of Celite®, the filtrate was concentrated *in vacuo* to obtain a crude product which was purified by column chromatography on silica gel (*n*-hexane/EtOAc, 3:1). The title compound **123** (6.03 g, 35.9 mmol, 79%) was obtained as a yellow solid.

^1H NMR (400 MHz, $\text{DMSO-}d_6$) δ 8.33 (d, $J=8.3$ Hz, 1H), 7.08 (d, $J=8.0$ Hz, 1H), 3.99 (s, 3H), 2.50 (s, 3H). ^{13}C NMR (101 MHz, $\text{DMSO-}d_6$) δ 162.6, 155.0, 135.9, 131.3, 116.5, 54.3, 24.1. HRMS (ESI): m/z calculated for $\text{C}_7\text{H}_8\text{N}_2\text{O}_3$ $[\text{M}+\text{H}]^+$ 169.0608, found 169.0603 ($\Delta m = -3.0$ ppm).

6-Methoxy-5-nitropicolinic acid (124)

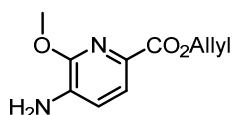
2-Methoxy-6-methyl-3-nitropyridine (**123**) (6.00 g, 35.7 mmol, 1.00 equiv) was dissolved in conc. H_2SO_4 (120 mL) and the solution was cooled down to 0 °C. CrO_3 (17.8 g, 178 mmol, 5.00 equiv) was added at that temperature portionwise and carefully over the time period of 5 min. After stirring at r.t. for 16 h, the reaction mixture was poured into a mixture of ice and water (~1 L) under vigorous stirring. The precipitate was isolated by filtration through a sintered funnel and dried under high vacuum to afford the title compound **124** (4.89 g, 24.6 mmol, 68%) as a colourless solid.

^1H NMR (400 MHz, $\text{DMSO}-d_6$) δ 13.72 (s, 1H), 8.54 (d, $J=8.0$ Hz, 1H), 7.79 (d, $J=8.0$ Hz, 1H), 4.07 (s, 3H). ^{13}C NMR (101 MHz, $\text{DMSO}-d_6$) δ 164.3, 155.0, 149.3, 136.4, 135.8, 118.2, 54.9.

Allyl 6-methoxy-5-nitropicolinate (124a)

6-Methoxy-5-nitropicolinic acid (**124**) (2.00 g, 10.1 mmol, 1.00 equiv) was dissolved in allyl alcohol (15 mL) and SOCl_2 (2.20 mL, 30.3 mmol, 3.00 equiv) was added dropwise. The reaction mixture was stirred at r.t. for 16 h before all volatiles were removed under reduced pressure. Purification of the crude product by column chromatography on silica gel (*n*-hexane/EtOAc, 3:1) afforded the title compound **124a** (2.23 g, 9.38 mmol, 93%) as an orange oil.

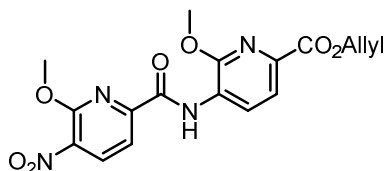
^1H NMR (400 MHz, $\text{DMSO}-d_6$) δ 8.57 (d, $J=8.0, 0.7$ Hz, 1H), 7.85 (d, $J=8.0$ Hz, 1H), 6.12–5.98 (m, 1H), 5.45 (dq, $J=17.3, 1.6$ Hz, 1H), 5.31 (dq, $J=10.5, 1.4$ Hz, 1H), 4.86 (dt, $J=5.4, 1.5$ Hz, 2H), 4.07 (s, 3H). ^{13}C NMR (101 MHz, $\text{DMSO}-d_6$) δ 162.4, 155.1, 147.9, 136.6, 136.1, 132.1, 118.5, 118.3, 66.0, 54.9. HRMS (ESI): m/z calculated for $\text{C}_{10}\text{H}_{10}\text{N}_2\text{O}_5$ $[\text{M}+\text{H}]^+$ 239.0662, found 239.0665 ($\Delta m = +1.3$ ppm).

Allyl 5-amino-6-methoxypicolinate (125)

Reduction of the nitro group according to GP1:

- EtOH (30 mL), AcOH (15 mL)
- nitropicolinate **124a** (2.15 g, 9.03 mmol, 1.00 equiv)
- Zn-dust (14.8 g)
- 0 °C, 2 h
- column chromatography: SiO₂, *n*-hexane/EtOAc, 4:1–2:1
- the title compound **125** (1.72 g, 8.22 mmol, 91%) was obtained as a brown oil

¹H NMR (400 MHz, DMSO-*d*₆) δ 7.56 (d, *J*=7.9 Hz, 1H), 6.87 (d, *J*=7.9 Hz, 1H), 6.08–5.94 (m, 1H), 5.88 (s, 2H), 5.43–5.33 (m, 1H), 5.27–5.19 (m, 1H), 4.72 (dt, *J*=5.3, 1.6 Hz, 2H), 3.91 (s, 3H). ¹³C NMR (101 MHz, DMSO-*d*₆) δ 164.1, 150.4, 137.1, 133.1, 129.3, 121.7, 117.3, 116.3, 64.3, 52.9. HRMS (ESI): *m/z* calculated for C₁₀H₁₂N₂O₃ [M+H]⁺ 209.0921, found 209.0918 (Δ*m* = –1.4 ppm).

O₂N-E(pyridine)-F(pyridine)-OAllyl (126)

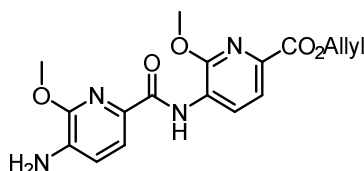
Peptide coupling using BTC according to GP4:

- benzoic acid **124** (1.14 g, 5.76 mmol, 2.00 equiv) in THF (30 mL)
- 2,4,6-collidine (6.11 mL, 46.1 mmol, 8.00 equiv based on **124**)
- BTC (513 mg, 1.73 mmol, 0.30 equiv based on **124**)
- aniline **125** (0.800 mg, 3.84 mmol, 1.00 equiv) in THF (15 mL)
- DIPEA (6.69 mL, 38.4 mmol, 10.0 equiv)
- column chromatography: SiO₂, 0.5% MeOH in CHCl₃
- the dipeptide **126** (1.25 g, 3.23 mmol, 84%) was obtained as a yellow solid

¹H NMR (400 MHz, CDCl₃) δ 10.35 (s, 1H), 8.85 (d, *J*=8.3 Hz, 1H), 8.46 (d, *J*=7.8 Hz, 1H), 8.01 (d, *J*=8.0 Hz, 1H), 7.86 (d, *J*=8.0 Hz, 1H), 5.99–6.15 (m, 1H), 5.46 (dq, *J*=17.1, 1.6 Hz, 1H), 5.31 (dq, *J*=10.5, 1.3 Hz, 1H), 4.87 (dt, *J*=5.6, 1.4 Hz, 2H), 4.28 (s, 3H), 4.18 (s, 3H). ¹³C NMR (101 MHz,

CDCl_3) δ 164.3, 160.5, 155.5, 152.9, 149.8, 139.1, 136.9, 136.4, 132.1, 125.5, 120.4, 118.5, 115.7, 66.0, 55.0, 54.5, 30.3. HRMS (ESI): m/z calculated for $\text{C}_{17}\text{H}_{16}\text{N}_4\text{O}_7$ $[\text{M}+\text{H}]^+$ 389.1092, found 389.1085 ($\Delta m = -1.8$ ppm).

$\text{H}_2\text{N-E(pyridine)-F(pyridine)-OAllyl}$ (**127**)

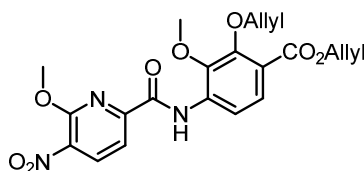


Reduction of the nitro group according to GP1:

- THF (15 mL), EtOH (35 mL), AcOH (10 mL)
- nitro dipeptide **126** (1.15 g, 2.96 mmol, 1.00 equiv)
- Zn-dust (15.5 g)
- 0 °C to r.t., 16 h
- column chromatography: SiO_2 , *n*-hexane/EtOAc, 3:1–1:2
- the title compound **127** (1.06 g, 2.96 mmol, quant.) was obtained as a yellow solid

^1H NMR (400 MHz, $\text{DMSO-}d_6$) δ 10.27 (s, 1H), 8.72 (d, $J=8.0$ Hz, 1H), 7.78 (d, $J=8.0$ Hz, 1H), 7.58 (d, $J=8.0$ Hz, 1H), 6.97 (d, $J=8.0$ Hz, 1H), 6.11–5.98 (m, 1H), 5.97 (s, 2H), 5.43 (dq, $J=17.2, 1.7$ Hz, 1H), 5.28 (dq, $J=10.5, 1.5$ Hz, 1H), 4.79 (dt, $J=5.3, 1.5$ Hz, 2H), 4.05 (s, 3H), 4.02 (s, 3H). ^{13}C NMR (101 MHz, $\text{DMSO-}d_6$) δ 163.5, 162.6, 152.1, 149.6, 137.4, 136.6, 132.6, 130.8, 126.5, 123.6, 120.4, 118.3, 117.8, 117.4, 65.0, 54.1, 52.9. HRMS (ESI): m/z calculated for $\text{C}_{17}\text{H}_{18}\text{N}_4\text{O}_5$ $[\text{M}+\text{H}]^+$ 359.1350, found 359.1355 (+1.39 ppm).

$\text{O}_2\text{N-E(pyridine)-F(Allyl)-OAllyl}$ (**128**)



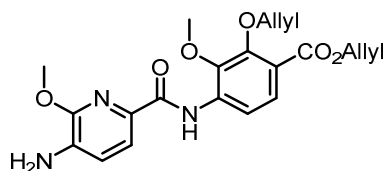
Peptide coupling using BTC according to GP4:

- benzoic acid **124** (1.35 g, 6.84 mmol, 1.50 equiv) in THF (15 mL)
- 2,4,6-collidine (7.25 mL, 54.7 mmol, 8.00 equiv based on **124**)
- BTC (609 mg, 2.05 mmol, 0.30 equiv based on **124**)
- aniline **110** (1.20 g, 4.56 mmol, 1.00 equiv) in THF (5 mL)

- DIPEA (7.94 mL, 45.6 mmol, 10.0 equiv)
- column chromatography: SiO₂, *n*-hexane/EtOAc, 7:1–5:1
- the dipeptide **128** (1.83 g, 4.10 mmol, 90%) was obtained as a yellow solid

¹H NMR (400 MHz, DMSO-*d*₆) δ 10.44 (s, 1H), 8.70–8.63 (m, 1H), 8.23 (d, *J*=8.7 Hz, 1H), 7.92 (d, *J*=8.0 Hz, 1H), 7.58 (d, *J*=8.7 Hz, 1H), 6.16–5.96 (m, 2H), 5.46–5.34 (m, 2H), 5.32–5.20 (m, 2H), 4.77 (dt, *J*=5.5, 1.5 Hz, 2H), 4.54 (dt, *J*=5.7, 1.4 Hz, 2H), 4.21 (s, 3H), 3.97 (s, 3H). ¹³C NMR (101 MHz, DMSO-*d*₆) δ 164.3, 159.7, 154.6, 151.2, 149.2, 142.6, 137.6, 136.1, 135.1, 133.8, 132.5, 126.5, 121.1, 118.2, 117.8, 115.7, 113.8, 74.6, 65.2, 61.2, 55.0. HRMS (ESI): *m/z* calculated for C₂₁H₂₁N₃O₈ [M+H]⁺ 444.1401, found 444.1407 (Δ*m* = +1.35 ppm).

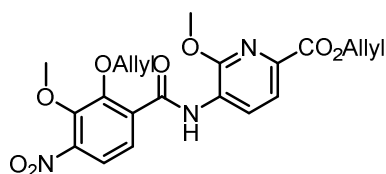
H₂N-E(pyridine)-F(Allyl)-OAllyl (**129**)



Reduction of the nitro group according to GP1:

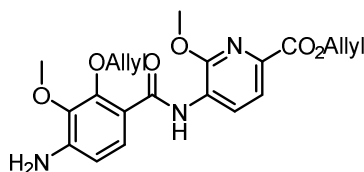
- THF (12.5 mL), EtOH (37.5 mL), AcOH (10 mL)
- nitro dipeptide **128** (1.80 g, 4.06 mmol, 1.00 equiv)
- Zn-dust (13.3 g)
- 0 °C to r.t., 16 h
- column chromatography: SiO₂, *n*-hexane/EtOAc, 3:1
- the title compound **129** (1.58 g, 3.81 mmol, 94%) was obtained as a yellow solid

¹H NMR (400 MHz, DMSO-*d*₆) δ 10.41 (s, 1H), 8.36–8.27 (m, 1H), 7.64–7.54 (m, 2H), 7.03–6.95 (m, 1H), 6.16–5.96 (m, 2H), 5.95 (s, 2H), 5.47–5.34 (m, 2H), 5.31–5.19 (m, 2H), 4.76 (dt, *J*=5.5, 1.5 Hz, 2H), 4.54 (dt, *J*=5.7, 1.4 Hz, 2H), 4.05 (s, 3H), 3.95 (s, 3H). ¹³C NMR (101 MHz, DMSO) δ 164.4, 162.1, 151.4, 149.6, 141.9, 137.2, 136.6, 134.0, 132.6, 131.3, 126.7, 119.4, 118.3, 118.1, 117.6, 117.5, 113.0, 74.6, 65.0, 60.9, 53.0. HRMS (ESI): *m/z* calculated for C₂₁H₂₃N₃O₆ [M+H]⁺ 414.1660, found 414.1649.

O₂N-E(Allyl)-F(pyridine)-OAllyl (130)

Peptide coupling using BTC according to GP4:

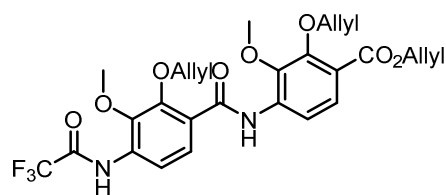
- benzoic acid **113** (1.46 g, 5.76 mmol, 1.50 equiv) in THF (15 mL)
- 2,4,6-collidine (6.11 mL, 46.1 mmol, 8.00 equiv based on **113**)
- BTC (513 mg, 1.73 mmol, 0.30 equiv based on **113**)
- aniline **110** (800 mg, 3.84 mmol, 1.00 equiv) in THF (5 mL)
- DIPEA (6.69 mL, 38.4 mmol, 10.0 equiv)
- column chromatography: SiO₂, *n*-hexane/EtOAc, 6:1
- the dipeptide **130** (1.18 g, 3.84 mmol, 69%) was obtained as a yellow solid

H₂N-E(Allyl)-F(pyridine)-OAllyl (131)

Reduction of the nitro group according to GP1:

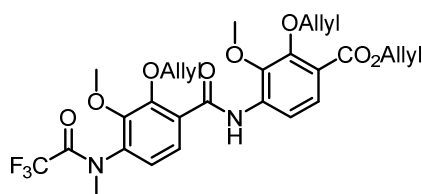
- THF (15 mL), EtOH (30 mL), AcOH (8 mL)
- nitro dipeptide **130** (1.10 g, 2.48 mmol, 1.00 equiv)
- Zn-dust (14.8 g)
- 0 °C to r.t., 16 h
- column chromatography: SiO₂, *n*-hexane/EtOAc, 3:1–1:1
- the title compound **131** (889 mg, 2.15 mmol, 87%) was obtained as a yellow solid

¹H NMR (400 MHz, DMSO-*d*₆) δ 10.41 (s, 1H), 8.31 (d, *J*=8.8, 0.8 Hz, 1H), 7.60 (dd, *J*=7.9, 0.8 Hz, 1H), 7.57 (d, *J*=8.8, 0.9 Hz, 1H), 6.99 (d, *J*=7.9 Hz, 1H), 6.06 (d, 2H), 5.95 (s, 2H), 5.45–5.35 (m, 2H), 5.30–5.20 (m, 2H), 4.76 (dt, *J*=5.5, 1.5 Hz, 2H), 4.54 (dt, *J*=5.7, 1.4 Hz, 2H), 4.05 (s, 3H), 3.95 (s, 3H). ¹³C NMR (101 MHz, DMSO-*d*₆) δ 164.4, 162.1, 151.4, 149.6, 141.9, 137.2, 136.6, 134.0, 132.6, 131.3, 126.7, 119.4, 118.3, 118.1, 117.6, 117.5, 113.0, 74.6, 65.0, 60.9, 53.0. HRMS (ESI): *m/z* calculated for C₂₁H₂₃N₃O₆ [M+H]⁺ 414.1660, found 414.1668 (Δ*m* = +1.9 ppm).

N-Trifluoroacetamidobenzamidobenzoate (133)

A solution of dipeptide **132** (1.00 g, 2.13 mmol, 1.00 equiv) in CH₂Cl₂ (25 mL) was treated with triethylamine (300 μL, 2.16 mmol, 1.01 equiv) and cooled down to 0 °C. TFAA (304 μL, 2.16 mmol, 1.01 equiv) was added and the reaction mixture was stirred at r.t. for 16 h. After removing the volatiles under reduced pressure, the residue was taken up in EtOAc. The solution was washed with 10% HCl_(aq.) (3×), H₂O, brine, dried over anhydrous Na₂SO₄ and concentrated under reduced pressure to afford title compound **133** (1.12 g, 1.98 mmol, 93%) as a yellow powder.

¹H NMR (500 MHz, DMSO-*d*₆) δ 11.08 (s, 1H), 10.57 (s, 1H), 8.28 (d, *J*=8.8 Hz, 1H), 7.77 (d, *J*=8.6 Hz, 1H), 7.57 (d, *J*=8.8 Hz, 1H), 7.46 (d, *J*=8.6 Hz, 1H), 6.15–5.98 (m, 3H), 5.45–5.34 (m, 3H), 5.31–5.26 (m, 1H), 5.29–5.21 (m, 2H), 4.80–4.74 (m, 4H), 4.56–4.51 (m, 2H), 3.92 (s, 3H), 3.87 (s, 3H). ¹³C NMR (126 MHz, DMSO-*d*₆) δ 164.4, 162.4, 155.1, 151.1, 149.8, 147.0, 142.7, 136.3, 133.9, 132.7, 132.6, 126.4, 126.2, 125.2, 121.5, 120.6, 120.1, 118.1, 117.8, 115.1, 75.1, 74.5, 65.1, 61.0, 60.9. HRMS (ESI): *m/z* calculated for C₂₇H₂₇F₃N₂O₈ [M+H]⁺ 565.1792, found 565.1783 (Δ*m* = -1.6 ppm).

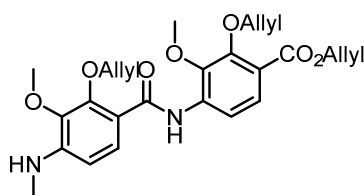
N-Methyl-N-trifluoroacetamidobenzamidobenzoate (134)

To a solution of the *N*-trifluoroacetylated dipeptide **133** (1.12 g, 1.98 mmol, 1.00 equiv) in dry CH₂Cl₂ (15 mL), was added NaH (60 wt.%, 83.3 mg, 2.08 mmol, 1.05 equiv) portionwise at 0 °C and the solution was stirred at that temperature for 30 min. MeI (618 μmol, 9.92 mmol, 5.00 equiv) was then added the reaction mixture was stirred for at r.t. 16 h. All volatiles were removed *in vacuo*, the residue was taken up in EtOAc and washed with 10% HCl_(aq.) (3×) and brine. The organic phase was dried over anhydrous Na₂SO₄ and concentrated under reduced pressure to obtain a crude product, which was purified by column chromatography on silica gel (*n*-hexane/EtOAc, 8:1–2:1). The title compound **134** (726 mg, 1.25 mmol, 63%) was

obtained as a brown oil.

^1H NMR (400 MHz, $\text{DMSO-}d_6$) δ 10.57 (s, 1H), 8.26 (d, $J=8.8$ Hz, 1H), 7.76 (d, $J=8.5$, 1.0 Hz, 1H), 7.57 (d, $J=8.7$, 1.0 Hz, 1H), 7.40 (d, $J=8.5$ Hz, 1H), 6.14–5.97 (m, 3H), 5.45–5.35 (m, 2H), 5.34–5.21 (m, 4H), 4.79–4.71 (m, 4H), 4.57–4.50 (m, 2H), 3.95–3.89 (m, 6H), 3.33 (s, 3H). ^{13}C NMR (101 MHz, $\text{DMSO-}d_6$) δ 164.5, 151.2, 142.9, 136.2, 134.0, 132.6, 132.3, 126.2, 120.8, 118.2, 117.9, 115.3, 74.9, 74.6, 65.2, 61.2, 61.1, 54.9. HRMS (ESI): m/z calculated for $\text{C}_{28}\text{H}_{29}\text{F}_3\text{N}_2\text{O}_8$ $[\text{M}+\text{H}]^+$ 579.1949, found 579.1945 ($\Delta m = -0.7$ ppm).

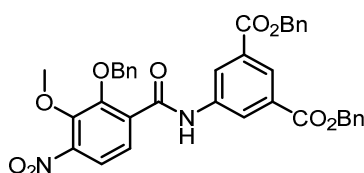
***N*-Methyl-aminobenzamidobenzoate (135)**



To a solution of trifluoroacetylated dipeptide **134** (404 mg, 718 μmol , 1.00 equiv) in a mixture of MeOH (20 mL) and H_2O (10 mL) was added K_2CO_3 (109 mg, 790 μmol , 1.10 equiv) and the reaction mixture was stirred at r.t. for 16 h. After removing MeOH under reduced pressure, the aq. residue was diluted with H_2O and extracted with EtOAc (3 \times). The combined organic phases were dried over anhydrous Na_2SO_4 and concentrated *in vacuo*. The crude product was purified by column chromatography on silica gel (*n*-hexane/EtOAc, 7:1–6:1) to afford the title compound **135** (291 mg, 625 μmol , 87%) as a yellow oil.

^1H NMR (400 MHz, $\text{DMSO-}d_6$) δ 10.64 (s, 1H), 8.36 (d, $J=8.8$ Hz, 1H), 7.71 (d, $J=8.8$ Hz, 1H), 7.54 (d, $J=8.7$ Hz, 1H), 6.48 (d, $J=9.0$ Hz, 1H), 6.23–6.17 (m, 1H), 6.16–5.97 (m, 3H), 5.45–5.33 (m, 3H), 5.31–5.19 (m, 3H), 4.80–4.73 (m, 3H), 4.55–4.49 (m, 2H), 3.90 (s, 3H), 3.75 (s, 3H), 2.78 (d, $J=4.9$ Hz, 3H). ^{13}C NMR (101 MHz, $\text{DMSO-}d_6$) δ 164.5, 163.1, 151.1, 149.6, 147.7, 142.0, 137.9, 137.3, 134.1, 133.1, 132.7, 127.7, 126.4, 119.7, 119.3, 118.1, 117.8, 114.4, 112.4, 105.4, 74.8, 74.5, 65.0, 60.9, 59.9, 29.3. HRMS (ESI): m/z calculated for $\text{C}_{26}\text{H}_{30}\text{N}_2\text{O}_7$ $[\text{M}+\text{H}]^+$ 483.2126, found 483.2119 ($\Delta m = -1.4$ ppm).

5-(4-Nitrobenzamido)isophthalic acid (137)

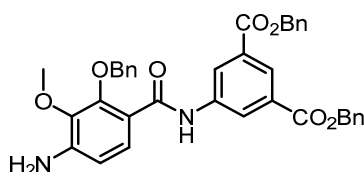


Peptide coupling using BTC according to GP4:

- benzoic acid **119** (382 mg, 1.26 mmol, 1.30 equiv) in THF (15 mL)
- 2,4,6-collidine (1.34 mL, 10.1 mmol, 8.00 equiv based on **119**)
- BTC (115 mg, 388 μ mol 0.30 equiv based on **119**)
- aniline **136** (350 mg, 0.986 mmol, 1.00 equiv) in THF (5 mL)
- DIPEA (1.69 mL, 9.86 mmol, 10.0 equiv)
- the title compound **137** (626 mg, 0.986 mmol, quant.) was obtained as a yellow gum

^1H NMR (400 MHz, DMSO- d_6) δ 10.86 (s, 1H), 8.56 (d, $J=1.6$ Hz, 2H), 8.29 (t, $J=1.6$ Hz, 1H), 7.77 (d, $J=8.4$ Hz, 1H), 7.53–7.31 (m, 15H), 7.22–7.15 (m, 3H), 5.42–5.39 (m, 4H), 5.10 (s, 2H), 4.00 (s, 3H). ^{13}C NMR (101 MHz, DMSO- d_6) δ 164.5, 163.7, 150.0, 146.1, 145.7, 139.5, 136.1, 136.0, 135.8, 130.8, 128.6, 128.5, 128.3, 128.2, 128.1, 128.1, 124.9, 124.3, 123.7, 119.5, 76.1, 66.7, 66.3, 62.3, 54.9, 30.4. HRMS (ESI): m/z calculated for $\text{C}_{37}\text{H}_{30}\text{N}_2\text{O}_9$ $[\text{M}+\text{H}]^+$ 647.2037, found 647.2024 ($\Delta m = -2.0$ ppm).

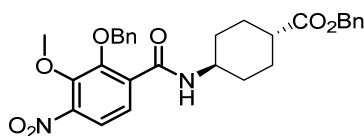
5-(4-Aminobenzamido)isophthalic acid (**138**)



Reduction of the nitro group according to GP1:

- THF (10 mL), EtOH (20 mL), AcOH (5 mL)
- nitro dipeptide **137** (600 mg, 928 μ mol, 1.00 equiv)
- Zn-dust (5.0 g)
- 0 $^\circ\text{C}$, 30 min
- the title compound **138** (572 mg, 928 μ mol, quant.) was obtained as a brown gum

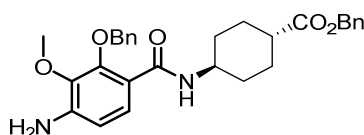
^1H NMR (400 MHz, DMSO- d_6) δ 10.19 (s, 1H), 8.39 (d, $J=1.6$ Hz, 2H), 8.19 (t, $J=1.6$ Hz, 1H), 7.51–7.32 (m, 13H), 7.25–7.17 (m, 3H), 6.56 (d, $J=8.6$ Hz, 1H), 5.72 (s, 2H), 5.42–5.37 (m, 4H), 5.09 (s, 2H), 3.80 (s, 3H). ^{13}C NMR (101 MHz, DMSO- d_6) δ 164.7, 164.3, 150.8, 146.6, 140.1, 138.0, 136.5, 135.9, 130.5, 128.5, 128.4, 128.4, 128.2, 128.1, 126.2, 124.0, 124.0, 118.2, 114.9, 109.9, 75.8, 66.6, 59.7. HRMS (ESI): m/z calculated for $\text{C}_{37}\text{H}_{32}\text{N}_2\text{O}_7$ $[\text{M}+\text{H}]^+$ 617.2288, found 617.2282 ($\Delta m = -1.0$ ppm).

4-(4-nitrobenzamido)cyclohexanecarboxylate (140)

Peptide coupling using BTC according to GP4:

- benzoic acid **119** (507 mg, 1.67 mmol, 1.50 equiv) in THF (25 mL)
- 2,4,6-collidine (1.77 mL, 13.4 mmol, 8.00 equiv based on **119**)
- BTC (153 mg, 0.501 mmol 0.30 equiv based on **119**)
- aniline **139** (300 mg, 1.29 mmol, 1.00 equiv) in THF (5 mL)
- DIPEA (2.24 mL, 12.9 mmol, 10.0 equiv)
- column chromatography: SiO₂, *n*-hexane/EtOAc, 5:1–3:1
- the title compound **140** (573 mg, 1.11 mmol, 86%) was obtained as a colourless oil

¹H NMR (400 MHz, DMSO-*d*₆) δ 8.30 (d, *J*=7.7 Hz, 1H), 7.71–7.67 (m, 1H), 7.49–7.29 (m, 11H), 5.10–5.07 (m, 4H), 3.94 (s, 3H), 3.74–3.62 (m, 1H), 2.34–2.24 (m, 1H), 1.97–1.82 (m, 4H), 1.50–1.37 (m, 2H), 1.25–1.12 (m, 2H). ¹³C NMR (101 MHz, DMSO-*d*₆) δ 174.4, 163.6, 150.0, 146.0, 145.2, 136.4, 136.3, 128.4, 128.3, 128.3, 127.9, 127.7, 123.8, 119.2, 75.9, 65.3, 62.2, 54.9, 47.8, 41.4, 30.8, 27.4.

4-(4-aminobenzamido)cyclohexanecarboxylate (141)

Reduction of the nitro group according to GP1:

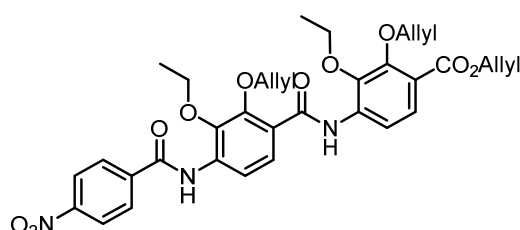
- EtOH (25 mL), AcOH (5 mL)
- nitro dipeptide **140** (512 mg, 987 μmol, 1.00 equiv)
- Zn-dust (10.0 g)
- 0 °C, 1 h
- the title compound **141** (482 mg, 987 μmol, quant.) was obtained as a yellow oil

¹H NMR (400 MHz, DMSO-*d*₆) δ 7.67 (d, *J*=7.6 Hz, 1H), 7.52–7.29 (m, 11H), 6.50 (d, *J*=8.7 Hz, 1H), 5.55 (s, 2H), 5.10–5.05 (m, 4H), 3.75 (s, 3H), 3.64–3.51 (m, 1H), 2.23–2.13 (m, 1H), 1.88–1.73 (m, 4H), 1.44–1.30 (m, 2H), 0.95–0.80 (m, 2H). ¹³C NMR (101 MHz, DMSO-*d*₆) δ 174.4,

172.0, 163.7, 150.9, 145.9, 137.9, 136.7, 136.3, 128.6, 128.5, 128.4, 128.4, 127.9, 127.7, 126.2, 114.2, 109.7, 75.4, 65.3, 59.6, 47.0, 41.5, 31.0, 27.4, 21.1, 20.7, 14.1. HRMS (ESI): m/z calculated for $C_{29}H_{32}N_2O_5$ $[M+H]^+$ 489.2384, found 489.2375 ($\Delta m = -1.8$ ppm).

Syntheses of Modified C-D-E-F Tetrapeptides

O₂N-D-E(Ethoxy-Allyl)-F(Ethoxy-Allyl)-OAllyl (204)

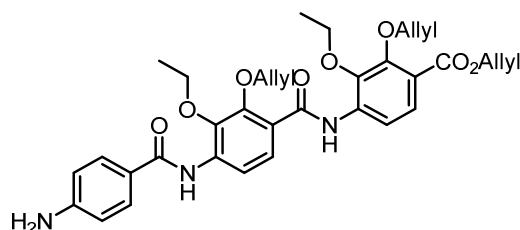


Peptide coupling according to GP5:

- amino dipeptide **109** (275 mg, 550 μ mol, 1.00 equiv) in THF (15 mL)
- *p*NBC (306 mg, 1.65 mmol, 3.00 equiv)
- Et₃N (280 μ L, 1.65 mmol, 3.00 equiv)
- the title compound **204** (341 mg, 528 μ mol, 96%) was obtained as a yellow solid

¹H NMR (400 MHz, DMSO-*d*₆) δ 10.65 (s, 1H), 10.19 (s, 1H), 8.39 (d, $J=8.8$ Hz, 2H), 8.06 (d, $J=8.9$ Hz, 2H), 7.78–7.85 (m, 2H), 7.53–7.58 (m, 2H), 5.97–6.14 (m, 3H), 5.21–5.44 (m, 6H), 4.75–4.78 (m, 4H), 4.55 (d, $J=5.7$ Hz, 1H), 4.52 (d, $J=5.6$ Hz, 1H), 4.05–4.19 (m, 4H), 1.31–1.38 (m, 6H). ¹³C NMR (101 MHz, DMSO-*d*₆) δ 171.1, 165.8, 164.5, 164.2, 162.3, 151.2, 149.9, 149.4, 144.2, 141.3, 139.5, 136.9, 134.0, 132.6, 132.5, 130.7, 130.2, 129.3, 126.2, 125.4, 124.0, 123.7, 120.3, 118.1, 117.7, 114.7, 75.3, 74.4, 69.9, 69.2, 65.1, 15.5, 15.3, 14.9. HRMS (ESI): m/z calculated for $C_{34}H_{35}N_3O_{10}$ $[M+H]^+$ 646.2395, found 646.2393 ($\Delta m = -0.3$ ppm).

H₂N-D-E(Ethoxy-Allyl)-F(Ethoxy-Allyl)-OAllyl (205)



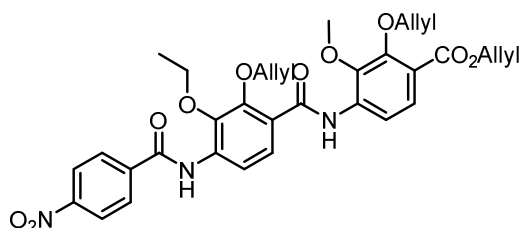
Reduction of the nitro group according to GP2:

- nitro tripeptide **204** (300 mg, 465 μ mol, 1.00 equiv)
- EtOAc (15 mL)

- $\text{SnCl}_2 \cdot 2 \text{H}_2\text{O}$ (735 mg, 3.26 mmol, 7.00 equiv)
- column chromatography: SiO_2 , 1–5% MeOH in CH_2Cl_2
- dipeptide **205** (172 mg, 279 μmol , 60%) was obtained as a yellow oil

^1H NMR (400 MHz, $\text{DMSO-}d_6$) δ 10.65 (s, 1H), 9.13 (s, 1H), 8.33 (d, $J=8.8$ Hz, 1H), 8.04 (d, $J=8.8$ Hz, 1H), 7.78 (d, $J=8.8$ Hz, 1H), 7.69 (d, $J=8.7$ Hz, 2H), 7.56 (d, $J=8.8$ Hz, 1H), 6.63 (d, $J=8.6$ Hz, 2H), 5.98–6.14 (m, 3H), 5.89 (s, 2H), 5.23–5.44 (m, 6H), 4.76 (t, $J=7.5$ Hz, 4H), 4.55 (d, $J=5.7$ Hz, 2H), 4.13 (q, $J=7.0$ Hz, 2H), 4.17 (q, $J=7.0$ Hz, 2H), 1.35–1.39 (m, 6H). ^{13}C NMR (101 MHz, $\text{DMSO-}d_6$) δ 164.7, 164.5, 162.4, 152.7, 151.2, 149.5, 142.2, 141.1, 137.4, 137.0, 134.0, 132.6, 129.2, 126.3, 125.6, 121.8, 120.3, 120.1, 119.9, 118.1, 117.7, 117.4, 114.6, 112.8, 75.3, 74.4, 69.2, 69.1, 65.1, 15.6, 15.4. HRMS (ESI): m/z calculated for $\text{C}_{34}\text{H}_{37}\text{N}_3\text{O}_8$ $[\text{M}+\text{H}]^+$ 616.2653, found 616.2654 ($\Delta m = -0.2$ ppm).

$\text{O}_2\text{N-D-E(Ethoxy-Allyl)-F(Allyl)-OAllyl (208)$

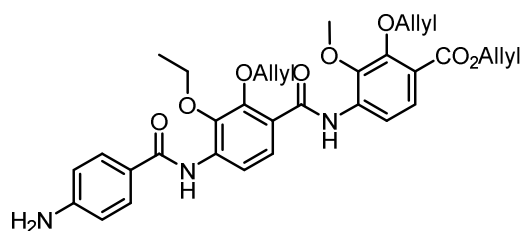


Peptide coupling according to GP5:

- amino dipeptide **112** (252 mg, 522 μmol , 1.00 equiv) in THF (10 mL)
- *pNBC* (194 mg, 1.04 mmol, 2.00 equiv)
- Et_3N (218 μL , 1.57 mmol, 3.00 equiv)
- the title compound **208** (328 mg, 522 μmol , quant.) was obtained as a yellow solid

^1H NMR (400 MHz, $\text{DMSO-}d_6$) δ 10.65 (s, 1H), 10.21 (s, 1H), 8.43–8.36 (m, 2H), 8.35–8.30 (m, 1H), 8.24–8.16 (m, 2H), 7.82 (s, 2H), 7.57 (d, $J=8.7$ Hz, 1H), 6.18–5.96 (m, 3H), 5.46–5.37 (m, 2H), 5.41–5.33 (m, 1H), 5.33–5.22 (m, 3H), 4.85–4.80 (m, 2H), 4.80–4.74 (m, 2H), 4.57–4.50 (m, 2H), 4.14 (q, $J=7.0$ Hz, 2H), 3.92 (s, 3H), 1.34 (t, $J=7.0$ Hz, 3H). ^{13}C NMR (101 MHz, $\text{DMSO-}d_6$) δ 165.8, 164.5, 164.2, 162.4, 151.1, 149.9, 149.4, 144.2, 142.6, 139.8, 136.5, 136.2, 133.98, 132.7, 132.7, 130.7, 129.3, 126.3, 125.4, 123.9, 123.8, 123.7, 120.4, 120.0, 119.9, 118.2, 117.9, 114.9, 75.1, 74.6, 69.2, 65.1, 61.0, 15.6.

H₂N-D-E(Ethoxy-Allyl)-F(Allyl)-OAllyl (209)



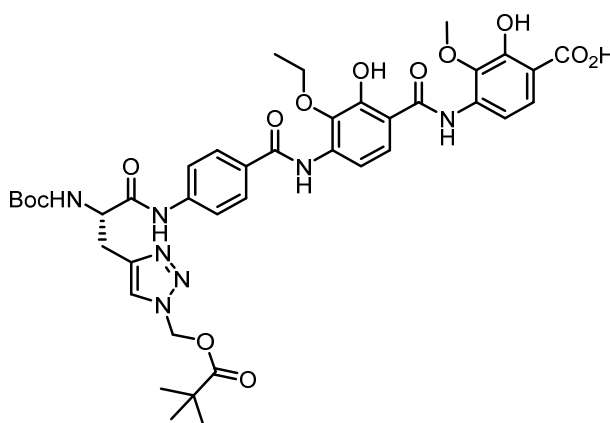
Reduction of the nitro group according to GP2:

- nitro tripeptide **208** (300 mg, 475 μ mol, 1.00 equiv)
- EtOAc (20 mL)
- SnCl₂ · 2 H₂O (643 mg, 2.85 mmol, 6.00 equiv)
- dipeptide **209** (284 mg, 475 μ mol, quant.) was obtained as a yellow solid

¹H NMR (400 MHz, DMSO-*d*₆) δ 10.66 (s, 1H), 9.17 (s, 1H), 8.34 (d, *J*=8.8 Hz, 1H), 8.03 (d, *J*=8.8 Hz, 1H), 7.80 (d, *J*=8.8 Hz, 1H), 7.73–7.68 (m, 2H), 7.57 (d, *J*=8.8 Hz, 1H), 6.68–6.62 (m, 2H), 6.17–5.98 (m, 3H), 5.45–5.35 (m, 3H), 5.32–5.21 (m, 3H), 4.84–4.79 (m, 2H), 4.77 (dt, *J*=5.5, 1.5 Hz, 2H), 4.57–4.50 (m, 2H), 4.15 (q, *J*=7.0 Hz, 2H), 3.92 (s, 3H), 1.37 (t, *J*=7.0 Hz, 3H).

¹³C NMR (101 MHz, DMSO-*d*₆) δ 164.7, 164.5, 162.5, 152.5, 151.1, 149.6, 142.4, 142.1, 137.51, 136.6, 134.0, 132.7, 132.7, 129.3, 126.3, 125.7, 121.7, 120.2, 120.0, 118.1, 117.9, 117.4, 114.8, 113.0, 75.0, 74.6, 69.2, 65.1, 61.0, 15.6. HRMS (ESI): *m/z* calculated for C₃₃H₃₅N₃O₈ [M+H]⁺ 602.2497, found 602.2493 ($\Delta m = -0.7$ ppm).

Boc-AzaHis(POM)-D-E(Ethoxy)-F-OH (210)



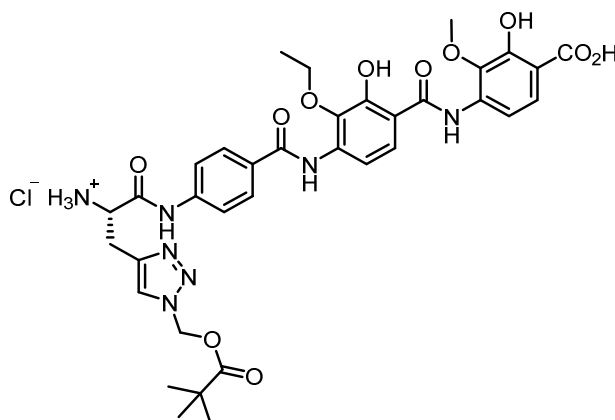
Pd-mediated allyl-deprotection according to GP8:

- allyl-protected tetrapeptide (187 mg, 196 μ mol, 1.00 equiv) in THF (10 mL)
- morpholine (338 μ L, 3.92 mmol, 20 equiv)

- Pd(PPh₃)₄ (90.6 mg, 78.4 μmol, 0.40 equiv)
- column chromatography: SiO₂, 7–15% MeOH in CH₂Cl₂
- the title compound **211** (122 mg, 147 μmol, 75%) was obtained as a beige solid

¹H NMR (400 MHz, DMSO-*d*₆) δ 10.90 (s, 1H), 10.53 (s, 1H), 9.56 (s, 1H), 8.01–7.92 (m, 3H), 7.78 (t, *J*=8.3 Hz, 3H), 7.60 (d, *J*=8.6 Hz, 1H), 7.52 (d, *J*=8.8 Hz, 1H), 7.45 (d, *J*=8.6 Hz, 1H), 7.23 (d, *J*=8.0 Hz, 1H), 6.29 (s, 2H), 4.44–4.38 (m, 1H), 4.02 (q, *J*=7.0 Hz, 2H), 3.86 (s, 3H), 3.18–2.96 (m, 2H), 1.38–1.27 (m, 12H), 1.08 (s, 9H). ¹³C NMR (101 MHz, DMSO-*d*₆) δ 176.5, 164.5, 163.95, 139.0, 135.8, 128.5, 124.8, 118.8, 116.1, 69.9, 68.5, 59.5, 42.7, 38.2, 28.2, 27.8, 26.5, 15.4. HRMS (ESI): *m/z* calculated for C₄₀H₄₇N₇O₁₃ [M+H]⁺ 834.3305, found 834.3306 (Δ*m* = –0.1 ppm).

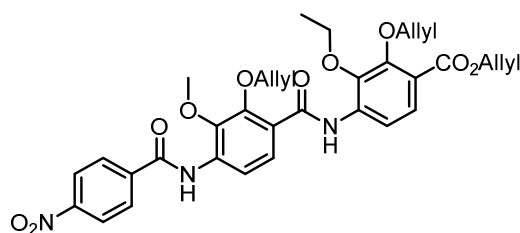
H₂N-AzaHis(POM)-D-E(Ethoxy)-F-OH (**211**)*HCl



Boc-deprotection according to GP7:

- Boc-protected tetrapeptide **210** (105 mg, 126 μmol, 1.00 equiv)
- 4 N HCl in 1,4-dioxane (7 mL)
- the title compound **211** (125 mg, 126 μmol, quant.) was obtained as a colourless solid

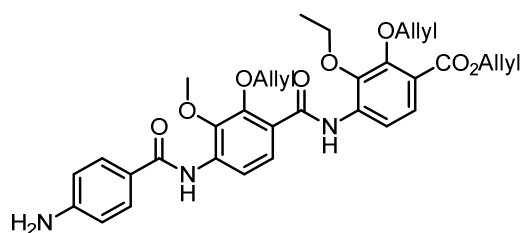
¹H NMR (400 MHz, DMSO-*d*₆) δ 11.45 (s, 1H), 11.35 (s, 1H), 11.14 (s, 1H), 9.67 (s, 1H), 8.64 (s, 3H), 8.17 (s, 1H), 8.04–7.94 (m, 3H), 7.81 (d, *J*=8.8 Hz, 1H), 7.77 (d, *J*=8.5 Hz, 2H), 7.58 (d, *J*=8.9 Hz, 1H), 7.54 (d, *J*=8.8 Hz, 1H), 6.27 (s, 2H), 4.48–4.40 (m, 1H), 3.99 (q, *J*=6.9 Hz, 2H), 3.91 (s, 3H), 3.40–3.32 (m, 2H), 1.32 (t, *J*=7.0 Hz, 3H), 1.06 (s, 9H). ¹³C NMR (101 MHz, DMSO-*d*₆) δ 176.4, 172.0, 166.8, 164.5, 163.5, 154.5, 150.0, 140.9, 137.6, 136.3, 129.3, 128.6, 125.0, 119.0, 110.3, 69.9, 60.2, 38.1, 26.4, 15.3. HRMS (ESI): *m/z* calculated for C₃₅H₄₀N₇O₁₁⁺ [M]⁺ 734.2786, found 734.2806 (Δ*m* = +2.7 ppm).

O₂N-D-E(Allyl)-F(Ethoxy-Allyl)-OAllyl (212)

Peptide coupling according to GP5:

- amino dipeptide **112** (340 mg, 705 μ mol, 1.00 equiv) in THF (10 mL)
- *p*NBC (262 mg, 1.41 mmol, 2.00 equiv)
- Et₃N (295 μ L, 2.11 mmol, 3.00 equiv)
- column chromatography: SiO₂, 0.3–0.5% MeOH in CH₂Cl₂
- the title compound **212** (436 mg, 691 μ mol, 98%) was obtained as a yellow solid

¹H NMR (400 MHz, DMSO-*d*₆) δ 10.66 (s, 1H), 10.24 (s, 1H), 8.42–8.30 (m, 3H), 8.21–8.17 (m, 2H), 7.88 (d, *J*=8.7 Hz, 1H), 7.81 (d, *J*=8.7 Hz, 1H), 7.57 (d, *J*=8.8 Hz, 1H), 6.16–5.98 (m, 3H), 5.46–5.32 (m, 3H), 5.32–5.20 (m, 3H), 4.80–4.71 (m, 4H), 4.59–4.52 (m, 2H), 4.14 (q, *J*=7.0 Hz, 2H), 1.38 (t, *J*=7.1 Hz, 3H). ¹³C NMR (101 MHz, DMSO) δ 164.5, 164.4, 162.3, 151.3, 149.7, 149.3, 145.1, 141.4, 140.0, 136.9, 135.9, 134.0, 132.7, 132.6, 130.7, 129.5, 126.3, 125.4, 123.9, 123.8, 123.6, 120.5, 120.3, 119.5, 118.1, 117.7, 114.7, 75.4, 74.5, 69.3, 65.1, 60.9, 15.4. HRMS (ESI): *m/z* calculated for C₃₃H₃₃N₃O₁₀ [M+H]⁺ 632.2239, found 632.2227 ($\Delta m = -1.9$ ppm).

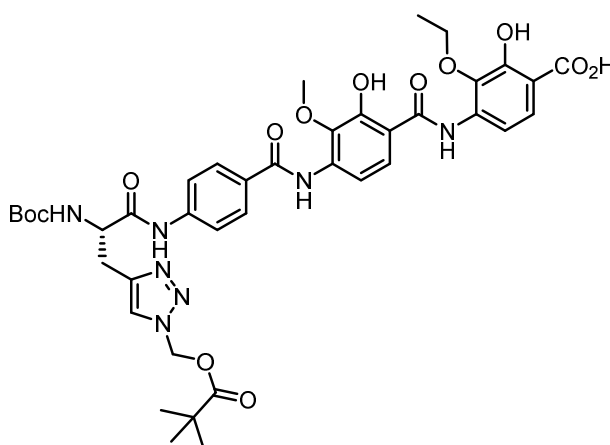
H₂N-D-E(Allyl)-F(Ethoxy-Allyl)-OAllyl (213)

Reduction of the nitro group according to GP2:

- nitro tripeptide **212** (400 mg, 633 μ mol, 1.00 equiv)
- EtOAc (20 mL)
- SnCl₂ · 2 H₂O (857 mg, 3.80 mmol, 6.00 equiv)
- dipeptide **213** (379 mg, 633 μ mol, quant.) was obtained as a yellow solid

^1H NMR (400 MHz, $\text{DMSO-}d_6$) δ 10.67 (s, 1H), 9.20 (s, 1H), 8.35 (d, $J=8.8$ Hz, 1H), 8.03 (d, $J=8.9$ Hz, 1H), 7.78 (d, $J=8.8$ Hz, 1H), 7.78–7.67 (m, 2H), 7.57 (d, $J=8.8$ Hz, 1H), 6.67–6.59 (m, 2H), 6.17–5.96 (m, 3H), 5.90 (s, 2H), 5.46–5.38 (m, 1H), 5.41–5.36 (m, 1H), 5.35 (dq, $J=6.1, 1.5$ Hz, 1H), 5.30–5.21 (m, 3H), 4.80–4.71 (m, 4H), 4.59–4.52 (m, 2H), 4.13 (q, $J=7.0$ Hz, 2H), 1.38 (t, $J=7.0$ Hz, 3H). ^{13}C NMR (101 MHz, DMSO) δ 165.0, 164.5, 162.4, 152.7, 151.3, 149.4, 143.4, 141.2, 137.1, 137.1, 134.0, 132.7, 132.6, 129.5, 126.3, 125.6, 121.9, 120.5, 120.1, 120.0, 118.1, 117.7, 117.5, 114.6, 112.7, 75.4, 74.5, 69.2, 65.1, 60.8, 15.4. HRMS (ESI): m/z calculated for $\text{C}_{33}\text{H}_{35}\text{N}_3\text{O}_8$ $[\text{M}+\text{H}]^+$ 602.2497, found 602.2494 ($\Delta m = -0.5$ ppm).

Boc-AzaHis(POM)-D-E-F(Ethoxy)-OH (**214**)

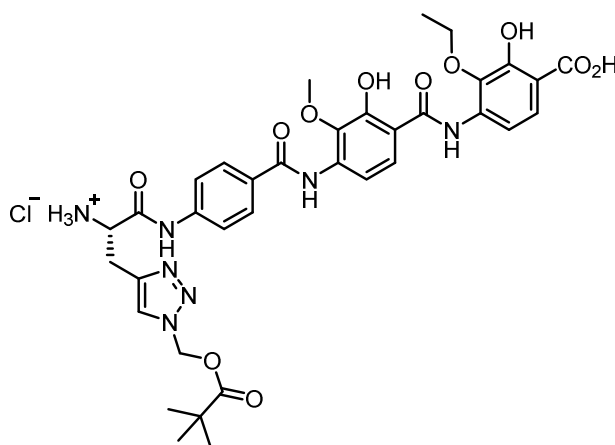


Pd-mediated allyl-deprotection according to GP8:

- allyl-protected tetrapeptide (195 mg, 204 μmol , 1.00 equiv) in THF (15 mL)
- morpholine (353 μL , 4.09 mmol, 20 equiv)
- $\text{Pd}(\text{PPh}_3)_4$ (94.5 mg, 81.8 μmol , 0.40 equiv)
- column chromatography: SiO_2 , 7–15% MeOH in CH_2Cl_2
- the title compound **214** (109 mg, 131 μmol , 64%) was obtained as a beige solid

^1H NMR (400 MHz, $\text{DMSO-}d_6$) δ 11.56 (s, 1H), 10.81 (s, 1H), 10.53 (s, 1H), 9.63 (s, 1H), 8.01–7.93 (m, 3H), 7.84–7.75 (m, 3H), 7.73 (d, $J=8.6$ Hz, 1H), 7.55 (d, $J=8.9$ Hz, 1H), 7.48 (d, $J=8.6$ Hz, 1H), 7.23 (d, $J=8.0$ Hz, 1H), 6.29 (s, 2H), 4.46–4.36 (m, 1H), 4.14 (q, $J=7.0$ Hz, 2H), 3.78 (s, 3H), 3.19–2.96 (m, 2H), 1.38–1.24 (m, 12H), 1.09 (s, 9H). ^{13}C NMR (101 MHz, $\text{DMSO-}d_6$) δ 176.5, 164.8, 163.5, 155.9, 155.4, 143.5, 142.3, 140.2, 135.6, 135.5, 128.7, 125.1, 124.7, 124.2, 118.7, 116.4, 108.3, 78.3, 69.9, 67.3, 60.4, 56.0, 38.2, 28.2, 27.9, 26.5, 18.6, 15.5. HRMS (ESI): m/z calculated for $\text{C}_{40}\text{H}_{47}\text{N}_7\text{O}_{13}$ $[\text{M}+\text{H}]^+$ 834.3305, found 834.3302 ($\Delta m = -0.4$ ppm).

H₂N-AzaHis(POM)-D-E-F(Ethoxy)-OH*HCl (215)

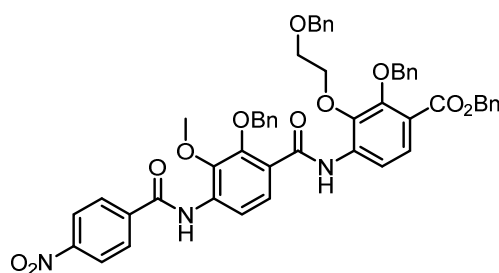


Boc-deprotection according to GP7:

- Boc-protected tetrapeptide **214** (88.0 mg, 106 μ mol, 1.00 equiv)
- 4 N HCl in 1,4-dioxane (5 mL)
- the title compound **215** (80.0 mg, 103 μ mol, 98%) was obtained as a colourless solid

¹H NMR (400 MHz, DMSO-*d*₆) δ 11.65 (s, 1H), 11.51 (s, 1H), 11.34 (s, 1H), 11.08 (s, 1H), 9.71 (s, 1H), 8.64 (s, 3H), 8.16 (s, 1H), 8.07 (d, *J*=8.9 Hz, 1H), 8.01–7.93 (m, 2H), 7.81 (d, *J*=8.8 Hz, 1H), 7.76 (d, *J*=8.8 Hz, 2H), 7.57 (t, *J*=8.5 Hz, 2H), 6.27 (s, 2H), 4.43 (s, 1H), 4.16 (q, *J*=7.0 Hz, 2H), 3.77 (s, 3H), 3.43–3.32 (m, 2H), 1.38 (t, *J*=7.0 Hz, 3H), 1.07 (s, 9H). HRMS (ESI): *m/z* calculated for C₃₅H₄₀N₇O₁₁⁺ [M]⁺ 734.2786, found 734.2811 (Δm = +3.4 ppm).

Ethylene glycol-containing nitro tripeptide (216)

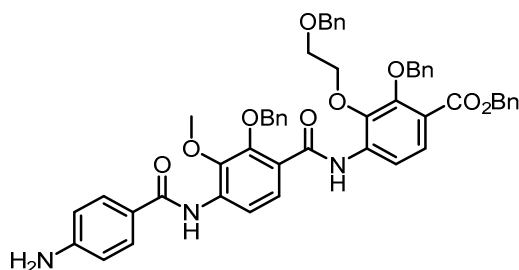


Peptide coupling according to GP5:

- amino dipeptide **121** (180 mg, 244 μ mol, 1.00 equiv) in THF (7 mL)
- *p*NBC (90.4 mg, 487 μ mol, 2.00 equiv)
- Et₃N (102 μ L, 731 μ mol, 3.00 equiv)
- column chromatography: SiO₂, *n*-hexane/EtOAc, 4:1
- the title compound **216** (203 mg, 229 μ mol, 94%) was obtained as a yellow solid

^1H NMR (400 MHz, $\text{DMSO-}d_6$) δ 10.45 (s, 1H), 10.26 (s, 1H), 8.42–8.37 (m, 2H), 8.28 (d, $J=8.8$ Hz, 1H), 8.23–8.19 (m, 2H), 7.85 (d, $J=8.7$ Hz, 1H), 7.69 (d, $J=8.7$ Hz, 1H), 7.59 (d, $J=8.8$ Hz, 1H), 7.46–7.42 (m, 2H), 7.41–7.31 (m, 11H), 7.29–7.24 (m, 3H), 7.20–7.15 (m, 3H), 7.09–7.05 (m, 2H), 5.30 (s, 2H), 5.16 (s, 2H), 4.98 (s, 2H), 4.27 (s, 2H), 4.09–4.01 (m, 2H), 3.86 (s, 3H), 3.57–3.50 (m, 2H). ^{13}C NMR (101 MHz, $\text{DMSO-}d_6$) δ 164.6, 164.4, 162.5, 151.0, 149.6, 149.3, 145.32, 141.4, 140.0, 137.8, 137.0, 136.7, 136.1, 135.6, 135.5, 129.5, 129.2, 128.6, 128.5, 128.5, 128.3, 128.24, 128.1, 128.1, 127.4, 127.3, 126.4, 124.9, 123.6, 120.2, 114.7, 76.2, 75.2, 72.5, 72.0, 68.5, 66.3, 60.9. HRMS (ESI): m/z calculated for $\text{C}_{52}\text{H}_{45}\text{N}_3\text{O}_{11}$ $[\text{M}+\text{H}]^+$ 888.3127, found 888.3116 ($\Delta m = -1.2$ ppm).

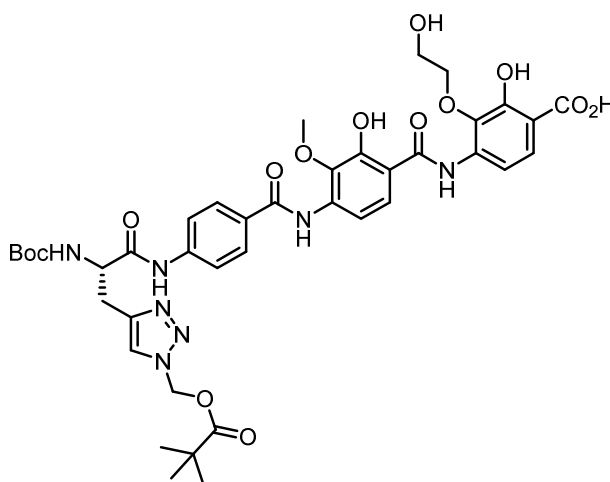
Ethylene glycol-containing amino tripeptide (**217**)



Reduction of the nitro group according to GP1:

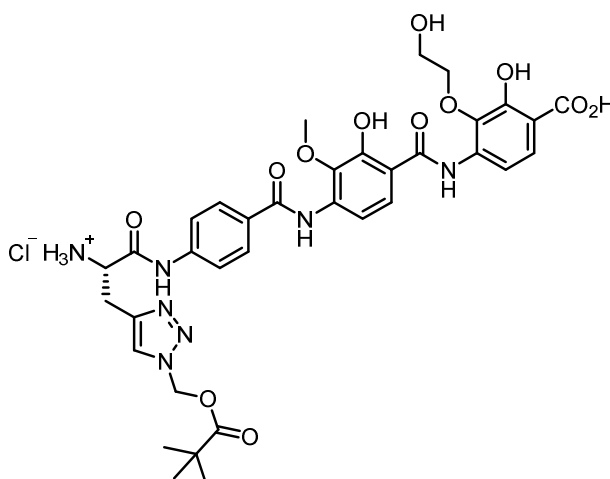
- EtOH (15 mL), AcOH (4 mL)
- nitro tripeptide **216** (190 mg, 214 μmol , 1.00 equiv)
- Zn-dust (2.0 g)
- 0 °C, 2 h
- the title compound **217** (171 mg, 199 μmol , 93%) was obtained as a yellow oil

^1H NMR (400 MHz, $\text{DMSO-}d_6$) δ 10.46 (s, 1H), 9.20 (s, 1H), 8.28 (d, $J=8.8$ Hz, 1H), 8.01 (d, $J=8.8$ Hz, 1H), 7.75–7.70 (m, 2H), 7.66 (d, $J=8.8$ Hz, 1H), 7.61–7.56 (m, 1H), 7.48–7.41 (m, 2H), 7.41–7.31 (m, 11H), 7.29–7.23 (m, 3H), 7.20–7.14 (m, 3H), 7.06 (dd, $J=6.7, 2.8$ Hz, 2H), 6.68–6.60 (m, 2H), 5.90 (s, 2H), 5.76 (s, 1H), 5.30 (s, 2H), 5.15 (s, 2H), 4.98 (s, 2H), 4.27 (s, 2H), 4.08–4.03 (m, 3H), 3.87 (s, 3H), 3.57–3.50 (m, 2H). HRMS (ESI): m/z calculated for $\text{C}_{52}\text{H}_{47}\text{N}_3\text{O}_9$ $[\text{M}+\text{H}]^+$ 858.3385, found 858.3383 ($\Delta m = -0.2$ ppm).

Ethylene glycol-containing tetrapeptide (218)

A solution of the benzyl-protected tetrapeptide (100 mg, 82.6 μmol , 1.00 equiv) in EtOAc (10 mL) was purged with N_2 for 5 min, then Pd (10 wt.% on activated carbon, 10 mg) was added. The resulting suspension was purged with N_2 for 5 min followed by H_2 for 5 min. The reaction mixture was stirred at r.t. under a H_2 -atmosphere for 12 h. The suspension was filtered through a pad of Celite[®] and the filtrate concentrated under reduced pressure to afford the title compound **218** (67.0 mg, 78.4 μmol , 95%) as a colourless solid.

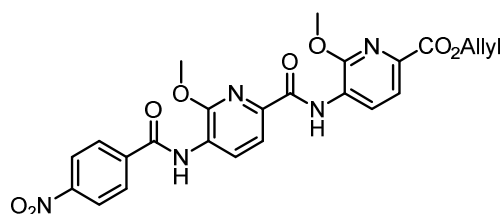
^1H NMR (500 MHz, $\text{DMSO-}d_6$) δ 11.78 (s, 2H), 10.63 (s, 1H), 10.43 (s, 1H), 9.56 (s, 1H), 8.05–7.89 (m, 4H), 7.88–7.61 (m, 5H), 7.58 (d, $J=8.8$ Hz, 1H), 7.19 (d, $J=8.1$ Hz, 1H), 6.29 (s, 2H), 4.45–4.37 (m, 1H), 4.17 (t, $J=5.2$ Hz, 2H), 3.83 (s, 3H), 3.74 (t, $J=5.2$ Hz, 2H), 3.16–2.97 (m, 2H), 1.39–1.25 (m, 9H), 1.09 (s, 9H). ^{13}C NMR (126 MHz, $\text{DMSO-}d_6$) δ 176.4, 171.9, 165.5, 164.8, 154.5, 151.7, 143.5, 142.2, 139.4, 137.3, 136.1, 135.5, 128.7, 125.2, 124.1, 118.7, 114.4, 110.8, 78.28, 74.2, 69.8, 60.4, 59.8, 38.2, 28.1, 26.4. HRMS (ESI): m/z calculated for $\text{C}_{40}\text{H}_{47}\text{N}_7\text{O}_{14}$ $[\text{M}+\text{H}]^+$ 850.3254, found 850.3260 ($\Delta m = +0.7$ ppm).

Ethylene glycol-containing tetrapeptide hydrochloride (219)

Boc-deprotection according to GP7:

- Boc-protected tetrapeptide **218** (67 mg, 79 μmol , 1.00 equiv)
- 4 N HCl in 1,4-dioxane (3 mL)
- the title compound **228** (61 mg, 76 μmol , 98%) was obtained as a colourless solid

HRMS (ESI): m/z calculated for $\text{C}_{35}\text{H}_{40}\text{N}_7\text{O}_{12}^+$ $[\text{M}]^+$ 750.2735, found 750.2711 ($\Delta m = -3.2$ ppm).

O₂N-D-E(Pyridine)-F(Pyridine)-OAllyl (220)

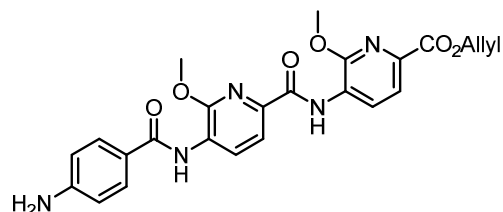
Peptide coupling according to GP5:

- amino dipeptide **127** (1.19 g, 3.32 mmol, 1.00 equiv) in THF (24 mL)
- *pNBC* (1.23 g, 6.64 mmol, 2.00 equiv)
- Et_3N (1.39 mL, 9.96 mmol, 3.00 equiv)
- column chromatography: SiO_2 , $\text{CHCl}_3/\text{MeOH}$, 9:0.05–9:0.2
- the title compound **220** (1.48 g, 2.92 mmol, 88%) was obtained as a yellow solid

^1H NMR (400 MHz, CDCl_3) δ 10.39 (s, 1H), 8.97 (d, $J=8.1$ Hz, 1H), 8.89 (d, $J=8.1$ Hz, 1H), 8.57 (s, 1H), 8.42–8.37 (m, 2H), 8.11–8.07 (m, 2H), 8.01 (dd, $J=8.1, 0.5$ Hz, 1H), 7.86 (dd, $J=8.1, 0.5$ Hz, 1H), 6.07 (ddt, $J=17.2, 10.5, 5.7$ Hz, 1H), 5.46 (dq, $J=17.2, 1.6$ Hz, 1H), 5.31 (dq, $J=10.4, 1.3$ Hz,

1H), 4.87 (dt, $J=5.6, 1.5$ Hz, 2H), 4.25 (s, 3H), 4.19 (s, 3H). HRMS (ESI): m/z calculated for $C_{24}H_{21}N_5O_8$ $[M+H]^+$ 508.1463, found 508.1473 ($\Delta m = +2.0$ ppm).

H₂N-D-E(Pyridine)-F(Pyridine)-OAllyl (221)

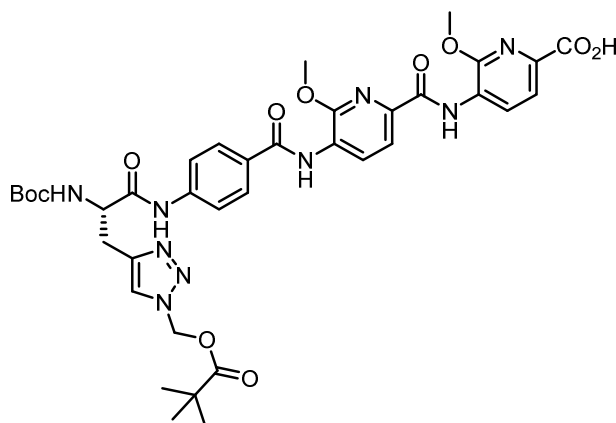


Reduction of the nitro group according to GP1:

- THF (10 mL), EtOH (30 mL), AcOH (10 mL)
- nitro tripeptide **220** (1.40 g, 2.76 mmol, 1.00 equiv)
- Zn-dust (18.0 g)
- 0 °C to r.t., 16 h
- column chromatography: SiO₂, CHCl₃/MeOH, 9:0.25
- the title compound **221** (638 mg, 1.32 mmol, 48%) was obtained as a beige solid

¹H NMR (400 MHz, DMF-*d*₇) δ 10.50 (s, 1H), 9.16 (s, 1H), 8.88 (d, $J=8.1$ Hz, 1H), 8.82 (d, $J=8.0$ Hz, 1H), 7.92 (d, $J=8.1$ Hz, 2H), 7.89–7.81 (m, 2H), 6.83–6.75 (m, 2H), 6.20–6.05 (m, 1H), 6.09 (s, 2H), 5.50 (dq, $J=17.2, 1.7$ Hz, 1H), 5.31 (dq, $J=10.5, 1.5$ Hz, 1H), 4.87 (dt, $J=5.4, 1.5$ Hz, 2H), 4.24 (s, 3H), 4.18 (s, 3H). ¹³C NMR (101 MHz, DMF-*d*₇) δ 166.6, 165.0, 154.6, 154.0, 139.9, 139.0, 134.0, 130.6, 128.9, 128.8, 127.6, 125.5, 121.4, 121.3, 118.5, 117.8, 114.1, 66.4, 55.1, 54.9. HRMS (ESI): m/z calculated for $C_{24}H_{23}N_5O_6$ $[M+H]^+$ 478.1718, found 478.1721 ($\Delta m = +0.6$ ppm).

Boc-AzaHis(POM)-D-E(Pyridine)-F(Pyridine)-OH (222)

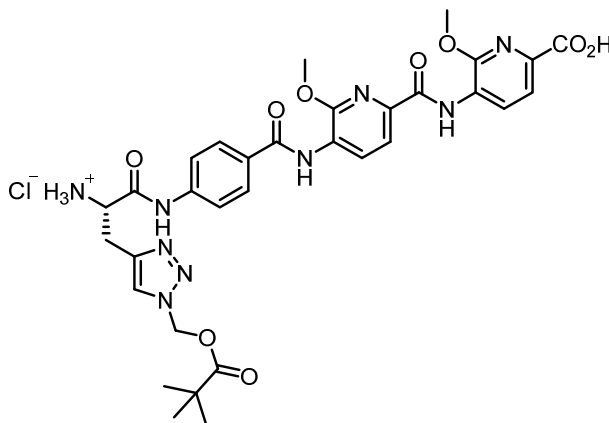


Pd-mediated allyl-deprotection according to GP8:

- allyl-protected tetrapeptide (230 mg, 277 μmol , 1.00 equiv) in THF (10 mL)
- morpholine (358 μL , 4.16 mmol, 15 equiv)
- $\text{Pd}(\text{PPh}_3)_4$ (96.1 mg, 83.2 μmol , 0.30 equiv)
- column chromatography: SiO_2 , 5–15% MeOH in CH_2Cl_2
- the title compound **222** (144 mg, 177 μmol , 64%) was obtained as a yellow solid

^1H NMR (400 MHz, $\text{DMSO}-d_6$) δ 10.59 (s, 1H), 10.41 (s, 1H), 9.69 (s, 1H), 8.73 (d, $J=7.9$ Hz, 1H), 8.53 (d, $J=7.9$ Hz, 1H), 8.02–7.94 (m, 3H), 7.85 (d, $J=8.0$ Hz, 1H), 7.82–7.75 (m, 3H), 7.67–7.50 (m, 3H), 7.22 (d, $J=8.0$ Hz, 1H), 6.29 (s, 2H), 4.42 (s, 1H), 4.14 (s, 3H), 4.08 (s, 3H), 3.18–2.98 (m, 2H), 1.38–1.25 (m, 9H), 1.09 (s, 9H). ^{13}C NMR (101 MHz, $\text{DMSO}-d_6$) δ 176.5, 170.8, 165.9, 165.0, 161.7, 155.3, 153.9, 152.4, 143.5, 142.5, 139.9, 133.2, 132.2, 132.0, 131.5, 131.5, 130.8, 128.8, 128.8, 128.7, 128.0, 126.6, 125.1, 124.8, 124.2, 119.8, 118.7, 116.4, 78.3, 69.9, 55.0, 54.3, 53.9, 38.2, 28.2, 27.8, 26.5, 18.8. HRMS (ESI): m/z calculated for $\text{C}_{37}\text{H}_{43}\text{N}_9\text{O}_{11}$ $[\text{M}+\text{H}]^+$ 790.3155, found 790.3151 ($\Delta m = -0.5$ ppm).

H_2N -AzaHis(POM)-D-E(Pyridine)-F(Pyridine)-OH*HCl (223)

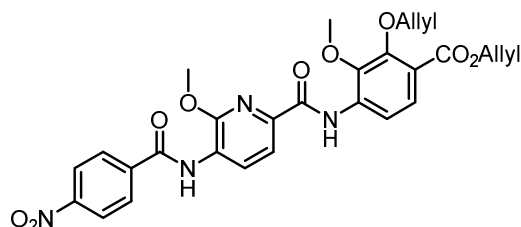


The Boc-protected tetrapeptide **222** (100 mg, 127 μmol , 1.00 equiv) was dissolved in CH_2Cl_2 (3 mL) and TFA (3 mL) was added. The reaction mixture was stirred at r.t. for 15 min, then all volatiles were removed under reduced pressure. The residue was taken up in 0.1 N $\text{HCl}_{(\text{aq})}$ and little CH_3CN and freeze-dried to afford the analytically pure title compound **223** (100 mg, 124 μmol , 98%) as a colourless solid.

^1H NMR (400 MHz, $\text{DMSO}-d_6$) δ 10.84 (s, 1H), 10.44 (s, 1H), 9.74 (s, 1H), 8.76 (d, $J=8.0$ Hz, 1H), 8.53 (d, $J=7.9$ Hz, 1H), 8.44 (s, 3H), 8.10 (s, 1H), 8.00 (d, $J=8.5$ Hz, 2H), 7.88 (d, $J=8.0$ Hz, 1H), 7.81 (d, $J=8.0$ Hz, 1H), 7.71 (d, $J=8.7$ Hz, 2H), 7.66–7.52 (m, 3H), 6.29 (s, 2H), 4.31 (s, 1H), 4.15

(s, 3H), 4.09 (s, 3H), 3.38–3.23 (m, 2H), 1.08 (s, 9H). HRMS (ESI): m/z calculated for $C_{32}H_{36}N_9O_9^+$ $[M]^+$ 690.2636, found 690.2637 ($\Delta m = +0.1$ ppm).

O₂N-D-E(Pyridine)-F(Allyl)-OAllyl (**224**)

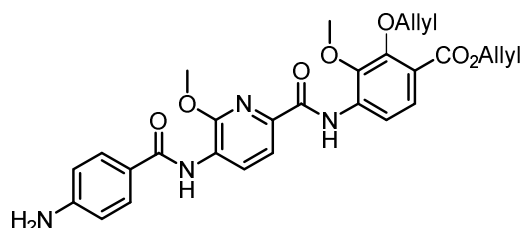


Peptide coupling according to GP5:

- amino dipeptide **129** (1.48 g, 3.58 mmol, 1.00 equiv) in THF (30 mL)
- *p*NBC (1.33 g, 7.16 mmol, 2.00 equiv)
- Et₃N (1.50 mL, 10.7 mmol, 3.00 equiv)
- the title compound **224** (1.80 g, 3.32 mmol, 90%) was obtained as a yellow solid

¹H NMR (400 MHz, CDCl₃) δ 10.48 (s, 1H), 8.94 (d, $J=8.1$ Hz, 1H), 8.56 (s, 1H), 8.44–8.33 (m, 3H), 8.11–8.03 (m, 2H), 8.00 (d, $J=8.0$ Hz, 1H), 7.69 (d, $J=8.8$ Hz, 1H), 6.23–5.97 (m, 2H), 5.46–5.36 (m, 2H), 5.33–5.22 (m, 2H), 4.80 (dt, $J=5.8, 1.4$ Hz, 2H), 4.59 (dt, $J=5.9, 1.4$ Hz, 2H), 4.25 (s, 3H), 4.02 (s, 3H). ¹³C NMR (101 MHz, CDCl₃) δ 165.1, 163.7, 161.7, 152.0, 151.7, 150.2, 142.8, 141.0, 139.6, 136.3, 134.0, 132.4, 128.5, 127.6, 127.4, 125.8, 124.3, 120.7, 118.6, 118.1, 117.8, 114.3, 75.3, 65.8, 61.3, 54.3. HRMS (ESI): m/z calculated for $C_{28}H_{26}N_4O_9$ $[M+H]^+$ 563.1757, found 563.1773 ($\Delta m = +2.8$ ppm).

H₂N-D-E(Pyridine)-F(Allyl)-OAllyl (**225**)



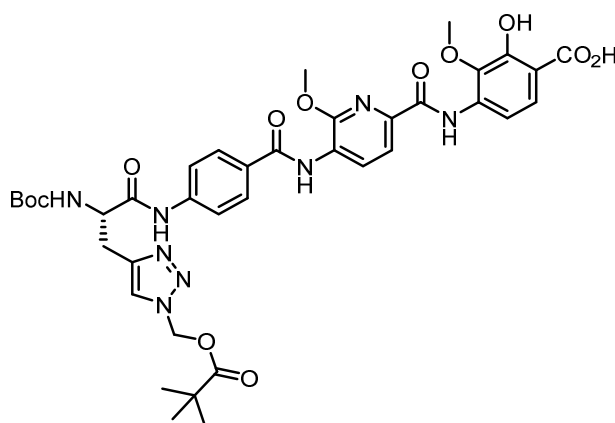
Reduction of the nitro group according to GP1:

- THF (15 mL), EtOH (35 mL), AcOH (10 mL)
- nitro tripeptide **224** (1.75 g, 3.11 mmol, 1.00 equiv)
- Zn-dust (15.3 g)
- 0 °C to r.t., 16 h

- column chromatography: SiO₂, CH₂Cl₂/MeOH, 9:0.2–9:1
- the title compound **221** (957 mg, 1.80 mmol, 58%) was obtained as a beige solid

¹H NMR (400 MHz, CDCl₃) δ 10.49 (s, 1H), 8.94 (d, *J*=8.1 Hz, 1H), 8.45–8.39 (m, 2H), 7.95 (d, *J*=8.1 Hz, 1H), 7.75–7.67 (m, 3H), 6.76–6.68 (m, 2H), 6.22–6.10 (m, 1H), 6.10–5.97 (m, 1H), 5.44 (q, *J*=1.6 Hz, 1H), 5.41–5.37 (m, 1H), 5.27 (ddt, *J*=11.1, 9.9, 1.4 Hz, 2H), 4.80 (dt, *J*=5.8, 1.4 Hz, 2H), 4.60 (dt, *J*=5.9, 1.4 Hz, 2H), 4.21 (s, 3H), 4.01 (s, 3H). ¹³C NMR (101 MHz, CDCl₃) δ 165.5, 165.1, 162.2, 152.0, 151.5, 150.7, 142.7, 139.5, 136.6, 134.0, 132.4, 129.2, 127.6, 127.1, 126.5, 123.3, 120.4, 118.6, 118.1, 117.9, 114.4, 114.3, 75.3, 65.7, 61.2, 54.1. HRMS (ESI): *m/z* calculated for C₂₈H₂₈N₄O₇ [M+H]⁺ 533.2031, found 533.2032 (Δ*m* = +0.2 ppm).

Boc-AzaHis(POM)-D-E(Pyridine)-F-OH (**226**)

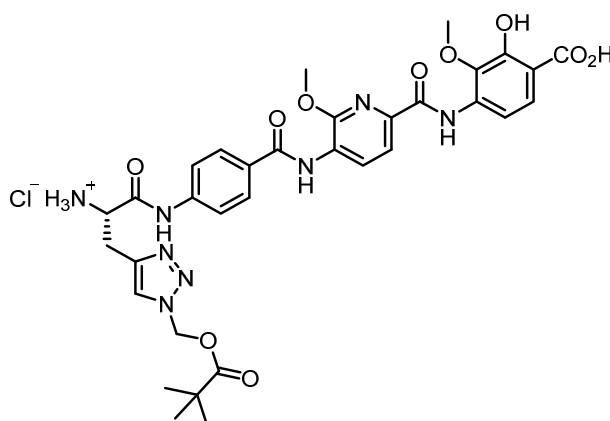


Pd-mediated allyl-deprotection according to GP8:

- allyl-protected tetrapeptide (220 mg, 249 μmol, 1.00 equiv) in THF (7 mL)
- morpholine (429 μL, 5.00 mmol, 20 equiv)
- Pd(PPh₃)₄ (86.2 mg, 74.6 μmol, 0.30 equiv)
- column chromatography: SiO₂, 5–25% MeOH in CH₂Cl₂
- the title compound **226** (140 mg, 174 μmol, 70%) was obtained as a yellow solid

¹H NMR (400 MHz, DMSO-*d*₆) δ 10.55 (s, 1H), 10.49 (s, 1H), 9.71 (s, 1H), 8.49 (d, *J*=7.9 Hz, 1H), 8.01–7.94 (m, 3H), 7.83 (d, *J*=7.9 Hz, 1H), 7.80–7.76 (m, 2H), 7.74 (d, *J*=8.6 Hz, 1H), 7.49 (d, *J*=8.5 Hz, 1H), 7.24 (d, *J*=8.0 Hz, 1H), 6.29 (s, 2H), 4.46–4.36 (m, 1H), 4.14 (s, 3H), 3.93 (s, 3H), 3.18–2.96 (m, 2H), 1.38–1.25 (m, 9H), 1.09 (s, 9H). ¹³C NMR (126 MHz, DMSO-*d*₆) δ 176.4, 165.0, 160.7, 153.9, 142.4, 141.2, 135.9, 128.7, 128.1, 125.9, 124.1, 118.7, 116.0, 105.3, 78.28, 69.9, 59.5, 53.8, 38.2, 28.1, 26.4. HRMS (ESI): *m/z* calculated for C₃₈H₄₄N₈O₁₂ [M+H]⁺ 805.3151, found 805.3154 (Δ*m* = +0.4 ppm).

H₂N-AzaHis(POM)-D-E(Pyridine)-F-OH*HCl (227)

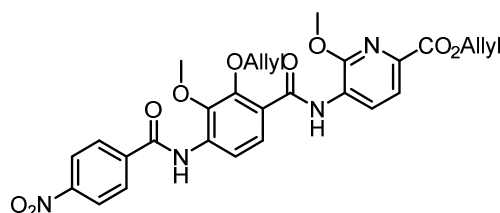


Boc-deprotection according to GP7:

- Boc-protected tetrapeptide **226** (95.0 mg, 118 μ mol, 1.00 equiv)
- 4 N HCl in 1,4-dioxane (5 mL)
- the title compound **227** (87.5 mg, 118 μ mol, quant.) was obtained as a colourless solid

¹H NMR (400 MHz, DMSO-*d*₆) δ 11.33 (s, 1H), 10.60 (s, 1H), 9.77 (s, 1H), 8.63 (s, 3H), 8.50 (d, *J*=8.0 Hz, 1H), 8.16 (s, 1H), 8.02–7.96 (m, 3H), 7.86 (d, *J*=7.9 Hz, 1H), 7.77 (d, *J*=8.7 Hz, 2H), 7.60 (d, *J*=8.7 Hz, 1H), 6.28 (s, 2H), 4.43 (s, 1H), 4.14 (s, 3H), 3.96 (s, 3H), 3.39–3.33 (m, 2H), 1.07 (s, 9H). HRMS (ESI): *m/z* calculated for C₃₃H₃₇N₈O₁₀⁺ [M]⁺ 705.2633, found 705.2628 (Δm = –0.7 ppm).

O₂N-D-E(Allyl)-F(Pyridine)-OAllyl (228)



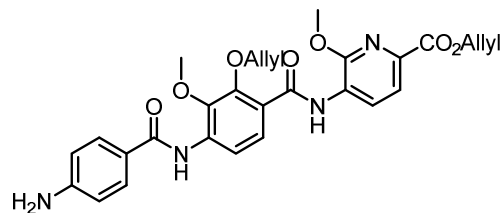
Peptide coupling according to GP5:

- amino dipeptide **131** (830 mg, 2.32 mmol, 1.00 equiv) in THF (25 mL)
- *p*NBC (862 g, 4.65 mmol, 2.00 equiv)
- Et₃N (971 μ L, 6.97 mmol, 3.00 equiv)
- the title compound **228** (1.06 g, 2.09 mmol, 90%) was obtained as a yellow solid

¹H NMR (400 MHz, CDCl₃) δ 10.65 (s, 1H), 8.93 (d, *J*=8.1 Hz, 1H), 8.70 (s, 1H), 8.43 (d, *J*=8.9 Hz, 1H), 8.41–8.33 (m, 2H), 8.10–8.02 (m, 3H), 7.82 (dd, *J*=8.2, 0.5 Hz, 1H), 6.19–6.00 (m, 2H),

5.48–5.38 (m, 2H), 5.36–5.27 (m, 2H), 4.85 (dt, $J=5.6, 1.5$ Hz, 2H), 4.75 (dt, $J=6.2, 1.2$ Hz, 2H), 4.16 (s, 3H), 4.06 (s, 3H). ^{13}C NMR (101 MHz, CDCl_3) δ 164.6, 163.3, 163.1, 152.9, 150.2, 149.5, 141.7, 140.0, 138.1, 136.0, 132.3, 128.5, 127.8, 127.0, 126.2, 124.3, 122.5, 120.7, 120.3, 118.5, 115.8, 75.8, 66.0, 61.6, 54.2. HRMS (ESI): m/z calculated for $\text{C}_{28}\text{H}_{26}\text{N}_4\text{O}_9$ $[\text{M}+\text{H}]^+$ 563.1773, found 563.1785 ($\Delta m = +2.1$ ppm).

H₂N-D-E(Allyl)-F(Pyridine)-OAllyl (229)

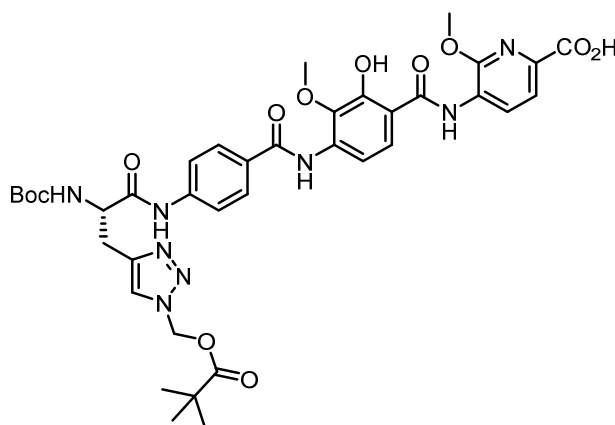


Reduction of the nitro group according to GP1:

- THF (30 mL), EtOH (10 mL), AcOH (10 mL)
- nitro tripeptide **228** (1.00 g, 1.78 mmol, 1.00 equiv)
- Zn-dust (11.6 g)
- r.t., 2 h
- column chromatography: SiO_2 , $\text{CH}_2\text{Cl}_2/\text{MeOH}$, 9:0.1–9:0.3
- the title compound **229** (880 mg, 1.66 mmol, 93%) was obtained as a beige solid

^1H NMR (400 MHz, CDCl_3) δ 10.68 (s, 1H), 8.93 (d, $J=8.1$ Hz, 1H), 8.57 (s, 1H), 8.44 (d, $J=9.0$ Hz, 1H), 8.02 (d, $J=9.0$ Hz, 1H), 7.82 (d, $J=8.1$ Hz, 1H), 7.77–7.69 (m, 2H), 6.78–6.70 (m, 2H), 6.21–5.99 (m, 2H), 5.48–5.38 (m, 2H), 5.33–5.27 (m, 2H), 4.85 (dt, $J=5.6, 1.4$ Hz, 2H), 4.75 (dt, $J=6.2, 1.3$ Hz, 2H), 4.15 (s, 3H), 4.01 (s, 3H). ^{13}C NMR (101 MHz, CDCl_3) δ 165.1, 164.7, 163.5, 152.9, 150.3, 149.5, 141.3, 137.9, 137.3, 135.9, 132.5, 132.3, 129.2, 127.7, 127.2, 126.1, 125.6, 123.9, 121.0, 120.7, 119.9, 118.4, 115.6, 114.6, 75.6, 68.1, 66.0, 61.3, 60.8, 54.1, 34.3, 30.4, 29.8, 29.5, 21.3. HRMS (ESI): m/z calculated for $\text{C}_{28}\text{H}_{28}\text{N}_4\text{O}_7$ $[\text{M}+\text{H}]^+$ 533.2031, found 533.2017 ($\Delta m = -2.6$ ppm).

Boc-AzaHis(POM)-D-E-F(Pyridine)-OH (230)

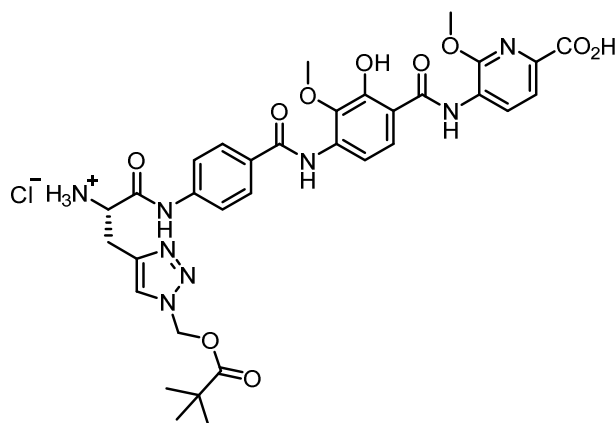


Pd-mediated allyl-deprotection according to GP8:

- allyl-protected tetrapeptide (300 mg, 339 μmol , 1.00 equiv) in THF (10 mL)
- morpholine (585 μL , 6.78 mmol, 20 equiv)
- Pd(PPh₃)₄ (118 mg, 102 μmol , 0.30 equiv)
- column chromatography: SiO₂, 5–25% MeOH in CH₂Cl₂
- the title compound **226** (245 mg, 305 μmol , 90%) was obtained as a colourless solid

¹H NMR (500 MHz, DMSO-*d*₆) δ 10.68 (s, 1H), 9.49 (s, 1H), 8.81 (d, *J* = 8.0 Hz, 1H), 8.00 (s, 1H), 7.97–7.92 (m, 2H), 7.82–7.76 (m, 2H), 7.74 (d, *J*=8.0 Hz, 2H), 7.44 (d, *J*=8.8 Hz, 1H), 7.19 (d, *J*=8.1 Hz, 1H), 6.28 (s, 2H), 4.48–4.40 (m, 1H), 4.05 (s, 3H), 3.79 (s, 3H), 3.17–3.01 (m, 2H), 1.37–1.26 (m, 9H), 1.09 (s, 9H). ¹³C NMR (126 MHz, DMSO-*d*₆) δ 176.4, 170.7, 165.7, 164.6, 155.3, 152.7, 143.5, 142.2, 140.4, 128.7, 128.5, 126.0, 125.0, 124.2, 119.8, 118.7, 115.7, 78.3, 69.9, 60.1, 54.0, 38.2, 28.1, 27.9, 26.5. HRMS (ESI): *m/z* calculated for C₃₈H₄₄N₈O₁₂ [M+H]⁺ 805.3151, found 805.3156 (Δm = +0.6 ppm).

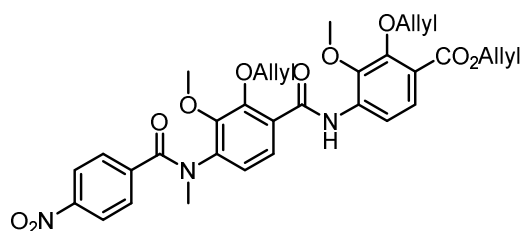
H₂N-AzaHis(POM)-D-E-F(Pyridine)-OH*HCl (231)



The Boc-protected tetrapeptide **230** (220 mg, 273 μmol , 1.00 equiv) was dissolved in CH_2Cl_2 (5 mL) and TFA (5 mL) was added. The reaction mixture was stirred at r.t. for 15 min, then all volatiles were removed under reduced pressure. The residue was taken up in 0.1 N $\text{HCl}_{(\text{aq.})}$ and little CH_3CN and freeze-dried to afford the analytically pure title compound **231** (202 mg, 273 μmol , quant.) as a colourless solid.

^1H NMR (400 MHz, $\text{DMSO-}d_6$) δ 11.76 (s, 1H), 11.08 (s, 1H), 10.90 (s, 1H), 9.72 (s, 1H), 9.09 (s, 1H), 8.79 (d, $J=8.1$ Hz, 1H), 8.56–8.47 (m, 3H), 8.10 (s, 1H), 8.02–7.96 (m, 2H), 7.82 (d, $J=8.8$ Hz, 1H), 7.77 (d, $J=8.0$ Hz, 1H), 7.70 (d, $J=8.7$ Hz, 2H), 7.58 (d, $J=8.9$ Hz, 1H), 6.28 (s, 2H), 4.37–4.29 (m, 1H), 4.07 (s, 3H), 3.76 (s, 3H), 3.15–3.05 (m, 2H), 1.07 (s, 9H). ^{13}C NMR (101 MHz, $\text{DMSO-}d_6$) δ 176.5, 166.9, 165.5, 164.8, 163.9, 158.9, 158.5, 158.2, 152.7, 150.0, 141.3, 140.9, 140.2, 138.5, 136.1, 129.5, 128.9, 126.3, 125.1, 119.1, 117.9, 115.8, 115.0, 69.9, 68.0, 63.4, 60.6, 54.2, 52.8, 42.8, 38.2, 26.5, 23.9. HRMS (ESI): m/z calculated for $\text{C}_{33}\text{H}_{37}\text{N}_8\text{O}_{10}^+$ $[\text{M}]^+$ 705.2633, found 705.2630 ($\Delta m = -0.4$ ppm).

***N*-Methylated nitro tripeptide (232)**

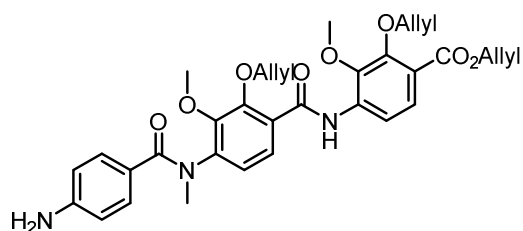


Peptide coupling according to GP5:

- amino dipeptide **135** (156 mg, 323 μmol , 1.00 equiv) in THF (15 mL)
- *p*NBC (120 mg, 646 μmol , 2.00 equiv)
- pyridine (78.1 μL , 970 μmol , 3.00 equiv)
- column chromatography: SiO_2 , *n*-hexane/EtOAc, 4:1–2:1
- the title compound **232** (135 mg, 217 μmol , 67%) was obtained as a yellow gum

HRMS (ESI): m/z calculated for $\text{C}_{33}\text{H}_{33}\text{N}_3\text{O}_{10}$ $[\text{M}+\text{H}]^+$ 632.2239, found 632.2231 ($\Delta m = -1.3$ ppm).

N-Methylated amino tripeptide (**233**)

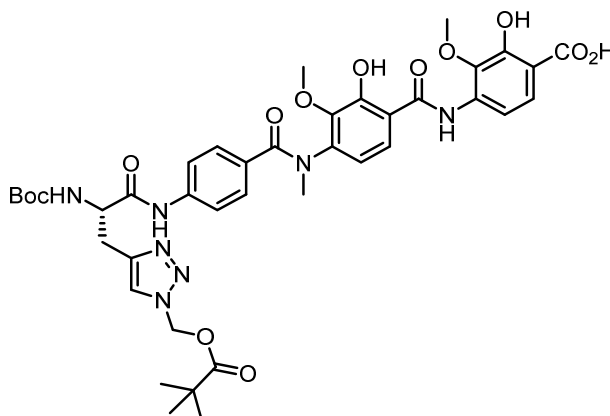


Reduction of the nitro group according to GP1:

- EtOH (15 mL), AcOH (3 mL)
- nitro tripeptide **228** (135 mg, 214 μmol , 1.00 equiv)
- Zn-dust (2.0 g)
- 0 °C, 30 min
- the title compound **233** (125 mg, 205 μmol , 96%) was obtained as a yellow oil

^1H NMR (500 MHz, $\text{DMSO-}d_6$) δ 10.61 (s, 1H), 8.28 (d, $J=8.8$ Hz, 1H), 7.72 (d, $J=8.6$ Hz, 1H), 7.55 (d, $J=8.8$ Hz, 1H), 7.24 (d, $J=8.6$ Hz, 1H), 7.04–6.99 (m, 2H), 6.33–6.29 (m, 2H), 6.12–5.98 (m, 2H), 5.82 (ddt, $J=16.9, 10.2, 6.6$ Hz, 1H), 5.48–5.44 (m, 2H), 5.39 (tq, $J=17.3, 1.7$ Hz, 2H), 5.29–5.26 (m, 1H), 5.25–5.21 (m, 1H), 5.16–5.12 (m, 1H), 5.10–5.05 (m, 1H), 4.77 (dt, $J=5.5, 1.5$ Hz, 2H), 4.56–4.50 (m, 4H), 3.91 (s, 3H), 3.75 (s, 3H), 3.29 (s, 3H). ^{13}C NMR (126 MHz, DMSO) δ 170.2, 164.4, 162.1, 151.0, 150.7, 149.8, 148.1, 143.6, 142.5, 136.3, 133.9, 132.6, 132.0, 130.1, 126.2, 125.4, 123.8, 121.9, 120.9, 120.4, 118.1, 117.8, 114.8, 111.9, 74.8, 74.5, 65.1, 61.0, 60.8, 37.6. HRMS (ESI): m/z calculated for $\text{C}_{33}\text{H}_{35}\text{N}_3\text{O}_8$ $[\text{M}+\text{H}]^+$ 602.2497, found 602.2491 ($\Delta m = -1.0$ ppm).

N-Methylated tetrapeptide (**234**)



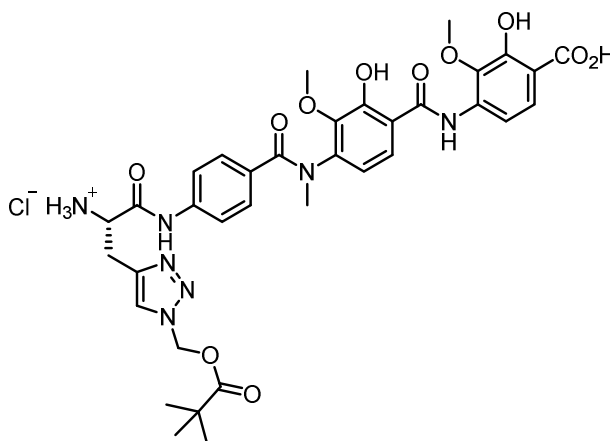
Pd-mediated allyl-deprotection according to GP8:

- allyl-protected tetrapeptide (138 mg, 145 μmol , 1.00 equiv) in THF (8 mL)

- morpholine (188 μL , 2.17 mmol, 15 equiv)
- $\text{Pd}(\text{PPh}_3)_4$ (50.1 mg, 43.4 μmol , 0.30 equiv)
- column chromatography: SiO_2 , 5–15% MeOH in CH_2Cl_2
- the title compound **234** (78.0 mg, 94.0, 65%) was obtained as a colourless solid

^1H NMR (400 MHz, $\text{DMSO}-d_6$) δ 11.50 (s, 1H), 10.83 (s, 1H), 10.22 (s, 1H), 7.93 (s, 1H), 7.75 (d, $J=8.7$ Hz, 1H), 7.62 (d, $J=8.5$ Hz, 1H), 7.43 (t, $J=8.7$ Hz, 3H), 7.30 (d, $J=8.4$ Hz, 2H), 7.14 (d, $J=8.0$ Hz, 1H), 6.97 (s, 1H), 6.25 (s, 2H), 4.35–4.24 (m, 1H), 3.79 (s, 3H), 3.68 (s, 3H), 3.09–2.87 (m, 2H), 1.33–1.11 (m, 9H), 1.06 (s, 9H). HRMS (ESI): m/z calculated for $\text{C}_{40}\text{H}_{47}\text{N}_7\text{O}_{13}$ $[\text{M}+\text{H}]^+$ 834.3305, found 834.3281 ($\Delta m = -2.9$ ppm).

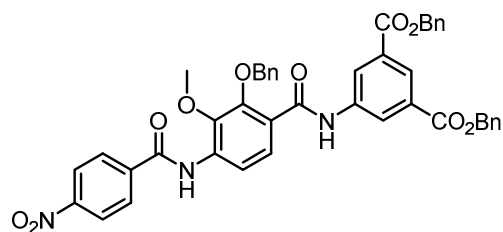
N-Methylated tetrapeptide (235)



Boc-deprotection according to GP7:

- Boc-protected tetrapeptide **234** (70 mg, 84 μmol , 1.00 equiv)
- 4 N HCl in 1,4-dioxane (10 mL)
- the title compound **235** (64 mg, 84 μmol , quant.) was obtained as a colourless solid

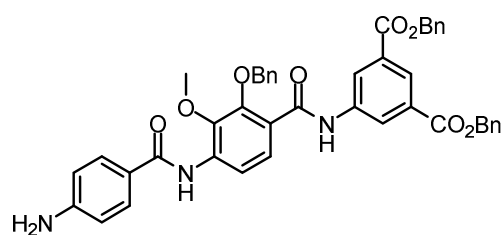
^1H NMR (400 MHz, $\text{DMSO}-d_6$) δ 11.53 (s, 1H), 11.11 (s, 1H), 11.06 (s, 1H), 8.53 (s, 4H), 8.10 (s, 1H), 7.98 (d, $J=8.9$ Hz, 1H), 7.77 (d, $J=8.7$ Hz, 1H), 7.55 (d, $J=8.9$ Hz, 1H), 7.44 (d, $J=8.4$ Hz, 2H), 7.32 (d, $J=8.4$ Hz, 2H), 7.03 (d, $J=8.7$ Hz, 1H), 6.23 (d, $J=1.1$ Hz, 2H), 4.31 (s, 1H), 3.85 (s, 3H), 3.68 (s, 3H), 3.34–3.22 (m, 2H), 1.03 (d, $J=0.9$ Hz, 9H).

Isophthalic acid-containing nitro tripeptide (236)

Peptide coupling according to GP5:

- amino dipeptide **138** (445 mg, 0.722 mmol, 1.00 equiv) in THF (15 mL)
- *p*NBC (268 mg, 1.44 mmol, 2.00 equiv)
- Et₃N (302 μL, 2.16 mmol, 3.00 equiv)
- the title compound **236** (431 mg, 0.563 mmol, 78%) was obtained as a yellow solid

¹H NMR (400 MHz, DMSO-*d*₆) δ 10.66 (s, 1H), 10.23 (s, 1H), 8.58 (d, *J*=1.6 Hz, 2H), 8.43–8.35 (m, 2H), 8.29–8.25 (m, 1H), 8.25–8.18 (m, 2H), 7.72 (d, *J*=8.5 Hz, 1H), 7.53–7.46 (m, 4H), 7.45–7.34 (m, 9H), 7.24–7.17 (m, 3H), 5.41 (s, 4H), 5.09 (s, 2H), 3.93 (s, 3H). ¹³C NMR (101 MHz, DMSO-*d*₆) δ 164.6, 164.3, 149.4, 149.3, 145.9, 140.0, 139.9, 136.5, 135.8, 134.1, 130.7, 129.3, 128.5, 128.2, 128.2, 128.2, 128.1, 124.5, 124.3, 123.6, 120.1, 75.7, 66.7, 60.9. HRMS (ESI): *m/z* calculated for C₄₄H₃₅N₃O₁₀ [M+H]⁺ 766.2395, found 766.2400 (Δ*m* = +0.7 ppm).

Isophthalic acid-containing amino tripeptide (237)

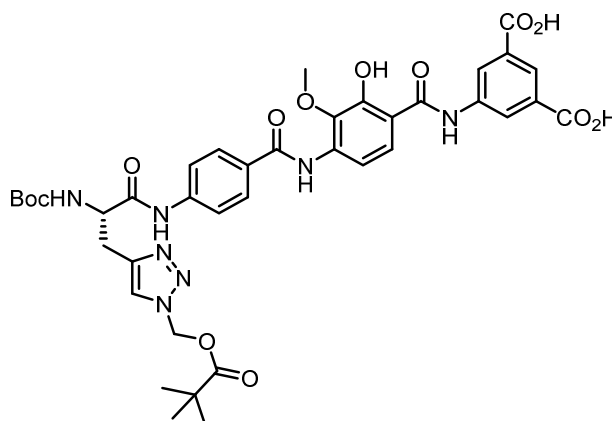
Reduction of the nitro group according to GP1:

- THF (10 mL), EtOH (20 mL), AcOH (5 mL)
- nitro tripeptide **236** (400 mg, 522 μmol, 1.00 equiv)
- Zn-dust (3.0 g)
- 0 °C, 30 min
- the title compound **237** (383 mg, 522 μmol, quant.) was obtained as a yellow oil

¹H NMR (400 MHz, DMSO-*d*₆) δ 10.59 (s, 1H), 9.20 (s, 1H), 8.57 (d, *J*=1.6 Hz, 2H), 8.26 (t, *J*=1.6 Hz, 1H), 7.89 (d, *J*=8.5 Hz, 1H), 7.78–7.70 (m, 2H), 7.53–7.33 (m, 12H), 7.25–7.17 (m, 3H),

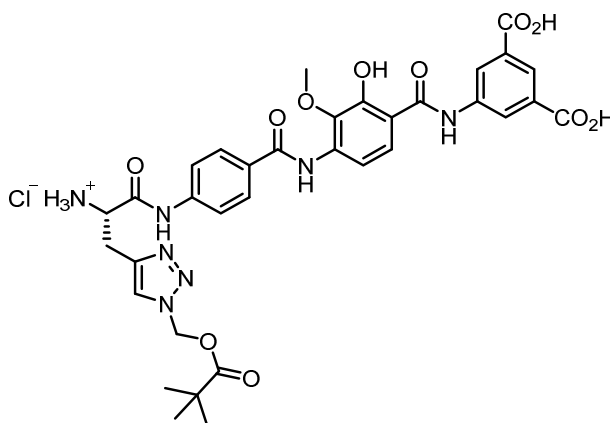
6.69–6.60 (m, 2H), 5.85 (s, 2H), 5.41 (s, 4H), 5.08 (s, 2H), 3.94 (s, 3H). ^{13}C NMR (101 MHz, DMSO- d_6) δ 165.0, 164.6, 164.6, 152.5, 149.3, 144.1, 139.9, 136.5, 135.8, 135.5, 130.6, 129.3, 128.5, 128.3, 128.2, 128.1, 126.0, 124.5, 124.3, 123.8, 120.2, 118.0, 112.7, 75.7, 66.6, 60.9, 30.4. HRMS (ESI): m/z calculated for $\text{C}_{44}\text{H}_{37}\text{N}_3\text{O}_8$ $[\text{M}+\text{H}]^+$ 736.2653, found 736.2648 ($\Delta m = -0.7$ ppm).

Isophthalic acid-containing tetrapeptide (238)



A solution of the benzyl-protected tetrapeptide (250 mg, 230 μmol , 1.00 equiv) in a mixture of MeOH (15 mL) and EtOAc (15 mL) was purged with N_2 for 5 min, then Pd (10 wt.% on activated carbon, 25 mg) was added. The resulting suspension was purged with N_2 for 5 min followed by H_2 for 5 min. The reaction mixture was stirred at r.t. under a H_2 -atmosphere for 2 h. The suspension was filtered through a pad of Celite[®] and the filtrate concentrated under reduced pressure to afford the crude product, which was purified by column chromatography on silica gel (3–20% MeOH in CH_2Cl_2). The title compound **238** (141 mg, 172 μmol , 75%) was obtained as a colourless solid.

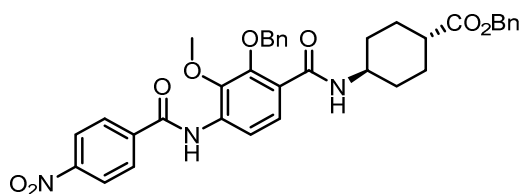
^1H NMR (400 MHz, DMSO- d_6) δ 12.28–12.23 (m, 2H), 10.51–10.46 (m, 1H), 9.34 (s, 1H), 8.52 (s, 2H), 8.31–8.27 (m, 1H), 8.02–7.89 (m, 3H), 7.82–7.73 (m, 3H), 7.46–7.41 (m, 1H), 7.22 (d, $J=7.6$ Hz, 1H), 6.29 (s, 2H), 4.44–4.38 (m, 1H), 3.87 (s, 3H), 3.18–2.95 (m, 2H), 1.42–1.23 (m, 9H), 1.09 (s, 9H). ^{13}C NMR (101 MHz, DMSO- d_6) δ 176.5, 167.8, 164.5, 155.4, 143.5, 142.2, 128.9, 128.5, 128.4, 124.2, 123.3, 118.8, 78.3, 69.9, 59.7, 55.0, 38.2, 28.2, 26.5. HRMS (ESI): m/z calculated for $\text{C}_{39}\text{H}_{43}\text{N}_7\text{O}_{13}$ $[\text{M}+\text{H}]^+$ 818.2992, found 818.3008 ($\Delta m = +2.0$ ppm).

Isophthalic acid-containing tetrapeptide (239)

Boc-deprotection according to GP7:

- Boc-protected tetrapeptide **238** (120 mg, 147 μmol , 1.00 equiv)
- 4 N HCl in 1,4-dioxane (7 mL)
- the title compound **239** (110 mg, 147 μmol , quant.) was obtained as a colourless solid

^1H NMR (400 MHz, $\text{DMSO-}d_6$) δ 13.32 (s, 2H), 12.30 (s, 1H), 11.39 (s, 1H), 10.81 (s, 1H), 9.56 (s, 1H), 8.67 (s, 3H), 8.61 (d, $J=1.5$ Hz, 2H), 8.25 (t, $J=1.6$ Hz, 1H), 8.17 (s, 1H), 7.96 (t, $J=8.6$ Hz, 3H), 7.81–7.72 (m, 2H), 7.63 (d, $J=8.9$ Hz, 1H), 6.27 (s, 2H), 4.44 (s, 1H), 3.87 (s, 3H), 3.56–3.30 (m, 2H), 1.07 (s, 9H). ^{13}C NMR (101 MHz, $\text{DMSO-}d_6$) δ 176.4, 168.4, 166.8, 166.4, 164.7, 153.95, 141.5, 140.9, 139.0, 138.7, 136.2, 131.7, 129.3, 128.7, 125.8, 125.6, 125.0, 123.1, 119.0, 112.6, 112.6, 69.9, 60.2, 52.6, 38.2, 30.4, 27.1, 26.5. HRMS (ESI): m/z calculated for $\text{C}_{34}\text{H}_{36}\text{N}_7\text{O}_{11}^+$ [M] $^+$ 718.2473, found 718.2462 ($\Delta m = -1.5$ ppm).

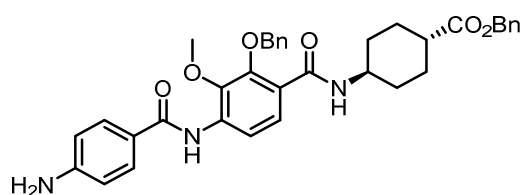
Cyclohexane-containing nitro tripeptide (240)

Peptide coupling according to GP5:

- amino dipeptide **141** (457 mg, 0.935 mmol, 1.00 equiv) in THF (15 mL)
- *p*NBC (347 mg, 1.87 mmol, 2.00 equiv)
- Et_3N (391 μL , 2.81 mmol, 3.00 equiv)
- the title compound **240** (564 mg, 0.889 mmol, 95%) was obtained as a colourless solid

^1H NMR (400 MHz, $\text{DMSO-}d_6$) δ 10.16 (s, 1H), 8.42–8.34 (m, 2H), 8.24–8.16 (m, 2H), 8.04 (d, $J=7.7$ Hz, 1H), 7.66 (d, $J=8.5$ Hz, 1H), 7.52–7.47 (m, 2H), 7.46–7.31 (m, 9H), 5.12–5.06 (m, 4H), 3.87 (s, 3H), 3.73–3.59 (m, 1H), 2.32–2.20 (m, 1H), 1.95–1.80 (m, 4H), 1.50–1.35 (m, 2H), 1.18–1.03 (m, 2H). ^{13}C NMR (101 MHz, DMSO) δ 174.4, 164.2, 164.0, 149.6, 149.3, 145.7, 140.0, 136.7, 136.3, 133.7, 129.3, 128.5, 128.4, 128.4, 128.3, 127.9, 127.7, 127.4, 123.9, 123.6, 119.8, 75.5, 65.3, 60.9, 47.5, 41.5, 30.9, 27.4.

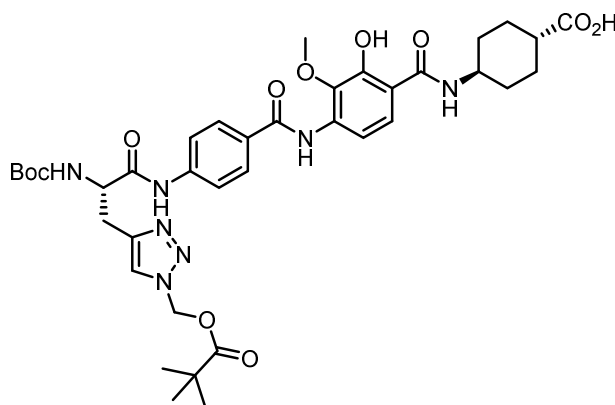
Cyclohexane-containing amino tripeptide (**241**)



Reduction of the nitro group according to GP1:

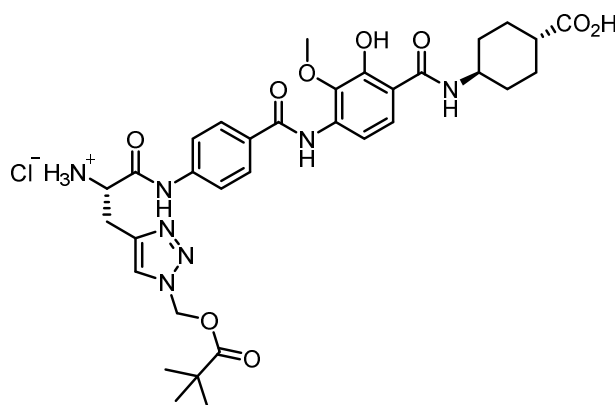
- THF (5 mL), EtOH (25 mL), AcOH (5 mL)
- nitro tripeptide **240** (100 mg, 157 μmol , 1.00 equiv)
- Zn-dust (1.0 g)
- 0 $^\circ\text{C}$, 15 min
- the title compound **241** (95.0 mg, 157 μmol , quant.) was obtained as a yellow oil

^1H NMR (400 MHz, $\text{DMSO-}d_6$) δ 9.13 (s, 1H), 7.96 (d, $J=7.7$ Hz, 1H), 7.83 (d, $J=8.6$ Hz, 1H), 7.73–7.68 (m, 2H), 7.52–7.48 (m, 2H), 7.46–7.31 (m, 10H), 6.65–6.59 (m, 2H), 5.83 (s, 2H), 5.11–5.06 (m, 4H), 3.88 (s, 3H), 3.71–3.59 (m, 1H), 2.29–2.19 (m, 1H), 1.94–1.79 (m, 4H), 1.48–1.35 (m, 2H), 1.14–1.01 (m, 2H). ^{13}C NMR (101 MHz, $\text{DMSO-}d_6$) δ 174.4, 164.9, 163.9, 152.5, 149.4, 143.8, 136.6, 136.3, 135.1, 129.3, 128.5, 128.4, 128.4, 128.3, 127.9, 127.7, 125.0, 124.2, 120.3, 117.7, 112.7, 75.5, 65.3, 60.8, 47.4, 41.5, 30.9, 27.4. HRMS (ESI): m/z calculated for $\text{C}_{36}\text{H}_{37}\text{N}_3\text{O}_6$ $[\text{M}+\text{H}]^+$ 608.2755, found 608.2771 ($\Delta m = +2.6$ ppm).

Cyclohexane-containing tetrapeptide (242)

A solution of the benzyl-protected tetrapeptide (100 mg, 104 μmol , 1.00 equiv) in a mixture of MeOH (5 mL) and EtOAc (5 mL) was purged with N_2 for 5 min, then Pd (10 wt.% on activated carbon, 10 mg) was added. The resulting suspension was purged with N_2 for 5 min followed by H_2 for 5 min. The reaction mixture was stirred at r.t. under a H_2 -atmosphere for 2 h. The suspension was filtered through a pad of Celite[®] and the filtrate concentrated under reduced pressure to afford the title compound **242** (78.0 mg, 100 μmol , 96%) as a colourless solid.

^1H NMR (400 MHz, $\text{DMSO-}d_6$) δ 10.41 (s, 1H), 9.36 (s, 1H), 8.77 (s, 1H), 7.97 (d, $J=7.7$ Hz, 1H), 7.92 (d, $J=8.7$ Hz, 2H), 7.75 (d, $J=8.5$ Hz, 2H), 7.66 (d, $J=8.9$ Hz, 1H), 7.52 (d, $J=8.8$ Hz, 1H), 7.18 (d, $J=7.9$ Hz, 1H), 6.29 (s, 2H), 4.44–4.37 (m, 1H), 3.85 (s, 3H), 3.16–2.95 (m, 2H), 2.18 (s, 1H), 2.04–1.84 (m, 3H), 1.52–1.19 (m, 13H), 1.09 (s, 9H). ^{13}C NMR (101 MHz, $\text{DMSO-}d_6$) δ 176.4, 176.4, 168.7, 164.6, 143.4, 142.1, 138.7, 135.3, 128.7, 128.5, 121.9, 118.7, 69.8, 59.9, 47.7, 41.8, 38.1, 31.0, 28.1, 27.7, 26.4. HRMS (ESI): m/z calculated for $\text{C}_{38}\text{H}_{49}\text{N}_7\text{O}_{11}$ $[\text{M}+\text{H}]^+$ 780.3563, found 780.3565 ($\Delta m = +0.3$ ppm).

Cyclohexane-containing tetrapeptide (243)

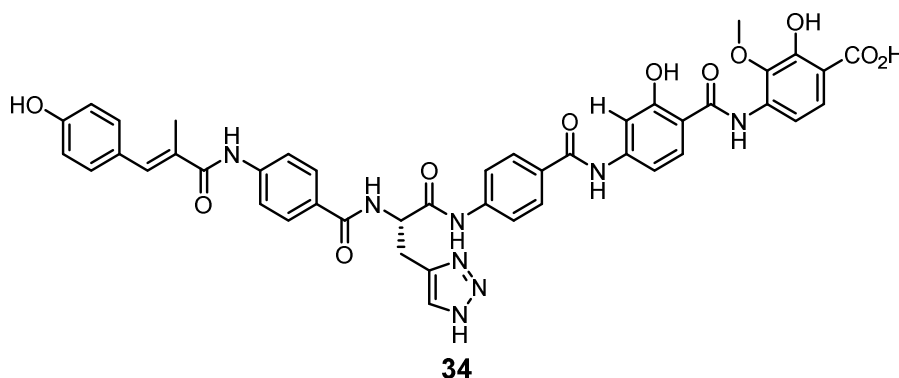
Boc-deprotection according to GP7:

- Boc-protected tetrapeptide **242** (60 mg, 77 μmol , 1.00 equiv)
- 4 N HCl in 1,4-dioxane (5 mL)
- the title compound **243** (55 mg, 77 μmol , quant.) was obtained as a colourless solid

HRMS (ESI): m/z calculated for $\text{C}_{33}\text{H}_{42}\text{N}_7\text{O}_9^+$ $[\text{M}]^+$ 680.3044, found 680.3059 ($\Delta m = +2.2$ ppm).

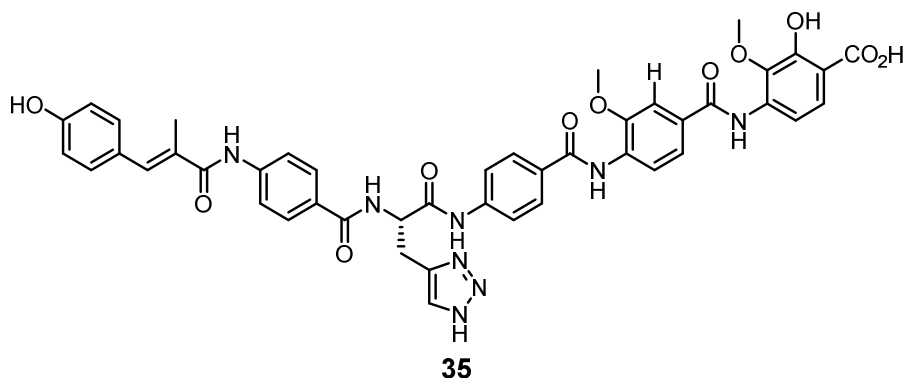
Final Assembly of E-F Derivatives of Albicidin

Final Derivative 34

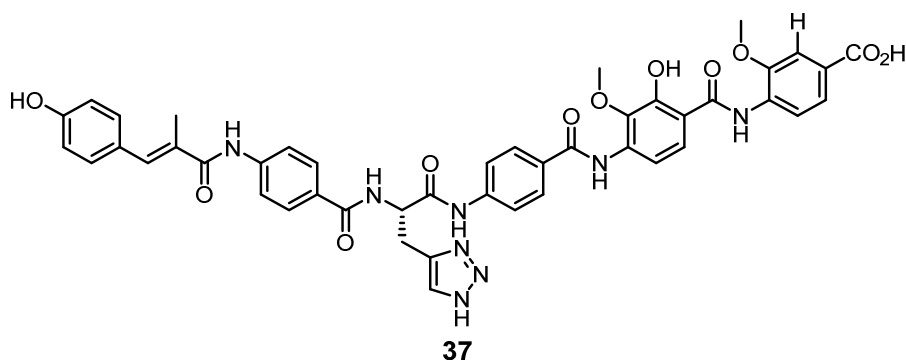


Synthetic protocol according to GP8. The title compound **34** (10 mg, 12 μmol , 8% over two steps) was obtained as a colourless solid. ^1H NMR (DMSO- d_6 , 500 MHz) δ 11.70–12.00 (m, 1H), 10.89–11.25 (m, 1H), 10.48–10.56 (m, 1H), 10.30–10.41 (m, 1H), 10.08 (s, 1H), 9.80 (br. s., 1H), 8.70 (d, $J=7.6$ Hz, 1H), 8.11 (d, $J=8.9$ Hz, 1H), 7.92–8.02 (m, 3H), 7.73–7.91 (m, 7H), 7.61–7.73 (m, 1H), 7.49–7.61 (m, $J=8.9$ Hz, 1H), 7.35 (d, $J=8.5$ Hz, 3H), 7.27 (s, 1H), 6.84 (d, $J=8.7$ Hz, 2H), 4.86–4.96 (m, 1H), 3.77–3.90 (m, 3H), 3.20–3.32 (m, 2H), 2.11 (d, $J=1.1$ Hz, 3H). HRMS (ESI): m/z calculated for $\text{C}_{44}\text{H}_{38}\text{N}_8\text{O}_{11}$ $[\text{M}+\text{H}]^+$, 855.2733 found 855.2741 ($\Delta m = +0.9$ ppm).

Final Derivative 35

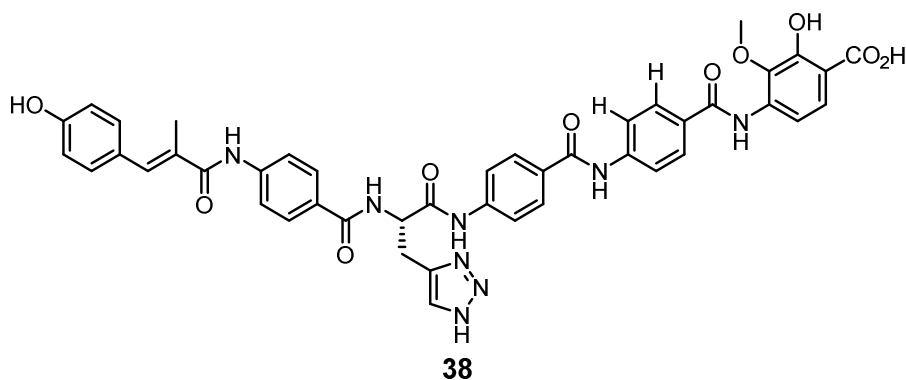


Final Derivative 37



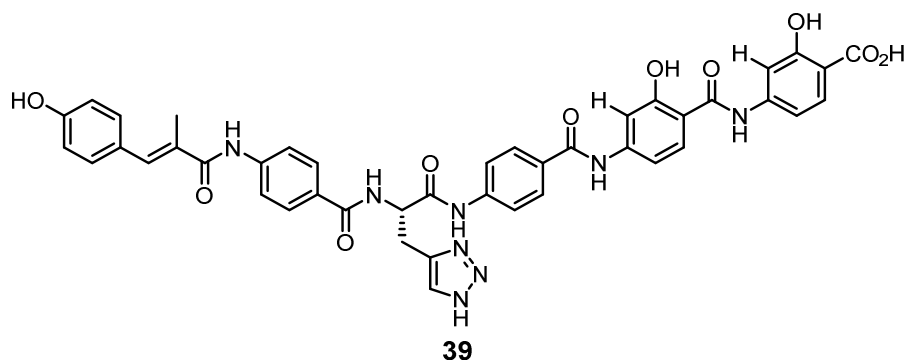
Synthetic protocol according to GP8. The title compound **37** (20 mg, 23 μmol , 19% over two steps) was obtained as a colourless solid. ^1H NMR (DMSO- d_6 , 400 MHz) δ 11.59 (br. s., 1H), 11.02 (s, 1H), 10.54 (s, 1H), 10.10 (s, 1H), 9.66 (s, 1H), 8.72 (d, $J=7.5$ Hz, 1H), 8.49 (d, $J=8.3$ Hz, 1H), 7.98 (d, $J=8.8$ Hz, 2H), 7.75–7.92 (m, 7H), 7.69 (s, 1H), 7.54–7.66 (m, 3H), 7.35 (d, $J=8.5$ Hz, 2H), 7.27 (s, 1H), 6.84 (d, $J=8.8$ Hz, 2H), 4.86–4.97 (m, 1H), 3.98 (s, 3H), 3.78 (s, 3H), 3.19–3.35 (m, 2H), 2.12 (s, 3H). HRMS (ESI): m/z calculated for $\text{C}_{45}\text{H}_{40}\text{N}_8\text{O}_{11}$ $[\text{M}+\text{H}]^+$ 869.2889, found 869.2901 ($\Delta m = +1.4$ ppm).

Final Derivative 38



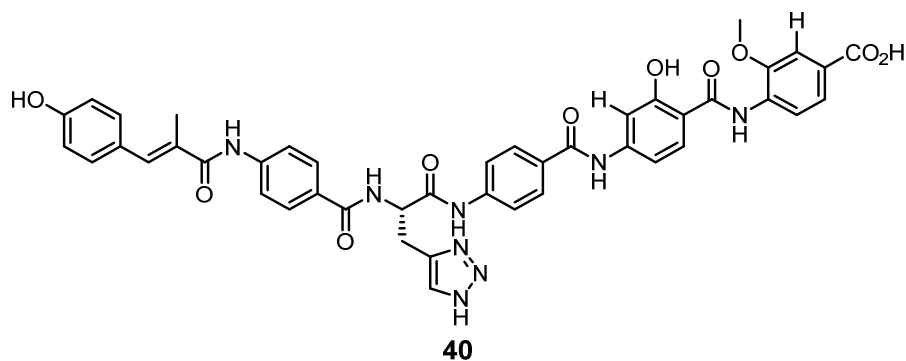
Synthetic protocol according to GP8. The title compound **38** (8.0 mg, 9.5 μmol , 5% over two steps) was obtained as a colourless solid. ^1H NMR (DMSO- d_6 , 400 MHz) δ 10.52 (s, 1H), 10.44 (s, 1H), 10.08 (s, 1H), 9.79 (br. s., 1H), 9.48 (s, 1H), 8.67–8.73 (m, 1H), 7.91–8.03 (m, 6H), 7.76–7.90 (m, 6H), 7.53–7.68 (m, 3H), 7.35 (d, $J=8.5$ Hz, 2H), 7.26 (s, 1H), 6.84 (d, $J=8.5$ Hz, 2H), 4.85–4.96 (m, 1H), 3.89 (s, 3H), 2.11 (s, 3H). HRMS (ESI): m/z calculated for $\text{C}_{44}\text{H}_{38}\text{N}_8\text{O}_{10}$ $[\text{M}+\text{H}]^+$ 839.2784, found 839.2787 ($\Delta m = +0.4$ ppm).

Final Derivative 39



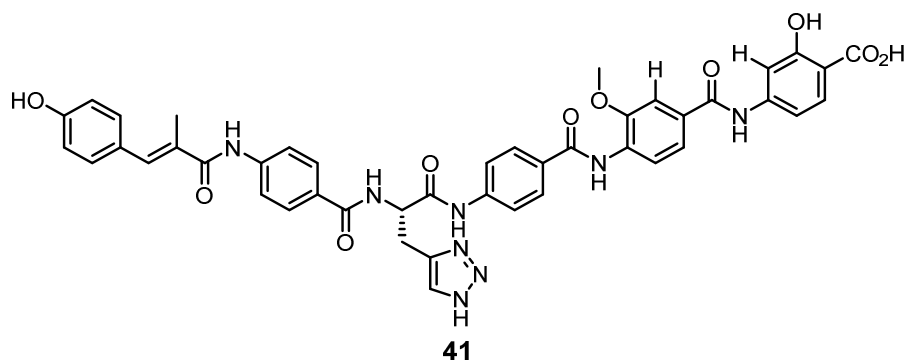
Synthetic protocol according to GP8. The title compound **39** (6.0 mg, 7.3 μmol , 6% over two steps) was obtained as a colourless solid. ^1H NMR (DMSO- d_6 , 500 MHz) δ 10.51 (br. s., 1H), 10.40 (br. s., 1H), 10.08 (br. s., 1H), 9.79 (br. s., 1H), 9.43 (br. s., 1H), 8.64–8.75 (m, $J=5.0$, 2.5 Hz, 1H), 8.11 (d, $J=7.9$ Hz, 1H), 7.97 (d, $J=7.8$ Hz, 2H), 7.71–7.90 (m, 8H), 7.59–7.68 (m, 3H), 7.54 (br. s., 1H), 7.30–7.40 (m, $J=7.6$ Hz, 3H), 7.26 (br. s., 1H), 6.84 (d, $J=7.6$ Hz, 2H), 4.85–4.97 (m, 1H), 2.11 (br. s., 3H). HRMS (ESI): m/z calculated for $\text{C}_{43}\text{H}_{36}\text{N}_8\text{O}_{10}$ $[\text{M}+\text{H}]^+$ 825.2627, found 825.2608 ($\Delta m = -2.3$ ppm).

Final Derivative 40



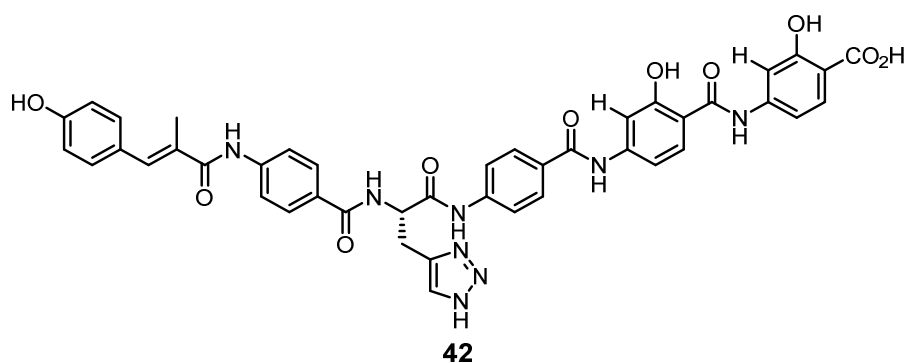
Synthetic protocol according to GP8. The title compound **40** (30 mg, 36 μmol , 23% over two steps) was obtained as a colourless solid. ^1H NMR (DMSO- d_6 , 400 MHz) δ 11.84 (s, 1H), 11.05 (s, 1H), 10.50 (s, 1H), 10.36 (s, 1H), 10.08 (s, 1H), 9.77 (s, 1H), 8.69 (d, $J=7.5$ Hz, 1H), 8.60 (d, $J=8.3$ Hz, 1H), 7.93–8.02 (m, 3H), 7.72–7.92 (m, 8H), 7.64–7.72 (m, 1H), 7.59–7.64 (m, 1H), 7.56 (d, $J=1.8$ Hz, 1H), 7.31–7.39 (m, 3H), 7.26 (s, 1H), 6.84 (d, $J=8.8$ Hz, 2H), 3.97 (s, 3H), 2.08–2.14 (m, $J=1.3$ Hz, 3H). HRMS (ESI): m/z calculated for $\text{C}_{44}\text{H}_{38}\text{N}_8\text{O}_{10}$ $[\text{M}+\text{H}]^+$ 839.2784, found 839.2783 ($\Delta m = -0.1$ ppm).

Final Derivative 41

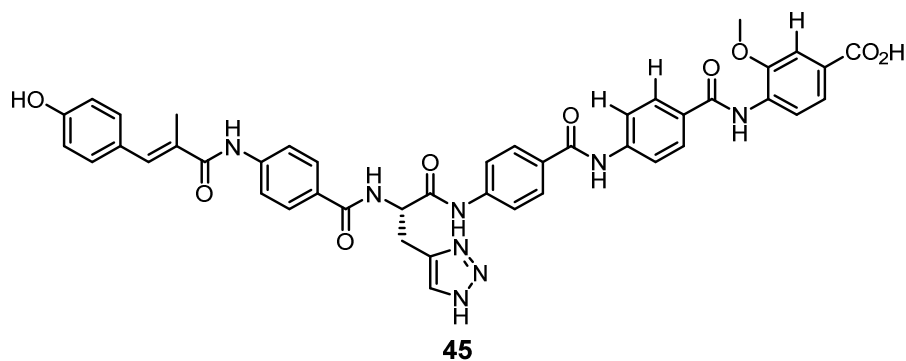


Synthetic protocol according to GP8. The title compound **41** (4.0 mg, 4.8 μmol , 2% over two steps) was obtained as a colourless solid. ^1H NMR (DMSO- d_6 , 500 MHz) δ 10.51 (s, 1H), 10.40 (s, 1H), 10.08 (s, 1H), 9.79 (br. s., 1H), 9.43 (s, 1H), 8.66–8.73 (m, $J=8.2$ Hz, 1H), 8.11 (d, $J=8.1$ Hz, 1H), 7.97 (d, $J=8.7$ Hz, 2H), 7.74–7.91 (m, 6H), 7.60–7.66 (m, 2H), 7.52–7.56 (m, 1H), 7.30–7.38 (m, $J=8.7$ Hz, 3H), 7.26 (s, 1H), 6.84 (d, $J=8.7$ Hz, 2H), 4.85–4.98 (m, 1H), 3.97 (s, 3H), 2.11 (d, $J=1.1$ Hz, 3H). HRMS (ESI): m/z calculated for $\text{C}_{44}\text{H}_{38}\text{N}_8\text{O}_{10}$ $[\text{M}+\text{H}]^+$ 839.2784, found 839.2796 (+1.4 ppm).

Final Derivative 42

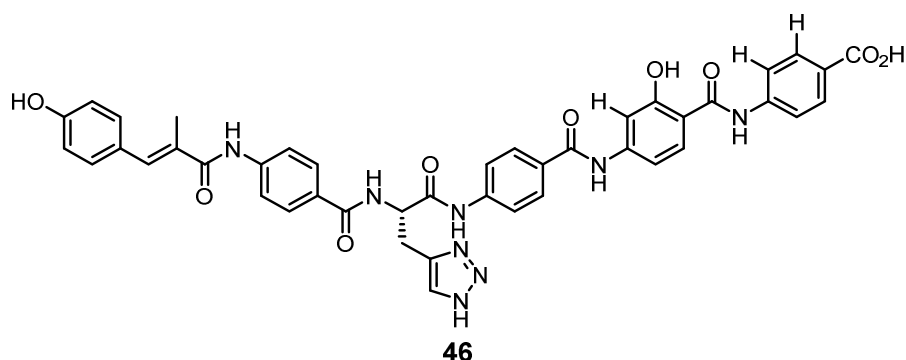


Synthetic protocol according to GP8. The title compound **42** (25 mg, 27 μmol , 22% over two steps) was obtained as a colourless solid. ^1H NMR (DMSO- d_6 , 500 MHz) δ 10.44 (s, 1H), 10.00 (s, 1H), 9.69 (s, 1H), 9.46 (s, 1H), 9.36 (s, 1H), 8.56–8.66 (m, $J=8.1$ Hz, 1H), 8.04 (d, $J=8.2$ Hz, 1H), 7.97 (d, $J=8.2$ Hz, 1H), 7.90 (d, $J=8.9$ Hz, 2H), 7.77–7.82 (m, 2H), 7.73 (dd, $J=14.3, 8.8$ Hz, 4H), 7.50–7.61 (m, $J=1.7$ Hz, 5H), 7.28 (d, $J=8.7$ Hz, 2H), 7.20 (s, 1H), 6.77 (d, $J=8.7$ Hz, 2H), 4.80–4.89 (m, 1H), 3.90 (s, 3H), 3.87 (s, 3H), 3.13–3.22 (m, 2H), 2.05 (d, $J=1.2$ Hz, 3H). HRMS (ESI): m/z calculated for $\text{C}_{45}\text{H}_{40}\text{N}_8\text{O}_{10}$ $[\text{M}+\text{H}]^+$ 853.2940, found 853.2949 ($\Delta m = +1.1$ ppm).



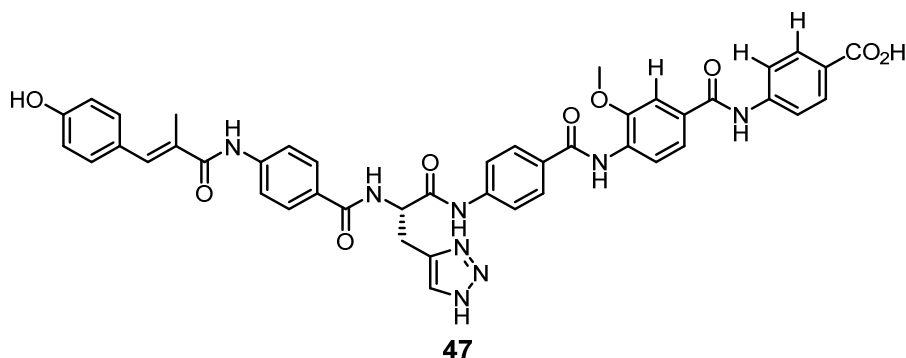
Synthetic protocol according to GP8. The title compound **45** (10 mg, 12 μmol , 18% over two steps) was obtained as a colourless solid. ^1H NMR (DMSO- d_6 , 400 MHz) δ 12.50–12.99 (m, 1H), 10.53 (br. s., 1H), 10.44 (s, 1H), 10.09 (s, 1H), 9.79 (s, 1H), 9.43 (s, 1H), 8.71 (br. s., 2H), 8.08–8.16 (m, $J=8.5$ Hz, 1H), 7.72–8.07 (m, 13H), 7.51–7.72 (m, 3H), 7.35 (d, $J=8.3$ Hz, 2H), 7.26 (s, 1H), 6.84 (d, $J=8.5$ Hz, 2H), 4.86–4.96 (m, 1H), 3.94 (s, 3H), 3.15–3.32 (m, $J=10.3$ Hz, 4H), 2.07–2.16 (m, 3H). HRMS (ESI): m/z calculated for $\text{C}_{44}\text{H}_{38}\text{N}_8\text{O}_9$ $[\text{M}+\text{H}]^+$ 823.2835, found 823.2834 (–1.2 ppm).

Final Derivative 46



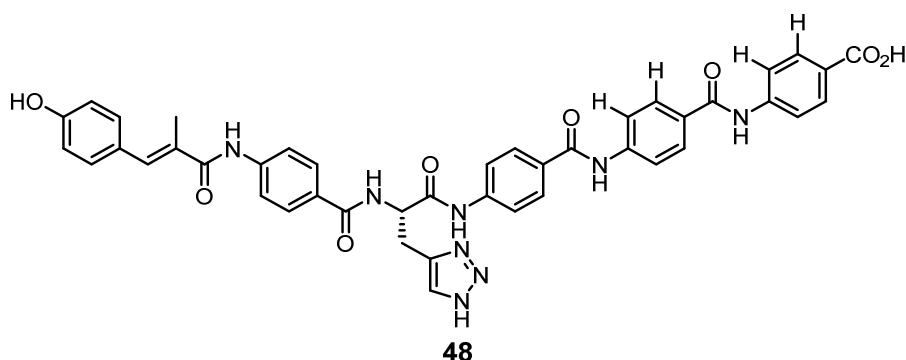
Synthetic protocol according to GP8. The title compound **46** (4.0 mg, 5.0 μmol , 12% over two steps) was obtained as a colourless solid. ^1H NMR (DMSO- d_6 , 700 MHz) δ 11.91 (s, 1H), 10.48–10.54 (m, 1H), 10.34 (s, 1H), 10.08 (s, 1H), 9.77 (s, 1H), 8.66–8.72 (m, $J=7.3$ Hz, 1H), 7.92–8.02 (m, $J=8.8$ Hz, 1H), 7.83–7.91 (m, $J=8.8$ Hz, 1H), 7.81 (d, $J=8.8$ Hz, 1H), 7.78 (d, $J=8.8$ Hz, 1H), 7.66–7.72 (m, $J=1.7$ Hz, 1H), 7.33–7.37 (m, 3H), 7.26 (s, 1H), 6.84 (d, $J=8.5$ Hz, 1H), 4.87–4.94 (m, 1H), 3.21–3.31 (m, 2H), 2.09–2.13 (m, $J=1.1$ Hz, 3H). HRMS (ESI): m/z calculated for $\text{C}_{43}\text{H}_{36}\text{N}_8\text{O}_9$ $[\text{M}+\text{H}]^+$ 809.2678, found 809.2672 ($\Delta m = -0.7$ ppm).

Final Derivative 47



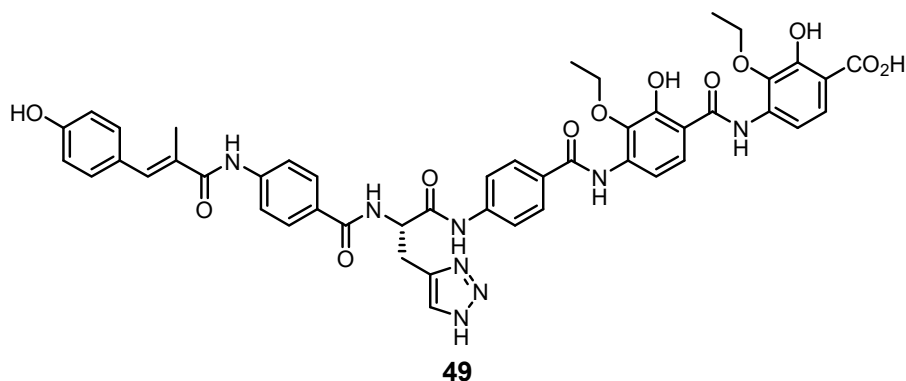
Synthetic protocol according to GP8. The title compound **47** (20 mg, 24 μmol , 9% over two steps) was obtained as a colourless solid. $^1\text{H NMR}$ ($\text{DMSO-}d_6$, 700 MHz) δ 12.73 (br. s., 1H), 10.51 (br. s., 1H), 10.47 (s, 1H), 10.07 (s, 1H), 9.76 (s, 1H), 9.43 (s, 1H), 8.66–8.72 (m, 1H), 8.11 (d, $J=8.1$ Hz, 1H), 7.90–8.00 (m, $J=8.8$ Hz, 6H), 7.85–7.88 (m, 2H), 7.81 (d, $J=8.8$ Hz, 2H), 7.78 (d, $J=8.8$ Hz, 2H), 7.62–7.70 (m, 3H), 7.35 (d, $J=8.5$ Hz, 2H), 7.26 (s, 1H), 6.84 (d, $J=8.8$ Hz, 2H), 4.89–4.94 (m, 1H), 3.98 (s, 3H), 3.20–3.27 (m, 2H), 2.11 (s, 3H). HRMS (ESI): m/z calculated for $\text{C}_{44}\text{H}_{38}\text{N}_8\text{O}_9$ $[\text{M}+\text{H}]^+$ 823.2835, found 823.2849 ($\Delta m = +1.7$ ppm).

Final Derivative 48



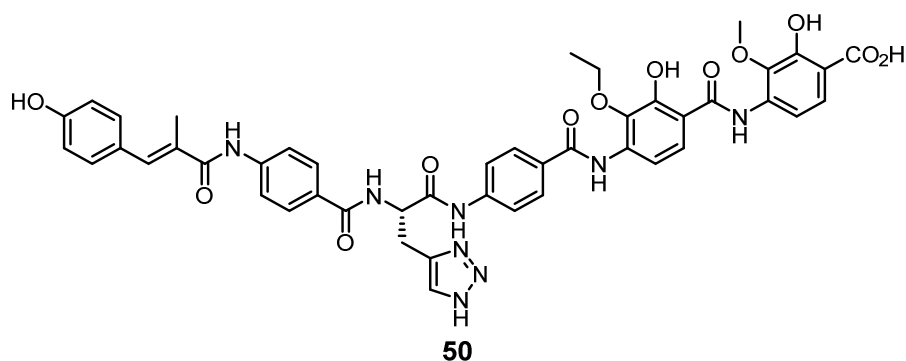
Synthetic protocol according to GP8. The title compound **48** (11 mg, 14 μmol , 12% over two steps) was obtained as a colourless solid. $^1\text{H NMR}$ ($\text{DMSO-}d_6$, 400 MHz) δ 10.63 (s, 1H), 10.44 (s, 1H), 10.42 (s, 1H), 10.10 (s, 1H), 8.80 (d, $J=7.3$ Hz, 1H), 8.24–8.40 (m, 2H), 7.96–8.03 (m, 6H), 7.85–7.95 (m, 7H), 7.77–7.84 (m, 4H), 7.68 (s, 1H), 7.35 (d, $J=8.5$ Hz, 2H), 7.26 (s, 1H), 6.84 (d, $J=8.5$ Hz, 2H), 4.86–4.95 (m, 1H), 3.21–3.36 (m, $J=4.8$ Hz, 2H), 2.11 (d, $J=1.0$ Hz, 3H). HRMS (ESI): m/z calculated for $\text{C}_{45}\text{H}_{41}\text{N}_9\text{O}_{10}$ $[\text{M}+\text{H}]^+$ 793.2729, found 793.2718 ($\Delta m = -1.4$ ppm).

Final Derivative 49



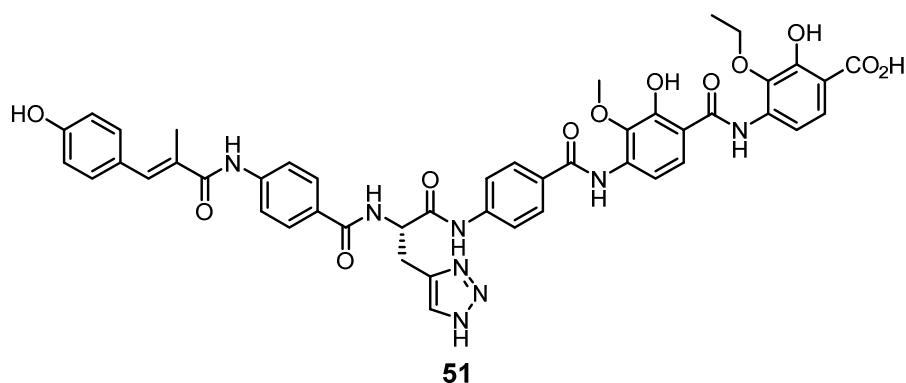
Synthetic protocol according to GP8. The title compound **49** (25 mg, 27 μmol , 25% over two steps) was obtained as a colourless solid. ^1H NMR (DMSO- d_6 , 400 MHz) δ 11.42 (s, 1H), 11.08 (s, 1H), 10.54 (s, 1H), 10.09 (s, 1H), 9.63 (s, 1H), 8.72 (d, $J=7.3$ Hz, 1H), 8.06 (d, $J=9.0$ Hz, 1H), 7.97 (d, $J=8.5$ Hz, 2H), 7.75–7.92 (m, 7H), 7.69 (br. s., 1H), 7.57 (dd, $J=8.4, 7.7$ Hz, 2H), 7.35 (d, $J=8.5$ Hz, 2H), 7.26 (s, 1H), 6.84 (d, $J=8.5$ Hz, 2H), 4.86–4.96 (m, 1H), 4.17 (q, $J=7.0$ Hz, 2H), 4.00 (q, $J=7.0$ Hz, 2H), 3.18–3.37 (m, 2H), 2.11 (s, 3H), 1.37 (t, $J=7.0$ Hz, 3H), 1.32 (t, $J=7.0$ Hz, 3H); HRMS (ESI): m/z calculated for $\text{C}_{47}\text{H}_{44}\text{N}_8\text{O}_{12}$ $[\text{M}+\text{H}]^+$ 913.3152, found 913.3154 ($\Delta m = +0.2$ ppm).

Final Derivative 50



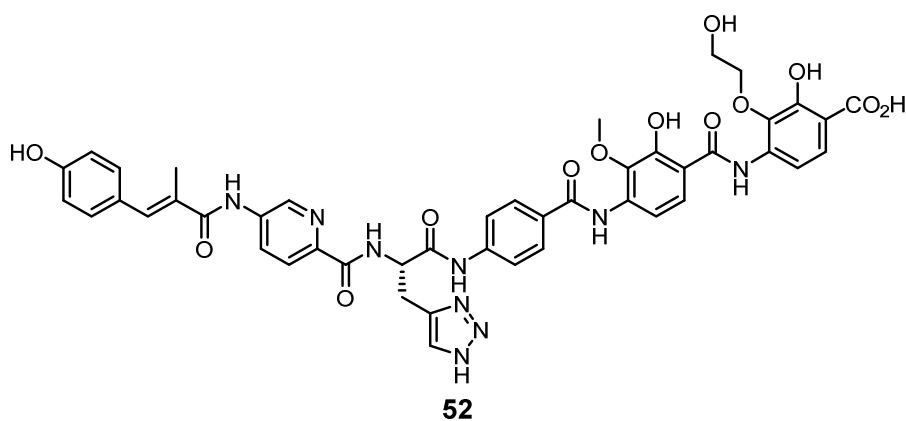
Synthetic protocol according to GP8. The title compound **50** (23 mg, 26 μmol , 21% over two steps) was obtained as a colourless solid. ^1H NMR (DMSO- d_6 , 400 MHz) δ 11.45 (br. s., 1H), 11.17 (s, 1H), 10.54 (s, 1H), 10.10 (s, 1H), 9.64 (s, 1H), 8.72 (d, $J=7.5$ Hz, 1H), 8.05 (d, $J=9.0$ Hz, 1H), 7.98 (d, $J=8.8$ Hz, 2H), 7.75–7.91 (m, 7H), 7.70 (s, 1H), 7.58 (dd, $J=12.5, 8.8$ Hz, 2H), 7.35 (d, $J=8.5$ Hz, 2H), 7.26 (s, 1H), 6.84 (d, $J=8.5$ Hz, 2H), 4.84–4.99 (m, 1H), 3.99 (q, $J=7.0$ Hz, 2H), 3.92 (s, 3H), 3.16–3.39 (m, 2H), 2.11 (s, 3H), 1.32 (t, $J=7.0$ Hz, 3H). HRMS (ESI): m/z calculated for $\text{C}_{46}\text{H}_{42}\text{N}_8\text{O}_{12}$ $[\text{M}+\text{H}]^+$ 899.2995, found 899.2992 ($\Delta m = -0.3$ ppm).

Final Derivative 51



Synthetic protocol according to GP8. The title compound **51** (18 mg, 20 μmol , 20% over two steps) was obtained as a colourless solid. ^1H NMR (DMSO- d_6 , 400 MHz) δ 11.51 (s, 1H), 11.08 (s, 1H), 10.55 (s, 1H), 10.10 (s, 1H), 9.67 (s, 1H), 8.72 (d, $J=7.8$ Hz, 1H), 8.08 (d, $J=8.8$ Hz, 1H), 7.97 (d, $J=8.5$ Hz, 2H), 7.75–7.92 (m, 7H), 7.69 (s, 1H), 7.54–7.63 (m, 2H), 7.31–7.40 (m, $J=8.8$ Hz, 2H), 7.26 (s, 1H), 6.79–6.90 (m, $J=8.5$ Hz, 2H), 4.91 (d, $J=6.8$ Hz, 1H), 4.17 (q, $J=7.1$ Hz, 2H), 3.78 (s, 3H), 3.19–3.36 (m, 2H), 2.11 (s, 3H), 1.39 (t, $J=7.0$ Hz, 3H). HRMS (ESI): m/z calculated for $\text{C}_{46}\text{H}_{42}\text{N}_8\text{O}_{12}$ $[\text{M}+\text{H}]^+$ 899.2995, found 899.2995 ($\Delta m = \pm 0.0$ ppm).

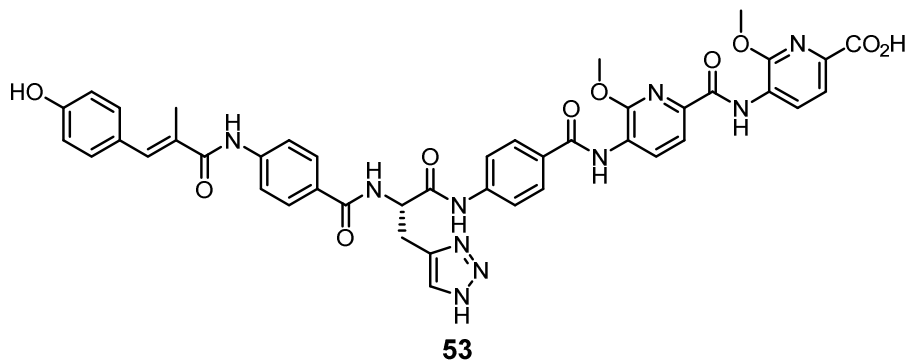
Final Derivative 52



Synthetic protocol according to GP8. The title compound **52** (9.0 mg, 9.8 μmol , 14% over two steps) was obtained as a colourless solid. ^1H NMR (500 MHz, DMSO- d_6) δ 11.75 (s, 1H), 11.64 (s, 1H), 10.64 (s, 1H), 10.56 (s, 1H), 10.35 (s, 1H), 9.80 (s, 1H), 9.60 (s, 1H), 8.98 (d, $J=2.5$ Hz, 1H), 8.83–8.74 (m, 1H), 8.37–8.31 (m, 1H), 8.01 (d, $J=8.6$ Hz, 1H), 7.99–7.93 (m, 3H), 7.81–7.73 (m, 3H), 7.66–7.57 (m, 3H), 7.41–7.35 (m, 2H), 7.35–7.31 (m, 1H), 6.88–6.82 (m, 2H), 4.99 (q, $J=6.8$ Hz, 1H), 4.17 (t, $J=5.2$ Hz, 2H), 3.82 (s, 3H), 3.74 (t, $J=5.2$ Hz, 2H), 3.34 (d, $J=6.5$ Hz, 2H),

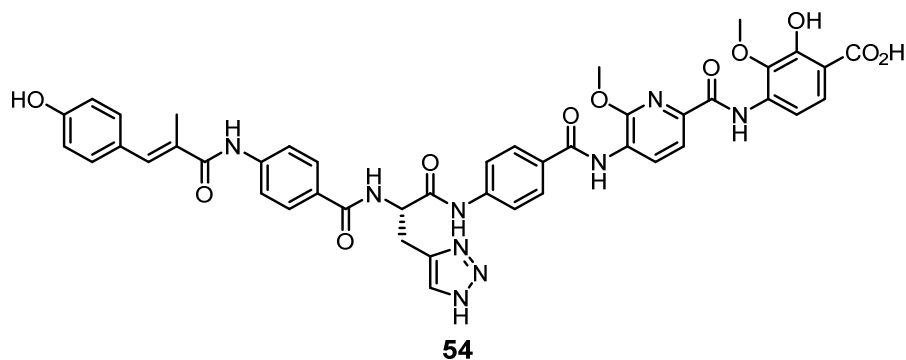
2.14 (d, $J=1.4$ Hz, 3H). HRMS (ESI): m/z calculated for $C_{46}H_{42}N_8O_{13}$ $[M+H]^+$ 916.2897, found 916.2880 ($\Delta m = -1.9$ ppm).

Final Derivative 53



Synthetic protocol according to GP8. The title compound **53** (19 mg, 22 μ mol, 20% over two steps) was obtained as a colourless solid. ^1H NMR (DMSO- d_6 , 400 MHz) δ 10.63 (s, 1H), 10.56 (s, 1H), 10.10 (s, 1H), 9.74 (s, 1H), 8.73 (d, $J=7.0$ Hz, 1H), 8.53 (d, $J=8.0$ Hz, 1H), 8.07 (d, $J=8.8$ Hz, 1H), 7.98 (d, $J=8.8$ Hz, 2H), 7.75–7.92 (m, 7H), 7.61–7.73 (m, 2H), 7.35 (d, $J=8.3$ Hz, 2H), 7.26 (s, 1H), 6.84 (d, $J=8.5$ Hz, 2H), 4.78–5.03 (m, 1H), 4.15 (s, 3H), 3.98 (s, 3H), 3.19–3.38 (m, 2H), 2.11 (s, 3H). HRMS (ESI): m/z calculated for $C_{44}H_{39}N_9O_{11}$ $[M+H]^+$ 870.2842, found 870.2883 ($\Delta m = +4.7$ ppm).

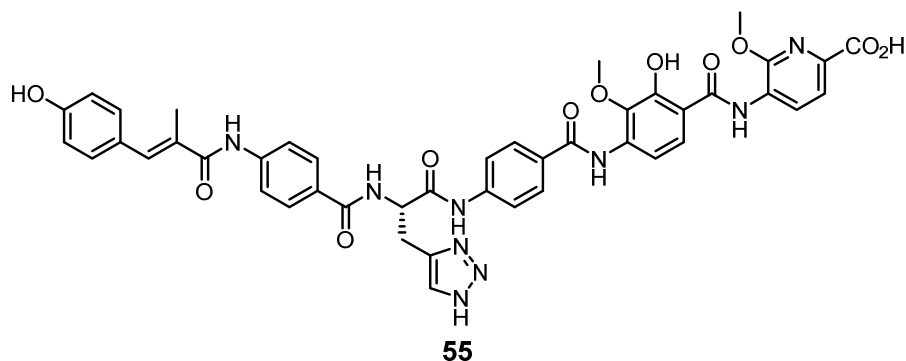
Final Derivative 54



Synthetic protocol according to GP8. The title compound **54** (4.0 mg, 46 μ mol, 4% over two steps) was obtained as a colourless solid. ^1H NMR (DMSO- d_6 , 500 MHz) δ 11.59–11.62 (m, 1H), 11.02 (s, 1H), 10.50 (br. s., 1H), 10.07 (s, 1H), 9.75 (s, 1H), 9.65 (s, 1H), 8.78 (d, $J=8.1$ Hz, 1H), 8.66–8.72 (m, $J=7.2$ Hz, 1H), 7.97 (d, $J=8.9$ Hz, 2H), 7.84–7.89 (m, 2H), 7.75–7.84 (m, 6H), 7.64 (br. s., 1H), 7.60 (d, $J=8.9$ Hz, 1H), 7.35 (d, $J=8.7$ Hz, 2H), 7.26 (s, 1H), 6.84 (d, $J=8.7$ Hz, 2H),

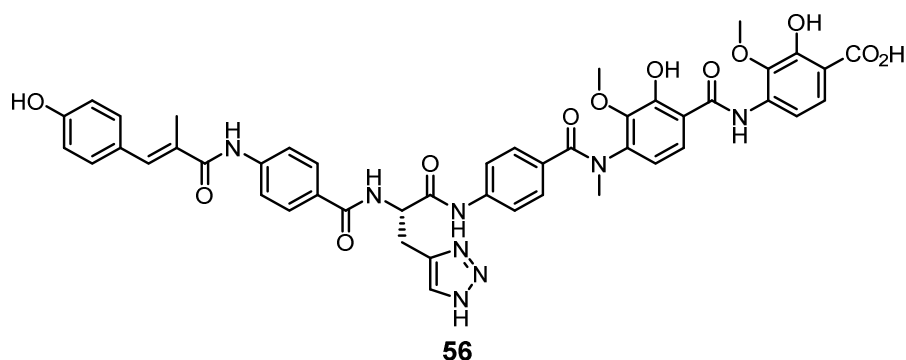
4.87–4.96 (m, 1H), 4.07 (s, 3H), 3.78 (s, 3H), 3.21–3.29 (m, 2H), 2.11 (d, $J=1.2$ Hz, 3H). HRMS (ESI): m/z calculated for $C_{44}H_{39}N_9O_{11}$ $[M+H]^+$ 868.2696, found 868.2673 ($\Delta m = -2.6$ ppm).

Final Derivative 55



Synthetic protocol according to GP8. The title compound **55** (14 mg, 16 μ mol, 13% over two steps) was obtained as a colourless solid. 1H NMR (DMSO- d_6 , 400 MHz) δ 10.55 (br. s., 1H), 10.44 (s, 1H), 10.09 (s, 1H), 9.79 (s, 1H), 9.71 (s, 1H), 8.66–8.82 (m, 2H), 8.54 (d, $J=7.8$ Hz, 1H), 7.98 (d, $J=8.8$ Hz, 2H), 7.75–7.92 (m, 8H), 7.65 (br. s., 1H), 7.35 (d, $J=8.5$ Hz, 2H), 7.26 (s, 1H), 6.84 (d, $J=8.5$ Hz, 2H), 4.83–5.00 (m, $J=5.8$ Hz, 1H), 4.15 (s, 3H), 4.09 (s, 3H), 3.18–3.30 (m, $J=9.5$ Hz, 2H), 2.11 (s, 3H). HRMS (ESI): m/z calculated for $C_{43}H_{38}N_{10}O_{10}$ $[M+H]^+$ 855.2845, found 855.2888 ($\Delta m = +5.0$ ppm).

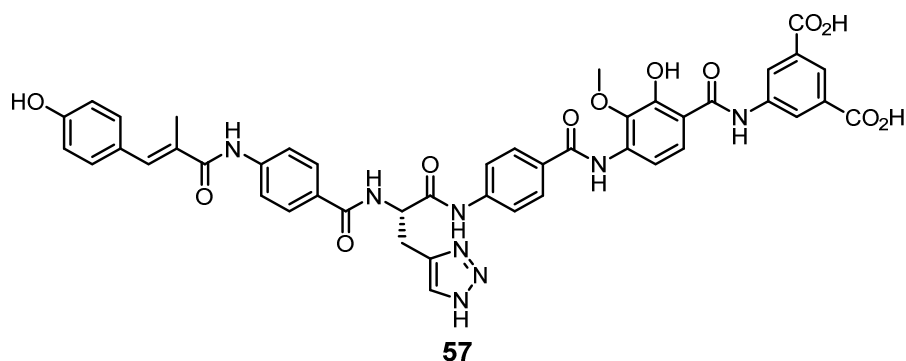
Final Derivative 56



Synthetic protocol according to GP8. The title compound **56** (8.0 mg, 89.0 μ mol, 11% over two steps) was obtained as a colourless solid. 1H NMR (DMSO- d_6 , 700 MHz) δ 11.56 (br. s., 1H), 11.48 (s, 1H), 11.12 (s, 1H), 10.27 (s, 1H), 10.05 (s, 1H), 9.70–9.84 (m, 1H), 8.61 (d, $J=7.5$ Hz, 1H), 8.02 (d, $J=8.8$ Hz, 1H), 7.73–7.85 (m, 5H), 7.64 (br. s., 1H), 7.57 (d, $J=8.8$ Hz, 1H), 7.47 (d, $J=8.5$ Hz, 2H), 7.29–7.38 (m, 4H), 7.25 (s, 1H), 7.04 (d, $J=8.8$ Hz, 1H), 6.84 (d, $J=8.5$ Hz, 2H),

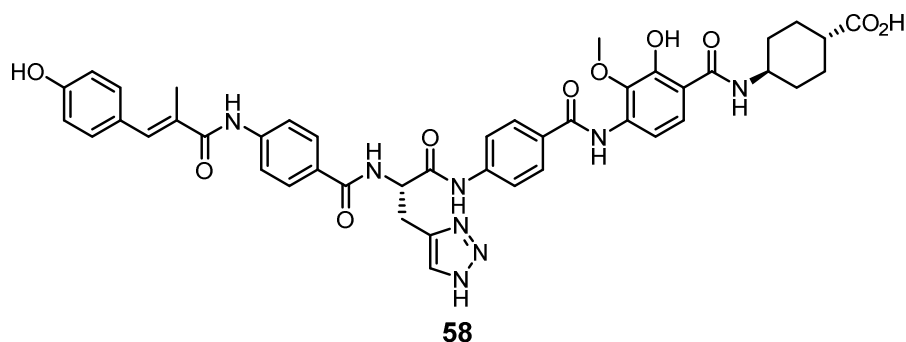
4.77–4.85 (m, 1H), 3.85 (s, 3H), 3.69 (s, 3H), 3.36 (s, 3H), 3.13–3.26 (m, 2H), 2.10 (s, 3H). HRMS (ESI): m/z calculated for $C_{46}H_{42}N_8O_{12}$ $[M+H]^+$ 899.2998, found 899.3000 ($\Delta m = +0.2$ ppm).

Final Derivative 57



Synthetic protocol according to GP8. The title compound **57** (12 mg, 14 μ mol, 11% over two steps) was obtained as a colourless solid. 1H NMR (400 MHz, $DMSO-d_6$) δ 12.25 (s, 1H), 10.69 (s, 1H), 10.54 (s, 1H), 10.09 (s, 1H), 9.80 (s, 1H), 9.55 (s, 1H), 8.72 (d, $J=7.6$ Hz, 1H), 8.60 (d, $J=1.5$ Hz, 2H), 8.26 (t, $J=1.6$ Hz, 1H), 7.96 (d, $J=8.6$ Hz, 2H), 7.91–7.75 (m, 7H), 7.67 (t, $J=7.9$ Hz, 2H), 7.38–7.32 (m, 2H), 7.26 (d, $J=1.7$ Hz, 1H), 6.88–6.80 (m, 2H), 4.96–4.87 (m, 1H), 3.87 (s, 3H), 3.35–3.19 (m, 2H), 2.11 (d, $J=1.4$ Hz, 3H). HRMS (ESI): m/z calculated for $C_{45}H_{38}N_8O_{12}$ $[M+H]^+$ 883.2682, found 883.2660 ($\Delta m = -2.5$ ppm).

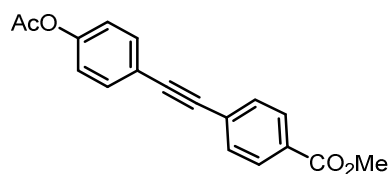
Final Derivative 58



1H NMR (500 MHz, $DMSO-d_6$) δ 13.38 (s, 1H), 10.54 (s, 1H), 10.08 (s, 1H), 9.78 (s, 1H), 9.42 (s, 1H), 8.70 (d, $J=7.6$ Hz, 1H), 8.59 (d, $J=7.8$ Hz, 1H), 7.93 (d, $J=8.7$ Hz, 2H), 7.87 (d, $J=8.7$ Hz, 2H), 7.84–7.76 (m, 4H), 7.67 (d, $J=8.6$ Hz, 2H), 7.55 (d, $J=8.8$ Hz, 1H), 7.38–7.32 (m, 2H), 7.26 (s, 1H), 6.87–6.82 (m, 2H), 4.95–4.87 (m, 1H), 3.85 (s, 3H), 3.34–3.20 (m, 2H), 2.18 (t, $J=7.6$ Hz, 1H), 2.11 (s, 3H), 2.00–1.87 (m, 4H), 1.49–1.36 (m, 4H), 1.25–1.21 (m, 1H). HRMS (ESI): m/z calculated for $C_{44}H_{44}N_8O_{10}$ $[M+H]^+$ 845.3253, found 845.3253 ($\Delta m = -0.1$ ppm).

5.2.3 Derivatives with Variations of the N-terminal A-B Building Blocks

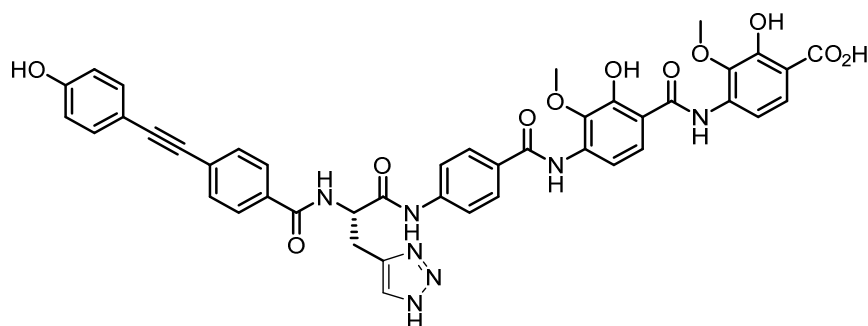
Methyl 4-((4-acetoxyphenyl)ethynyl)benzoate (**261**)



To a solution of methyl 4-iodobenzoate (245 mg, 1.53 mmol, 1.00 eq.) in Et₃N (15 mL) were added Pd(PPh₃)₂Cl₂ (10.7 mg, 15.3 μmol, 0.01 eq.) and CuI (2.91 mg, 15.3 μg, 0.01 eq.) at r.t. A solution of 4-ethynylphenyl acetate (**260**) (481 mg, 1.84 mmol, 1.20 eq.) in Et₃N (3 mL) was added dropwise to the first solution and the reaction mixture was stirred at r.t. for 16 h. The solution was diluted with toluene (30 mL) and washed with 10% HCl_(aq.) (3×) followed by brine. The organic phase was dried over anhydrous Na₂SO₄ and concentrated under reduced pressure. Purification of the crude product by column chromatography on silica gel (*n*-hexane/EtOAc, 7:1–5:1) afforded the desired product **261** (308 mg, 1.05 mmol, 69%) as an off-white solid.

¹H NMR (500 MHz, CDCl₃) δ 8.05–7.97 (m, 2H), 7.61–7.51 (m, 4H), 7.14–7.07 (m, 2H), 3.93 (s, 3H), 2.31 (s, 3H). ¹³C NMR (126 MHz, CDCl₃) δ 169.2, 166.7, 151.0, 133.1, 131.6, 129.7, 129.7, 128.0, 122.0, 120.5, 91.6, 88.8, 52.4, 21.3. HRMS (ESI): *m/z* calculated for C₁₈H₁₄O₄ [M+H]⁺ 295.0965, found 295.0962 (Δ*m* = -1.0 ppm).

Final Albicidin Derivative **247**

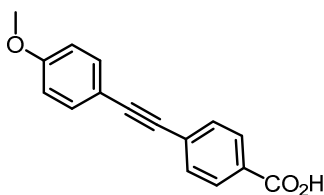


HATU (53 mg, 140 μmol, 1.5 eq.) was added to a solution of biaryl alkyne **262** (29 mg, 121 μmol, 1.3 eq.) in anhydrous DMF (3 mL) and the resulting solution was stirred at r.t for 15 min. A solution of tetrapeptide **284** (70 mg, 93 μmol, 1.0 eq.) and DIPEA (0.12 mL) in anhydrous DMF (1 mL) was added dropwise and the reaction mixture was stirred at r.t for 16 h. All volatiles were removed *in vacuo* and the residue was taken up in a mixture of THF (1
186

mL) and MeOH (1 mL), and 3 N KOH_(aq.) (1 mL) was added dropwise. After 30 min of stirring, 3 N HCl_(aq.) (1.1 mL) was added and the resulting suspension was evaporated under reduced pressure. The crude material was dissolved in DMSO, centrifuged, and the supernatant purified by HPLC (PLRP-S column, CH₃CN in H₂O). The title compound **247** (12 mg, 16% over two steps) was obtained as a colourless solid.

¹H NMR (500 MHz, DMSO-*d*₆) δ 11.52 (s, 1H), 11.17 (s, 1H), 10.52 (s, 1H), 9.99 (s, 1H), 9.66 (s, 1H), 8.92 (d, *J*=7.3 Hz, 1H), 8.06 (d, *J*=8.9 Hz, 1H), 7.98 (d, *J*=8.7 Hz, 2H), 7.91 (d, *J*=8.4 Hz, 2H), 7.75–7.84 (m, 3H), 7.56–7.64 (m, 4H), 7.41 (d, *J*=8.5 Hz, 2H), 6.82 (d, *J*=8.7 Hz, 2H), 4.89–4.99 (m, *J*=6.3 Hz, 1H), 3.92 (s, 3H), 3.79 (s, 3H), 3.21–3.41 (m, 2H). ¹³C NMR (126 MHz, DMSO-*d*₆) δ 133.7 (Ar), 131.4 (Ar), 129.1 (Ar), 128.3 (Ar), 126.1 (Ar), 119.2 (Ar), 116.3 (Ar), 115.3 (Ar), 110.7 (Ar), 60.6 (OMe), 61.0 (OMe), 54.8 (α-C), 29.4 (β-C). HRMS (ESI): *m/z* calculated for C₄₃H₃₅N₇O₁₁ [M+H]⁺ 826.2467, found 826.2454 (Δ*m* = -1.6 ppm), *t*_R = 8.38 min.

4-((4-Methoxyphenyl)ethynyl)benzoic acid (**266**)

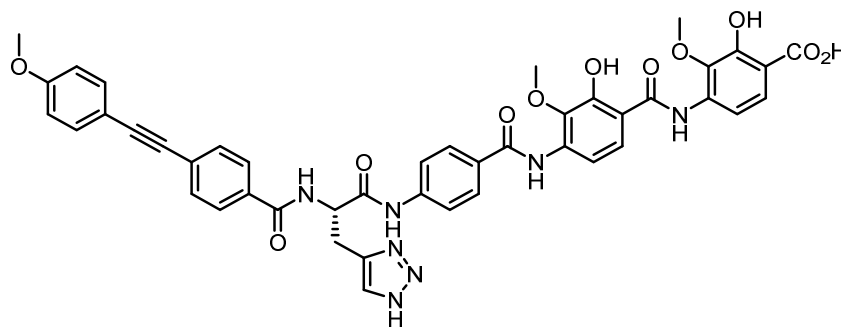


1-Ethynyl-4-methoxybenzene (**265**) (1.00 g, 7.56 mmol, 1.10 eq.) and methyl 4-iodobenzoate (1.80 g, 6.87 mmol, 1.00 eq.) were dissolved in dry THF (10 mL) and Pd(PPh₃)Cl₂ (0.241 g, 0.344 mmol, 0.050 eq.), CuI (0.078 g, 0.412 mmol, 0.060 eq.), and pyridine (1.5 mL) were successively added at 0 °C. After stirring for 2 h at r.t., the reaction mixture was diluted with toluene (30 mL), washed with 1 N HCl_(aq.) and H₂O (2×), dried over anhydrous MgSO₄, and concentrated *in vacuo*. The crude product was purified by trituration with MeOH and subsequent filtration through a pad of celite to afford methyl 4-((4-methoxyphenyl)ethynyl)benzoate (1.45 g, 5.43 mmol, 79%) as a brown solid. 4-((4-methoxyphenyl)ethynyl)benzoate (1.40 g, 5.26 mmol, 1.00 eq.) was then dissolved in a mixture of THF (15 mL) and MeOH (15 mL) and 3 N KOH_(aq.) (15 mL) was added dropwise. The reaction mixture was stirred at r.t. for 3 h before the organic solvents were removed *in vacuo*, the aq. residue was diluted with H₂O and acidified to pH ≈ 2 by the addition of 10% HCl_(aq.). The solution was extracted with EtOAc (3×) and the combined organic phases were dried over anhydrous MgSO₄ and concentrated under reduced pressure to obtain the analytically pure

title compound **266** (1.32 g, 5.26 mmol, quant.) as a brown solid.

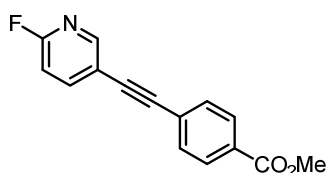
^1H NMR (400 MHz, $\text{DMSO-}d_6$) δ 13.12 (s, 1H), 7.99–7.91 (m, 2H), 7.67–7.59 (m, 2H), 7.57–7.49 (m, 2H), 7.05–6.96 (m, 2H), 3.80 (s, 3H). ^{13}C NMR (101 MHz, $\text{DMSO-}d_6$) δ 166.7, 159.9, 133.2, 131.3, 130.2, 129.6, 127.1, 114.5, 113.7, 92.4, 87.4, 55.3, 40.2, 40.2, 39.9, 39.7, 39.5, 39.3, 39.1, 38.9. HRMS (ESI): m/z calculated for $\text{C}_{16}\text{H}_{12}\text{O}_3$ $[\text{M}+\text{H}]^+$ 253.0859, found 253.0859 ($\Delta m = \pm 0.0$ ppm).

Final Derivative 248



Synthetic protocol analogous to compound **247**. The title compound **248** (4 mg, 9% over two steps) was obtained as a colorless solid. ^1H NMR (400 MHz, $\text{DMSO-}d_6$) δ 11.54 (s, 1H), 11.19 (s, 1H), 10.55 (s, 1H), 9.69 (s, 1H), 8.95 (d, $J=7.8$ Hz, 1H), 8.06 (d, $J=9.0$ Hz, 1H), 7.97 (d, $J=8.8$ Hz, 2H), 7.92 (d, $J=8.5$ Hz, 2H), 7.75–7.84 (m, 3H), 7.63 (d, $J=8.5$ Hz, 2H), 7.56–7.61 (m, 2H), 7.51–7.56 (m, 2H), 6.98–7.04 (m, 2H), 4.88–4.97 (m, 1H), 3.91 (s, 3H), 3.80 (s, 3H), 3.78 (s, 3H), 3.19–3.35 (m, $J=5.5$ Hz, 2H). ^{13}C NMR (101 MHz, $\text{DMSO-}d_6$) δ 133.4 (Ar), 131.4 (Ar), 129.0 (Ar), 128.1 (Ar), 128.1 (Ar), 125.8 (Ar), 125.6 (Ar), 119.1 (Ar), 115.2 (Ar), 114.9 (Ar), 110.8 (Ar), 60.8 (OMe), 60.8 (OMe), 55.7 (OMe), 54.5 (α -C), 27.6 (β -C). HRMS (ESI): m/z calculated for $\text{C}_{44}\text{H}_{37}\text{N}_7\text{O}_{11}$ $[\text{M}+\text{H}]^+$ 840.2624, found 840.2626 ($\Delta m = +0.2$ ppm), $t_R = 9.38$ min.

Methyl 4-((6-fluoropyridin-3-yl)ethynyl)benzoate (269)

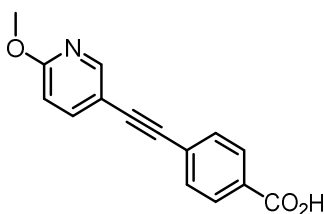


To a solution of 2-fluoro-5-iodopyridine (**267**) (500 mg, 2.24 mmol, 1.00 eq.) in dry THF (10 mL) were successively added Et_3N (5 mL), $\text{Pd}(\text{PPh}_3)_2\text{Cl}_2$ (15.7 mg, 22.4 μmol , 0.01 eq.), CuI (4.27 mg, 22.4 μg , 0.01 eq.) and methyl 4-ethynylbenzoate (**268**) (431 mg, 2.69 mmol,

1.20 eq.). The reaction mixture was stirred at r.t. for 16 h, then diluted with toluene (30 mL) and washed with 10% HCl_(aq.) (3×) followed by brine. The organic phase was dried over anhydrous Na₂SO₄ and concentrated under reduced pressure. Purification of the crude product by column chromatography on silica gel (*n*-hexane/EtOAc, 12:1–8:1) afforded the desired product **269** (561 mg, 2.20 mmol, 98%) as a yellow solid.

¹H NMR (500 MHz, CDCl₃) δ 8.41–8.39 (m, 1H), 8.05–8.02 (m, 2H), 7.93–7.88 (m, 1H), 7.60–7.56 (m, 2H), 6.97–6.93 (m, 1H), 3.92 (d, *J*=3.0 Hz, 3H). HRMS (ESI): *m/z* calculated for C₁₅H₁₀FNO₂ [M+H]⁺ 256.0768, found 256.0767 (Δ*m* = -0.4 ppm).

4-((6-Methoxypyridin-3-yl)ethynyl)benzoic acid (**270**)

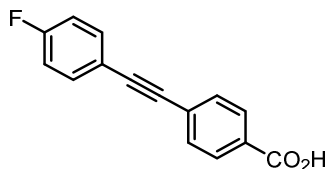


To a solution of fluoropyridine **269** (500 mg, 1.96 mmol, 1.00 eq.) in a mixture of MeOH (25 mL) and THF (25 mL) was added 3 N KOH_(aq.) (25 mL) and the reaction mixture was stirred at r.t. for 16 h. The solution was then acidified to pH ≈ 2 by the addition of 1 N HCl_(aq.) and the organic solvent evaporated under reduced pressure. The aq. residue was diluted with H₂O and extracted with CHCl₃ (3×). The combined organic phases were dried over anhydrous Na₂SO₄ and concentrated *in vacuo* to give the pure benzoic acid **270** (470 mg, 1.96 mmol, quant.) as a colourless solid.

¹H NMR (400 MHz, DMSO-*d*₆) δ 12.29 (br. s, 1H), 8.46–8.40 (m, 1H), 7.98 (d, *J*=8.0 Hz, 2H), 7.90 (dd, *J*=8.6, 2.4 Hz, 1H), 7.63 (d, *J*=8.0 Hz, 2H), 6.90 (dd, *J*=8.6, 0.8 Hz, 1H), 3.89 (s, 3H). ¹³C NMR (101 MHz, DMSO-*d*₆) δ 163.2, 150.1, 141.6, 131.2, 129.6, 112.0, 110.9, 90.1, 88.8, 53.6, 21.1. HRMS (ESI): *m/z* calculated for C₁₅H₁₁NO₃ [M-H]⁻ 252.0666, found 252.0669 (Δ*m* = +1.2 ppm).

129.7, 129.7, 128.0, 119.0, 119.0, 116.0, 115.8, 91.4, 88.5, 52.4. HRMS (ESI): m/z calculated for $C_{16}H_{11}FO_2$ $[M+H]^+$ 255.0816, found 255.0815 ($\Delta m = -0.4$ ppm).

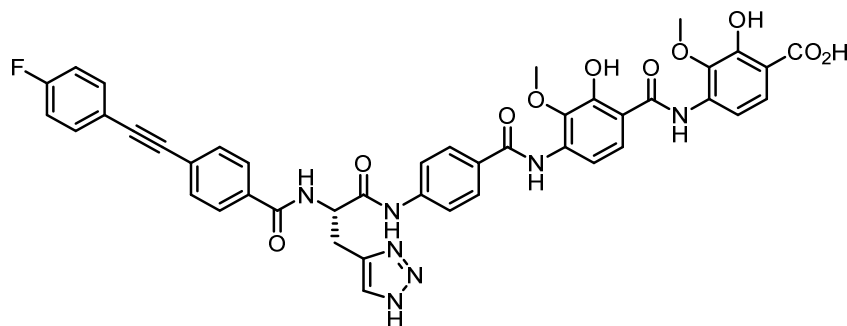
4-((4-Fluorophenyl)ethynyl)benzoic acid (**273**)



The diaryl alkyne **272** (250 mg, 980 μ mol, 1.00 eq.) was dissolved in a mixture of THF (30 mL) and MeOH (30 mL) and 3 N $KOH_{(aq)}$ (15 mL) was added dropwise at r.t. After stirring the reaction mixture for 16 h at r.t., the solution was acidified to $pH \approx 2$ by the addition of 1 N $HCl_{(aq)}$ before evaporating the organic solvents under reduced pressure. The aq. residue was diluted with H_2O and extracted with EtOAc (3 \times). The combined organic phases were dried over anhydrous Na_2SO_4 and concentrated under reduced pressure. Drying of the crude product under high vacuum yielded the analytically pure title compound **273** (224 mg, 934 μ mol, 95%) as a colourless solid.

1H NMR (400 MHz, $DMSO-d_6$) δ 13.11 (s, 1H), 8.01–7.93 (m, 2H), 7.70–7.61 (m, 4H), 7.35–7.25 (m, 2H). ^{13}C NMR (101 MHz, $DMSO-d_6$) δ 166.7, 163.6, 161.1, 134.0, 134.0, 131.5, 130.6, 129.6, 126.5, 118.3, 118.3, 116.3, 116.1, 91.0, 88.4. HRMS (ESI): m/z calculated for $C_{15}H_9FO_2$ $[M-H]^-$ 239.0514, found 239.0512 ($\Delta m = -0.8$ ppm).

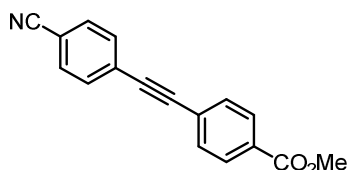
Final Derivative **250**



Synthetic protocol analogous to compound **247**. The title compound **250** (25 mg, 32% over two steps) was obtained as a colourless solid. 1H NMR (400 MHz, $DMSO-d_6$) δ 11.55 (s, 1H), 11.19 (s, 1H), 10.56 (s, 1H), 9.69 (s, 1H), 8.98 (d, $J=7.5$ Hz, 1H), 8.06 (d, $J=9.0$ Hz, 1H), 7.96 (dd, $J=8.5, 15.6$ Hz, 4H), 7.76–7.85 (m, 3H), 7.63–7.73 (m, 5H), 7.59 (dd, $J=5.4, 8.9$ Hz, 2H), 7.30 (t,

$J=8.9$ Hz, 2H), 4.88–4.99 (m, 1H), 3.92 (s, 3H), 3.78 (s, 3H), 3.19–3.37 (m, 2H). ^{13}C NMR (101 MHz, $\text{DMSO-}d_6$) δ 134.2 (Ar), 132.7 (Ar), 129.4 (Ar), 128.1 (Ar), 126.1 (Ar), 125.8 (Ar), 119.1 (Ar), 116.5 (Ar), 115.3 (Ar), 110.6 (Ar), 60.8 (OMe), 60.6 (OMe), 54.7 (α -C), 27.6 (β -C). HRMS (ESI): m/z calculated for $\text{C}_{43}\text{H}_{34}\text{FN}_7\text{O}_{10}$ $[\text{M}+\text{H}]^+$ 828.2424, found 828.2427 ($\Delta m = +0.4$ ppm) $t_{\text{R}} = 9.04$ min.

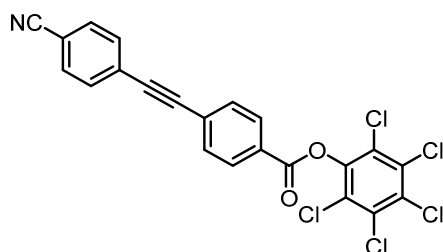
Methyl 4-((4-isocyanophenyl)ethynyl)benzoate (**275**)



To a solution of 1-iodo-4-isocyanobenzene (**274**) (1.20 g, 5.24 mmol, 1.00 eq.) in Et_3N (10 mL) were added $\text{Pd}(\text{PPh}_3)_4$ (60.5 mg, 52.4 μmol , 0.01 eq.), CuI (9.98 mg, 52.4 μmol , 0.01 eq.), and methyl 4-ethynylbenzoate (**268**) (1.01 mg, 6.29 mmol, 1.20 eq.). The reaction mixture was stirred at r.t. for 16 h, then diluted with toluene (30 mL) and washed with 10% $\text{HCl}_{(\text{aq.})}$ (3 \times) followed by brine. The organic phase was dried over anhydrous Na_2SO_4 and concentrated under reduced pressure. The crude product was purified by column chromatography on silica gel (n -hexane/ EtOAc , 6:1–3:1) to obtain the title compound **275** (1.52 g, 4.77 mmol, 91%) as a beige-coloured solid.

^1H NMR (500 MHz, CDCl_3) δ 8.07–8.02 (m, 2H), 7.68–7.63 (m, 2H), 7.63–7.56 (m, 4H), 3.93 (s, 3H). ^{13}C NMR (126 MHz, CDCl_3) δ 166.5, 132.3, 132.2, 131.8, 130.4, 129.8, 127.7, 126.9, 118.5, 112.2, 92.8, 90.4, 52.4. HRMS (ESI): m/z calculated for $\text{C}_{17}\text{H}_{11}\text{NO}_2$ $[\text{M}+\text{H}]^+$ 262.0863, found 262.0861 ($\Delta m = -0.8$ ppm).

Perchlorophenyl 4-((4-isocyanophenyl)ethynyl)benzoate (**276**)

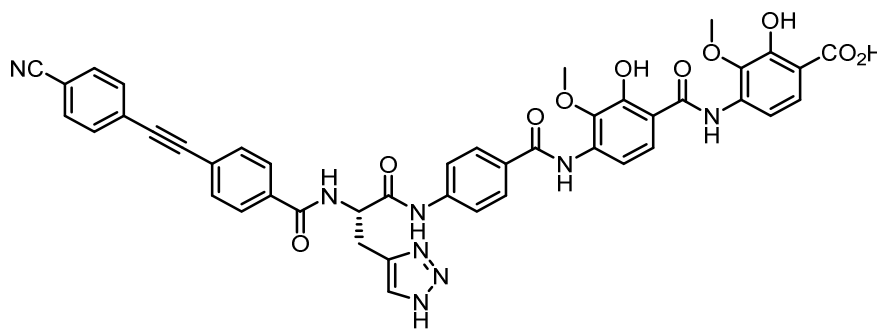


The methyl ester **275** (990 mg, 3.79 mmol, 1.00 eq.) was dissolved in a mixture of dry THF (30 mL) and MeOH (30 mL) and 3 N $\text{KOH}_{(\text{aq.})}$ (15 mL) was added dropwise at 0 °C. After stirring the reaction mixture for 2 h at 0 °C, the solution was acidified to $\text{pH} \approx 2$ by the addition of 1 N

HCl_(aq.) before evaporating the organic solvents under reduced pressure. The aq. residue was diluted with H₂O and extracted with EtOAc (3×). The combined organic phases were dried over anhydrous Na₂SO₄ and concentrated under reduced pressure. The crude product (210 mg) was used in the following step without further purification after confirming its formation by mass spectrometry. HRMS (ESI): *m/z* calculated for C₁₆H₉NO₂ [M-H]⁻ 246.0561, found 246.0556 ($\Delta m = -2.0$ ppm). 4-((4-Isocyanophenyl)ethynyl)benzoic acid (200 mg, 0.809 mmol, 1.00 eq.), pentachlorophenol (259 mg, 0.971 mmol, 1.20 eq.) DCC (217 mg, 1.05 mmol, 1.30 eq.) and DMAP (9.88 mg, 80.9 μ mol, 0.100 eq.) were dissolved in DMF (8 mL) and the reaction mixture was stirred at r.t. for 16 h. After removing DMF *in vacuo*, the residue was taken up CH₂Cl₂ and washed with 10% HCl_(aq.) (3×) followed by brine. The organic phase was dried over anhydrous Na₂SO₄ and concentrated under reduced pressure to obtain the crude product, which was purified by column chromatography on silica gel (*n*-hexane/EtOAc, 4:1–2:1) to afford the title compound **276** (150 mg, 307 μ mol, 65% over two steps) as a colourless solid.

¹H NMR (400 MHz, CDCl₃) δ 8.27–8.20 (m, 2H), 7.75–7.62 (m, 6H). ¹³C NMR (101 MHz, CDCl₃) δ 162.0, 144.2, 132.4, 132.2, 132.2, 132.1, 131.8, 130.7, 128.7, 127.9, 127.4, 127.3, 118.4, 112.4, 92.2, 91.5.

Final Derivative 251

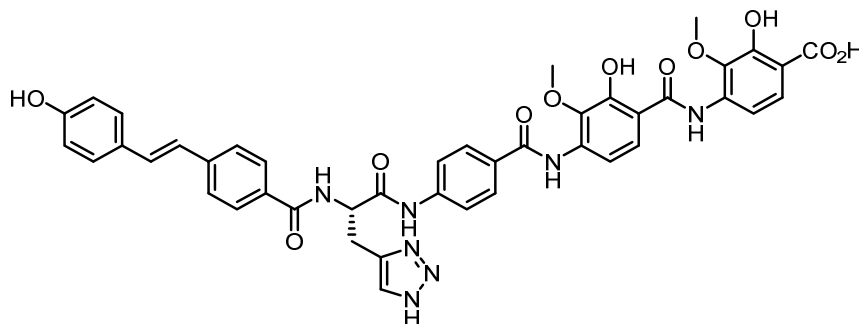


The tetrapeptide **285** (60 mg, 93.0 μ mol, 1.0 eq.) and the active ester **276** (52 mg, 102 μ mol, 1.1 eq.) were dissolved in a mixture of anhydrous DMF (5 mL) and triethylamine (0.10 mL, 744 μ mol, 8.0 eq.). The reaction mixture was stirred at r.t. for 16 h. All volatiles were removed *in vacuo* and the crude material was dissolved in DMSO and purified by HPLC (PLRP-S column, CH₃CN in H₂O). The title compound **251** (5.0 mg, 6%) was obtained as a colourless powder.

¹H NMR (400 MHz, DMSO-*d*₆) δ 11.54 (s, 1H), 11.17 (s, 1H), 10.56 (s, 1H), 9.68 (s, 1H), 9.01 (d,

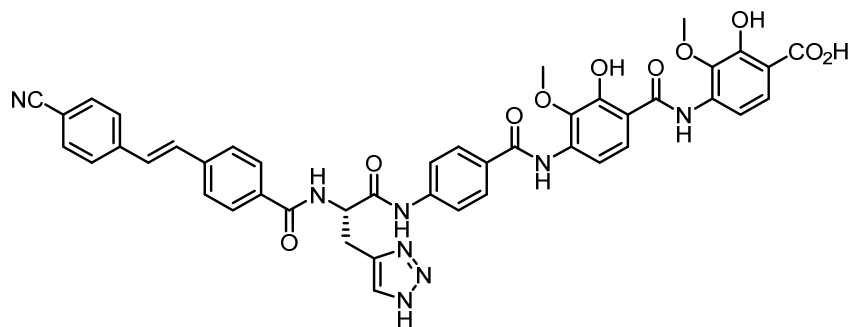
$J=8.0$ Hz, 1H), 7.77–7.83 (m, 5H), 7.73 (d, $J=8.5$ Hz, 2H), 7.60 (d, $J=3.5$ Hz, 1H), 7.57 (d, $J=3.8$ Hz, 1H), 4.88–4.99 (m, 1H), 3.92 (s, 3H), 3.78 (s, 3H). ^{13}C NMR (101 MHz, $\text{DMSO-}d_6$) δ 132.9 (Ar), 132.7 (Ar), 132.0 (Ar), 128.8 (Ar), 126.3 (Ar), 119.1 (Ar), 115.3 (Ar), 110.3 (Ar), 60.8 (OMe), 60.5 (OMe). HRMS (ESI): m/z calculated for $\text{C}_{44}\text{H}_{34}\text{N}_8\text{O}_{10}$ $[\text{M}+\text{H}]^+$ 835.2471, found 835.2469 ($\Delta m = -0.2$ ppm), $t_{\text{R}} = 9.38$ min.

Final Derivative 252

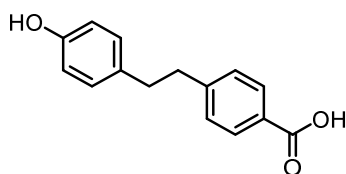


The tetrapeptide **284** (0.16 g, 0.22 mmol, 1.0 eq.) and the active ester **280** (0.11 g, 0.21 mmol, 1.0 eq.) were dissolved in a mixture of anhydrous DMF (3 mL) and triethylamine (0.29 mL, 2.1 mmol, 10 eq.). The mixture was stirred at r.t. for 16 h. All volatiles were removed *in vacuo* and the residue was taken up in a mixture of THF (2 mL) and MeOH (2 mL), and 3 N $\text{KOH}_{(\text{aq.})}$ (2 mL) was added dropwise at 0 °C. The ice bath was removed and after 15 min of stirring 3 N $\text{HCl}_{(\text{aq.})}$ (2.1 mL) was added and the resulting suspension was concentrated under reduced pressure. The crude material was dissolved in DMSO, centrifuged, and the supernatant was purified by HPLC (PLRP-S column, CH_3CN in H_2O). The title compound **252** (3.0 mg, 2% over two steps) was obtained as a colourless powder.

^1H NMR (500 MHz, $\text{DMSO-}d_6$) δ 10.82 (br. s, 1H), 10.59 (s, 1H), 9.61 (s, 1H), 8.79–8.84 (m, 1H), 7.97 (d, $J=9.0$ Hz, 2H), 7.88 (d, $J=8.4$ Hz, 2H), 7.80 (d, $J=8.9$ Hz, 3H), 7.66–7.70 (m, 1H), 7.60–7.66 (m, 2H), 7.55 (d, $J=8.9$ Hz, 1H), 7.41–7.51 (m, 3H), 7.28 (d, $J=16.5$ Hz, 1H), 7.07 (d, $J=16.5$ Hz, 1H), 6.77–6.84 (m, 2H), 4.90–4.96 (m, 1H), 3.86 (s, 3H), 3.79 (s, 3H). ^{13}C NMR (126 MHz, $\text{DMSO-}d_6$) δ 130.7 (Ar-CH), 128.9, 128.4, 128.2, 125.9, 125.2, 125.0, 124.7 (CH-Ar), 124.4, 119.0 (Ar), 115.9 (Ar), 114.6 (Ar), 107.8 (Ar), 60.6 (OMe), 59.8 (OMe), 54.6 (α -C), 27.5 (β -C). HRMS (ESI): m/z calculated for $\text{C}_{43}\text{H}_{37}\text{N}_7\text{O}_{11}$ $[\text{M}+\text{H}]^+$ 828.2624, found 828.2628 ($\Delta m = -0.4$ ppm), $t_{\text{R}} = 8.11$ min.

Final Derivative **253**

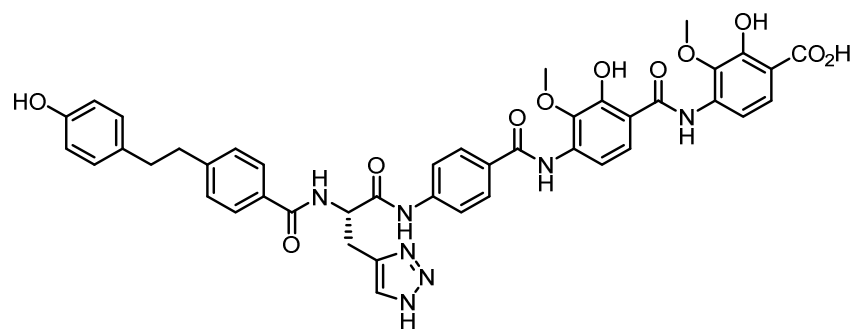
Synthetic protocol analogous to compound **252**. The title compound **253** (2.3 mg, 2% over two steps) was obtained as a colourless solid. ^1H NMR (500 MHz, $\text{DMSO-}d_6$) δ 11.54 (br. s, 1H), 11.17 (s, 1H), 10.58 (s, 1H), 9.67 (s, 1H), 8.86–8.91 (m, 1H), 8.02–8.08 (m, 1H), 7.97 (d, $J=8.7$ Hz, 2H), 7.93 (d, $J=8.1$ Hz, 2H), 7.77–7.87 (m, 8H), 7.75 (d, $J=8.4$ Hz, 2H), 7.69 (br s, 1H), 7.60–7.55 (m, 2H), 7.51 (d, $J=13.9$ Hz, 2H), 4.90–4.97 (m, 1H), 3.91 (s, 3H), 3.77–3.79 (m, 3H), 3.77–3.79 (m, 3H). ^{13}C NMR (126 MHz, $\text{DMSO-}d_6$) δ 133.1, 131.2 (Ar-CH), 129.8 (CH-Ar), 129.6 (Ar), 128.6 (Ar), 127.4 (Ar), 127.4 (Ar), 126.1 (Ar), 119.3 (Ar), 115.3 (Ar), 110.8 (Ar), 61.1 (OMe), 61.0 (OMe), 54.8 (α -C), 27.9 (β -C). HRMS (ESI): m/z calculated for $\text{C}_{44}\text{H}_{36}\text{N}_8\text{O}_{10}$ $[\text{M}+\text{H}]^+$ 837.2627, found 837.2631 ($\Delta m = -0.4$ ppm), $t_R = 8.87$ min.

4-(4-Hydroxyphenethyl)benzoic acid (**263**)

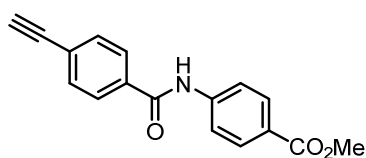
The alkyne **262** (350 mg, 1.46 mmol, 1.00 equiv) was dissolved in dry THF (5 mL) and the solution was purged with argon for 10 min. Palladium (10% on activated carbon, 155 mg) was added, the reaction mixture was saturated with H_2 and stirred at r.t. for 5 h under hydrogen atmosphere. The suspension was filtered over a pad of Celite[®], concentrated under reduced pressure, and the residue was dried under high vacuum to give the title compound **263** (317 mg, 1.31 mmol, 90%) as a colourless powder.

^1H NMR (500 MHz, $\text{DMSO-}d_6$) δ 12.75 (br s, 1H), 9.12 (s, 1H), 7.82–7.86 (m, 2H), 7.32 (d, $J=8.4$ Hz, 2H), 6.97–7.02 (m, 2H), 6.64–6.66 (m, 2H), 2.76–2.93 (m, 4H). ^{13}C NMR (126 MHz, $\text{DMSO-}d_6$) δ 167.8, 155.8, 147.6, 131.7, 129.7, 129.7, 129.1, 115.5, 37.8, 36.3. HRMS (ESI): m/z calculated for $\text{C}_{15}\text{H}_{13}\text{O}_3$ $[\text{M}-\text{H}]^-$ 241.0870, found 241.0864 ($\Delta m = -2.4$ ppm).

Final Derivative 254



Synthetic protocol analogous to compound **247**. The title compound **254** (4.0 mg, 2% over two steps) was obtained as a colourless solid. ^1H NMR (400 MHz, $\text{DMSO-}d_6$) δ 11.52 (s, 1H), 11.16 (s, 1H), 10.49 (s, 1H), 9.65 (s, 1H), 9.01–9.22 (m, 1H), 8.68–8.75 (m, 1H), 8.05 (d, $J=8.8$ Hz, 1H), 7.93–8.00 (m, 2H), 7.73–7.82 (m, 5H), 7.63–7.70 (m, 1H), 7.54–7.63 (m, 2H), 7.29 (d, $J=8.0$ Hz, 2H), 6.99 (d, $J=8.5$ Hz, 2H), 6.65 (d, $J=8.3$ Hz, 2H), 4.85–4.95 (m, 1H), 3.92 (s, 3H), 3.78 (s, 3H), 3.06–3.14 (m, 2H), 2.84–2.91 (m, 2H), 2.74–2.81 (m, 2H). ^{13}C NMR (101 MHz, $\text{DMSO-}d_6$) δ 129.8 (Ar), 129.4 (Ar), 119.2 (Ar), 127.9 (Ar), 128.8 (Ar), 115.6 (Ar), 60.5 (Ar), 60.9 (Ar), 46.1 (CH_2), 37.4 (CH_2), 36.1 (CH_2). HRMS (ESI): m/z calculated for $\text{C}_{43}\text{H}_{39}\text{N}_7\text{O}_{11}$ $[\text{M}+\text{H}]^+$ 830.2780, found 830.2780 ($\Delta m = 0$ ppm), $t_{\text{R}} = 8.23$ min.

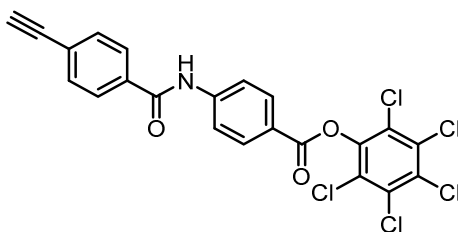
Methyl 4-(4-ethynylbenzamido)benzoate (**288**)

BTC (870 mg, 2.93 mmol, 0.45 eq.) was added to a solution of 4-Ethynylbenzoic acid (1.43 g, 9.77 mmol, 1.50 eq.) in dry THF (25 mL) and the solution was cooled down to 0 °C. 2,4,6-collidine (10.4 mL, 78.2 mmol, 12.0 eq.) was added dropwise and the resulting suspension was stirred at that temperature for 45 min. Subsequently, a premixed solution of methyl 4-aminobenzoate (985 mg, 6.52 mmol, 1.00 eq.) and DIPEA (11.4 mL, 65.2 mmol, 10.0 eq.) in dry THF (15 mL) was added dropwise to the suspension and the reaction mixture was stirred for 16 h while warming up to r.t. After removing all volatiles under reduced pressure, the residue was taken up in EtOAc and washed with 1 N $\text{HCl}_{(\text{aq.})}$ (3 \times), saturated aq. NaHCO_3 (3 \times), and brine. The organic phase was dried over anhydrous Na_2SO_4 and concentrated *in vacuo* to obtain the crude product, which was purified by column chromatography on silica gel (0.3–1%

MeOH in CH₂Cl₂) to afford the desired product **288** (0.859 g, 3.06 mmol, 47%) as colourless solid.

¹H NMR (400 MHz, DMSO-*d*₆) δ 10.64 (s, 1H), 8.02–7.92 (m, 6H), 7.68–7.62 (m, 2H), 4.44 (s, 1H), 3.83 (s, 3H). ¹³C NMR (101 MHz, DMSO-*d*₆) δ 165.8, 165.2, 143.5, 134.6, 131.8, 130.2, 128.2, 125.1, 124.5, 119.7, 83.3, 82.8, 52.0, 40.2, 40.2, 39.9, 39.7, 39.5, 39.3, 39.1, 38.9, 7.4. HRMS (ESI): *m/z* calculated for C₁₇H₁₃NO₃ [M+H]⁺ 280.0968, found 280.0967 (Δ*m* = -0.4 ppm).

Perchlorophenyl 4-(4-ethynylbenzamido)benzoate (**289**)



To a solution of methyl 4-(4-ethynylbenzamido)benzoate (**288**) (830 mg, 2.97 mmol, 1.00 eq.) in a mixture of THF (20 mL) and MeOH (20 mL) was added 3 N KOH_(aq.) (15 mL) and the reaction mixture was stirred at r.t. for 3 h. After removing the organic solvents *in vacuo*, the residue was taken up in EtOAc and washed with 1 N HCl_(aq.) (3×) and brine. The organic phase was dried over anhydrous Na₂SO₄ and concentrated under reduced pressure to obtain the crude product, which was purified by column chromatography on silica gel (3–20% MeOH in CH₂Cl₂) to afford 4-(4-ethynylbenzamido)benzoic acid (680 mg, 2.55 mmol, 86%).

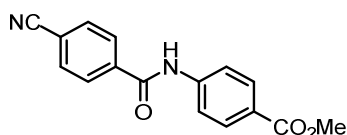
¹H NMR (400 MHz, DMSO-*d*₆) δ 12.39 (br. s, 1H), 10.41 (s, 1H), 8.01–7.81 (m, 6H), 7.55–7.51 (m, 2H), 3.85 (d, *J*=1.1 Hz, 1H). ¹³C NMR (101 MHz, DMSO-*d*₆) δ 166.9, 164.9, 142.8, 134.4, 131.3, 129.9, 127.7, 125.5, 125.0, 119.2, 82.3, 81.5. HRMS (ESI): *m/z* calculated for C₁₆H₁₁NO₃ [M+H]⁺ 266.0812, found 266.0811 (Δ*m* = -0.4 ppm).

To a solution of 4-(4-ethynylbenzamido)benzoic acid (150 mg, 566 μmol, 1.00 eq.) in DMF (5 mL) were successively added pentachlorophenol (166 mg, 622 μmol, 1.10 eq.), DCC (140 mg, 679 μmol, 1.20 eq.), and DMAP (6.91 mg, 56.6 μmol, 0.10 eq.) and the reaction mixture was stirred at r.t. for 16 h. After removing DMF under high vacuum, the residue was taken up in EtOAc and washed with 10% HCl_(aq.) (3×) followed by brine. The organic phase was dried over anhydrous Na₂SO₄ and concentrated under reduced pressure to obtain the crude product, which was purified by column chromatography on silica gel (0.3–15% MeOH in

To a solution of the alkyne derivative **255** (45 mg, 47 μmol , 1.0 eq.) and azidomethyl pivalate (5.1 μL , 47 μmol , 1.0 eq.) in a mixture of THF (2 mL) and H_2O (2 mL) was added $\text{CuSO}_4 \cdot 5 \text{H}_2\text{O}$ (0.58 mg, 2.3 μmol , 0.05 eq.). After purging the solution with N_2 for 5 min, sodium ascorbate (1.8 mg, 9.3 μmol , 0.20 eq.) was added and the reaction mixture was stirred at r.t. for 16 h. MeOH (2 mL) and 3 N $\text{KOH}_{(\text{aq.})}$ (2 mL) were added and the solution was stirred for another 15 min at r.t. After adding 3 N $\text{HCl}_{(\text{aq.})}$ (2.1 mL), the resulting suspension was concentrated under reduced pressure. The crude material was dissolved in DMSO, centrifuged, and the supernatant was purified by HPLC (PLRP-S column, CH_3CN in H_2O). The title compound **256** (15 mg, 36% over two steps) was obtained as a colourless powder.

^1H NMR (400 MHz, $\text{DMSO}-d_6$) δ 11.55 (s, 1H), 11.19 (s, 1H), 10.57 (s, 1H), 10.53 (s, 1H), 9.69 (s, 1H), 8.77 (d, $J=7.28$ Hz, 1H), 8.01–8.14 (m, 5H), 7.98 (d, $J=8.8$ Hz, 2H), 7.88–7.94 (m, 4H), 7.76–7.85 (m, 3H), 7.59 (dd, $J=3.8, 8.8$ Hz, 2H), 4.93 (q, $J=7.7$ Hz, 1H), 3.92 (s, 3H), 3.78 (s, 3H), 3.19–3.38 (m, 2H). ^{13}C NMR (101 MHz, $\text{DMSO}-d_6$) δ 129.1 (Ar), 128.9 (Ar), 128.7 (Ar), 126.1 (Ar), 126.0 (Ar), 125.9 (Ar), 119.8 (Ar), 118.9 (Ar), 115.1 (Ar), 110.4 (Ar), 60.8 (OMe), 60.5 (OMe), 54.7 ($\alpha\text{-C}$), 27.9 ($\beta\text{-C}$); HRMS (ESI): m/z calculated for $\text{C}_{44}\text{H}_{37}\text{N}_{11}\text{O}_{11}$ $[\text{M}+\text{H}]^+$ 896.2747, found 896.2734 ($\Delta m = -1.5$ ppm), $t_{\text{R}} = 7.34$ min.

Methyl 4-(4-cyanobenzamido)benzoate (**291**)

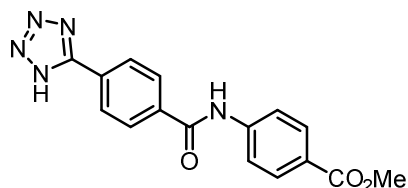


BTC (442 mg, 1.49 mmol, 0.45 eq.) was added to a solution of 4-cyanobenzoic acid (**290**) (730 mg, 4.96 mmol, 1.50 eq.) in dry THF (7 mL) and the solution was cooled down to 0 °C. 2,4,6-collidine (5.26 mL, 39.7 mmol, 12.0 eq.) was added dropwise and the resulting suspension was stirred at that temperature for 45 min. Subsequently, a premixed solution of methyl 4-aminobenzoate (500 mg, 3.31 mmol, 1.00 eq.) and DIPEA (5.76 mL, 33.1 mmol, 10.0 eq.) in dry THF (4 mL) was added dropwise to the suspension and the reaction mixture was stirred for 16 h while warming up to r.t. After removing all volatiles under reduced pressure, the residue was taken up in EtOAc and washed with 1 N $\text{HCl}_{(\text{aq.})}$ (3 \times), saturated aq. NaHCO_3 (3 \times), and brine. The organic phase was dried over anhydrous Na_2SO_4 and concentrated *in vacuo* to obtain the crude product, which was purified by recrystallization (*n*-

hexane/EtOAc, 5:1) to afford the title compound **291** (578 mg, 2.02 mmol, 61%) as colourless solid.

^1H NMR (400 MHz, $\text{DMSO-}d_6$) δ 10.78 (s, 1H), 8.15–8.07 (m, 2H), 8.07–8.01 (m, 2H), 8.01–7.91 (m, 4H), 3.84 (s, 3H). ^{13}C NMR (101 MHz, $\text{DMSO-}d_6$) δ 165.8, 164.6, 143.2, 138.5, 132.5, 130.1, 128.6, 124.7, 119.7, 118.2, 114.1, 51.9.

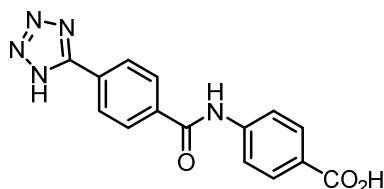
Methyl 4-(4-(1H-tetrazol-5-yl)benzamido)benzoate (**292**)



Methyl 4-(4-cyanobenzamido)benzoate (**291**) (200 mg, 714 μmol , 1.00 eq.), NaN_3 (58.0 mg, 892 μmol , 1.25 eq.), and L-proline (24.7 mg, 214 μmol , 0.30 eq.) were dissolved in DMF (6 mL) and stirred at 150 $^\circ\text{C}$ for 16 h. The solution was poured into ice-water (15 mL) under vigorous stirring and subsequently acidified to $\text{pH} \approx 2$ by the addition of conc. HCl(aq.) . The precipitate was isolated by filtration through a sintered funnel and dried under high vacuum to afford the pure title compound **292** (120 mg, 371 μmol , 52%) as a colourless solid.

^1H NMR (400 MHz, $\text{DMSO-}d_6$) δ 10.73 (s, 1H), 8.26–8.14 (m, 4H), 8.02–7.93 (m, 4H), 3.84 (s, 3H). ^{13}C NMR (101 MHz, $\text{DMSO-}d_6$) δ 165.8, 165.2, 143.5, 136.7, 130.2, 128.9, 127.3, 127.0, 124.5, 119.7, 52.0. HRMS (ESI): m/z calculated for $\text{C}_{16}\text{H}_{13}\text{N}_5\text{O}_3$ $[\text{M}+\text{H}]^+$ 324.1091, found 324.1090 ($\Delta m = +0.3$ ppm).

4-(4-(1H-Tetrazol-5-yl)benzamido)benzoic acid (**293**)



To a solution of methyl 4-(4-(1H-tetrazol-5-yl)benzamido)benzoate (**292**) (120 mg, 371 μmol , 1.00 eq.) in a mixture of THF (3 mL) and MeOH (3 mL) was added 3 N KOH(aq.) (3 mL) and the reaction mixture was stirred at r.t. for 1 h. After removing the organic solvents *in vacuo*, the residue was taken up in EtOAc and washed with 1 N HCl(aq.) (3 \times) and brine. The organic phase was dried over anhydrous Na_2SO_4 and concentrated under reduced pressure to obtain the title

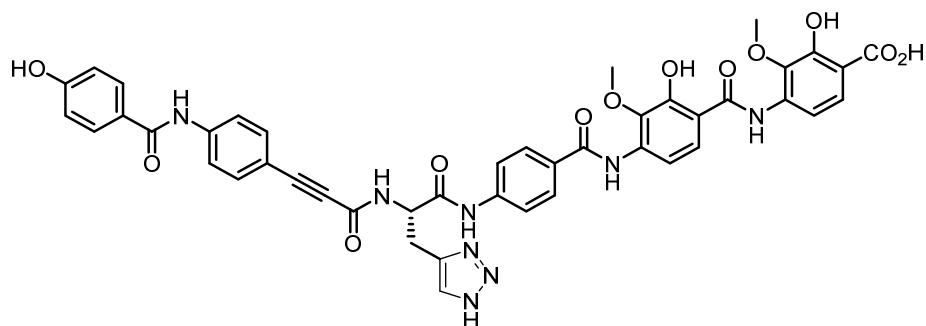
pressure, the residue was taken up in EtOAc and washed with 1 N HCl_(aq.) (3×), saturated aq. NaHCO₃ (3×), and brine. The organic phase was dried over anhydrous Na₂SO₄ and concentrated *in vacuo* to obtain the crude product, which was purified by column chromatography on silica gel (*n*-hexane/EtOAc, 6:1–3:1) to afford methyl 3-(4-(4-acetoxybenzamido)phenyl)propiolate (274 mg, 0.809 mmol, 71%) as colourless solid.

¹H NMR (400 MHz, DMSO-*d*₆) δ 10.59 (s, 1H), 8.03–7.97 (m, 2H), 7.94–7.89 (m, 2H), 7.71–7.64 (m, 2H), 7.34–7.29 (m, 2H), 3.78 (s, 3H), 2.31 (s, 3H). ¹³C NMR (101 MHz, DMSO-*d*₆) δ 169.0, 165.2, 153.7, 153.1, 141.9, 133.8, 129.4, 121.9, 120.0, 112.6, 86.6, 80.1, 52.9, 20.9. HRMS (ESI): *m/z* calculated for C₁₉H₁₅NO₅ [M+H]⁺ 338.1023, found 338.1024 (Δ*m* = +0.3 ppm).

To a solution of methyl 3-(4-(4-acetoxybenzamido)phenyl)propiolate (260 mg, 771 μmol, 1.00 eq.) in a mixture of THF (7 mL) and MeOH (7 mL) was added 3 N KOH_(aq.) (7 mL) and the reaction mixture was stirred at r.t. for 4 h. After removing the organic solvents *in vacuo*, the residue was taken up in EtOAc and washed with 1 N HCl_(aq.) (3×) and brine. The organic phase was dried over anhydrous Na₂SO₄ and concentrated under reduced pressure to obtain the title compound **297** (215 mg, 771 μmol, quant.).

¹H NMR (400 MHz, DMSO-*d*₆) δ 10.28 (s, 1H), 10.19 (s, 1H), 7.92–7.82 (m, 4H), 7.64–7.57 (m, 2H), 6.91–6.84 (m, 2H). ¹³C NMR (101 MHz, DMSO-*d*₆) δ 165.3, 160.9, 140.2, 132.3, 129.8, 124.9, 119.9, 116.1, 115.0, 48.6. HRMS (ESI): *m/z* calculated for C₁₆H₁₁NO₄ [M+H]⁺ 282.0761, found 282.0760 (Δ*m* = -0.4 ppm).

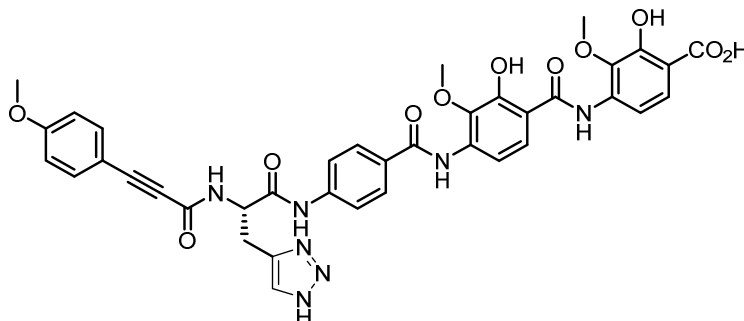
Final Derivative 258



Synthetic protocol analogous to compound **247**. The title compound **258** (4 mg, 4% over two steps) was obtained as a colourless solid. ¹H NMR (400 MHz, DMSO-*d*₆) δ 10.55 (br. s, 1H), 10.26 (s, 1H), 10.22 (s, 1H), 9.67 (br. s, 1H), 9.29 (br. s, 1H), 7.74–8.01 (m, 11H), 7.52–7.62 (m, 4H), 6.88 (d, *J*=8.8 Hz, 2H), 4.77–4.87 (m, 1H), 3.86–3.92 (m, 3H), 3.76–3.81 (m, 3H). HRMS

(ESI): m/z calculated for $C_{44}H_{36}N_8O_{12}$ $[M+H]^+$ 869.2525, found 869.2521 ($\Delta m = -0.5$ ppm), $t_R = 7.82$ min.

Final Derivative 259



Synthetic protocol analogous to compound **3**. The title compound **15** (15 mg, 25% over two steps) was obtained as a colourless solid. 1H NMR (400 MHz, $DMSO-d_6$) δ 3.06–3.25 (m, 2H) 3.78 (s, 3H) 3.81 (s, 3H) 3.92 (s, 3H) 4.81 (q, $J=7.9$ Hz, 1H) 7.03 (d, $J=8.8$ Hz, 2H) 7.52–7.62 (m, 4H) 7.67 (br. s., 1H) 7.76 (d, $J=8.8$ Hz, 2H) 7.81 (d, $J=8.8$ Hz, 1H) 7.97 (d, $J=8.8$ Hz, 2H) 8.06 (d, $J=9.0$ Hz, 1H) 9.23 (d, $J=8.0$ Hz, 1H) 9.69 (s, 1H) 10.53 (s, 1H) 11.19 (s, 1H) 11.55 (s, 1H). ^{13}C NMR (400 MHz, $DMSO-d_6$) δ 134.5 (Ar), 129.0 (Ar), 126.1 (Ar), 126.0 (Ar), 119.2 (Ar), 115.2 (Ar), 115.1 (Ar), 110.4 (Ar), 60.8 (OMe), 60.6 (OMe), 55.8 (OMe); HRMS (ESI): calculated for $C_{38}H_{33}N_7O_{11}$ $[M+H]^+$ 764.2311, found 764.2316 ($\Delta m = +0.7$ ppm).

5.3 Biological Assays

5.3.1 Microdilution Assay

MIC values were determined by Dipl. Biotechnol. MARIA SEIDEL according to the 9th edition of the Approved Standard M07-A9. The test was carried out for 18 different bacterial strains (*E. coli* DSM 1116 [Gram-negative], *E. coli* BW25113 [Gram-negative], *S. typhimurium* TA100 [Gram-negative], *B. subtilis* DSM10 [Gram-positive], *M. luteus* DSM1790 [Gram-positive], *M. phlei* DSM750 [Gram-positive], *E. coli* CIP res. [Gram-negative], *E. coli* CIP sens. [Gram-negative], *K. pneumoniae* CIP sens. [Gram-negative], *A. baumannii* CIP res. [Gram-negative], *P. aeruginosa* CIP res. [Gram-negative], *P. aeruginosa* CIP sens. [Gram-negative], *E. faecium* CIP res. [Gram-positive], *E. faecium* CIP sens. [Gram-positive], *S. aureus* CIP res. [Gram-positive], *S. aureus* CIP sens. [Gram-positive], S. Kentucky CIP res. [Gram-negative], S. Kentucky CIP sens. [Gram-negative]).

20 µL of cryo stock of each strain were inoculated in 20 mL LB medium (Lysogeny broth: 10 g/L peptone, 5 g/L yeast extract, 5 g/L NaCl) followed by incubation overnight at 37 °C, 200 rpm. The test inoculum was adjusted by the 0.5 McFarland Standard (OD₆₂₅ from 0.08 to 0.1). Within 15 min of preparation, the adjusted inoculum suspension was diluted in MHBII (BBL™ Mueller-Hinton Broth II, Becton, Dickinson and Company, New Jersey, USA) so that each well contained approximately 5×10^5 CFU/mL in a final volume of 100 µL. 95 µL of the inoculum were applied per well and 5 µL of the (diluted) antibiotic substance were added. Previously, the dry antibiotic compounds were dissolved in DMSO (100%) with a concentration of 2560 µg/mL, and the so obtained stock solutions were further diluted in DMSO (100%). 5 µL of each antibiotic dilution were applied to the microdilution tray to reach final concentrations of 8 µg/mL to 0.016 µg/mL. One row of each well plate served as a growth control without antibiotic substances and another row of the microdilution tray served as sterility control (only MHB II-media). The antimicrobial effect of the solvent (DMSO) was tested by adding 5 µL DMSO to several wells. Purity check and cell titer control were performed according to International Standard M07-A9 on Mueller-Hinton II Agar (Mueller Hinton II Broth, 15 g/L agar-agar). Both microdilution trays and agar plates were incubated at 37 °C for 20 h and subsequently analyzed by naked eye.

5.3.2 DNA Gyrase Inhibition Assay

DNA supercoiling experiments with DNA gyrase were performed by Dipl. Biotechnol. MARIA SEIDEL in a total volume of 30 μL gyrase buffer (protocol by NEB, Frankfurt, Germany). The incubations contained 0.5 μg relaxed pBR322 plasmid DNA (inspiralis Limited), 1.5 U DNA-gyrase (6 U/ μL) (NEB) and the final albicidin derivatives at a final concentration of 45 nM. The final DMSO concentration was 3%. Samples were incubated at 37 °C for 30 min and subsequently loaded on an agarose gel. Electrophoretic analysis was performed using a 1% agarose gel (100 V, 90 min). DNA bands were stained with ethidium bromide and visually analyzed.

6 References

- [1] C. L. Ventola, *Pharm. Ther.* **2015**, *40*, 277–283.
- [2] K. C. Nicolaou, S. Rigol, *J. Antibiot.* **2018**, *71*, 153–184.
- [3] V. M. D'Costa, C. E. King, L. Kalan, M. Morar, W. W. L. Sung, C. Schwarz, D. Froese, G. Zazula, F. Calmels, R. Debruyne et al., *Nature* **2011**, *477*, 457–461.
- [4] F. Prestinaci, P. Pezzotti, A. Pantosti, *Pathog. Glob. Health* **2015**, *109*, 309–318.
- [5] E. Y. Klein, T. P. van Boeckel, E. M. Martinez, S. Pant, S. Gandra, S. A. Levin, H. Goossens, R. Laxminarayan, *Proc. Natl. Acad. Sci. U.S.A.* **2018**, *115*, E3463–E3470.
- [6] P. Lopez-Vazquez, J. M. Vazquez-Lago, A. Figueiras, *J. Eval. Clin. Pract.* **2012**, *18*, 473–484.
- [7] T. C. Jenkins, A. Irwin, L. Coombs, L. Dealleaume, S. E. Ross, J. Rozwadowski, B. Webster, L. M. Dickinson, A. L. Sabel, T. D. Mackenzie et al., *Am. J. Med.* **2013**, *126*, 327–335.
- [8] C. L. Ventola, *Pharm. Ther.* **2015**, *40*, 344–352.
- [9] I. A. Rather, B.-C. Kim, V. K. Bajpai, Y.-H. Park, *Saudi J. Biol. Sci.* **2017**, *24*, 808–812.
- [10] W. Witte, *Int. J. Antimicrob. Agents* **2000**, *16*, 19–24.
- [11] P. Chittick, A. Sulka, R. V. Tauxe, A. M. Fry, *J. Food Prot.* **2006**, *69*, 1150–1153.
- [12] K. Jeannot, A. Bolard, P. Plésiat, *Int. J. Antimicrob. Agents* **2017**, *49*, 526–535.
- [13] F. S. Codjoe, E. S. Donkor, *Med. Sci.* **2017**, *6*, 1–28.
- [14] L. B. Rice, *J. Infect. Dis.* **2008**, *197*, 1079–1081.
- [15] D. Nagarjuna, G. Mittal, R. S. Dhanda, P. K. Verma, R. Gaiind, M. Yadav, *New Microbes New Infect.* **2015**, *7*, 57–66.
- [16] D. A. Enoch, S. H. Aliyu, *CMAJ* **2012**, *184*, 17–18.
- [17] A. Y. Peleg, D. C. Hooper, *N. Engl. J. Med.* **2010**, *362*, 1804–1813.
- [18] D. van Duin, D. L. Paterson, *Infect. Dis. Clin. North Am.* **2016**, *30*, 377–390.
- [19] A. H. Delcour, *Biochim. Biophys. Acta* **2009**, *1794*, 808–816.
- [20] J. Freeman, J. E. McGowan, *J. Infect. Dis.* **1978**, *138*, 811–819.
- [21] K. Bush, P. Courvalin, G. Dantas, J. Davies, B. Eisenstein, P. Huovinen, G. A. Jacoby, R. Kishony, B. N. Kreiswirth, E. Kutter et al., *Nat. Rev. Microbiol.* **2011**, *9*, 894–896.
- [22] WHO, "Antibacterial Agents in Clinical Development: An Analysis of the Antibacterial Clinical Development Pipeline, Including Tuberculosis", can be found under <https://apps.who.int/iris/bitstream/handle/10665/258965/WHO-EMP-IAU->

- 2017.11-eng.pdf;jsessionid=602C005142A4F4BFC8F775BDAF5FCFB8?sequence=1, **2017**.
- [23] J. O'Neill, "Antimicrobial Resistance: Tackling a Crisis for the Health and Wealth of Nations", can be found under https://amr-review.org/sites/default/files/AMR%20Review%20Paper%20-%20Tackling%20a%20crisis%20for%20the%20health%20and%20wealth%20of%20nations_1.pdf, **2014**.
- [24] World Bank Group, "Drug-Resistant Infections. A Threat to Our Economic Future", can be found under <http://documents.worldbank.org/curated/en/323311493396993758/pdf/final-report.pdf>, **2017**.
- [25] WHO, "Global Action Plan on Antimicrobial Resistance", can be found under https://apps.who.int/iris/bitstream/handle/10665/193736/9789241509763_eng.pdf?sequence=1, **2015**.
- [26] The Federal Government, "DART 2020. Fourth Interim Report 2019", can be found under https://www.bundesgesundheitsministerium.de/fileadmin/Dateien/5_Publikationen/Praevention/Broschueren/DART2020_4-Zwischenbericht_2019_EN.pdf, **2019**.
- [27] WHO, "Global Priority List of Antibiotic-Resistant Bacteria to Guide Research, Discovery, and Development of New Antibiotics", can be found under https://www.who.int/medicines/publications/WHO-PPL-Short_Summary_25Feb-ET_NM_WHO.pdf?ua=1, **2017**.
- [28] J. Bérny, *J. Antibiot.* **2012**, *65*, 385–395.
- [29] D. Gottlieb, *J. Antibiot.* **1976**, *29*, 987–1000.
- [30] M. Kawaguchi, K. Nonaka, R. Masuma, H. Tomoda, *J. Antibiot.* **2013**, *66*, 17–21.
- [31] M. G. Watve, R. Tickoo, M. M. Jog, B. D. Bhole, *Arch. Microbiol.* **2001**, *176*, 386–390.
- [32] R. E. d. L. Procópio, I. R. d. Silva, M. K. Martins, J. L. de Azevedo, J. M. de Araújo, *Braz. J. Infect. Dis.* **2012**, *16*, 466–471.
- [33] C. Walsh, *Nature* **2000**, *406*, 775–781.
- [34] J. Davies, D. Davies, *Microbiol. Mol. Biol. Rev.* **2010**, *74*, 417–433.
- [35] G. Cox, G. D. Wright, *Int. J. Med. Microbiol.* **2013**, *303*, 287–292.
- [36] C. M. Bébéar, S. Pereyre, *Curr. Drug Targets Infect. Disord.* **2005**, *5*, 263–271.
- [37] V. Yarlagadda, G. B. Manjunath, P. Sarkar, P. Akkapeddi, K. Paramanandham, B. R. Shome, R. Ravikumar, J. Haldar, *ACS Infect. Dis.* **2016**, *2*, 132–139.
- [38] M. M. Fernandes, K. Ivanova, J. Hoyo, S. Pérez-Rafael, A. Francesko, T. Tzanov, *ACS Appl. Mater. Interfaces* **2017**, *9*, 15022–15030.
- [39] X. Z. Li, D. M. Livermore, H. Nikaido, *Antimicrob. Agents Chemother.* **1994**, *38*, 1732–1741.
- [40] H. Tsubery, I. Ofek, S. Cohen, M. Eisenstein, M. Fridkin, *Mol. Pharmacol.* **2002**, *62*, 1036–1042.
- [41] P. J. Bergen, Z. P. Bulman, S. Saju, J. B. Bulitta, C. Landersdorfer, A. Forrest, J. Li, R. L. Nation, B. T. Tsuji, *Pharmacotherapy* **2015**, *35*, 34–42.
- [42] J. Seoane, T. Yankelevich, A. Dechesne, B. Merkey, C. Sternberg, B. F. Smets, *FEMS Microbiol. Ecol.* **2011**, *75*, 17–27.

- [43] A. R. Burmeister, *Evol. Med. Public Health* **2015**, 2015, 193–194.
- [44] M. Kolář, K. Urbánek, T. Látal, *Int. J. Antimicrob. Agents* **2001**, 17, 357–363.
- [45] S. Fossum, E. Crooke, K. Skarstad, *EMBO J.* **2007**, 26, 4514–4522.
- [46] B. G. Spratt, *Science* **1994**, 264, 388–393.
- [47] M. S. Ramirez, M. E. Tolmasky, *Drug Resist. Updat.* **2010**, 13, 151–171.
- [48] A. Kumar, H. P. Schweizer, *Adv. Drug. Deliv. Rev.* **2005**, 57, 1486–1513.
- [49] S. B. Levy, *Antimicrob. Agents Chemother.* **1992**, 36, 695–703.
- [50] J. M. Munita, C. A. Arias, *Microbiol. Spectr.* **2016**, 4.
- [51] S. R. Partridge, S. M. Kwong, N. Firth, S. O. Jensen, *Clin. Microbiol. Rev.* **2018**, 31.
- [52] A. San Millan, *Trends Microbiol.* **2018**, 26, 978–985.
- [53] M. Dolejska, C. C. Papagiannitsis, *Plasmid* **2018**, 99, 99–111.
- [54] M. Rozwandowicz, M. S. M. Brouwer, J. Fischer, J. A. Wagenaar, B. Gonzalez-Zorn, B. Guerra, D. J. Mevius, J. Hordijk, *J. Antimicrob. Chemother.* **2018**, 73, 1121–1137.
- [55] Y.-Y. Liu, Y. Wang, T. R. Walsh, L.-X. Yi, R. Zhang, J. Spencer, Y. Doi, G. Tian, B. Dong, X. Huang et al., *Lancet Infect. Dis.* **2016**, 16, 161–168.
- [56] "Superbugs: finding the path of least resistance", can be found under <https://www.nature.com/articles/d42473-019-00381-4>, **2020**.
- [57] G. A. Pankey, L. D. Sabath, *Clin. Infect. Dis.* **2004**, 38, 864–870.
- [58] M. A. Kohanski, D. J. Dwyer, J. J. Collins, *Nat. Rev. Microbiol.* **2010**, 8, 423–435.
- [59] A. Coates, Y. Hu, R. Bax, C. Page, *Nat. Rev. Drug Discov.* **2002**, 1, 895–910.
- [60] K. Bush, P. A. Bradford, *Cold Spring Harb. Perspect. Med.* **2016**, 6.
- [61] P. Sarkar, V. Yarlagadda, C. Ghosh, J. Haldar, *MedChemComm* **2017**, 8, 516–533.
- [62] L. L. Ling, T. Schneider, A. J. Peoples, A. L. Spoering, I. Engels, B. P. Conlon, A. Mueller, T. F. Schäberle, D. E. Hughes, S. Epstein et al., *Nature* **2015**, 517, 455–459.
- [63] K. Jin, I. H. Sam, K. H. L. Po, D.'a. Lin, E. H. Ghazvini Zadeh, S. Chen, Y. Yuan, X. Li, *Nat. Commun.* **2016**, 7, 12394.
- [64] F. von Nussbaum, R. D. Süßmuth, *Angew. Chem. Int. Ed.* **2015**, 54, 6684–6686.
- [65] K. Drlica, M. Malik, R. J. Kerns, X. Zhao, *Antimicrob. Agents Chemother.* **2007**, 52, 385–392.
- [66] M. Gellert, K. Mizuuchi, M. H. O'Dea, H. A. Nash, *Proc. Natl. Acad. Sci. U.S.A.* **1976**, 73, 3872–3876.
- [67] H. G. Floss, T.-W. Yu, *Chem. Rev.* **2005**, 105, 621–632.
- [68] D. Fernández-Villa, M. R. Aguilar, L. Rojo, *Int. J. Mol. Sci.* **2019**, 20, 1–30.
- [69] E. Goldberg, J. Bishara, *Clin. Microbiol. Infect.* **2012**, 18, 8–17.
- [70] P. D. Walzer, C. K. Kim, J. M. Foy, M. J. Linke, M. T. Cushion, *Antimicrob. Agents Chemother.* **1988**, 32, 96–103.
- [71] H. K. Johansen, T. G. Jensen, R. B. Dessau, B. Lundgren, N. Frimodt-Moller, *J. Antimicrob. Chemother.* **2000**, 46, 973–980.
- [72] M. H. Lepper, H. F. Dowling, *AMA Arch. Intern. Med.* **1951**, 88, 489–494.
- [73] R. Mehta, W. S. Champney, *Antimicrob. Agents Chemother.* **2002**, 46, 1546–1549.
- [74] B. A. Maguire, *Microbiol. Mol. Biol. Rev.* **2009**, 73, 22–35.

- [75] S. M. R. Hashemian, T. Farhadi, M. Ganjparvar, *Drug Des. Devel. Ther.* **2018**, *12*, 1759–1767.
- [76] D. M. Livermore, *J. Antimicrob. Chemother.* **2003**, *51*, ii9-16.
- [77] S. C. Verma, Z. Qian, S. L. Adhya, *PLoS Genet.* **2019**, *15*, e1008456.
- [78] T. M. Lohman, K. P. Bjornson, *Annu. Rev. Biochem.* **1996**, *65*, 169–214.
- [79] D. P. Snustad, M. J. Simmons, *Principles of Genetics*, John Wiley & Sons, Inc., New York, **2015**.
- [80] Y. Pommier, E. Leo, H. Zhang, C. Marchand, *Chem. Biol.* **2010**, *17*, 421–433.
- [81] B. J. Bradbury, M. J. Pucci, *Curr. Opin. Pharmacol.* **2008**, *8*, 574–581.
- [82] Y.-C. Tse-Dinh, *Infect. Disord. Drug Targets* **2007**, *7*, 3–9.
- [83] J. J. Champoux, *Annu. Rev. Biochem.* **2001**, *70*, 369–413.
- [84] L. Liu, C. Liu, B. Alberts, *Cell* **1980**, *19*, 697–707.
- [85] F. Collin, S. Karkare, A. Maxwell, *Appl. Microbiol. Biotechnol.* **2011**, *92*, 479–497.
- [86] M. Gellert, M. H. O'Dea, T. Itoh, J. Tomizawa, *Proc. Natl. Acad. Sci. U.S.A.* **1976**, *73*, 4474–4478.
- [87] J. Roca, J. C. Wang, *Cell* **1992**, *71*, 833–840.
- [88] J. Roca, J. C. Wang, *Cell* **1994**, *77*, 609–616.
- [89] D. B. Wigley, G. J. Davies, E. J. Dodson, A. Maxwell, G. Dodson, *Nature* **1991**, *351*, 624–629.
- [90] J. H. Morais Cabral, A. P. Jackson, C. V. Smith, N. Shikotra, A. Maxwell, R. C. Liddington, *Nature* **1997**, *388*, 903–906.
- [91] K. D. Corbett, R. K. Shultzaberger, J. M. Berger, *Proc. Natl. Acad. Sci. U.S.A.* **2004**, *101*, 7293–7298.
- [92] M. J. Edwards, R. H. Flatman, L. A. Mitchenall, C. E. M. Stevenson, T. B. K. Le, T. A. Clarke, A. R. McKay, H.-P. Fiedler, M. J. Buttner, D. M. Lawson et al., *Science* **2009**, *326*, 1415–1418.
- [93] G. Fu, J. Wu, W. Liu, D. Zhu, Y. Hu, J. Deng, X.-E. Zhang, L. Bi, D.-C. Wang, *Nucleic Acids Res.* **2009**, *37*, 5908–5916.
- [94] T.-J. Hsieh, T.-J. Yen, T.-S. Lin, H.-T. Chang, S.-Y. Huang, C.-H. Hsu, L. Farh, N.-L. Chan, *Nucleic Acids Res.* **2010**, *38*, 4173–4181.
- [95] E. M. Tretter, A. J. Schoeffler, S. R. Weisfield, J. M. Berger, *Proteins* **2010**, *78*, 492–495.
- [96] B. D. Bax, P. F. Chan, D. S. Eggleston, A. Fosberry, D. R. Gentry, F. Gorrec, I. Giordano, M. M. Hann, A. Hennessy, M. Hibbs et al., *Nature* **2010**, *466*, 935–940.
- [97] A. J. Schoeffler, A. P. May, J. M. Berger, *Nucleic Acids Res.* **2010**, *38*, 7830–7844.
- [98] M. Couturier, E. M. Bahassi, L. van Melderen, *Trends Microbiol.* **1998**, *6*, 269–275.
- [99] S. N. Dighe, T. A. Collet, *Eur. J. Med. Chem.* **2020**, DOI 10.1016/j.ejmech.2020.112326.
- [100] A. Maxwell, *Biochem. Soc. Trans.* **1999**, *27*, 48–53.
- [101] M. Durcik, T. Tomašič, N. Zidar, A. Zega, D. Kikelj, L. P. Mašič, J. Ilaš, *Expert Opin. Ther. Pat.* **2019**, *29*, 171–180.
- [102] M. Barančoková, D. Kikelj, J. Ilaš, *Future. Med. Chem.* **2018**, *10*, 1207–1227.

- [103] M.-H. Dao-Thi, L. van Melderen, E. de Genst, H. Afif, L. Buts, L. Wyns, R. Loris, *J. Mol. Biol.* **2005**, *348*, 1091–1102.
- [104] T. Khan, K. Sankhe, V. Suvarna, A. Sherje, K. Patel, B. Dravyakar, *Biomed. Pharmacother.* **2018**, *103*, 923–938.
- [105] D. J. Biedenbach, S. K. Bouchillon, M. Hackel, L. A. Miller, N. E. Scangarella-Oman, C. Jakielaszek, D. F. Sahm, *Antimicrob. Agents Chemother.* **2016**, *60*, 1918–1923.
- [106] C. Charrier, A.-M. Salisbury, V. J. Savage, T. Duffy, E. Moyo, N. Chaffer-Malam, N. Ooi, R. Newman, J. Cheung, R. Metzger et al., *Antimicrob. Agents Chemother.* **2017**, *61*, 1–13.
- [107] P. A. Bradford, A. A. Miller, J. O'Donnell, J. P. Mueller, *ACS Infect. Dis.* **2020**, DOI 10.1021/acsinfecdis.0c00021.
- [108] R. H. Flatman, A. J. Howells, L. Heide, H.-P. Fiedler, A. Maxwell, *Antimicrob. Agents Chemother.* **2005**, *49*, 1093–1100.
- [109] C. G. Smith, A. Dietz, W. T. Sokolski, G. M. Savage, *Antibiot. Chemother. (Northfield)* **1956**, *6*, 135–142.
- [110] H. Kawaguchi, H. Tsuikiura, M. Okanishi, T. Miyaki, T. Ohmori, K. Fujisawa, H. Koshiyama, *J. Antibiot.* **1965**, *18*, 1–10.
- [111] J. Schimana, H. P. Fiedler, I. Groth, R. Süsmuth, W. Beil, M. Walker, A. Zeeck, *J. Antibiot.* **2000**, *53*, 779–787.
- [112] R. Pozzi, M. Simone, C. Mazzetti, S. Maffioli, P. Monciardini, L. Cavaletti, R. Bamonte, M. Sosio, S. Donadio, *J. Antibiot.* **2011**, *64*, 133–139.
- [113] U. Galm, M. A. Desso, J. Schmidt, L. A. Wessjohann, L. Heide, *Chem. Biol.* **2004**, *11*, 173–183.
- [114] L. Heide, *Biotechnol. Adv.* **2009**, *27*, 1006–1014.
- [115] L. Heide, *Int. J. Med. Microbiol.* **2014**, *304*, 31–36.
- [116] C. Anderle, S. Hennig, B. Kammerer, S.-M. Li, L. Wessjohann, B. Gust, L. Heide, *Chem. Biol.* **2007**, *14*, 955–967.
- [117] L. Heide, B. Gust, C. Anderle, S.-M. Li, *Curr. Top. Med. Chem.* **2008**, *8*, 667–679.
- [118] A. Maxwell, D. M. Lawson, *Curr. Top. Med. Chem.* **2003**, *3*, 283–303.
- [119] M. J. Buttner, M. Schäfer, D. M. Lawson, A. Maxwell, *FEMS Microbiol. Rev.* **2018**, *42*.
- [120] C. Sissi, E. Vazquez, A. Chemello, L. A. Mitchenall, A. Maxwell, M. Palumbo, *Antimicrob. Agents Chemother.* **2010**, *54*, 213–220.
- [121] B. K. Bhuyan, S. P. Owen, A. Dietz, *Antimicrob. Agents Chemother.* **1964**, *10*, 91–96.
- [122] F. Reusser, *Biochemistry* **1973**, *12*, 1136–1142.
- [123] F. Reusser, *J. Antibiot.* **1979**, *32*, 1186–1192.
- [124] F. Reusser, B. Bannister, W. G. Tarpley, I. W. Althaus, B. A. Zapotocky, *Rubradirin derivatives for treatment of HIV infection*, W08808707, **1988**.
- [125] H. Welch, W. W. Wright, *Antibiot. Chemother. (Northfield)* **1955**, *5*, 670–673.
- [126] R. N. Jones, *Diagn. Micr. Infec. Dis.* **1989**, *12*, 363–365.
- [127] G. Rolland, P. Sensi, G. A. Ferrari, G. Maffll, M. T. Timbal, L. G. Silvestri, *Farmaco. Sci.* **1956**, *11*, 549–561.
- [128] R. W. Fairbrother, B. L. Williams, *The Lancet* **1956**, *268*, 1177–1179.

- [129] M. Finalnd, E. Foltz, J. E. Geraci, W. M. Kirby, E. L. Quinn, M. J. Romansky, E. M. Yow, *Antibiot. Annu.* **1958**, *6*, 1051–1072.
- [130] J. Berger, A. D. Batcho in *Journal of Chromatography Library* (Eds.: G. H. Wagman, M. J. Weinstein), Elsevier Science, Amsterdam, **2007**, pp. 101–158.
- [131] T. J. Walsh, S. L. Hansen, B. A. Tatem, F. Auger, H. C. Standiford, *J. Antimicrob. Chemother.* **1985**, *15*, 435–440.
- [132] FDA, "Determination that albamycin (novobiocin sodium) capsule, 250 milligrams, was withdrawn from sale for reasons of safety or effectiveness", can be found under <https://www.federalregister.gov/documents/2011/01/19/2011-1000/determination-that-albamycin-novobiocin-sodium-capsule-250-milligrams-was-withdrawn-from-sale-for>, **2011**.
- [133] D. C. Hooper, *Drugs* **1999**, *58 Suppl. 2*, 6–10.
- [134] K. J. Aldred, R. J. Kerns, N. Osheroff, *Biochemistry* **2014**, *53*, 1565–1574.
- [135] L. S. Redgrave, S. B. Sutton, M. A. Webber, L. J. V. Piddock, *Trends Microbiol.* **2014**, *22*, 438–445.
- [136] G. Y. Leshner, E. J. Froehlich, M. D. Gruett, J. H. Bailey, R. P. Brundage, *J. Med. Pharm. Chem.* **1962**, *91*, 1063–1065.
- [137] A. M. Emmerson, A. M. Jones, *J. Antimicrob. Chemother.* **2003**, *51 Suppl. S1*, 13–20.
- [138] P. C. Appelbaum, P. A. Hunter, *Int. J. Appl. Ceram. Technol.* **2000**, *16*, 5–15.
- [139] G. L. Patrick, *An Introduction to Medicinal Chemistry*, Oxford University Press, Oxford, **2017**.
- [140] E. L. Alapi, J. Fischer in *Analogue-Based Drug Discovery* (Eds.: J. Fischer, C. R. Ganellin), Wiley-VCH, Weinheim, **2006**, p. 500.
- [141] M. G. Bergeron, *Clin. Invest. Med* **1989**, *12*, 20–27.
- [142] G. Drusano, M.-T. Labro, O. Cars, P. Mendes, P. Shah, F. Sörgel, W. Weber, *Clin. Microbiol. Infect.* **1998**, *4*, 2S27–2S41.
- [143] WHO, "World Health Organization Model List of Essential Medicines: 21st list 2019", can be found under <https://apps.who.int/iris/bitstream/handle/10665/325771/WHO-MVP-EMP-IAU-2019.06-eng.pdf?ua=1>, **2019**.
- [144] M. V. de Almeida, M. F. Saraiva, M. V. N. de Souza, C. F. da Costa, F. R. C. Vicente, M. C. S. Lourenço, *Bioorg. Med. Chem. Lett.* **2007**, *17*, 5661–5664.
- [145] P. C. Sharma, A. Jain, S. Jain, R. Pahwa, M. S. Yar, *J. Enzyme Inhib. Med. Chem.* **2010**, *25*, 577–589.
- [146] J. C. McGregor, G. P. Allen, D. T. Bearden, *Ther. Clin. Risk Manag.* **2008**, *4*, 843–853.
- [147] T. D. M. Pham, Z. M. Ziora, M. A. T. Blaskovich, *MedChemComm* **2019**, *10*, 1719–1739.
- [148] K. Drlica, H. Hiasa, R. Kerns, M. Malik, A. Mustaev, X. Zhao, *Curr. Top. Med. Chem.* **2009**, *9*, 981–998.
- [149] L. J. Piddock, *Br. Med. J.* **1998**, *317*, 1029–1030.
- [150] J. A. García-Rodríguez, J. L. Muñoz Bellido, *Clin. Microbiol. Infect.* **2000**, *6*, 73–75.
- [151] H. E. Akalin, *Drugs* **1999**, *58 Suppl. 2*, 52–54.

- [152] E. E. Effa, Z. S. Lassi, J. A. Critchley, P. Garner, D. Sinclair, P. L. Olliaro, Z. A. Bhutta, *Cochrane Database Syst. Rev.* **2011**, *10*, 1–141.
- [153] J. Sendzik, H. Lode, R. Stahlmann, *Int. J. Antimicrob. Agents* **2009**, *33*, 194–200.
- [154] P. Rawla, M. L. El Helou, A. R. Vellipuram, *Cardiovasc. Hematol. Agents Med. Chem.* **2019**, *17*, 3–10.
- [155] R. Loebstein, A. Addis, E. Ho, R. Andreou, S. Sage, A. E. Donnenfeld, B. Schick, M. Bonati, M. Moretti, A. Lalkin et al., *Antimicrob. Agents Chemother.* **1998**, *42*, 1336–1339.
- [156] FDA, "FDA updates warnings for fluoroquinolone antibiotics on risks of mental health and low blood sugar adverse reactions", can be found under <https://www.fda.gov/news-events/press-announcements/fda-updates-warnings-fluoroquinolone-antibiotics-risks-mental-health-and-low-blood-sugar-adverse>, **2018**.
- [157] N. Nakada, H. Shimada, T. Hirata, Y. Aoki, T. Kamiyama, J. Watanabe, M. Arisawa, *Antimicrob. Agents Chemother.* **1993**, *37*, 2656–2661.
- [158] E. Goetschi, P. Angehrn, H. Gmuender, P. Hebeisen, H. Link, R. Masciadri, J. Nielsen, *Pharmacol. Ther.* **1993**, *60*, 367–380.
- [159] N. Nakada, H. Gmünder, T. Hirata, M. Arisawa, *Antimicrob. Agents Chemother.* **1994**, *38*, 1966–1973.
- [160] G. S. Bisacchi, J. I. Manchester, *ACS Infect. Dis.* **2015**, *1*, 4–41.
- [161] P. Angehrn, S. Buchmann, C. Funk, E. Goetschi, H. Gmuender, P. Hebeisen, D. Kostrewa, H. Link, T. Luebbers, R. Masciadri et al., *J. Med. Chem.* **2004**, *47*, 1487–1513.
- [162] J. M. Hamilton-Miller, *Antimicrob. Agents Chemother.* **1995**, *39*, 2375–2377.
- [163] R. Hirano, W. Sasamoto, A. Matsumoto, H. Itakura, O. Igarashi, K. Kondo, *J. Nutr. Sci. Vitaminol.* **2001**, *47*, 357–362.
- [164] J. K. Kemberling, J. A. Hampton, R. W. Keck, M. A. Gomez, S. H. Selman, *J. Urol.* **2003**, *170*, 773–776.
- [165] J. B. Calixto, M. M. Campos, M. F. Otuki, A. R. Santos, *Planta Med.* **2004**, *70*, 93–103.
- [166] K. Kono, I. Tataru, S. Takeda, K. Arakawa, Y. Hara, *Kansenshogaku Zasshi* **1994**, *68*, 1518–1522.
- [167] H. Gradisar, P. Pristovsek, A. Plaper, R. Jerala, *J. Med. Chem.* **2007**, *50*, 264–271.
- [168] H. Ikigai, T. Nakae, Y. Hara, T. Shimamura, *BBA Biomembranes* **1993**, *1147*, 132–136.
- [169] Y.-M. Zhang, C. O. Rock, *J. Biol. Chem.* **2004**, *279*, 30994–31001.
- [170] W.-H. Zhao, N. Asano, Z.-Q. Hu, T. Shimamura, *J. Pharm. Pharmacol.* **2003**, *55*, 735–740.
- [171] F.-Y. Fan, L.-X. Sang, M. Jiang, *Molecules* **2017**, *22*, 1–29.
- [172] A. Sudano Roccaro, A. R. Blanco, F. Giuliano, D. Rusciano, V. Enea, *Antimicrob. Agents Chemother.* **2004**, *48*, 1968–1973.
- [173] P. D. Stapleton, S. Shah, Y. Hara, P. W. Taylor, *Antimicrob. Agents Chemother.* **2006**, *50*, 752–755.

- [174] T. P. Tiwari, S. K. Bharti, H. D. Kaur, R. P. Dikshit, G. S. Hoondal, *Indian J. Med. Res.* **2005**, *122*, 80–84.
- [175] J. H. Daugrois, R. Boisne-Noc, P. Rott, *Plant Dis.* **2014**, *98*, 191–196.
- [176] M. Dal-Bianco, M. S. Carneiro, C. T. Hotta, R. G. Chapola, H. P. Hoffmann, A. A. F. Garcia, G. M. Souza, *Curr. Opin. Biotechnol.* **2012**, *23*, 265–270.
- [177] M. Royer, L. Costet, E. Vivien, M. Bes, A. Cousin, A. Damais, I. Pieretti, A. Savin, S. Megessier, M. Viard et al., *Mol. Plant Microbe Interact.* **2004**, *17*, 414–427.
- [178] M. S. Ntambo, J.-Y. Meng, P. C. Rott, M. Royer, L.-H. Lin, H.-L. Zhang, S.-J. Gao, *Plant. Pathol.* **2019**, *68*, 269–277.
- [179] R. G. Birch, *Phytopathology* **1983**, *73*, 1368.
- [180] R. G. Birch, S. S. Patil, *J. Gen. Microbiol.* **1985**, *131*, 1069–1075.
- [181] R. G. Birch, S. S. Patil, *Physiol. Mol. Plant Pathol.* **1987**, *30*, 199–206.
- [182] L. Zhang, R. G. Birch, *Proc. Natl. Acad. Sci. U.S.A.* **1997**, *94*, 9984–9989.
- [183] C. B. Monteiro-Vitorello, L. E. A. Camargo, M. A. van Sluys, J. P. Kitajima, D. Truffi, A. M. do Amaral, R. Harakava, J. C. F. de Oliveira, D. Wood, M. C. de Oliveira et al., *Mol. Plant Microbe Interact.* **2004**, *17*, 827–836.
- [184] S. M. Hashimi, M. K. Wall, A. B. Smith, A. Maxwell, R. G. Birch, *Antimicrob. Agents Chemother.* **2007**, *51*, 181–187.
- [185] J. Kretz, D. Kerwat, V. Schubert, S. Grätz, A. Pesic, S. Semsary, S. Cociancich, M. Royer, R. D. Süssmuth, *Angew. Chem. Int. Ed.* **2015**, *54*, 1969–1973.
- [186] R. G. Birch, S. S. Patil, *Antibiotic and process for the production thereof*, US4525354, **1985**.
- [187] L. Zhang, J. Xu, R. G. Birch, *J. Appl. Microbiol.* **1998**, *85*, 1023–1028.
- [188] E. Vivien, D. Pitorre, S. Cociancich, I. Pieretti, D. W. Gabriel, P. C. Rott, M. Royer, *Antimicrob. Agents Chemother.* **2007**, *51*, 1549–1552.
- [189] S. Cociancich, A. Pesic, D. Petras, S. Uhlmann, J. Kretz, V. Schubert, L. Vieweg, S. Duplan, M. Marguerettaz, J. Noëll et al., *Nat. Chem. Biol.* **2015**, *11*, 195–197.
- [190] P. C. Rott, L. Costet, M. J. Davis, R. Frutos, D. W. Gabriel, *J. Bacteriol.* **1996**, *178*, 4590–4596.
- [191] M. Royer, D. W. Gabriel, R. Frutos, P. Rott., *Complete biosynthetic gene set for synthesis of polyketide antibiotics, including the albicidin family, resistance genes, and uses thereof*, US0269988-A1, **2006**.
- [192] E. Vivien, S. Megessier, I. Pieretti, S. Cociancich, R. Frutos, D. W. Gabriel, P. C. Rott, M. Royer, *FEMS Microbiol. Lett.* **2005**, *251*, 81–89.
- [193] F. Lipmann, *Acc. Chem. Res.* **1973**, *6*, 361–367.
- [194] H. Kleinkauf, H. von Döhren, *Eur. J. Biochem.* **1990**, *192*, 1–15.
- [195] T. Stachelhaus, M. A. Marahiel, *FEMS Microbiol. Lett.* **1995**, *125*, 3–14.
- [196] R. D. Süssmuth, A. Mainz, *Angew. Chem. Int. Ed.* **2017**, *56*, 3770–3821.
- [197] G. Huang, L. Zhang, R. G. Birch, *Gene* **2000**, *258*, 193–199.
- [198] F. Dosselaere, J. Vanderleyden, *Crit. Rev. Microbiol.* **2001**, *27*, 75–131.
- [199] A. Nieweg, E. Bremer, *Microbiology* **1997**, *143*, 603–615.
- [200] H. Nikaido, *Antimicrob. Agents Chemother.* **1989**, *33*, 1831–1836.

- [201] R. Hancock, *Trends Microbiol.* **1997**, *5*, 37–42.
- [202] H. Nikaido, M. Vaara, *Microbiol. Rev.* **1985**, *49*, 1–32.
- [203] H. Nikaido, *Mol. Microbiol.* **1992**, *6*, 435–442.
- [204] K. Postle, *Mol. Microbiol.* **1990**, *4*, 2019–2025.
- [205] R. J. Kadner, *Mol. Microbiol.* **1990**, *4*, 2027–2033.
- [206] H. Killmann, R. Benz, V. Braun, *EMBO J.* **1993**, *12*, 3007–3016.
- [207] M. S. Weiss, A. Kreuzsch, E. Schiltz, U. Nestel, W. Welte, J. Weckesser, G. E. Schulz, *FEBS Lett.* **1991**, *280*, 379–382.
- [208] S. W. Cowan, T. Schirmer, G. Rummel, M. Steiert, R. Ghosh, R. A. Pauptit, J. N. Jansonius, J. P. Rosenbusch, *Nature* **1992**, *358*, 727–733.
- [209] A. Kreuzsch, G. E. Schulz, *J. Mol. Biol.* **1994**, *243*, 891–905.
- [210] R. Koebnik, K. P. Locher, P. van Gelder, *Mol. Microbiol.* **2000**, *37*, 239–253.
- [211] M. Luckey, H. Nikaido, *Proc. Natl. Acad. Sci. U.S.A.* **1980**, *77*, 167–171.
- [212] P. van Gelder, R. Dutzler, F. Dumas, R. Koebnik, T. Schirmer, *Protein Eng.* **2001**, *14*, 943–948.
- [213] C. Hardesty, C. Ferran, J. M. DiRienzo, *J. Bacteriol.* **1991**, *173*, 449–456.
- [214] T. Schirmer, T. A. Keller, Y. F. Wang, J. P. Rosenbusch, *Science* **1995**, *267*, 512–514.
- [215] R. Benz in *New Comprehensive Biochemistry, Vol. 27* (Eds.: J. M. Ghuysen, R. Hakenbeck), Elsevier, Amsterdam, **1994**, pp. 397–423.
- [216] H. Nikaido, *J. Biol. Chem.* **1994**, *269*, 3905–3908.
- [217] K. Hantke, *FEBS Lett.* **1976**, *70*, 109–112.
- [218] H. J. Krieger-Brauer, V. Braun, *Arch. Microbiol.* **1980**, *124*, 233–242.
- [219] H. Fsihi, B. Kottwitz, E. Bremer, *J. Biol. Chem.* **1993**, *268*, 17495–17503.
- [220] W. van Alphen, N. van Seim, B. Lugtenberg, *Mol. Gen. Genet.* **1978**, *159*, 75–83.
- [221] R. Benz, A. Schmid, C. Maier, E. Bremer, *Eur. J. Biochem.* **1988**, *176*, 699–705.
- [222] C. Maier, E. Bremer, A. Schmid, R. Benz, *J. Biol. Chem.* **1988**, *263*, 2493–2499.
- [223] E. Bremer, A. Middendorf, J. Martinussen, P. Valentin-Hansen, *Gene* **1990**, *96*, 59–65.
- [224] J. Ye, B. van den Berg, *EMBO J.* **2004**, *23*, 3187–3195.
- [225] R. G. Birch, J. M. Pemberton, W. V. Basnayake, *J. Gen. Microbiol.* **1990**, *136*, 51–58.
- [226] S. M. Hashimi, G. Huang, A. Maxwell, R. G. Birch, *Antimicrob. Agents Chemother.* **2008**, *52*, 1382–1390.
- [227] S. E. Critchlow, M. H. O'Dea, A. J. Howells, M. Couturier, M. Gellert, A. Maxwell, *J. Mol. Biol.* **1997**, *273*, 826–839.
- [228] O. A. Pierrat, A. Maxwell, *J. Biol. Chem.* **2003**, *278*, 35016–35023.
- [229] O. A. Pierrat, A. Maxwell, *Biochemistry* **2005**, *44*, 4204–4215.
- [230] J. M. Bostock, G. Huang, S. M. Hashimi, L. Zhang, R. G. Birch, *J. Appl. Microbiol.* **2006**, *101*, 151–160.
- [231] J. H. Tran, G. A. Jacoby, *Proc. Natl. Acad. Sci. U.S.A.* **2002**, *99*, 5638–5642.
- [232] C. Montero, G. Mateu, R. Rodriguez, H. Takiff, *Antimicrob. Agents Chemother.* **2001**, *45*, 3387–3392.

- [233] S. S. Hegde, M. W. Vetting, S. L. Roderick, L. A. Mitchenall, A. Maxwell, H. E. Takiff, J. S. Blanchard, *Science* **2005**, *308*, 1480–1483.
- [234] L. Zhang, R. G. Birch, *Lett. Appl. Microbiol.* **1996**, *22*, 132–136.
- [235] L. Zhang, R. G. Birch, *J. Appl. Microbiol.* **1997**, *82*, 448–454.
- [236] L. Zhang, J. Xu, R. G. Birch, *Nat. Biotechnol.* **1999**, *17*, 1021–1024.
- [237] L. Vieweg, J. Kretz, A. Pesic, D. Kerwat, S. Grätz, M. Royer, S. Cociancich, A. Mainz, R. D. Süßmuth, *J. Am. Chem. Soc.* **2015**, *137*, 7608–7611.
- [238] M. J. Walker, R. G. Birch, J. M. Pemberton, *Mol. Microbiol.* **1988**, *2*, 443–454.
- [239] L. Zhang, J. Xu, R. G. Birch, *Microbiology* **1998**, *144*, 555–559.
- [240] L.-X. Weng, J.-L. Xu, Q. Li, R. G. Birch, L.-H. Zhang, *Microbiology* **2003**, *149*, 451–457.
- [241] L.-X. Weng, L.-H. Wang, J.-L. Xu, J.-E. Wu, Q. Li, L.-H. Zhang, *Appl. Environ. Microbiol.* **2005**, *71*, 1445–1452.
- [242] W. V. Basnayake, R. G. Birch, *Microbiology* **1995**, *141* (Pt. 3), 551–560.
- [243] L. Rostock, R. Driller, S. Grätz, D. Kerwat, L. von Eckardstein, D. Petras, M. Kunert, C. Alings, F.-J. Schmitt, T. Friedrich et al., *Nat. Commun.* **2018**, *9*, 3095.
- [244] N. L. Brown, J. V. Stoyanov, S. P. Kidd, J. L. Hobman, *FEMS Microbiol. Rev.* **2003**, *27*, 145–163.
- [245] K. J. Newberry, R. G. Brennan, *J. Biol. Chem.* **2004**, *279*, 20356–20362.
- [246] K. J. Newberry, J. L. Huffman, M. C. Miller, N. Vazquez-Laslop, A. A. Neyfakh, R. G. Brennan, *J. Biol. Chem.* **2008**, *283*, 26795–26804.
- [247] S. Watanabe, A. Kita, K. Kobayashi, K. Miki, *Proc. Natl. Acad. Sci. U.S.A.* **2008**, *105*, 4121–4126.
- [248] T. Murakami, T. G. Holt, C. J. Thompson, *J. Bacteriol.* **1989**, *171*, 1459–1466.
- [249] D. J. Holmes, J. L. Caso, C. J. Thompson, *EMBO J.* **1993**, *12*, 3183–3191.
- [250] J. Habazettl, M. Allan, P. R. Jensen, H.-J. Sass, C. J. Thompson, S. Grzesiek, *Proc. Natl. Acad. Sci. U.S.A.* **2014**, *111*, E5498–E5507.
- [251] A. Sikandar, K. Cirnski, G. Testolin, C. Volz, M. Brönstrup, O. V. Kalinina, R. Müller, J. Koehnke, *J. Am. Chem. Soc.* **2018**, *140*, 16641–16649.
- [252] R. D. Süßmuth, J. Kretz, V. Schubert, A. Pesic, M. Hügelland, M. Royer, S. Cociancich, P. Rott, D. Kerwat, S. Grätz, *Albicidin derivatives, their use and synthesis*, WO2014125075A1, **2014**.
- [253] A. Yamamoto, K. Nakamura, K. Furukawa, Y. Konishi, T. Ogino, K. Higashiura, H. Yago, K. Okamoto, M. Otsuka, *Chem. Pharm. Bull.* **2002**, *50*, 47–52.
- [254] C. Stammer, *J. Org. Chem.* **1961**, *26*, 2556–2560.
- [255] D. V. Kashelkar, C. Ressler, *J. Am. Chem. Soc.* **1964**, *86*, 2467–2473.
- [256] S. Mojsov, A. R. Mitchell, R. B. Merrifield, *J. Org. Chem.* **1980**, *45*, 555–560.
- [257] S. Kato, T. Morie, *J. Heterocycl. Chem.* **1996**, *33*, 1171–1178.
- [258] M. S. Tichenor, D. B. Kastinsky, D. L. Boger, *J. Am. Chem. Soc.* **2004**, *126*, 8396–8398.
- [259] B. Thern, J. Rudolph, G. Jung, *Angew. Chem. Int. Ed.* **2002**, *41*, 2307–2309.
- [260] B. Thern, J. Rudolph, G. Jung, *Tetrahedron Lett.* **2002**, *43*, 5013–5016.

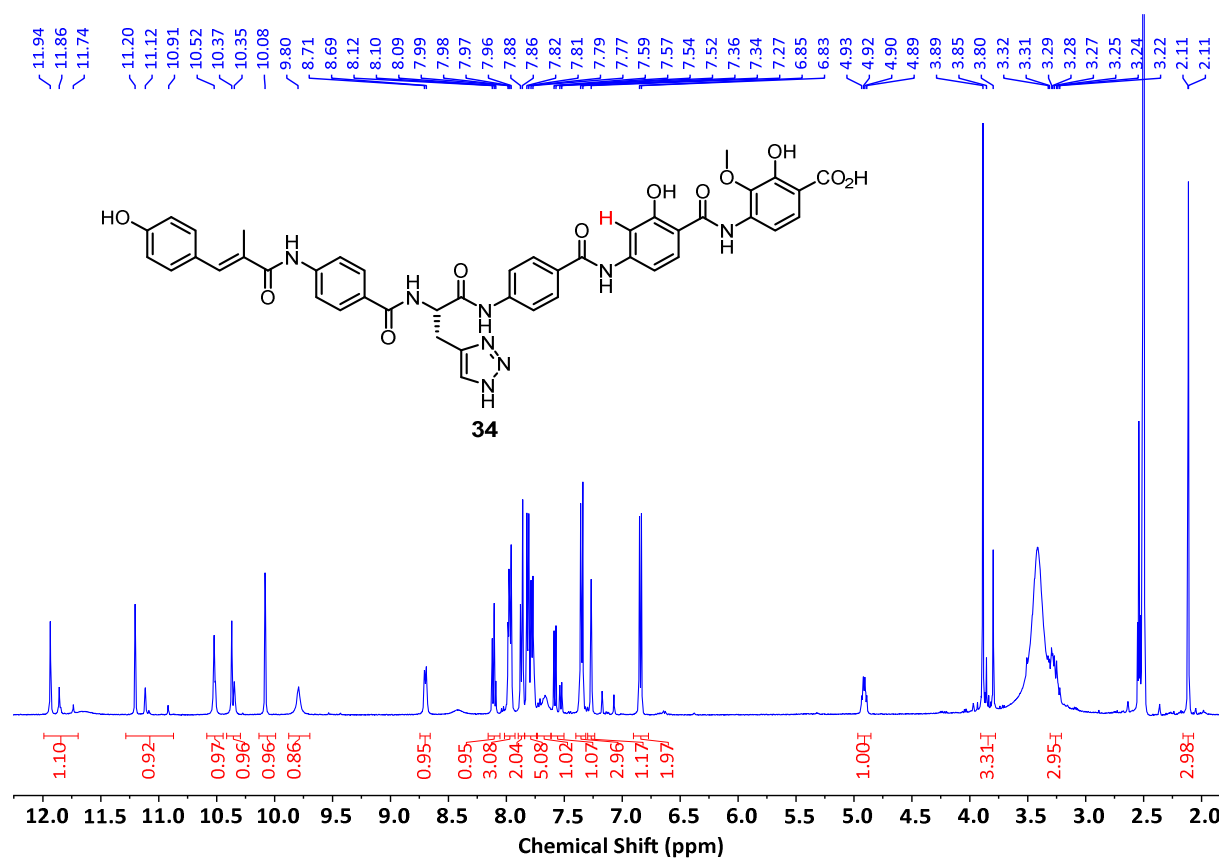
- [261] C. A. Lipinski, F. Lombardo, B. W. Dominy, P. J. Feeney, *Adv. Drug Delivery Rev.* **2001**, *46*, 3–26.
- [262] F. von Nussbaum, M. Brands, B. Hinzen, S. Weigand, D. Häbich, *Angew. Chem. Int. Ed.* **2006**, *45*, 5072–5129.
- [263] C. A. S. Bergström, P. Larsson, *Int. J. Pharm.* **2018**, *540*, 185–193.
- [264] P. Fasinu, V. Pillay, V. M. K. Ndesendo, L. C. Du Toit, Y. E. Choonara, *Biopharm. Drug Dispos.* **2011**, *32*, 185–209.
- [265] K. T. Savjani, A. K. Gajjar, J. K. Savjani, *ISRN Pharm.* **2012**, *2012*, 195727.
- [266] H. Nikaido, *Semin. Cell Dev. Biol.* **2001**, *12*, 215–223.
- [267] T. Bohnert, L.-S. Gan, *J. Pharm. Sci.* **2013**, *102*, 2953–2994.
- [268] N. J. Yang, M. J. Hinner, *Methods Mol. Biol.* **2015**, *1266*, 29–53.
- [269] D. Kerwat, S. Grätz, J. Kretz, M. Seidel, M. Kunert, J. B. Weston, R. D. Süßmuth, *ChemMedChem* **2016**, *11*, 1899–1903.
- [270] S. Grätz, D. Kerwat, J. Kretz, L. von Eckardstein, S. Semsary, M. Seidel, M. Kunert, J. B. Weston, R. D. Süßmuth, *ChemMedChem* **2016**, *11*, 1499–1502.
- [271] S. Baumann, J. Herrmann, R. Raju, H. Steinmetz, K. I. Mohr, S. Hüttel, K. Harmrolfs, M. Stadler, R. Müller, *Angew. Chem. Int. Ed.* **2014**, *53*, 14605–14609.
- [272] Y. J. Kim, H.-J. Kim, G.-W. Kim, K. Cho, S. Takahashi, H. Koshino, W.-G. Kim, *J. Nat. Prod.* **2016**, *79*, 2223–2228.
- [273] I. Behroz, P. Durkin, S. Grätz, M. Seidel, L. Rostock, M. Spinczyk, J. B. Weston, R. D. Süßmuth, *Chem. Eur. J.* **2019**, *25*, 16538–16543.
- [274] S. Roux, M. Ligeti, D.-A. Buisson, B. Rousseau, J.-C. Cintrat, *Amino Acids* **2010**, *38*, 279–286.
- [275] D. Petras, D. Kerwat, A. Pesic, B.-F. Hempel, L. von Eckardstein, S. Semsary, J. Arasté, M. Marguerettaz, M. Royer, S. Cociancich et al., *ACS Chem. Biol.* **2016**, *11*, 1198–1204.
- [276] E. P. Gillis, K. J. Eastman, M. D. Hill, D. J. Donnelly, N. A. Meanwell, *J. Med. Chem.* **2015**, *58*, 8315–8359.
- [277] B. K. Park, N. R. Kitteringham, *Drug Metab. Rev.* **1994**, *26*, 605–643.
- [278] B. K. Park, N. R. Kitteringham, P. M. O'Neill, *Annu. Rev. Pharmacol. Toxicol.* **2001**, *41*, 443–470.
- [279] L. B. Turner, I. Mueller-Harvey, A. B. McAllan, *Phytochemistry* **1993**, *33*, 791–796.
- [280] L. von Eckardstein, D. Petras, T. Dang, S. Cociancich, S. Sabri, S. Grätz, D. Kerwat, M. Seidel, A. Pesic, P. C. Dorrestein et al., *Chem. Eur. J.* **2017**, *23*, 15316–15321.
- [281] B. Cheng, R. Müller, D. Trauner, *Angew. Chem. Int. Ed.* **2017**, *56*, 12755–12759.
- [282] S. Hüttel, G. Testolin, J. Herrmann, T. Planke, F. Gille, M. Moreno, M. Stadler, M. Brönstrup, A. Kirschning, R. Müller, *Angew. Chem. Int. Ed.* **2017**, *56*, 12760–12764.
- [283] Y. Ito, I. Washio, M. Ueda, *Macromolecules* **2008**, *41*, 2778–2784.
- [284] B. Belleau, G. Malek, *J. Am. Chem. Soc.* **1968**, *90*, 1651–1652.
- [285] E. Valeur, M. Bradley, *Chem. Soc. Rev.* **2009**, *38*, 606–631.
- [286] S. Grätz, *Synthese von Derivaten von Albicidin zur Untersuchung von Struktur-Aktivitäts-Beziehungen*, Berlin, **2017**.

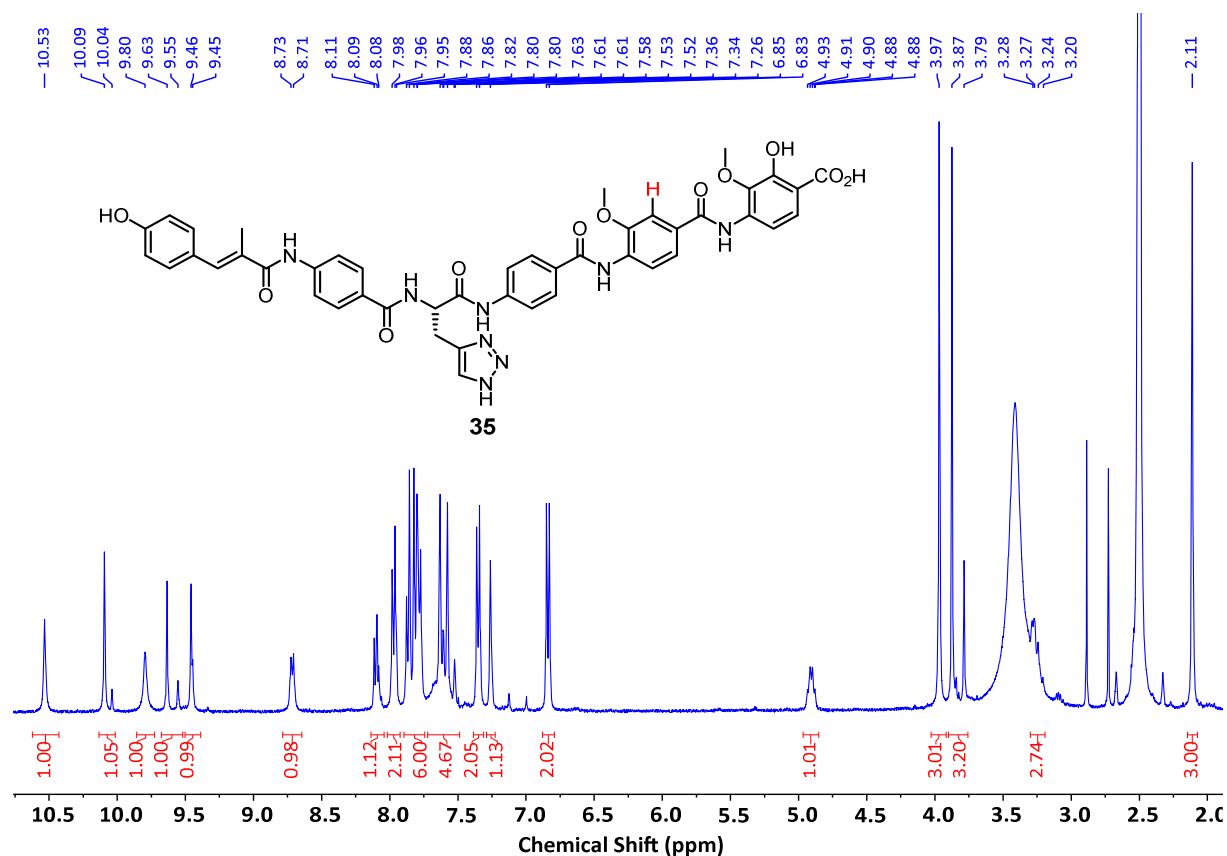
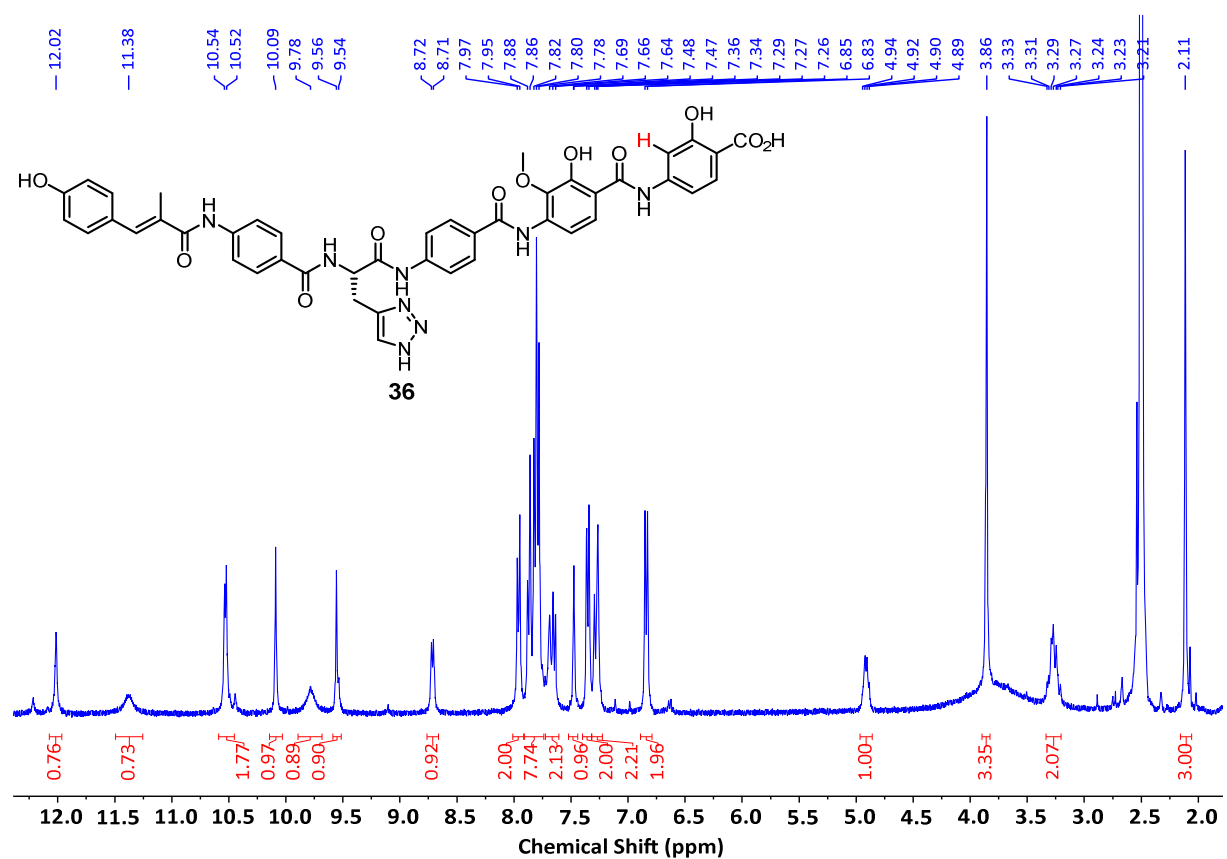
- [287] J. Clayden, W. J. Moran, P. J. Edwards, S. R. LaPlante, *Angew. Chem. Int. Ed.* **2009**, *48*, 6398–6401.
- [288] C. W. Ford, R. D. Hartley, *J. Sci. Food Agric.* **1989**, *46*, 301–310.
- [289] R. D. Hartley, E. C. Jones, *J. Chromatogr. A.* **1975**, *107*, 213–218.
- [290] G.H.N. Towers, B. Abeysekera, *Phytochemistry* **1984**, *23*, 951–952.
- [291] F. D. Lewis, J. E. Elbert, A. L. Uthagrove, P. D. Hale, *J. Am. Chem. Soc.* **1988**, *110*, 5191–5192.
- [292] F. D. Lewis, J. E. Elbert, A. L. Uthagrove, P. D. Hale, *J. Org. Chem.* **1991**, *56*, 553–561.
- [293] N. Sagawa, T. Shikata, *Phys. Chem. Chem. Phys.* **2014**, *16*, 13262–13270.
- [294] N. J. Harper, S. E. Fullerton, *J. Med. Pharm. Chem.* **1961**, *4*, 297–316.
- [295] T. T. Talele, *J. Med. Chem.* **2020**, *63*, 5625–5663.
- [296] E. de Clercq, *Int. J. Antimicrob. Agents* **2009**, *33*, 307–320.
- [297] Y. El Safadi, V. Vivet-Boudou, R. Marquet, *Appl. Microbiol. Biotechnol.* **2007**, *75*, 723–737.
- [298] A. E. Mutlib, H. Chen, G. Nemeth, L. S. Gan, D. D. Christ, *Drug Metab. Dispos.* **1999**, *27*, 1045–1056.
- [299] A. E. Mutlib, R. J. Gerson, P. C. Meunier, P. J. Haley, H. Chen, L. S. Gan, M. H. Davies, B. Gemzik, D. D. Christ, D. F. Krahn et al., *Toxicol. Appl. Pharmacol.* **2000**, *169*, 102–113.
- [300] I. N. White, *Biochem. J.* **1978**, *174*, 853–861.
- [301] F. P. Guengerich, *Mol. Pharmacol.* **1988**, *33*, 500–508.
- [302] A. Choudhary, R. T. Raines, *ChemBioChem* **2011**, *12*, 1801–1807.
- [303] M. M. Hann, P. G. Sammes, P. D. Kennewell, J. B. Taylor, *J. Chem. Soc., Chem. Commun.* **1980**, 234–235.
- [304] C. Ballatore, D. M. Hury, A. B. Smith, *ChemMedChem* **2013**, *8*, 385–395.
- [305] D. J. Sheffler, C. J. Wenthur, J. A. Bruner, S. J. S. Carrington, P. N. Vinson, K. K. Gogi, A. L. Blobaum, R. D. Morrison, M. Vamos, N. D. P. Cosford et al., *Bioorg. Med. Chem. Lett.* **2012**, *22*, 3921–3925.
- [306] C. J. Wenthur, R. Morrison, A. S. Felts, K. A. Smith, J. L. Engers, F. W. Byers, J. S. Daniels, K. A. Emmitte, P. J. Conn, C. W. Lindsley, *J. Med. Chem.* **2013**, *56*, 5208–5212.
- [307] H. J. Li, L. Wang, *Eur. J. Org. Chem.* **2006**, *22*, 5099–5102.
- [308] J. Santandrea, C. Minozzi, C. Cruché, S. K. Collins, *Angew. Chem. Int. Ed.* **2017**, *56*, 12255–12259.
- [309] S. Bhagat, V. Telvekar, *Synlett* **2018**, *29*, 874–879.

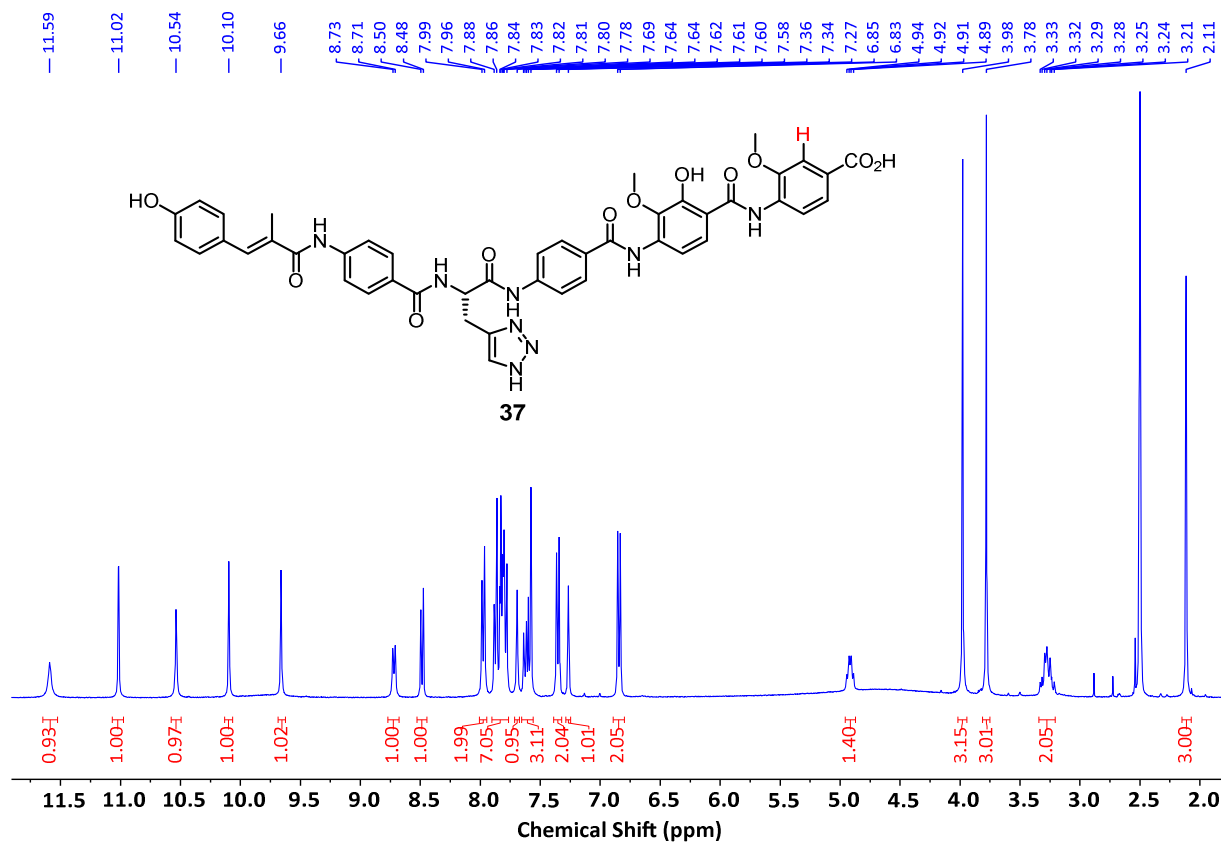
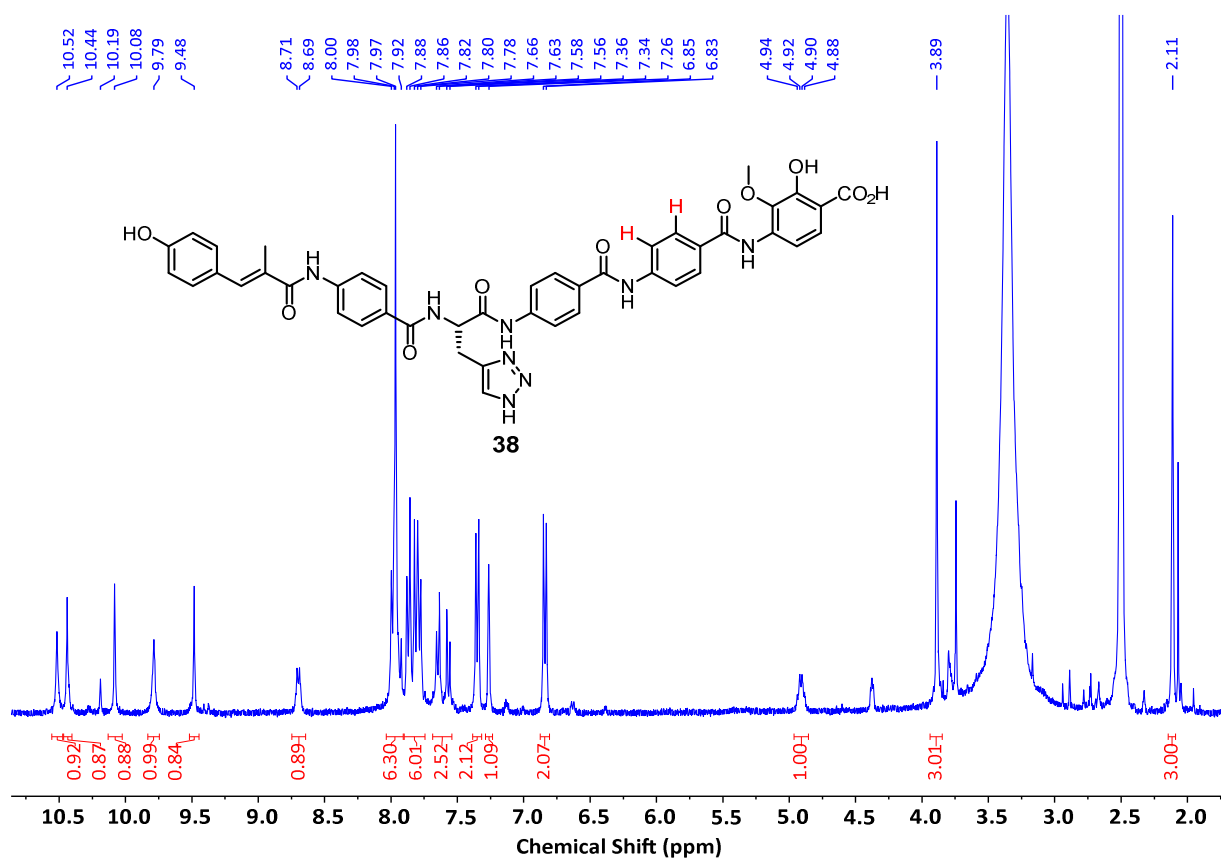
7 Appendix

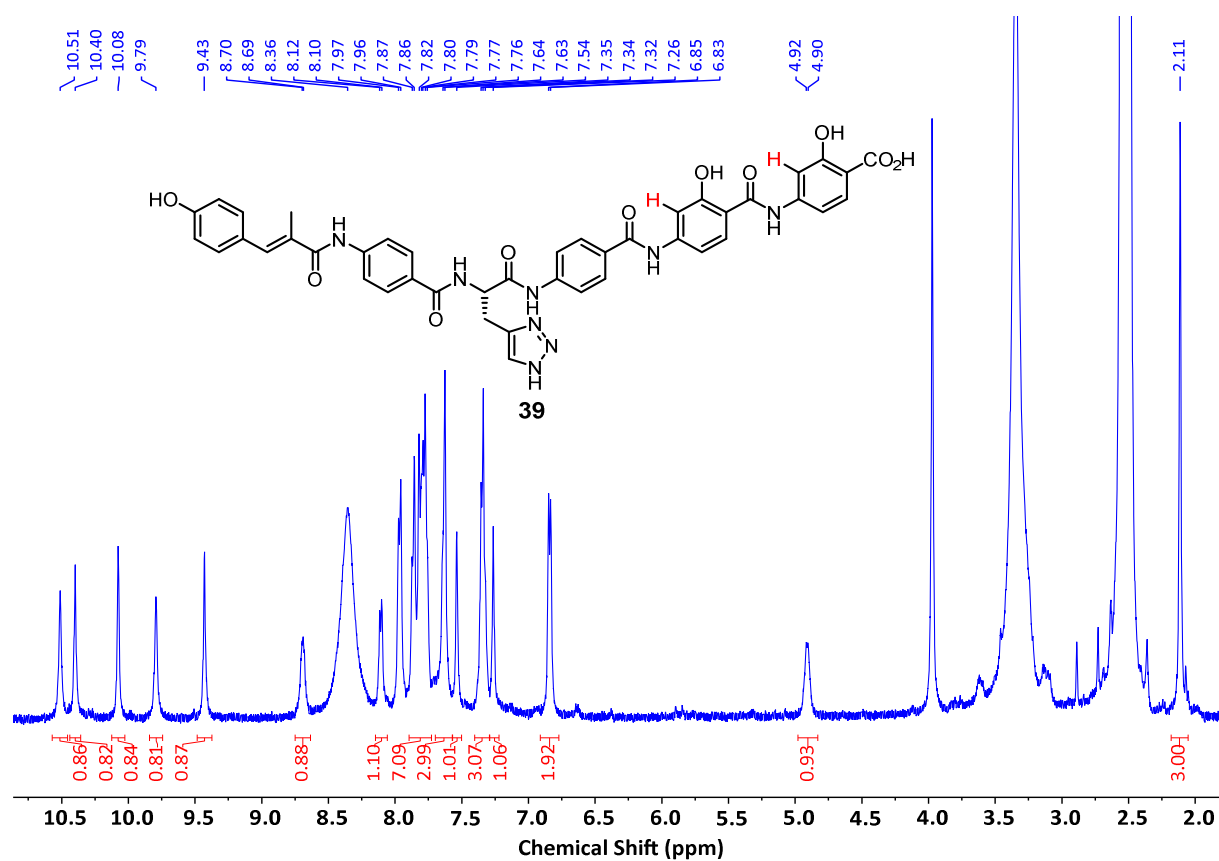
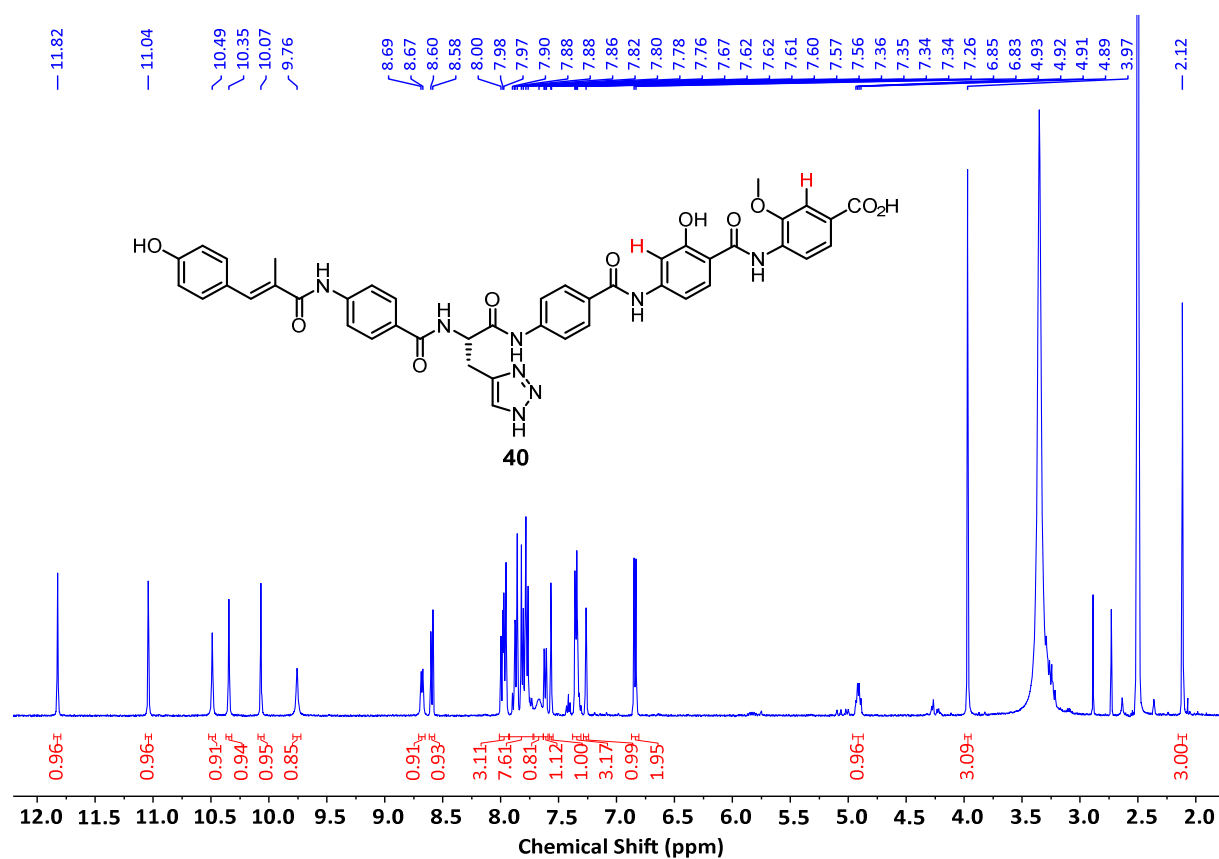
Selected NMR spectra of final albicidin derivatives with variations of the C-terminal dipeptide (**34–58**) and with modified A-B fragments (**247–259**), respectively, are shown below.

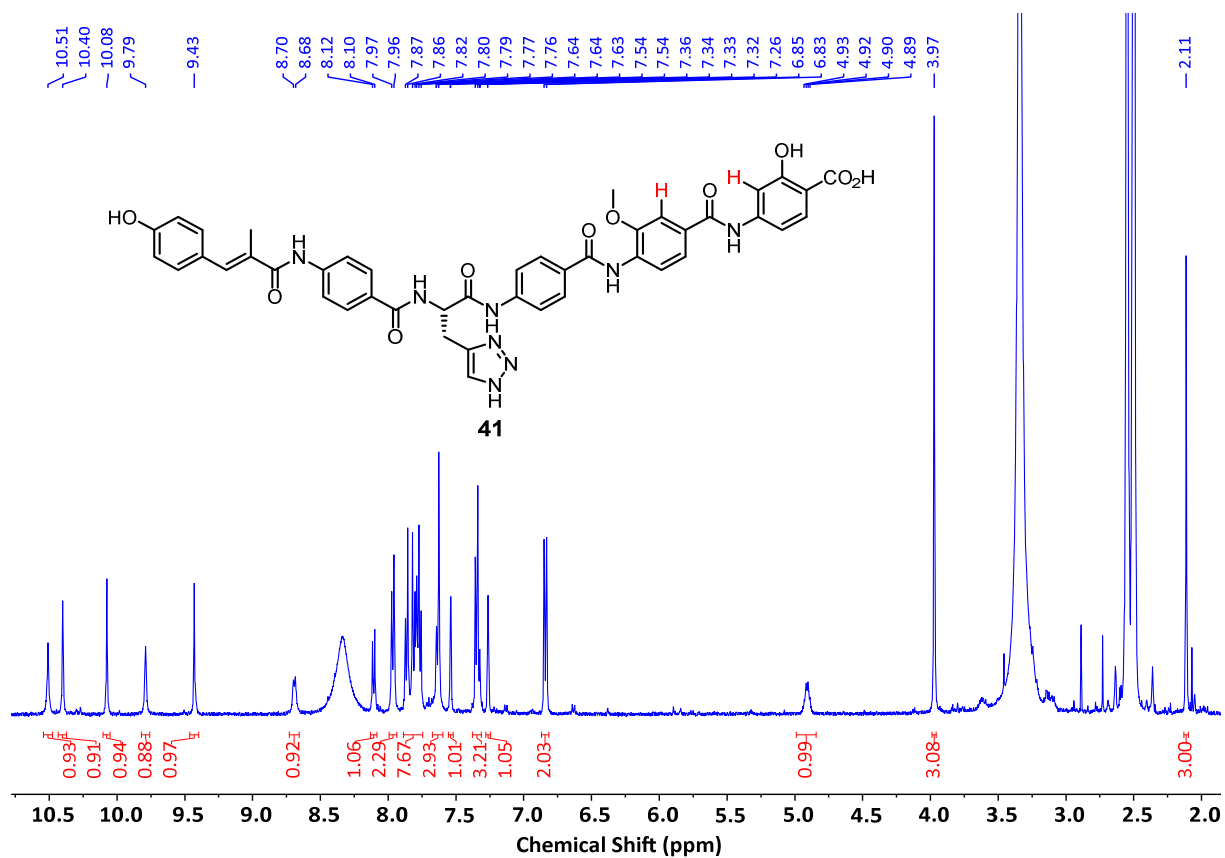
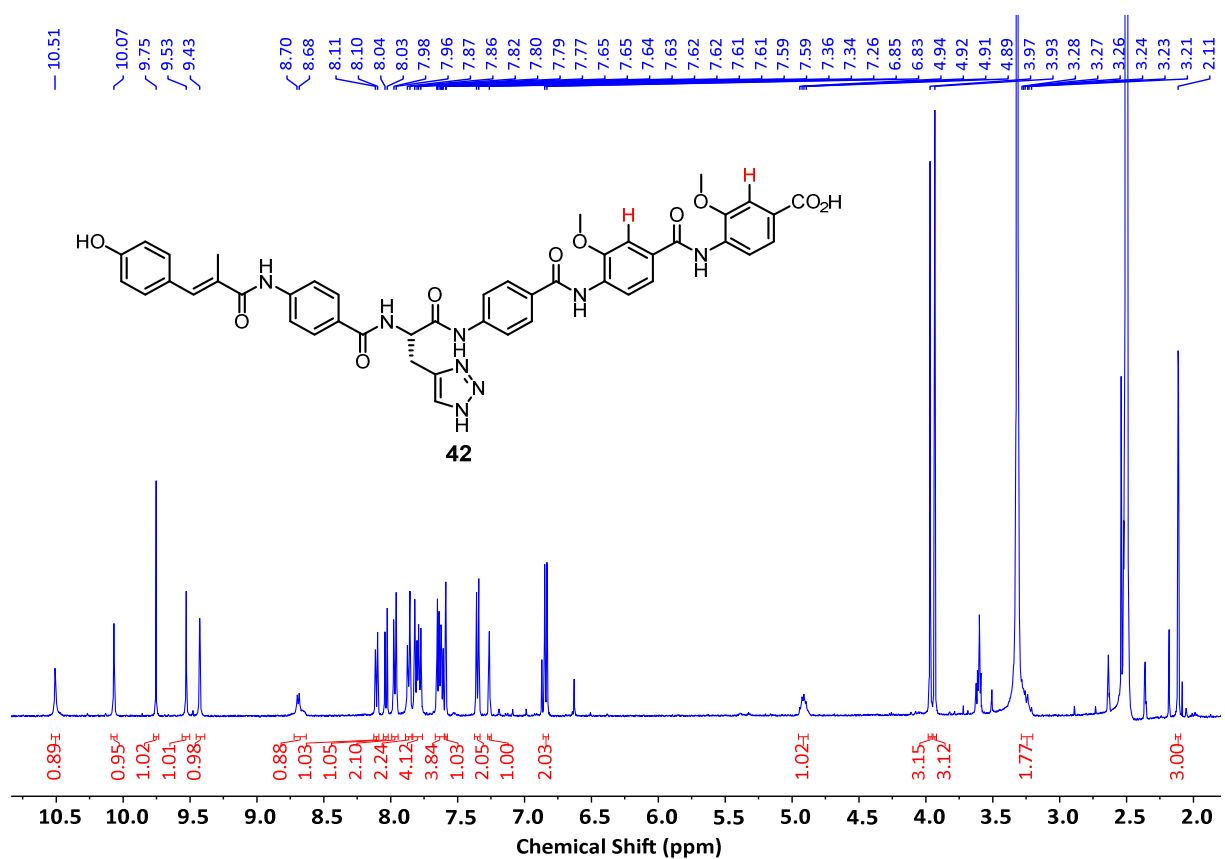
Final Derivative **34**

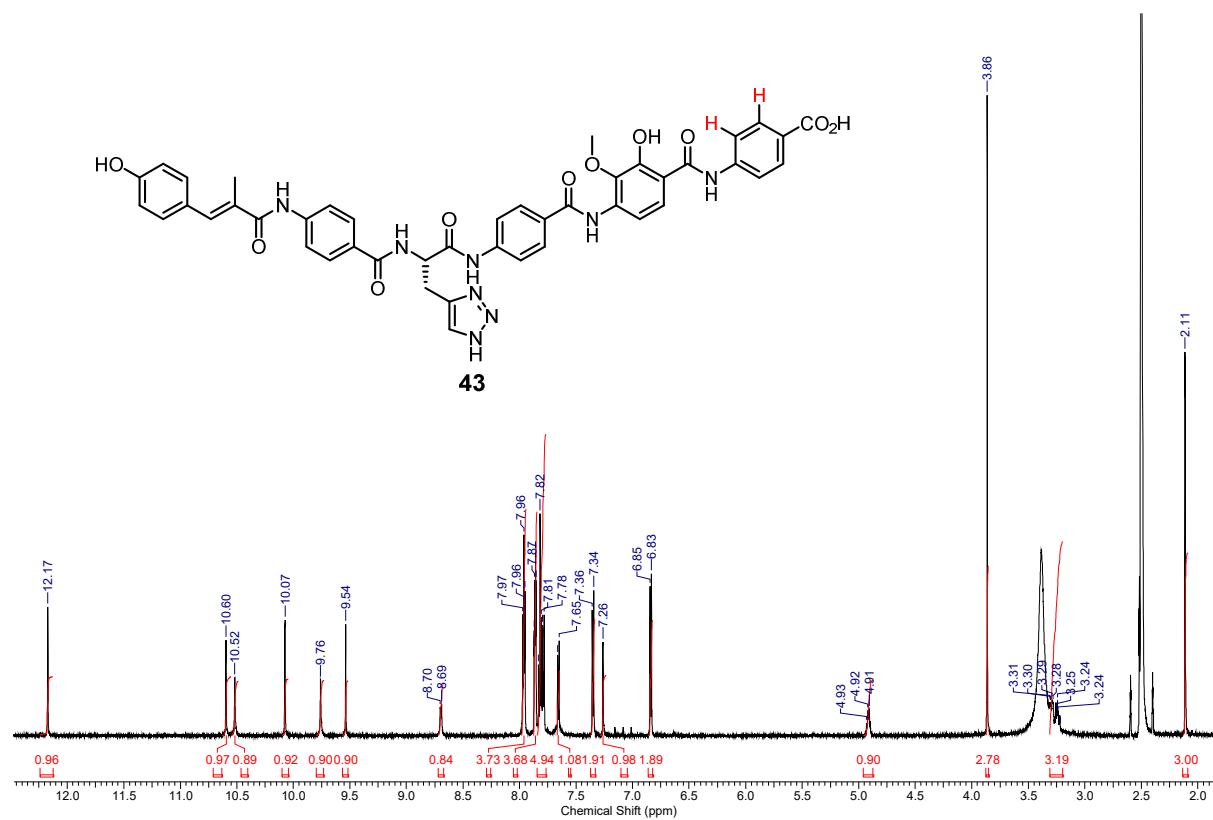
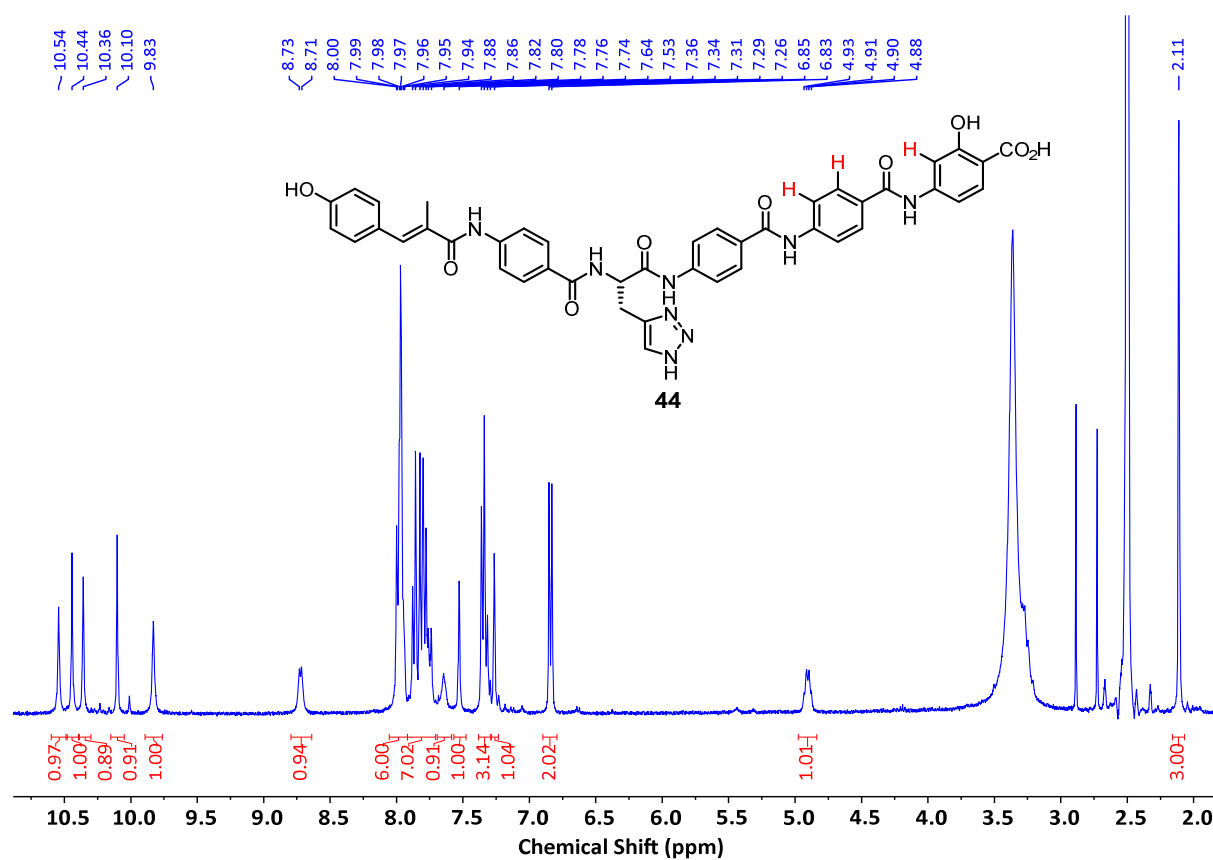


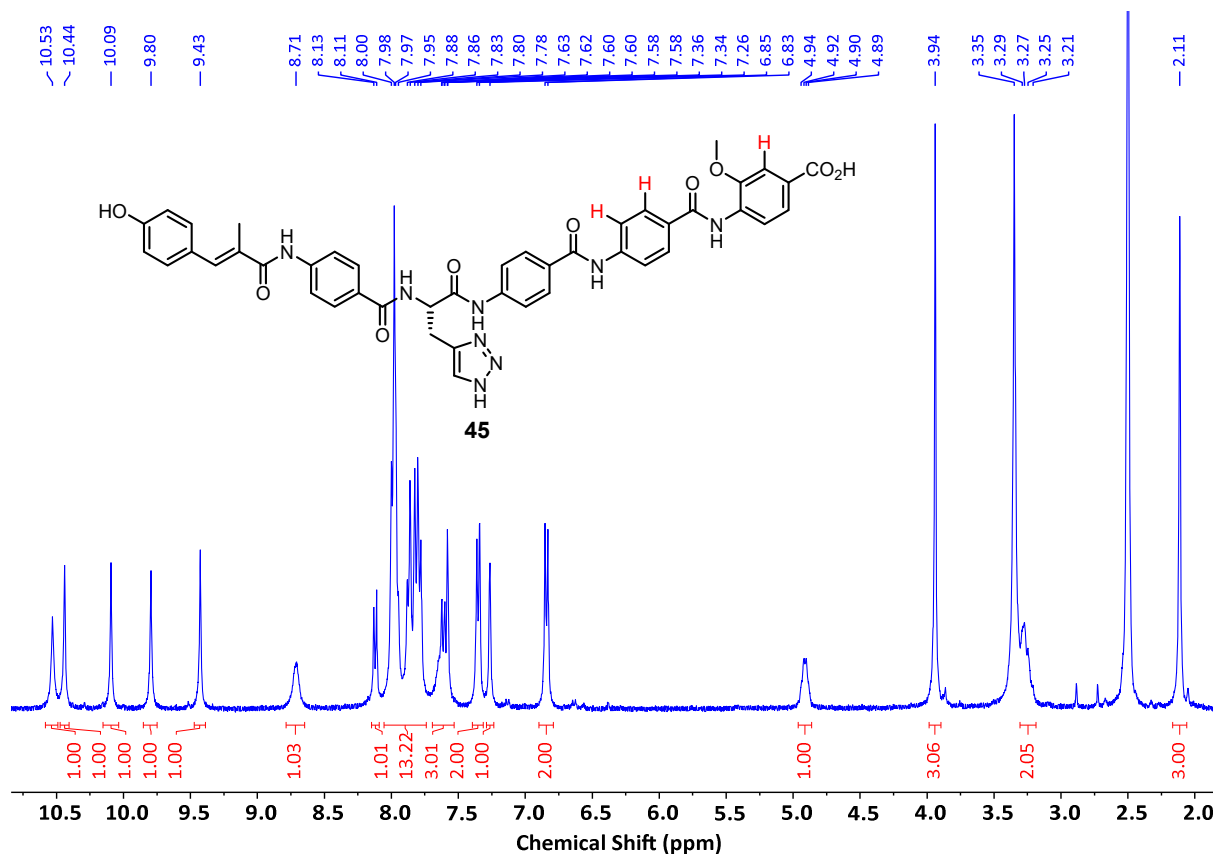
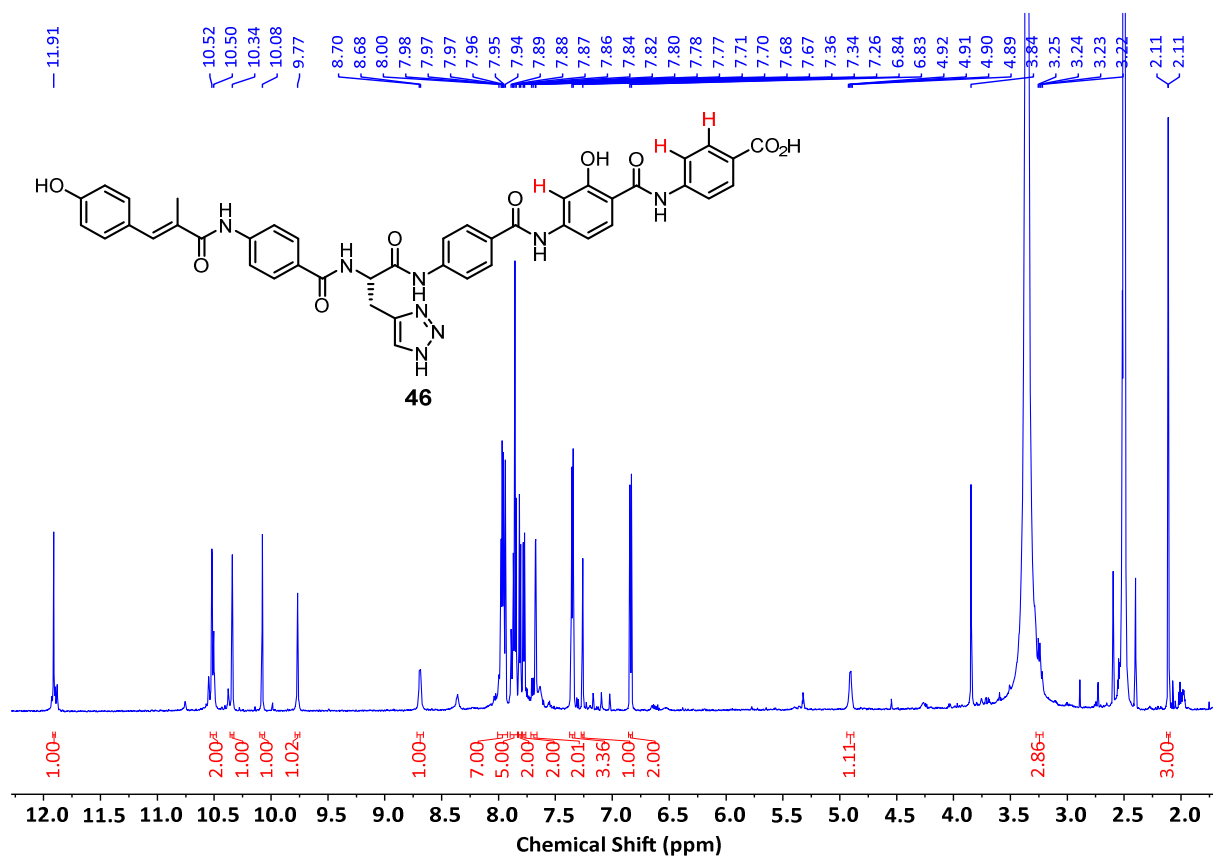
Final Derivative **35**Final Derivative **36**

Final Derivative **37**Final Derivative **38**

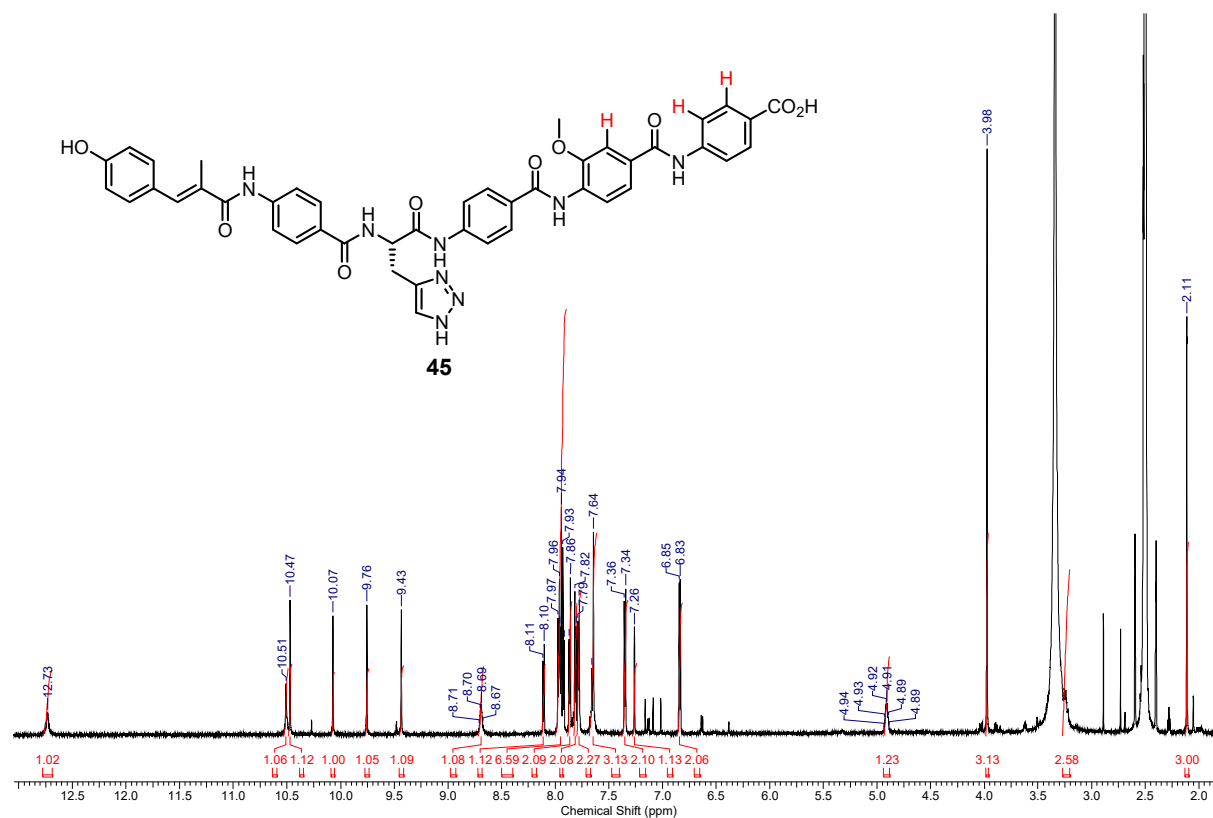
Final Derivative **39**Final Derivative **40**

Final Derivative **41**Final Derivative **42**

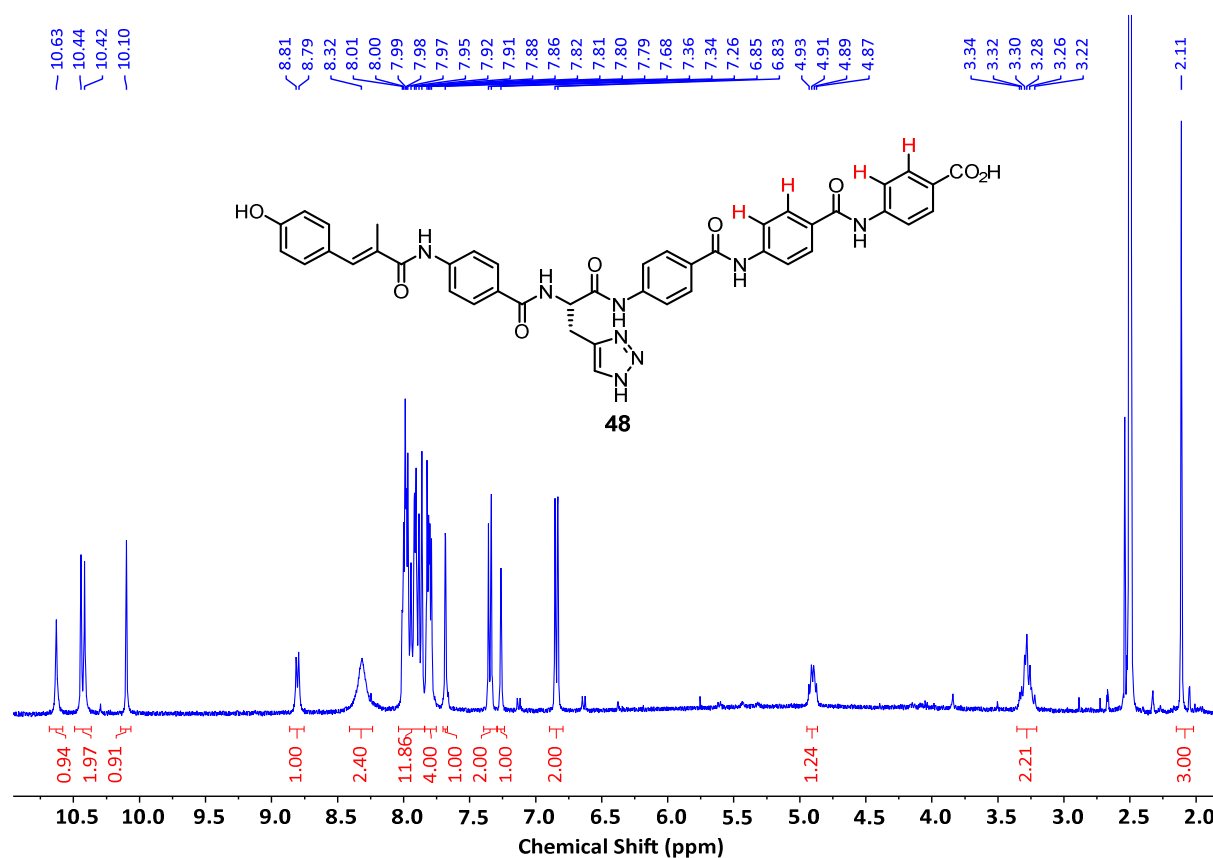
Final Derivative **43**Final Derivative **44**

Final Derivative **45**Final Derivative **46**

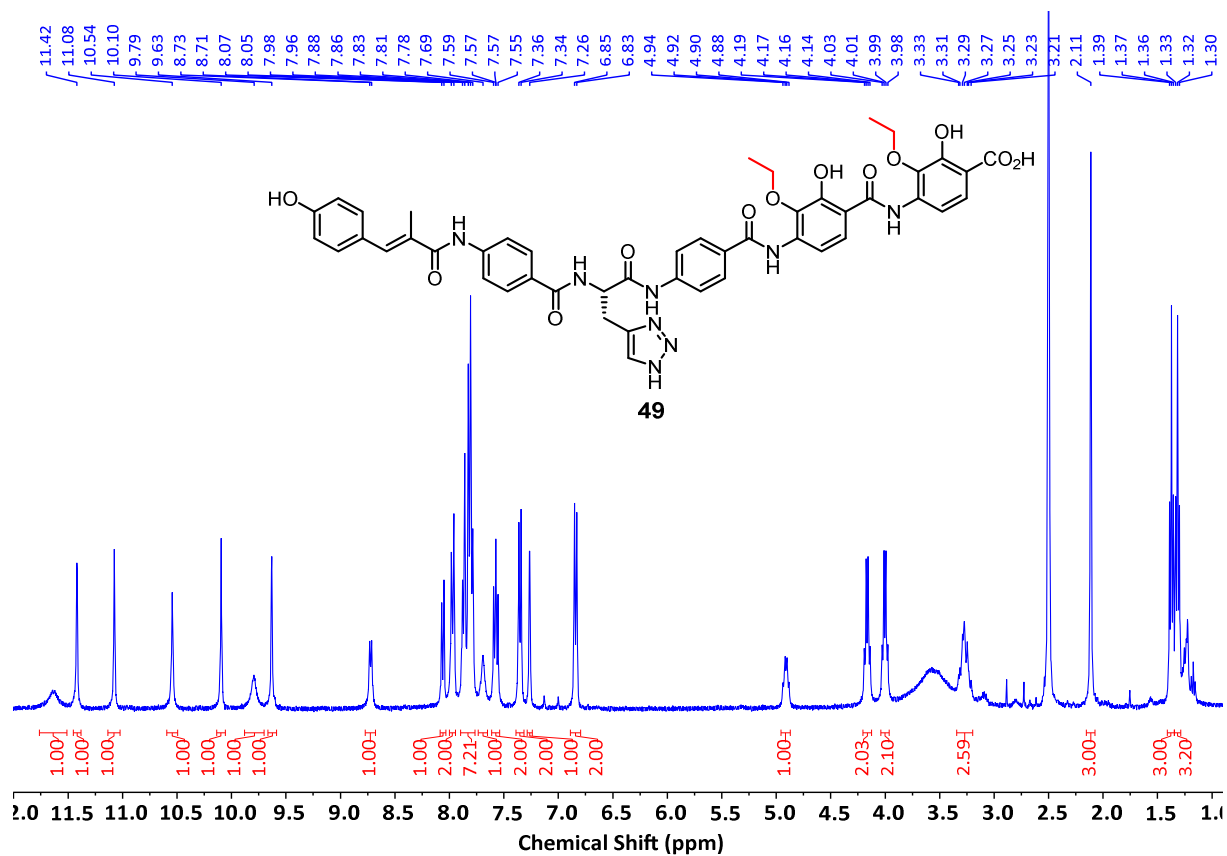
Final Derivative 47



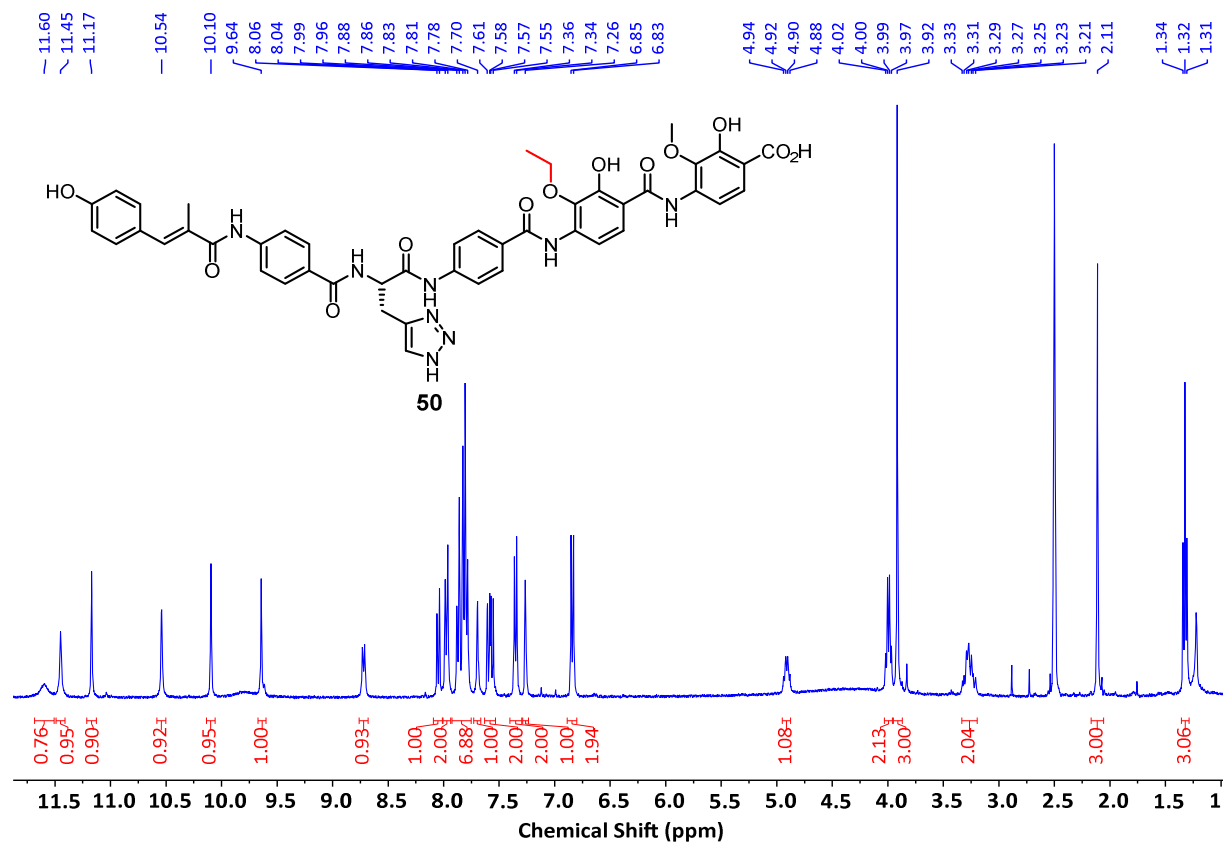
Final Derivative 48



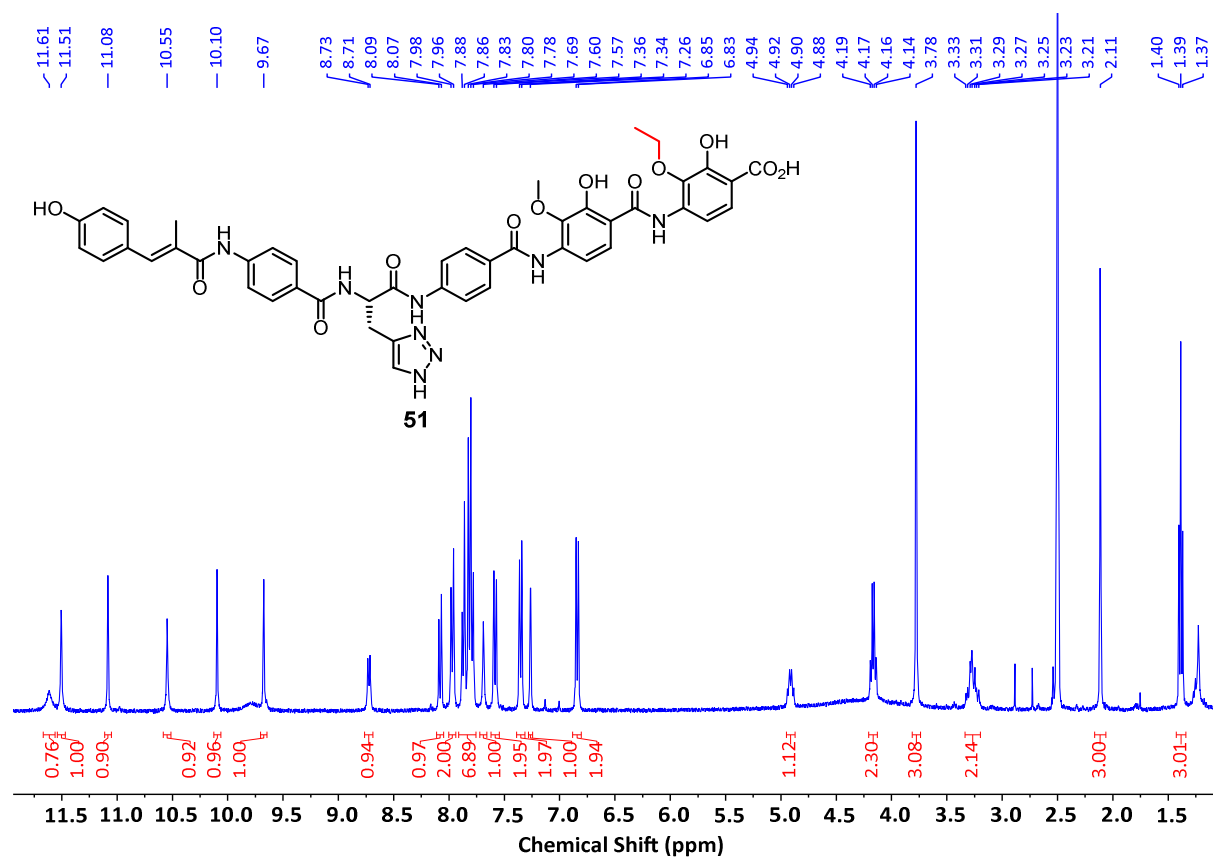
Final Derivative 49



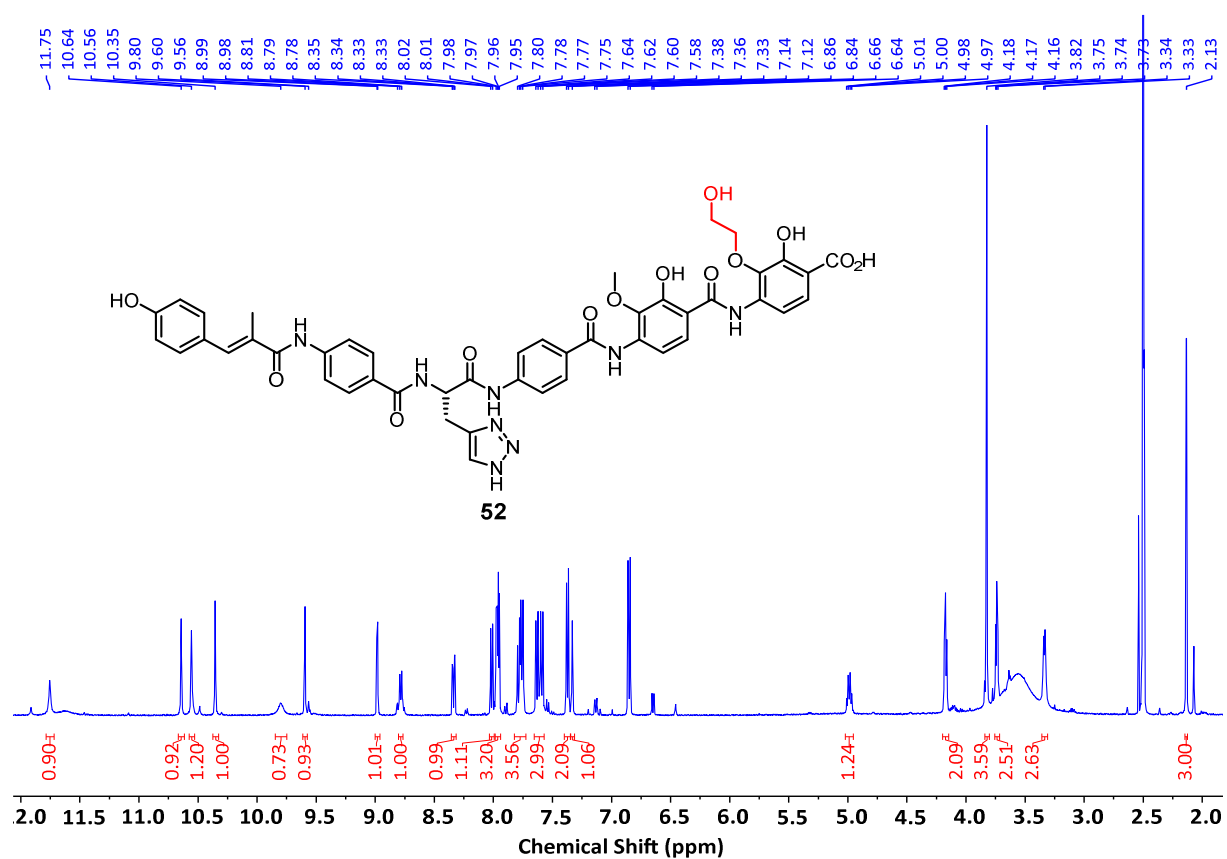
Final Derivative 50

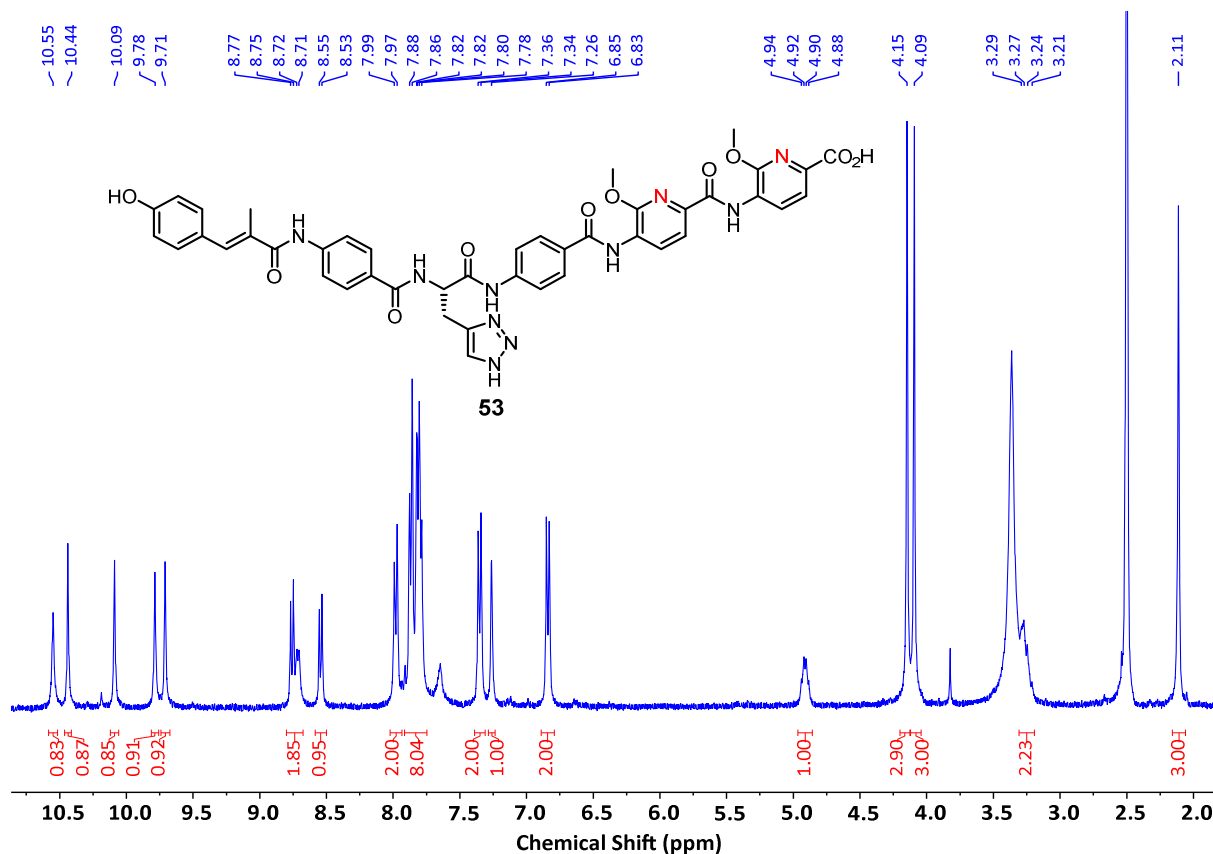
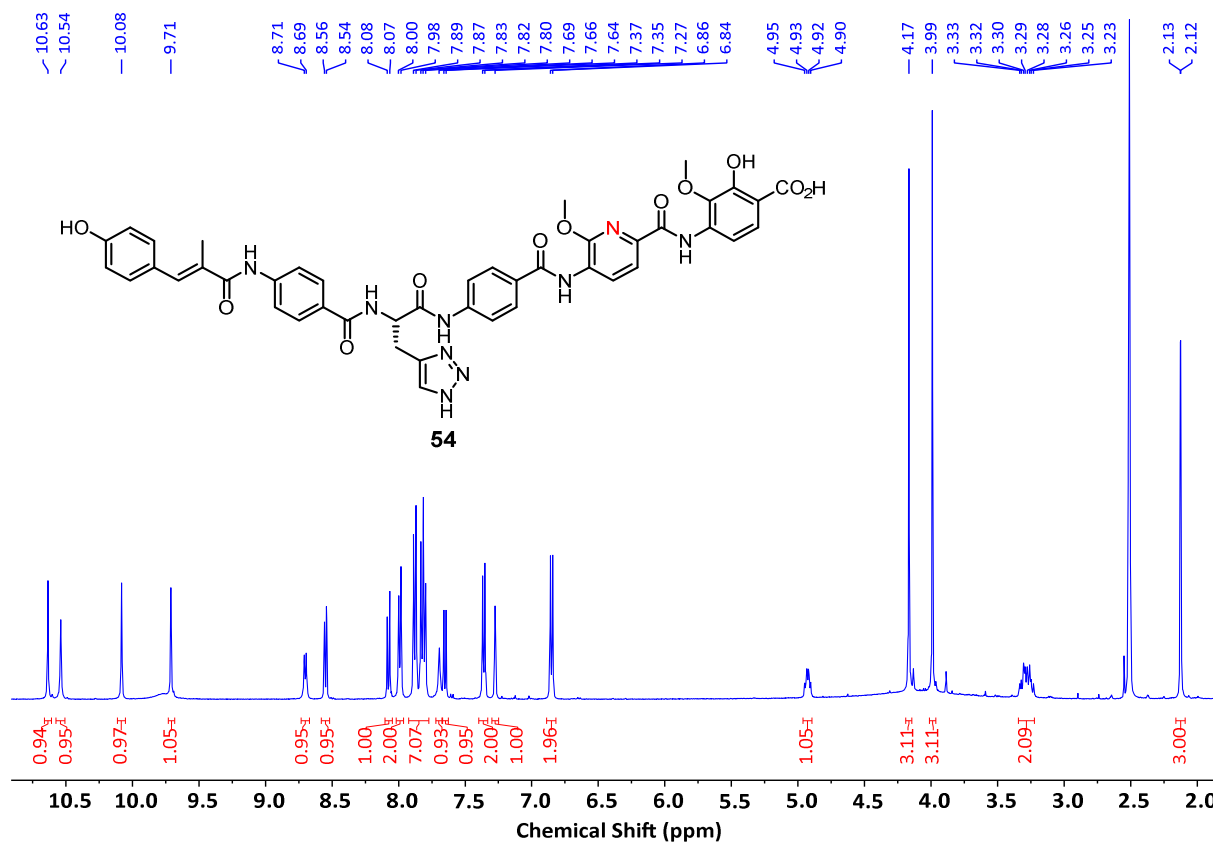


Final Derivative 51

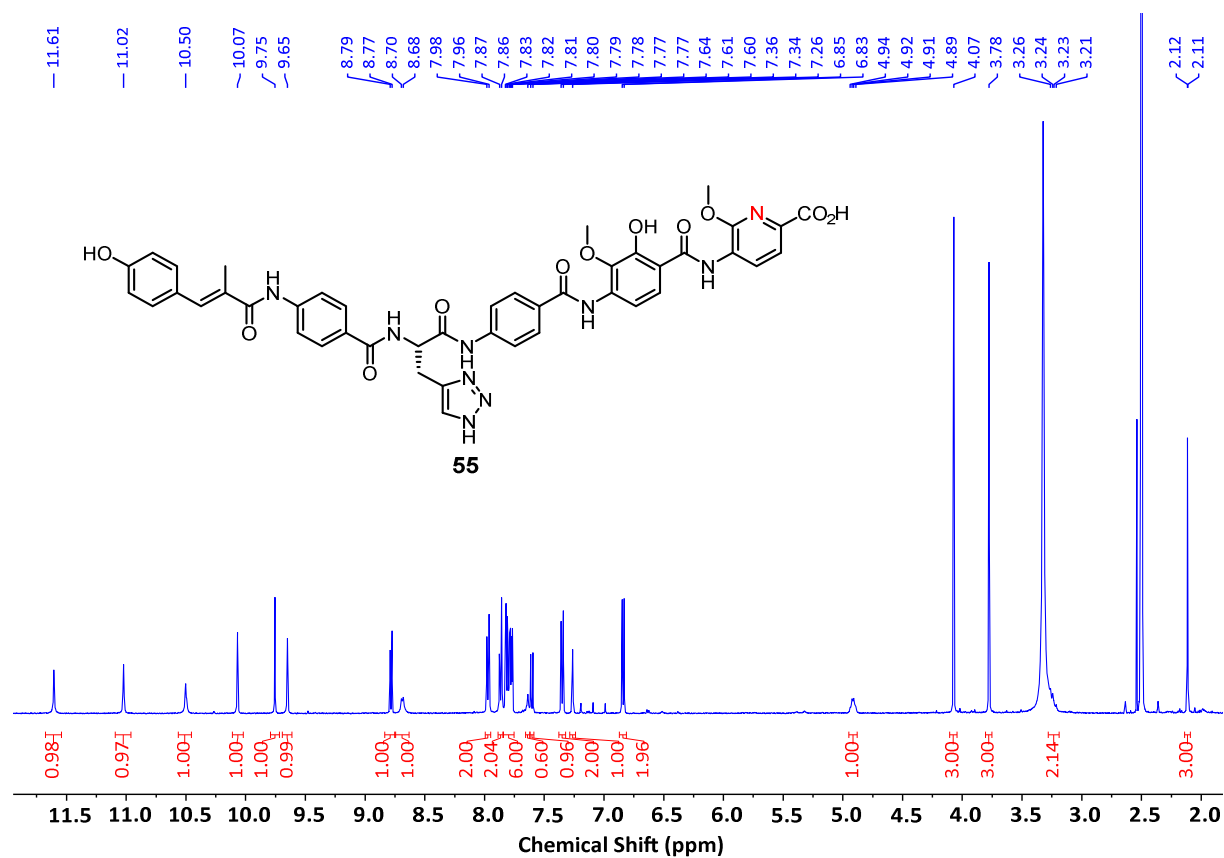


Final Derivative 52

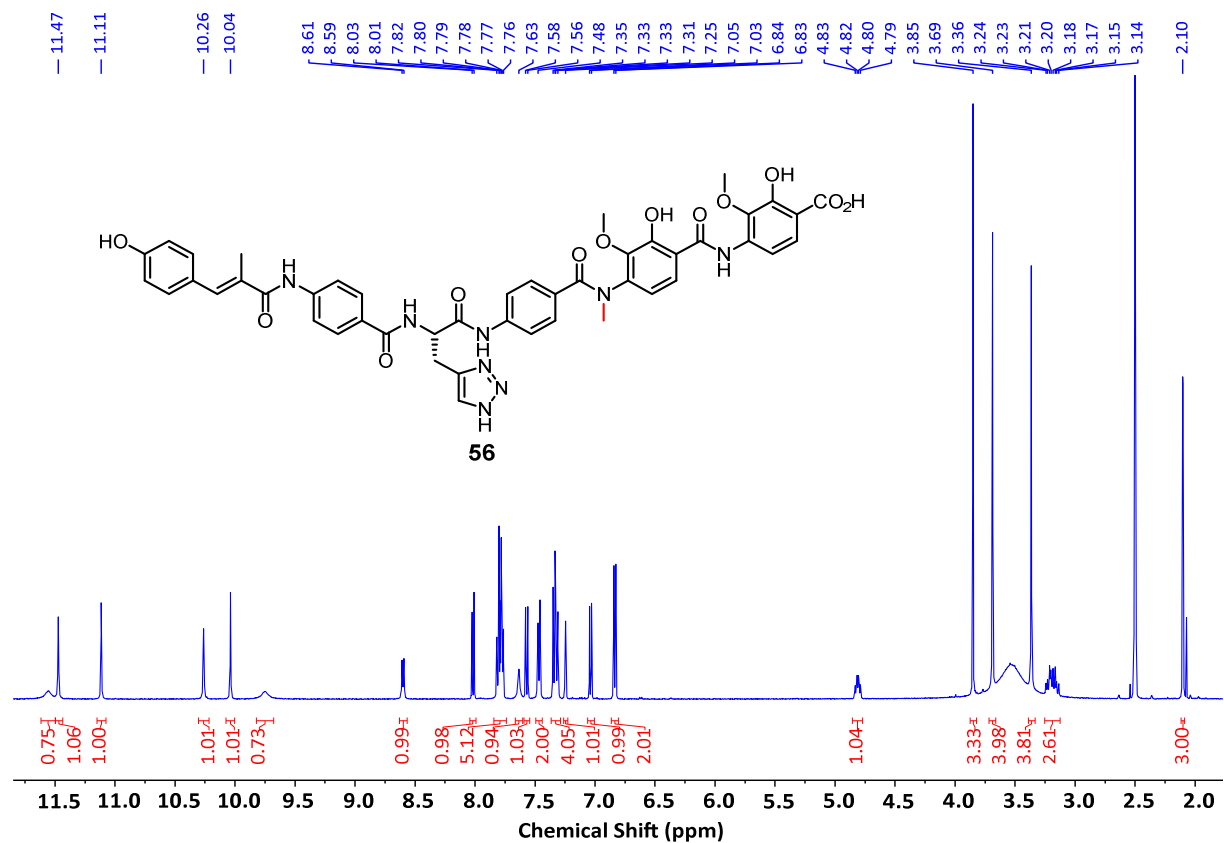


Final Derivative **53**Final Derivative **54**

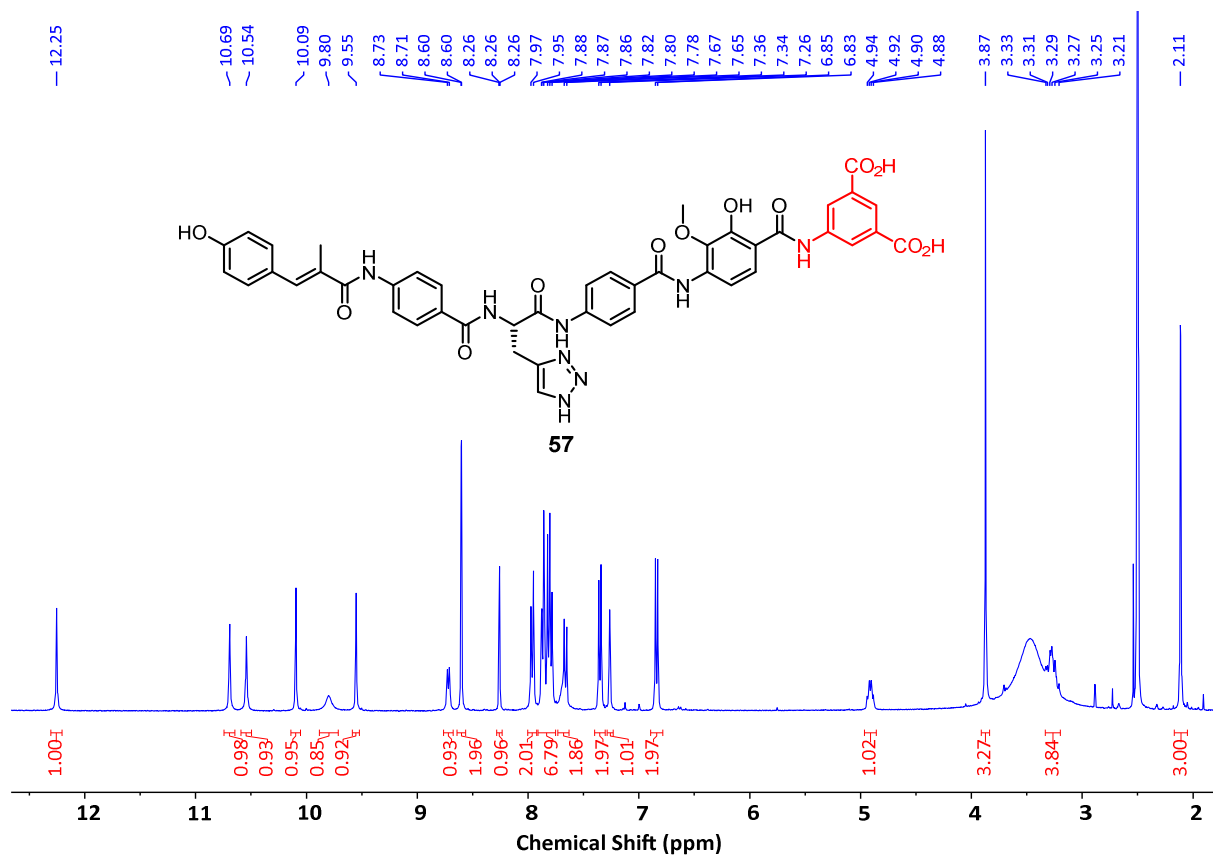
Final Derivative 55



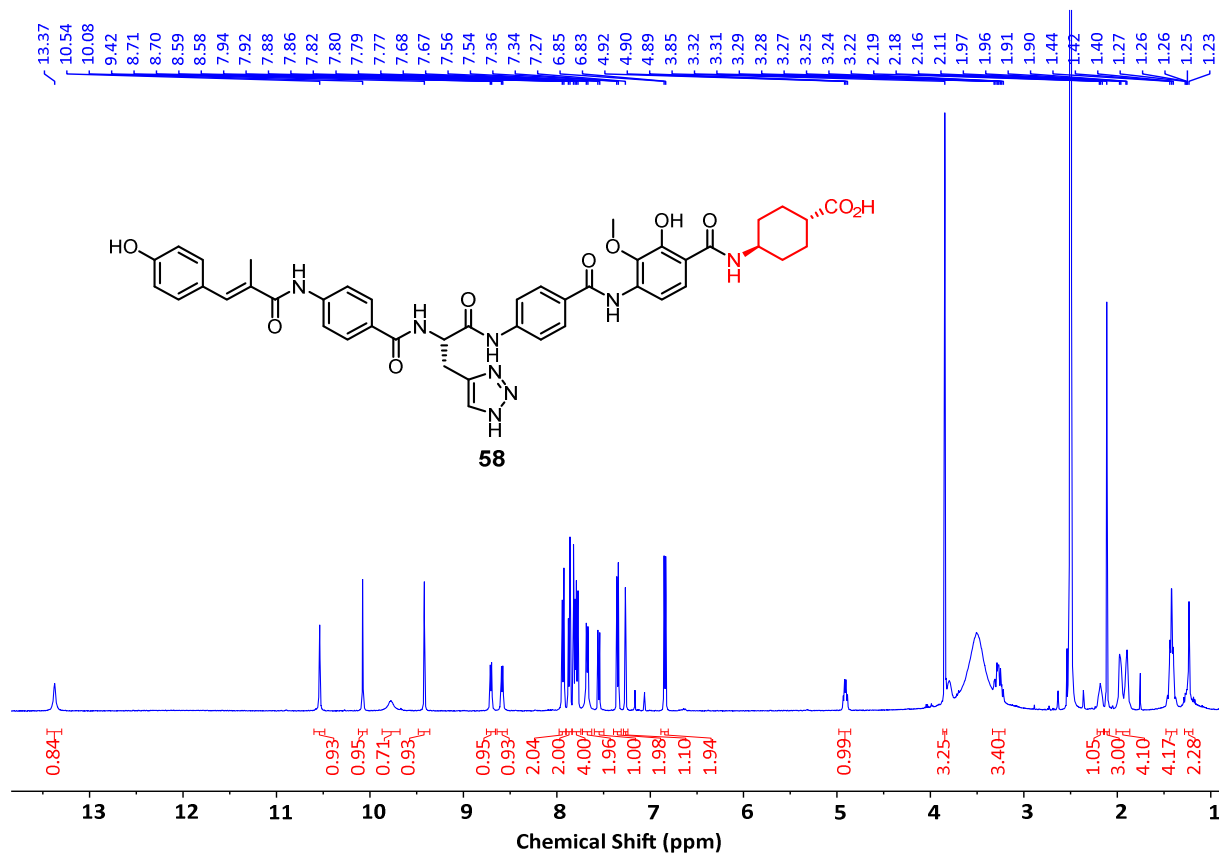
Final Derivative 56

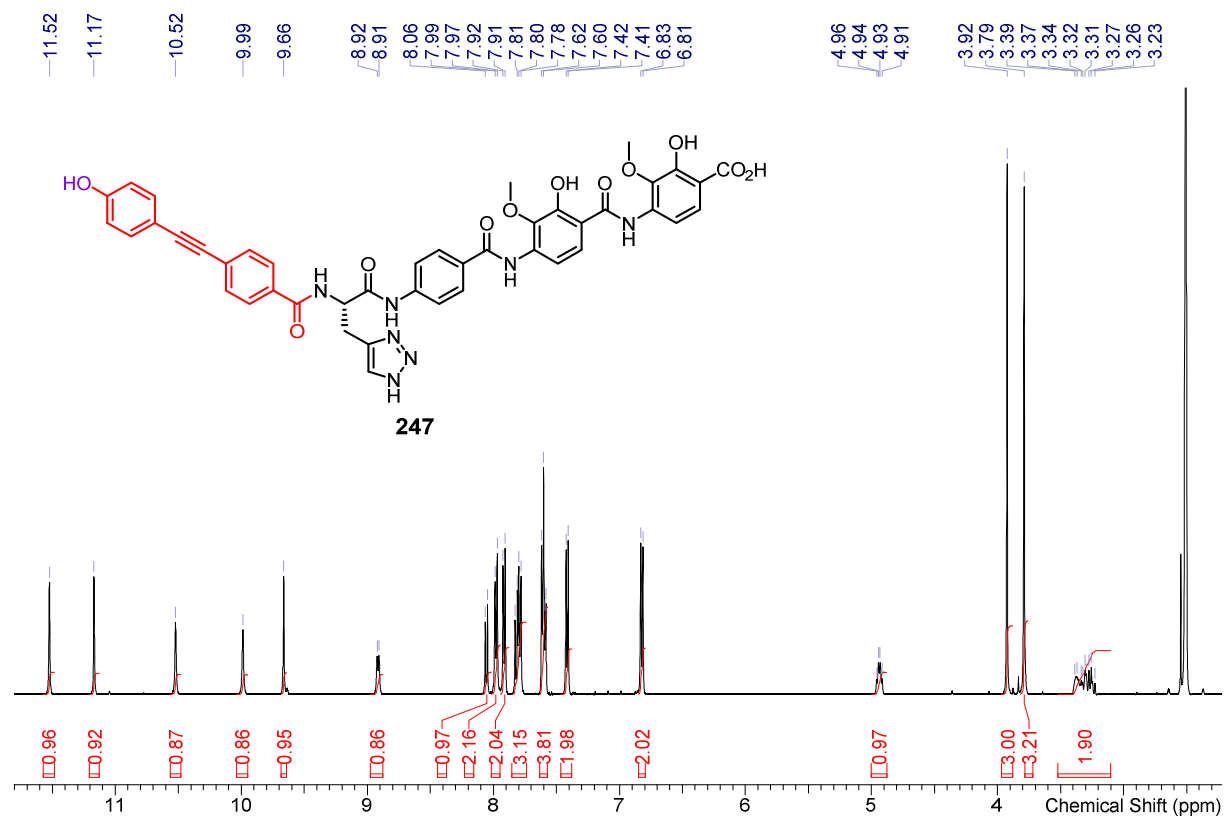
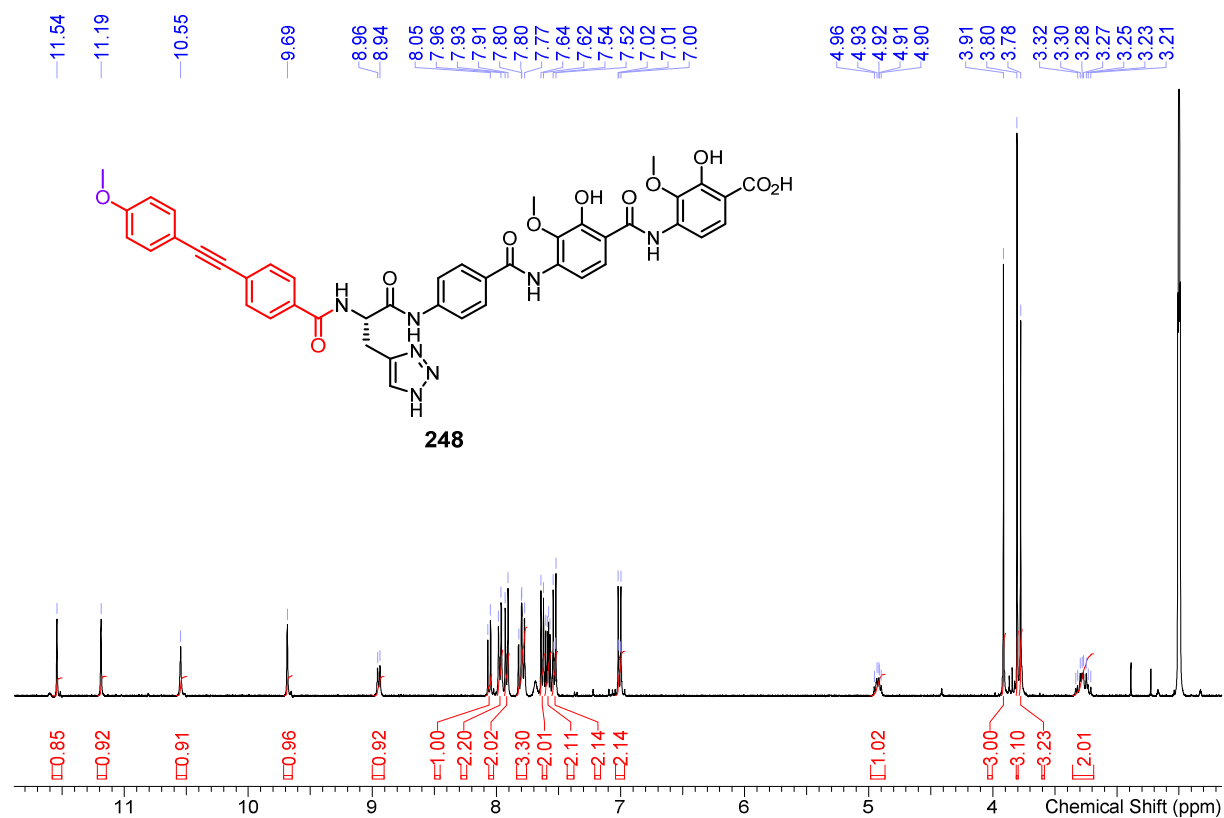


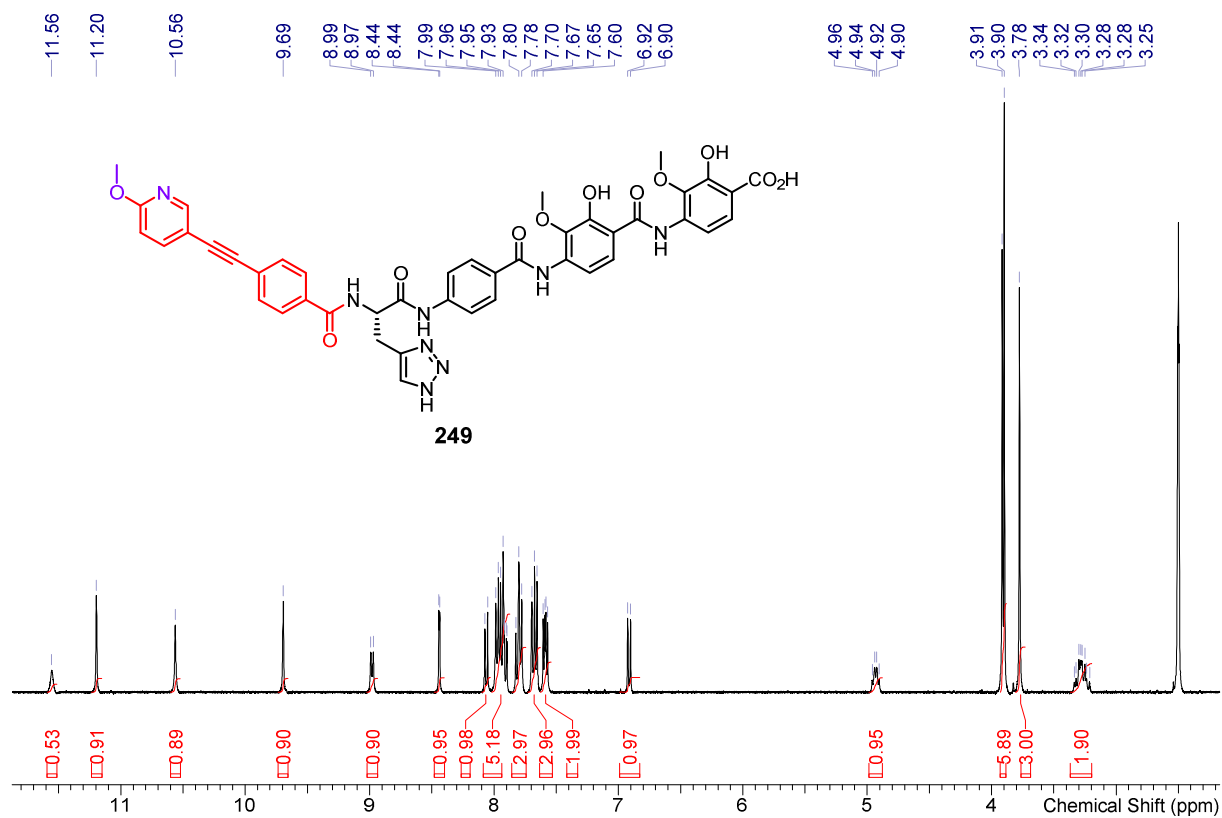
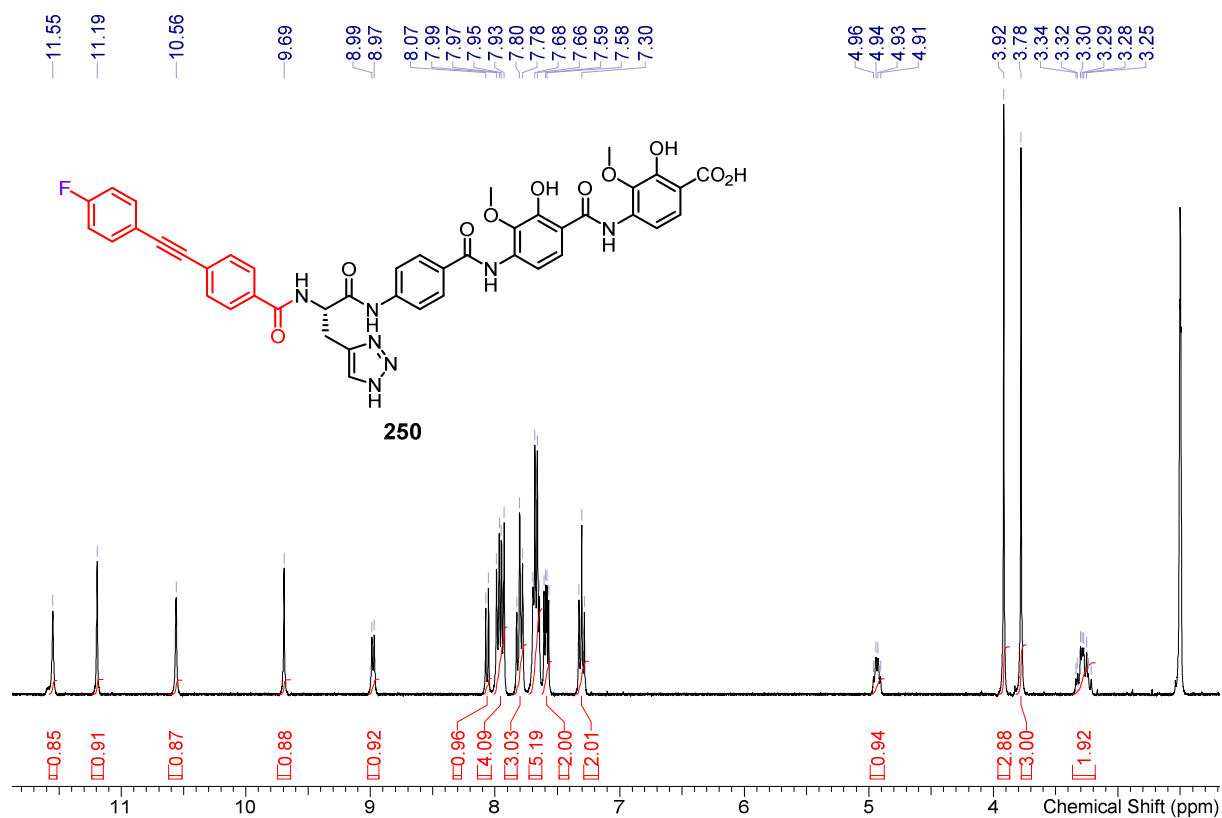
Final Derivative 57

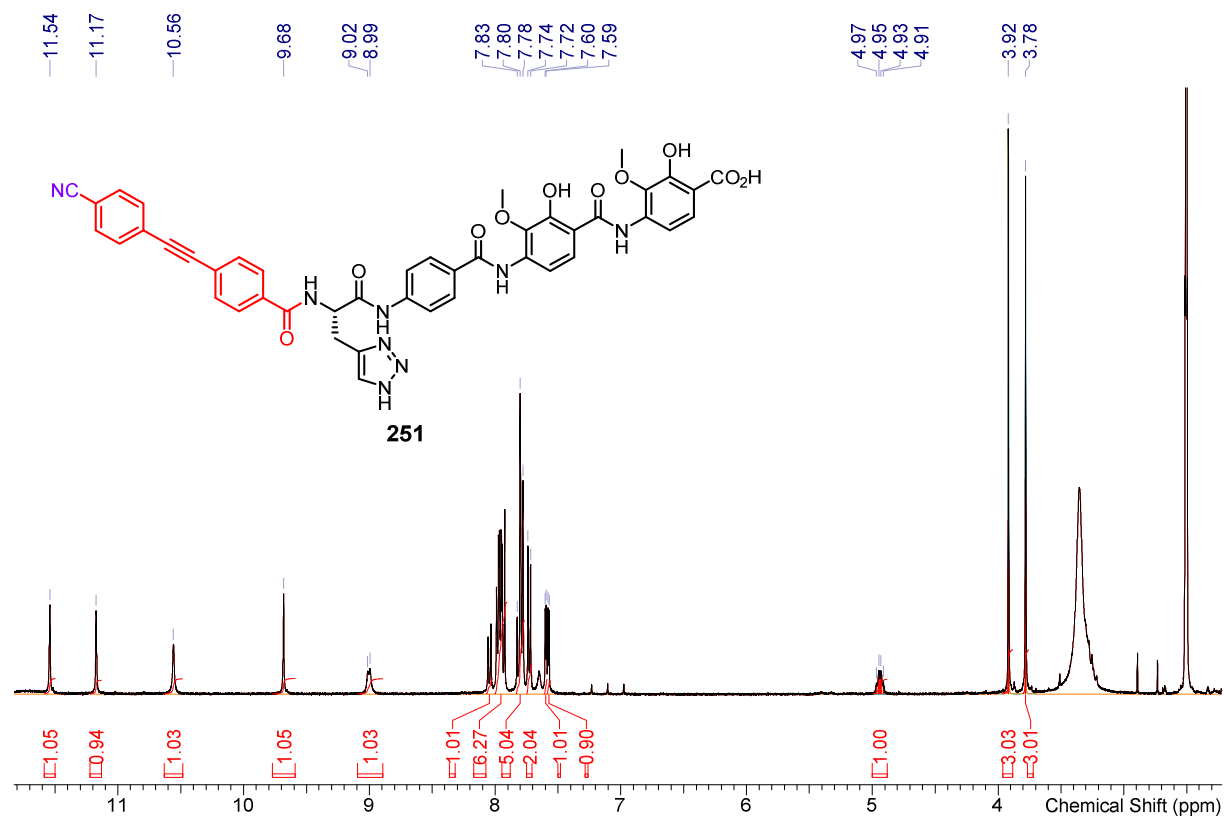
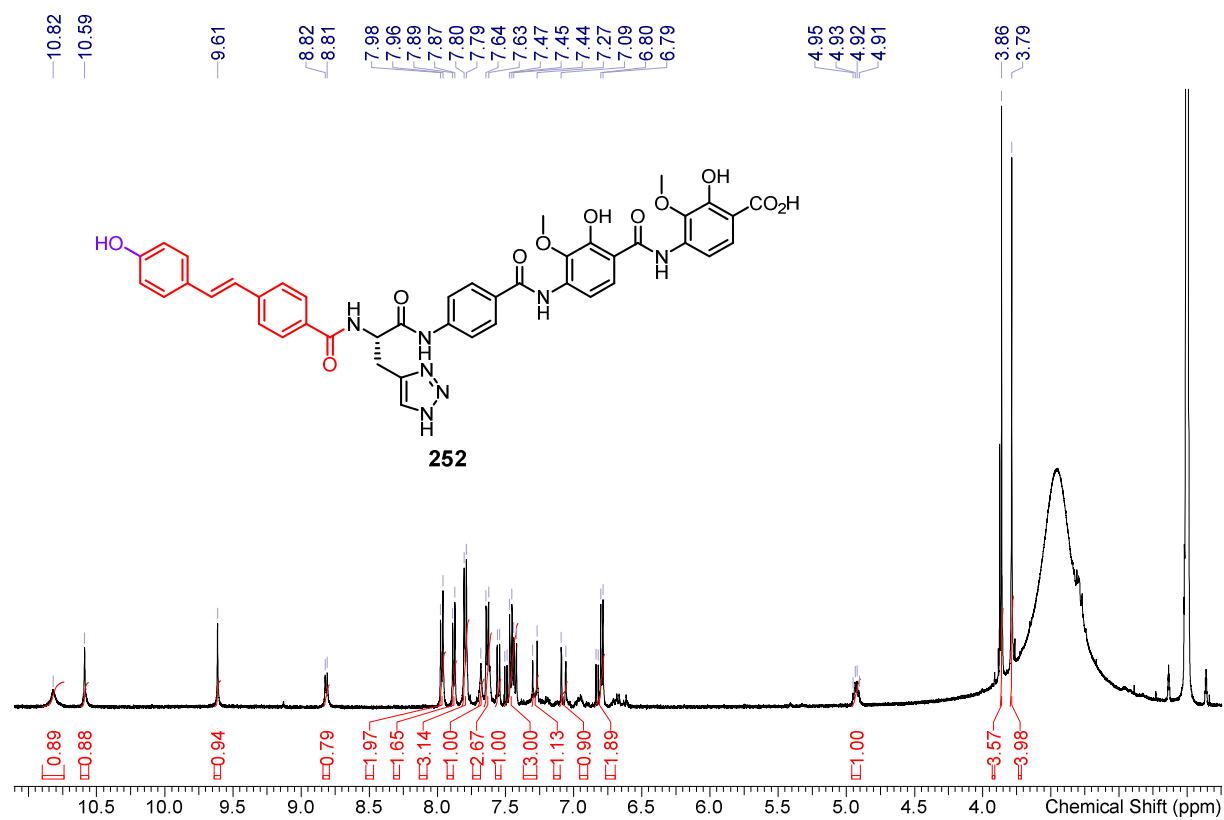


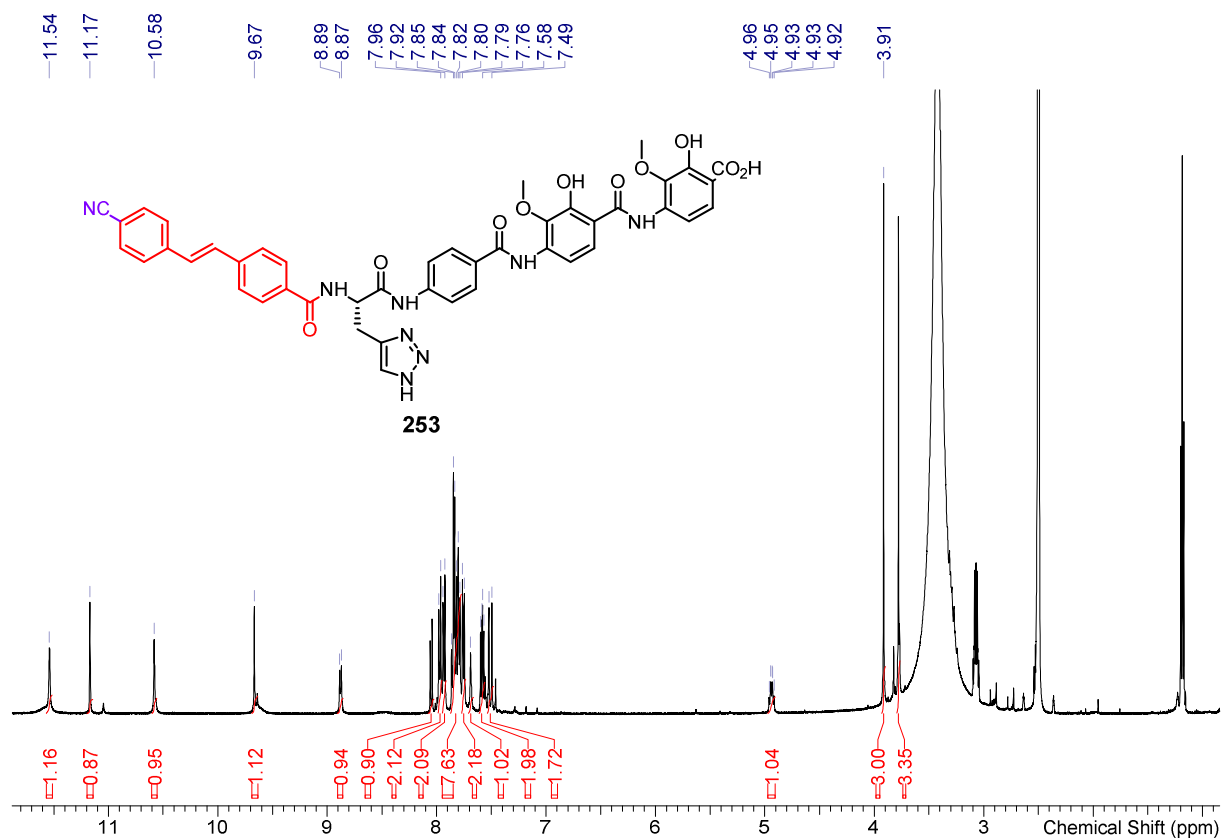
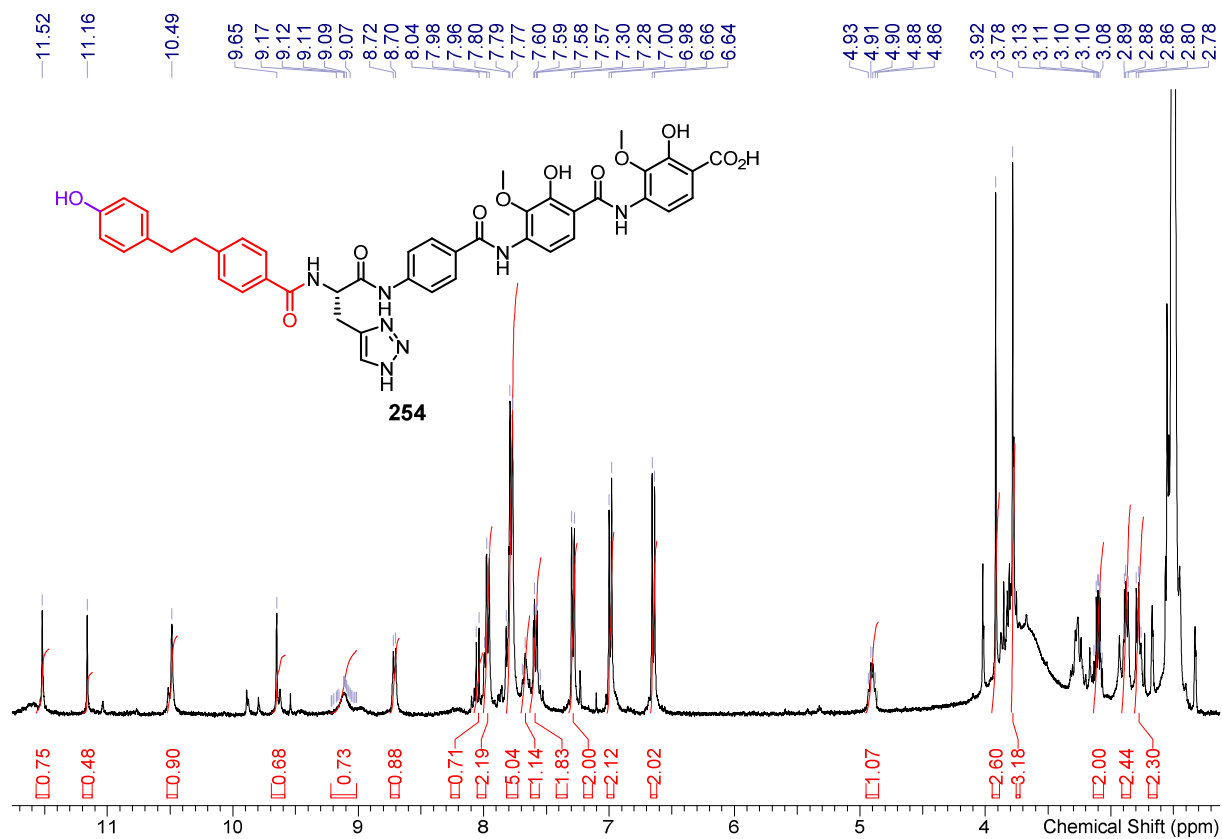
Final Derivative 58

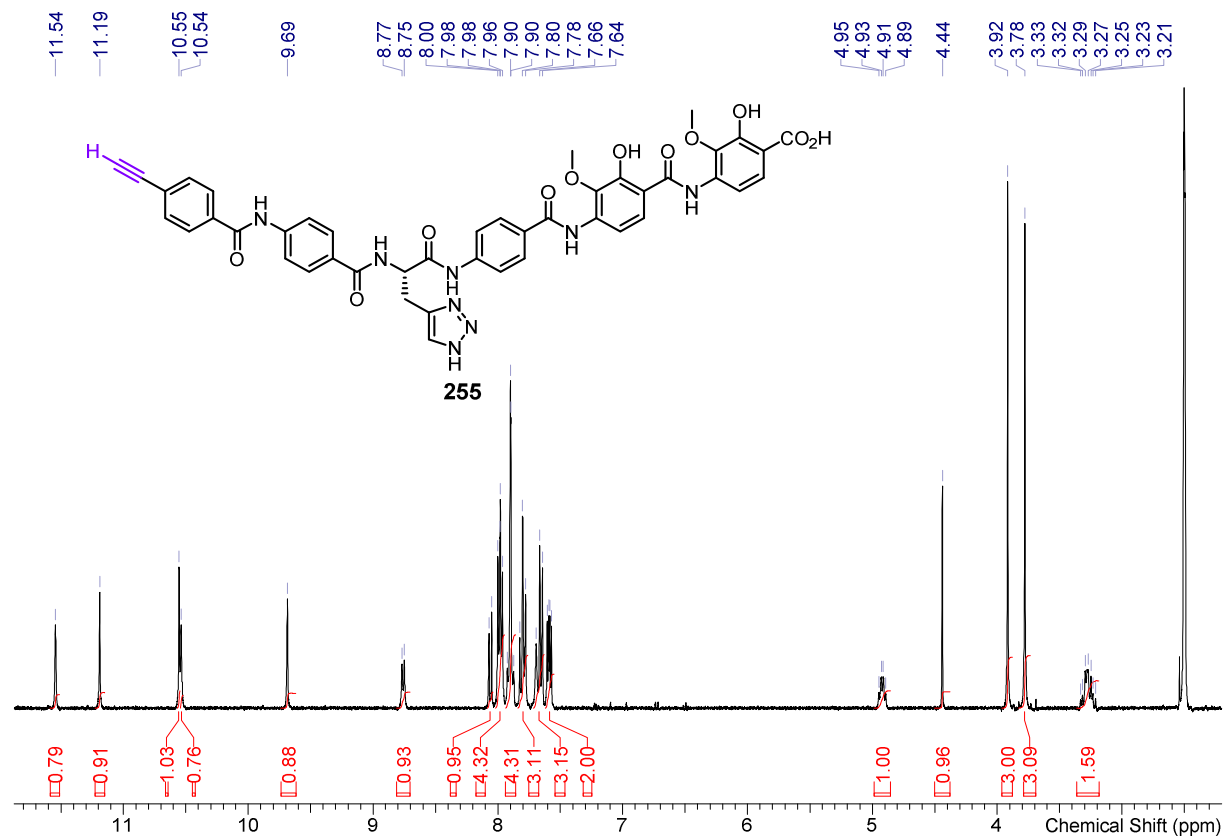
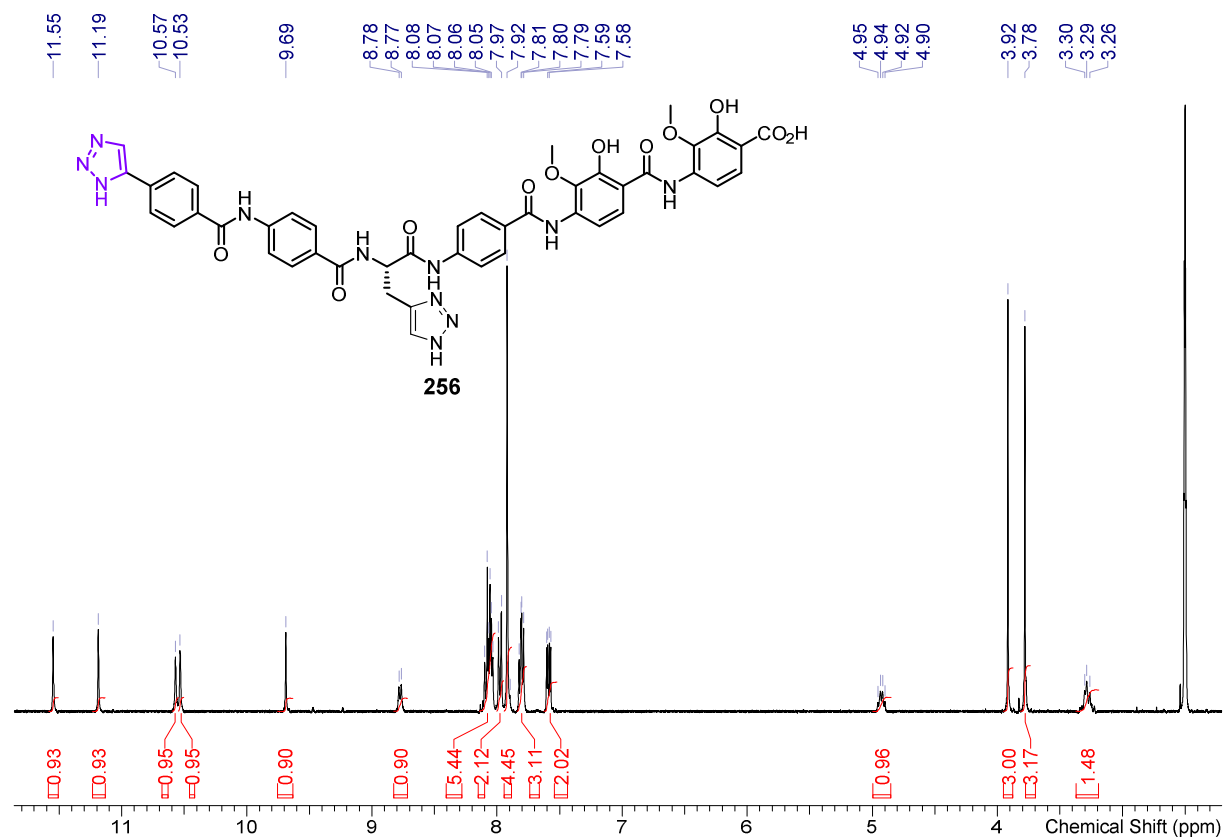


Final Derivative **247**Final Derivative **248**

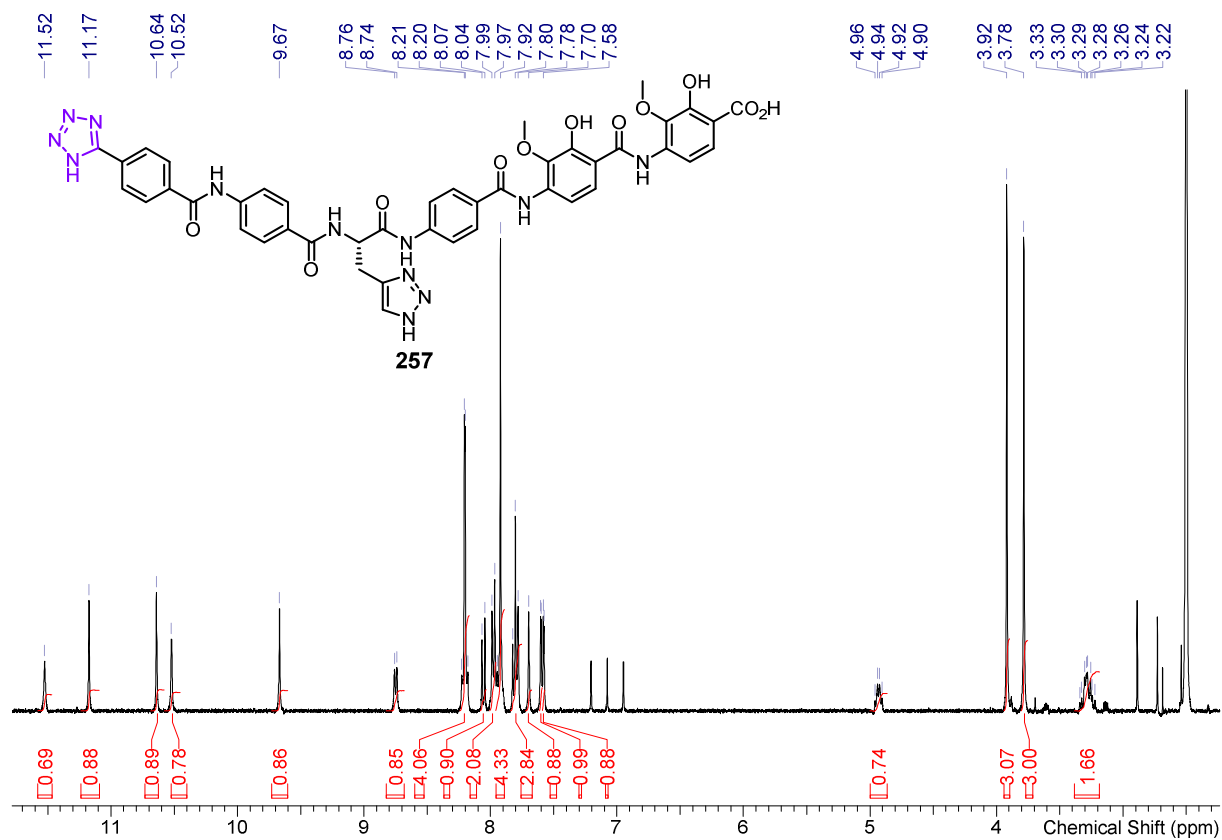
Final Derivative **249**Final Derivative **250**

Final Derivative **251**Final Derivative **252**

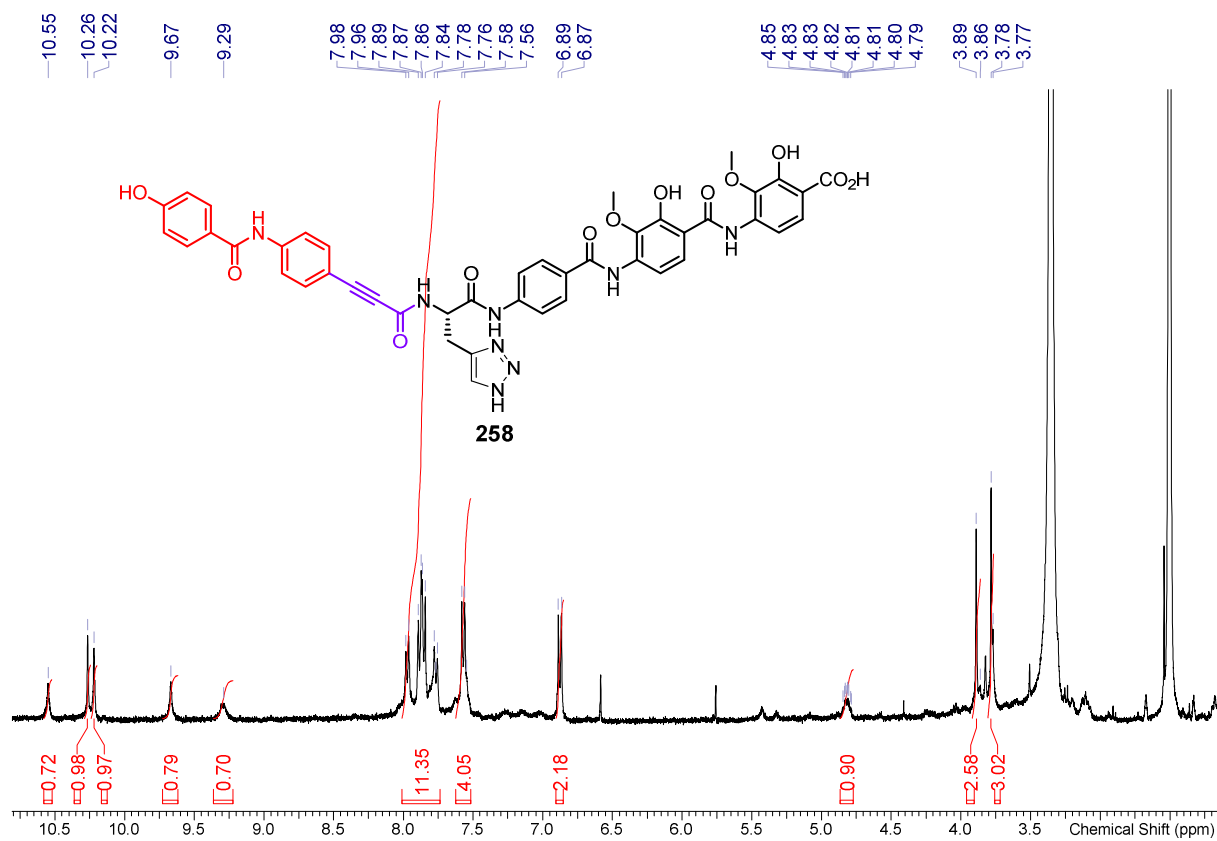
Final Derivative **253**Final Derivative **254**

Final Derivative **255**Final Derivative **256**

Final Derivative 257



Final Derivative 258



Final Derivative **259**